EXPERIMENTS, ANALYSIS AND DESIGN MODELS FOR SLAB ON PRESTRESSED CONCRETE GIRDER BRIDGE STRUCTURES

A Dissertation

by

DONGQI JIANG

Submitted to the Office of Graduate and Professional Studies of
Texas A&M University
in partial fulfillment of the requirements for the degree of

DOCTOR OF PHILOSOPHY

Chair of Committee,	John B. Mander
Co-Chair of Committee,	Mary Beth D. Hueste
Committee Members,	Gary T. Fry
	Mohammed E. Haque
Head of Department,	Robin Autenrieth

December 2015

Major Subject: Civil Engineering

ABSTRACT

A new class of spread slab beam bridge superstructure has recently been developed and implemented in Texas. In order to investigate its structural performance in general, and load distribution behavior in particular, comprehensive static and dynamic tests are performed on an in-service spread slab beam bridge, the US 69 Bridge located in Denison, Texas. Different computational techniques including the historic grillage analysis and the more rigorous finite element method (FEM) are utilized to model the moment and shear actions for this new bridge system. Satisfactory agreements are obtained with comparisons between experimental and computational results.

Current service load design practice reveals that the asymmetric AASHTO HS20 truck load and complicated LRFD LDF formulas bring unnecessary inconvenience to the design process. Alternative symmetric live load models and new design models with a familiar "*S/D*" format are developed in this dissertation for the purpose of providing bridge engineers a more straight-forward option to determine the moment and shear demands at the service load design or for the rapid checking of computer output. The applicability of the proposed design models for the prestressed concrete girder bridges commonly used in Texas and elsewhere is evaluated by comparing accuracy with more exacting FEM analysis results. Comparative results show that the proposed design formulas are mostly conservative for these bridge types.

Following service load design, the adequacy under factored ultimate strength conditions requires checking. Due to their expediency and ease of use, plastic limit

analysis methods are used to evaluate the reserve strength capacity of slab-on-beam bridge systems. It is shown that by taking a holistic view of several different potential failure modes the "balance" of the design can be judged in terms of a hierarchy of failure mechanisms. Therefore, it is possible to make minor adjustments to the design in order to obtain a preferred outcome.

The proposed design methods are adopted in the service load design of a multi-span spread slab beam bridge to explore the potential for extending the span length of this low profile bridge system. The design results indicate that span lengths up to 21.3 m are viable with only four spread slab beams. To achieve this span it is necessary to make at least three spans continuous and use load balancing principles along with some supplementary post-tensioning.

DEDICATION

To My Father and Mother

To All of Us Floating in the Sea of Destiny

ACKNOWLEDGEMENTS

I would like to express my gratitude to my committee chair, Dr. John Mander, and committee co-chair, Dr. Mary Beth Hueste for their invaluable guidance throughout my entire Ph.D. career. They can always provide creative thoughts and professional advice to lead the best direction of my research. This work would be impossible for me without their help and inspiration. I am also grateful to the Texas Department of Transportation and the Zachry Department of Civil Engineering for the financial support.

I would also like to thank my committee member, Dr. Gary Fry, for providing support during the bridge testing and valuable suggestions for my research work. Thanks also to Dr. Mohammed Haque for serving on my advisory committee.

I wish to express my appreciation to my project partners, Mr. Tevfik Terzioglu and Mr. Joel Petersen-Gauthier, for their constant help and support. I also would like to thank the department faculty and staff for their friendship and help during my life at the Texas A&M University.

Finally, my utmost gratitude goes to my father Mr. Bihai Jiang and mother Ms. Jianxia Tang for their constant encouragement and support during my journey at the Texas A&M University.

TABLE OF CONTENTS

Page

LIST OF FIGURES

Page

LIST OF TABLES

1 INTRODUCTION

1.1 BACKGROUND AND PROBLEM STATEMENT

1.1.1 Spread Slab Beam Bridge System

As a common alternative to the standard slab-on-I-girder bridge, prestressed concrete slab beam bridges have been used extensively in Texas and elsewhere. This bridge type is normally designed for up to 15 m long simply supported spans and it provides more clearance height due to a lower girder depth. However, previous design experience shows that it costs more when compared with traditional prestressed concrete I-girder bridges. In order to explore an economical and practical design solution for short-span bridges, the Texas Department of Transportation (TxDOT) developed a new bridge type using the same concept as spread box beam bridges in which the slab beams are spread apart with equal spacing.

Because this new bridge type was developed recently, its structural performance, especially the load distribution behavior, remains in question to bridge engineers. Therefore, TxDOT funded the Zachry Department of Civil Engineering at Texas A&M University and the Texas A&M Transportation Institute (TTI) to conduct Project 0-6722 "Spread Prestressed Concrete Slab Beam Bridges" to comprehensively investigate the behavior of the simply supported spread slab beam bridge system and provide design recommendations before it comes to extensive use. The study presented in this dissertation includes part of the research work in this project, mainly focusing on field experimental tests of an in-service simply supported spread slab beam bridge, the US 69 Bridge located

in the City of Denison, and computational modeling of the spread slab beam bridge system using both historic grillage and more rigorous finite element method (FEM) techniques.

1.1.2 Design Models for Slab on Prestressed Concrete Girder Bridge Structures

In highway bridge design, live loads plus their dynamic impact effects are one of the major components causing moment and shear demands. The American Association of State Highway and Transportation Officials (AASHTO) Load and Resistance Factor Design (LRFD) Bridge Design Specifications designate the live load model as the superposition of the design truck/tandem load and a uniformly distributed lane load, called the HL-93 live load model. However, design experience indicates that the asymmetric AASHTO HS20 truck load that is part of the HL-93 live load model brings inconvenience to determine the maximum moment value and critical load position. In this dissertation, an alternative symmetric live load model is developed in an attempt to provide bridge engineers a more direct and simpler option for rapid design. The reliability of the proposed live load model is validated by comparing its moment and shear force envelops with the "exact" actions generated by the HL-93 live load model.

The structural analysis for the bridge superstructure can be a complex problem due to the high degree of indeterminacy in the structure. To simplify the design, the American Association of State Highway (AASHO) Standard Bridge Design Specifications (AASHO 1931) introduced the concept of load sharing amongst girders and provided a "*S*-over" method for defining the load distribution factor (LDF). The historic "*S*-over" formula has been extensively utilized by bridge engineers due to its straight-forward concept and simple format. Since the advent of the AASHTO LRFD Bridge Design

Specifications in 1994, empirically derived power functions have been adopted. Although the LRFD formulas may have generated slightly more accurate design values for bridge structures within the range of the specified geometric characteristics, they are criticized by practitioners for the limited range of applicability, and their undue complexity sometimes requiring an iterative design procedure. In this dissertation, new design models with a "*S/D*" format are developed for the purpose of providing bridge engineers a more straight-forward option to determine the moment and shear demands in the service load design phase. The applicability of the proposed design models for the simply supported and continuous prestressed concrete girder bridges commonly used in Texas and elsewhere is evaluated by comparing to finite element method (FEM) analysis results.

The evaluation of the ultimate load capacity of bridge superstructures is a necessary part of design checking. Plastic methods of analysis are adopted in this dissertation to predict the overstrength capacity of slab-on-beam bridge decks at the ultimate collapse load. Different types of limiting behavior modes, including slab-only mechanisms, a beam-only mechanism, and mixed beam-slab mechanisms, are considered and analyzed with upper bound yield line theory and lower bound strip methods. The limit analysis methods are applied to two realistic spread slab beam bridges investigated in TxDOT Project 0-6722. Based on the plastic overstrength analysis results, important concepts regarding the "balance" of design with respect to the hierarchy of failure mechanisms are provided.

The proposed design methods are applied in the service load design of a multi span spread slab beam bridge to explore the span capability of this new bridge system. In the

design process, a new precast prestressed concrete panel (PCP) with thicker depth and longer span length is developed to facilitate accelerated bridge construction by negating the need for field placement of deck reinforcing steel.

1.2 OBJECTIVES AND SCOPE

The research work described in this dissertation is mainly concerned with (1) the load distribution behavior of the prestressed concrete spread slab beam bridge system and (2) new design models for slab on prestressed concrete girder bridge structures. The specific objectives in this study shall include:

1. Perform comprehensive static and dynamic tests on an in-service spread slab beam bridge, the US 69 Bridge, to investigate the structural performance in general and the load distribution behavior in particular for this new class of bridge.
2. Develop computational models with grillage and FEM techniques for the spread slab beam bridge system and validate the modeling techniques by comparing with experimental results.
3. Propose a symmetric alternative live load model for rapid design purposes and evaluate the reliability by comparing its moment and shear force envelops with the "exact" actions generated by the AASHTO LRFD HL-93 live load model.
4. Develop new design models to determine the moment and shear demands of simply supported and continuous girder bridge structures in the service load design phase.
5. Verify the applicability of proposed design models for slab on prestressed concrete girder bridges commonly used in Texas and elsewhere, including the prestressed

concrete I-girder bridge, the prestressed concrete slab beam bridge and the prestressed concrete spread slab beam bridge.

6. Investigate the overstrength capacity of slab-on-beam bridge decks by utilizing plastic analysis methods, including upper bound yield line theory and lower bound strip methods.
7. Perform a preliminary design example for a multi-span prestressed concrete spread slab beam bridge by adopting the alternative live load models and proposed design methods to explore the span capability of this new bridge system.

1.3 METHODOLOGY

Seven main tasks are carried out in order to achieve the research objectives.

1.3.1 Task 1: Review Literature and Document State-of-the-Practice

Comprehensive review and synthesis of available literature was performed to fully document the state-of-the-practice and state-of-the-art on issues involved in this research. Because the spread slab beam bridge was suggested by TxDOT recently, very limited information about the new type of bridge was found. Literature about full-scale bridge field test programs and experimental LDF value determination were reviewed to get a better idea of the instrumentation selection and arrangement. Besides, relevant publications about the bridge modeling and analysis were also included in the review process, which is helpful for researchers to be familiar with common computational techniques and to find applicable strategies to model the tested bridge. The literature covered in this review largely dealt with the development of the design models using the

live load distribution factor method, which provides insight to develop new design models for bridge structures. Finally, useful sources on plastic analysis methods for slab-on-beam bridge structures at the ultimate limit state were also included in the literature review.

1.3.2 Task 2: Field Tests of US 69 Bridge

A recently constructed spread slab beam bridge on US 69 North in the City of Denison, Texas (Grayson County) was temporarily instrumented and tested to measure the structural responses under vehicular loading. The experimental program at the US 69 Bridge provides a good opportunity to evaluate the in-service performance of a spread slab beam bridge system with more closely spaced slab beams. The instrumentation included strain gages, linear variable differential transformer (LVDT) transducers, string potentiometers, and accelerometers. The bearing pad deformations obtained using LVDTs at the bearing pad level were used to infer shear distribution factors between beams. Strain gages were installed at approximately mid-span on the bottom surface of the slab beams and on the top surface of the deck to determine flexural distribution factors. String potentiometers were also installed to measure the deflection profiles of the girders. Dynamic response parameters, including natural frequencies and mode shapes, of the bridge were also obtained using the accelerometer data.

1.3.3 Task 3: Computational Analysis of Spread Slab Beam Bridges

Although moment and shear LDF values were determined experimentally from the field test, the experimental conditions cannot represent all parameters affecting the load distribution behavior. Therefore, it is crucial to find a reliable computational modeling

technique to thoroughly investigate the structural behavior of spread slab beam bridges. Computational models using both historic grillage analysis and more computationally rigorous FEM techniques were developed to simulate the moment and shear actions of the tested bridge and determine computational LDF values. The accuracy of grillage and FEM models were evaluated by comparing computational results with experimental values.

1.3.4 Task 4: Alternative Symmetric Live Load Models

An alternative symmetric live load model was developed in an attempt to provide bridge engineers a more direct and simpler option for rapid design. To verify the reliability of the proposed live load models, the moment and shear force envelops were calculated for a wide range of simple spans and then compared with the "exact" actions generated by the AASHTO LRFD HL-93 live load model.

1.3.5 Task 5: Design Models for Slab on Prestressed Concrete Girder Bridge Structures

New design models were developed to determine girder moment and shear demands of slab on prestressed concrete girder bridge structures in the service load design phase. In order to verify the applicability of the proposed design models, a parametric study on extensive bridge configurations covering different girder spacing, span length, bridge width and number of lane was conducted using the FEM analysis technique. These bridge configurations include various bridge types commonly used in Texas and elsewhere: the prestressed concrete I-girder bridge, the prestressed concrete slab beam bridge and the prestressed concrete spread slab beam bridge. For each bridge type, both simply supported

and continuous cases were investigated. The moment and shear force values calculated from the proposed design models for each bridge configuration were compared with the "exact" FEM solutions to verify the applicability of the proposed design models.

1.3.6 Plastic Overstrength Analysis of Slab-on-beam Bridges

Plastic methods of analysis were utilized to predict the overstrength capacity of slab-on-beam bridge decks at the ultimate collapse load. Different types of limiting behavior modes, including slab-only mechanisms, a beam-only mechanism and mixed beam-slab mechanisms, were considered and analyzed with upper bound yield line theory and lower bound strip methods. The limit analysis methods were then applied to two realistic spread slab beam bridge prototypes investigated in Project 0-6722, Riverside and US 69 Bridges, to determine their reserve strength capacities.

1.3.7 Preliminary Design of a Multiple Span Spread Slab Beam Bridge

The alternative live load model, proposed design models and plastic analysis methods were applied in the service load design of a multiple span spread slab beam bridge to explore the span capability of this new bridge system. In the design process, a longitudinally prestressed PCP was developed to facilitate accelerated bridge construction by negating the need for field placement of deck reinforcing steel.

1.4 RESEARCH QUESTIONS

The investigation on the design and performance of slab-on-beam bridges in general and spread slab beam bridges in particular presented herein deals with the following research questions:

Q1: What is the structural performance in general and the load distribution behavior in particular of the in-service spread slab beam bridge system?

Q2: How can one effectively and efficiently experimentally infer from field observations the load distribution factors for shear for an in-service bridge structure?

Q3: Do secondary elements, such as the guardrail and sidewalk, significantly affect the load distribution behavior of a spread slab beam bridge?

Q4: What contemporary method of computational modeling is most appropriate for an accurate analysis of a slab-on-beam bridge? And how do these temporary methods compare with the historical grillage approach used in the AASHTO LRFD Specification development?

Q5: For rapid bridge analysis and design, is there a simple and expedient alternative live load model that has similar load effects with the current AASHTO LRFD HL-93 live load model?

Q6: As current AASHTO LRFD equations for LDFs for flexure and shear are somewhat complex, often necessitating iterative designs, is there a more straightforward way to determine the moment and shear demands for both simply supported and continuous slab-on-beam bridges?

Q7: For checking the reserve strength capacity of slab-on-beam bridges (especially for the new class of spread slab beam bridge), are the classical plastic analysis methods applicable?

Q8: In special circumstances, is it possible to extend the span capability of a spread slab beam bridge by making the bridge continuous over several supports?

Q9: By design, are there any expedient methods to improve the constructability of spread slab beam bridges?

1.5 ORGANIZATION OF DISSERTATION

This dissertation is structured with ten major sections. The first section is the background information on the research problems and the dissertation outline. Section 2 presents the comprehensive literature review conducted on the development of the LDF design method, experimental test program, computational modeling and plastic analysis methods. In Section 3, a comprehensive static and dynamic test on the US 69 Bridge and results analysis are described. The fourth section covers the computational analysis of the tested spread slab beam bridge. Section 5 introduces the alternative symmetric live load model for rapid design. In Section 6, new design models based on the lane loading concept are proposed and their applicability to simply supported bridge configurations is presented. Section 7 discusses the applicability of proposed design models to continuous bridge configurations. Section 8 presents the plastic analysis methods for slab-on-beam bridges at ultimate limit state and their application to two realistic spread slab beam bridges. In Section 9, a preliminary design of a multi-span spread slab beam bridge was performed by adopting the proposed design methods. The final section presents the research summary, conclusions, recommendations and potential future research work.

2 LITERATURE REVIEW

2.1 GENERAL

A comprehensive review of available literature on the issues involved in the research work is described in this section, from which it is helpful to get a full knowledge of what has been completed in this research area. The shortcomings of the existing achievements are also included to provide the basis for the research study in this dissertation. One major topic discussed by this literature review is the background, development and evaluation of the live load distribution factor (LDF) method, including the historic "*S*-over" method, AASHTO LRFD power function LDF equations and simplified LDF approaches proposed by other researchers. Relevant publications about the prestressed concrete spread slab beam bridge system, bridge field experimental test program, computational modeling techniques and plastic methods of analysis for bridge structure are also covered in the review.

2.2 PRESTRESSED CONCRETE SPREAD SLAB BEAM BRIDGE SYSTEM

As an economical solution for short to medium spans, prestressed concrete girder bridges have been used effectively in Texas and elsewhere for more than 60 years. In particular, the precast, prestressed concrete I-girder is the most common example in Texas and it is very popular because of the simple geometry, easy erection and low fabrication cost. However, its applicability in locations with low clearance is limited due to the high girder depth. In that situation, the prestressed concrete slab beam bridge is often selected as an

alternative because of its shallow geometric characteristic. This bridge type is normally designed for up to 15 m long simply supported spans and a typical 203 mm thick deck slab is cast to be composite with precast prestressed concrete slab beams. Figure 2.1 provides the plan view and transverse section of a typical prestressed concrete slab beam bridge designed by the Texas Department of Transportation (TxDOT). Details about the prestressing and mild steel reinforcing arrangement are shown in Figure 2.2.

While prestressed concrete slab beam bridges are used extensively in Texas, previous design experience shows that they are more expensive than traditional prestressed concrete I-girder bridges on a per-square-foot basis. In order to explore an economical and practical design solution for short-span bridges with a low beam depth, a new bridge type, known as spread slab beam bridge, was developed by TxDOT using the same concept as a spread box beam bridge in which the beams are spread apart with equal spacing. It is suggested that precast prestressed concrete panels (PCPs) be placed between girders transversely to work as stay-in-place (SIP) forms. The contractors show strong preference that no overhangs exist at both edges of the deck slab (Holt 2011). Figure 2.3(a) presents the transverse section of a typical prestressed concrete spread slab beam bridge without slab overhangs. The design details of a typical prestressed concrete spread slab beam bridge deck with PCPs are shown in Figure 2.3(b). The deck thickness presented in Figure 2.3(b) is 203 mm (8 in.), consisting of a 102 mm (4 in.) thick PCPs between girders and 102 mm (4 in.) thick reinforced concrete deck cast on the top.

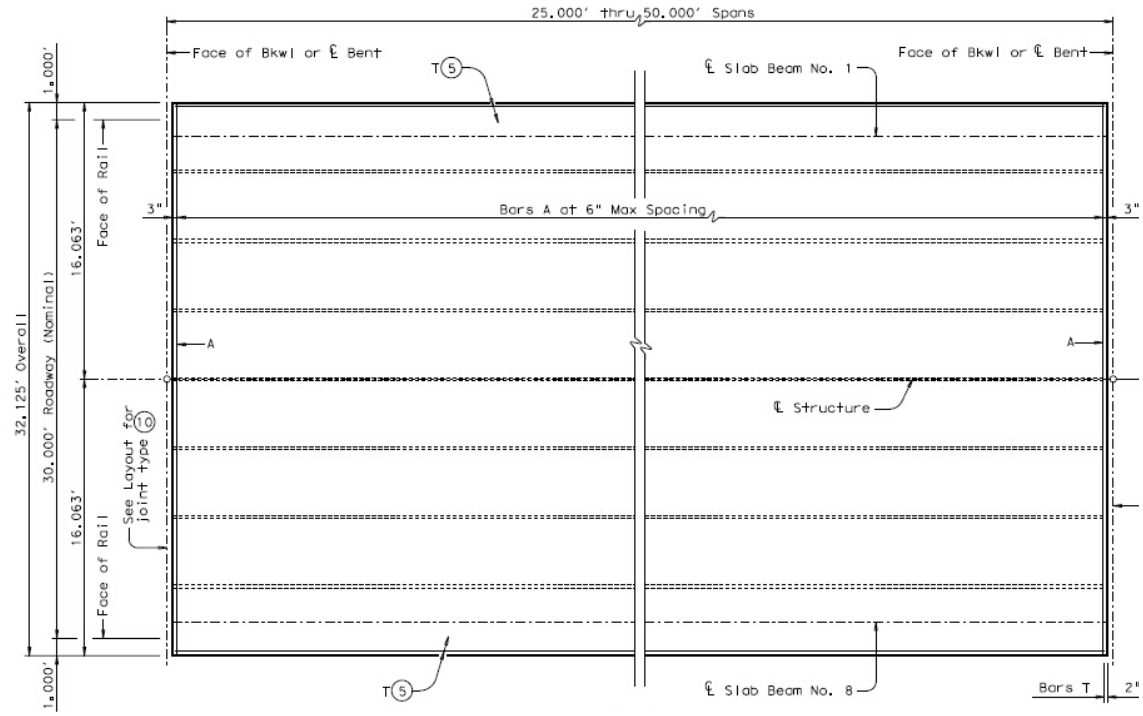

(a) Typical Plan View

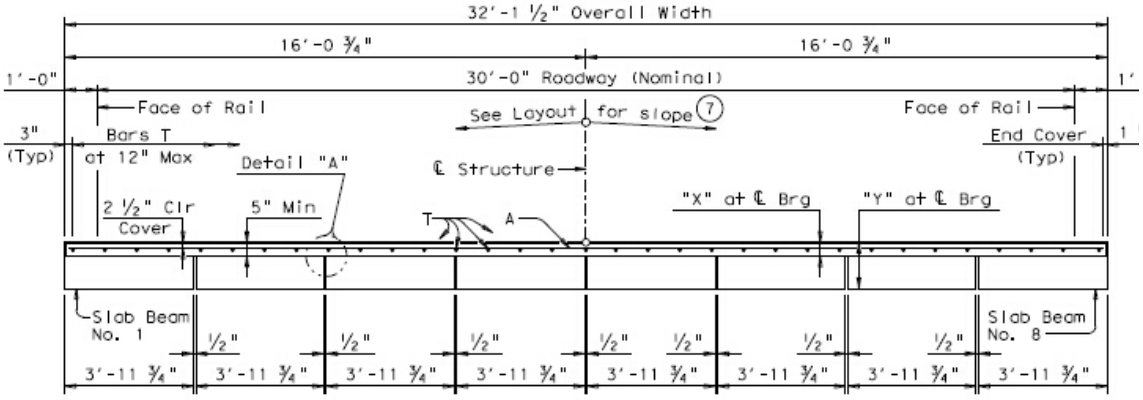

(b) Typical Transverse Section

Note: 1 inch = 25.4 mm

Figure 2.1. Typical TxDOT Prestressed Concrete Slab Beam Bridge (TxDOT 2012).

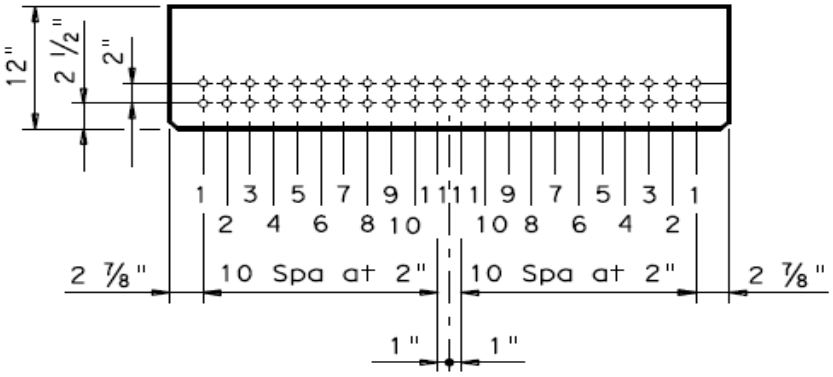

(a) 4SB12 Slab Beam Prestressing Locations

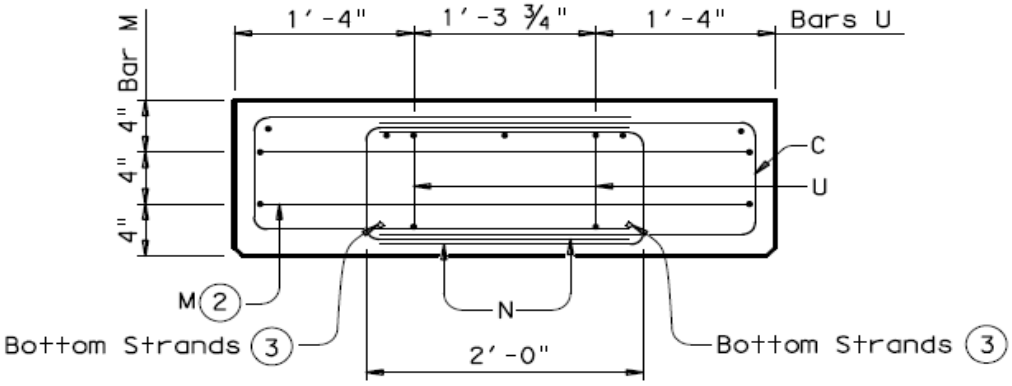

(b) 4SB12 Slab Beam Mild Steel Reinforcing

Note: 1 inch = 25.4 mm

Figure 2.2. Typical Details of TxDOT 4SB12 Prestressed Concrete Slab Beams (TxDOT 2012).

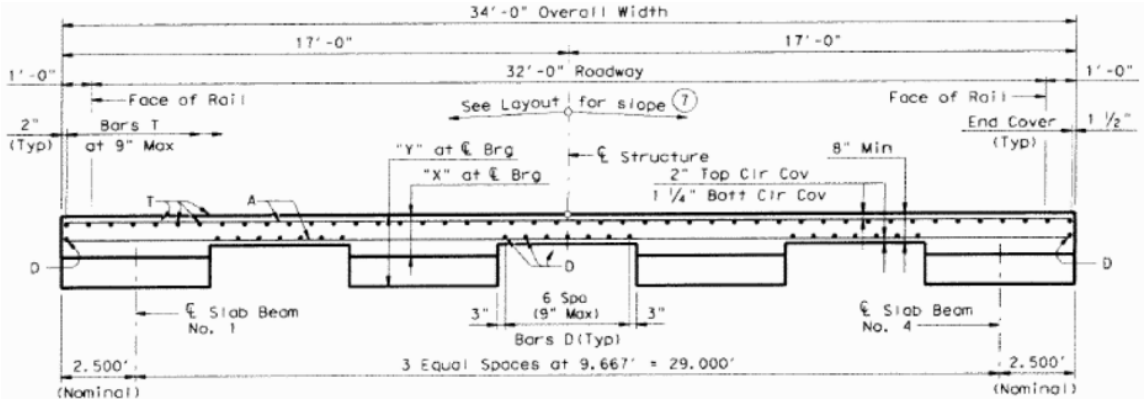

(a) Transverse Section of a Typical Spread Slab Beam Bridge

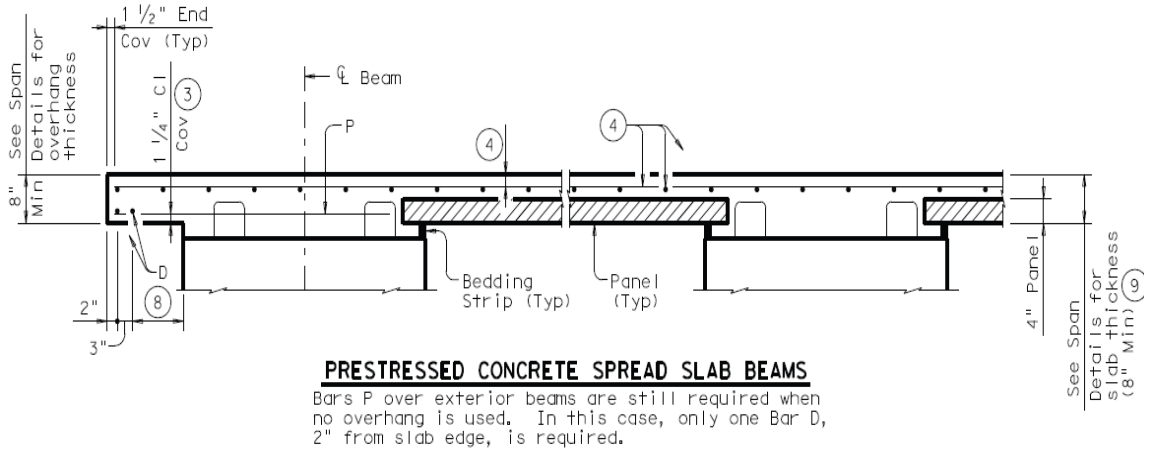

(b) Details of Bridge Deck with PCPs

Note: 1 inch = 25.4 mm

Figure 2.3. Transverse Section and Deck Details of a Typical Prestressed Concrete Spread Slab Beam Bridge (TxDOT 2012)

Once the slab beams are spread out across the bridge transverse section, it is obvious that less material, labor and girder transportation are required although more CIP PCP placement activities are needed during the construction process. Because this bridge system was developed recently, very limited information was found in the literature. The structural behavior of this new type of bridge, especially the load distribution behavior amongst individual slab beams, is unclear to bridge engineers. Therefore, one major objective of the research work in this dissertation is to investigate the load distribution behavior of the spread slab beam bridge system through experimental testing and computational analysis.

2.3 LIVE LOAD DISTRIBUTION FACTOR (LDF) METHOD

The analysis for slab-on-girder bridges is a highly complex problem due to a high degree of indeterminacy in the structure. Since the 1930's, the concept of LDF was extensively utilized by bridge engineers to determine the moments and shear forces of individual girders, which is necessary for the new bridge design or existing bridge evaluation. In the past century, many scholars and practitioners have made great efforts to evaluate the reliability and accuracy of code specified LDF formulas and further develop a simplified LDF method. Note that the LDF equations developed in the early days were expressed with US customary units, thus these achievements are described herein with their original unit system to avoid bias caused by unit conversion. In this section, a robust and comprehensive literature review on the development of the LDF method and relevant topics are covered. All publications are classified into four categories: development of the historic "*S*-over" method and relevant publications, development of AASHTO LRFD

empirical LDF approach and relevant articles, evaluation of "*S*-over" method and LRFD LDF approach and other simplified LDF methods.

2.3.1 Background and Development of the AASHTO "*S*-over" Method

2.3.1.1 Development of AASHTO "S-over" Formula in Early Stage (1931-1950s)

The historic concept of live LDF was introduced to the structural design of bridge decks in the first edition of the American Association of State Highway Officials (AASHO) Bridge Standard Design Specifications (AASHO 1931) to determine the wheel load distribution of stringers and floor beams. The design moment value was considered as the fraction of a wheel load to each stringer or floor beam and the fraction factors were given in the form of a "*S*-over" formulation where *S* is defined as the spacing of stringers or floor beams in feet and the denominator value varies with different bridge configurations. Table 2.1 lists the moment distribution factor equations for interior stringers specified in the AASHO Standard Bridge Design Specifications (AASHO 1931). It is seen from Table 2.1 that only one general formula "*S/6.0*" was provided for concrete bridges and no detailed classifications for different bridge types were given. It is worth mentioning that in the first edition of AASHO Bridge Standard Design Specifications, no lateral distribution of the wheel load was specified to determine the shear forces and reactions in stringers or floor beams.

Since the "*S*-over" fraction factor of wheel loads was introduced in AASHO Standard Bridge Specifications in 1931, this simplified method became popular and has been extensively used in the design of highway bridges because it allows bridge engineers

to uncouple the transverse and longitudinal effects of the wheel loads and calculate the maximum moment values of each girder by multiplying the fraction factor to a one-dimensional single beam analysis. In the academic field, significant research work was accomplished on the load distribution behavior of different slab-on-beam bridge systems, and they provide more reliable denominator values to improve the accuracy and applicability of "*S*-over" formulas for various bridge types. The "*S*-over" formulas in the subsequent AASHO/AASHTO Standard Bridge Design Specifications have been modified and updated as these new research results became available.

Table 2.1. Moment Distribution Factors for Interior Stringers (AASHO 1931).

	One traffic lane		**Two or more traffic lanes**	
	Fraction of a wheel load to each stringer	Limiting stringer spacing (ft)	Fraction of a wheel load to each stringer	Limiting stringer spacing (ft)
Plank	*S/4.0*	4.0	*S/3.5*	5.0
4 in. thick strip or wood block on 4 in. plank subfloor	*S/4.5*	4.5	*S/3.75*	5.5
6 in. or more thick strip	*S/5.0*	5.0	*S/4.0*	6.0
Concrete	*S/6.0*	6.0	*S/4.5*	10.0

Note: 1 inch = 25.4 mm

Westergaard (1930) developed the closed form solutions of the homogeneous elastic slabs under wheel loads using theory of elasticity, which has been adopted by the AASHO Standard Bridge Design Specification (AASHO 1931) to determine the design moment values in bridge deck slabs. Jensen (1938), Newmark (1938) and Jensen et al. (1943) offered analytical solutions to different bridge deck situations based on Westergaard's pilot work.

Newmark (1938) investigated the effects of concentrated or distributed loads on rectangular slabs continuous over rigid or flexible beams. Reciprocal relations between slabs and supporting beams were studied using an elastic foundation approach. Furthermore, Newmark and Siess (1942) applied his previous analysis method to study the moment distribution in simple-span right I-beam bridges, in which the concrete deck slab was supported by steel beams. Moment distribution factors were determined for a number of bridge configurations with different span lengths, and the dominator, *D*, expression for the distribution factor of wheel loads was suggested, as shown in Equation (2.1) in US customary units. It is stated by Newmark and Siess (1942) that the following formula was also applicable to concrete girder bridge structures.

$$D = 4.4 + 0.42\frac{L}{10\sqrt{H}} \tag{2.1}$$

where L = span length, ft; $H = \frac{E_b I_b}{LN}$, stiffness ratio of the beam to deck slab; $N = \frac{E_s I_s}{1-\mu^2}$, stiffness of the deck slab element; E_b, E_s = modulus of elasticity for the beam and deck concrete; I_b, I_s = moment of inertia for the cross section of the beam and deck slab.

Although the moment distribution behavior of a slab-on-beam bridge system was determined using an analytical method, the denominator expression was not user-friendly to bridge engineers for design purposes. In order to further simplify the formula, Newmark (1943) conducted a parametric study for a number of bridge cases with different girder spacings (1.52-2.44 m) and span lengths (6.10-24.4 m) using Equation (2.1). Based on the parametric study results, the typical "*D*" value for commonly used bridge configurations was determined and the distribution factor expression was updated to "*S/5.5*".

A series of laboratory test programs was also conducted by the Engineering Experiment Station, University of Illinois, to investigate the moment distribution behavior. The accuracy of the denominator expression was verified using fifteen quarter-scale simply-supported right I-beam bridges with different span lengths (Newmark 1949). Subsequent experiments on simply-supported skew and continuous right I-beam bridges were performed to evaluate the applicability of "*S/5.5*" formula to the I-beam bridges with continuity and small skew angles (Newmark 1946; Newmark et al. 1948; Siess and Viest 1953). The simple formula, "*S/5.5*", was then quickly adopted in the third edition of the AASHTO Standard Bridge Design Specifications (AASHTO 1941). Also, shear distribution factors began to be taken into account in the AASHTO Specifications at that time. Shear LDFs were considered the same as the values for moment action in the design.

2.3.1.2 Development of LDF formulas in AASHTO Standard Specifications since 1950s

Since the 1950s, the prosperity in the transportation industry brought rapid development in bridge design and construction. Some new bridge types came into use, such as multi-beam precast concrete beam bridges, prestressed concrete spread box beam bridges, etc. Many scholars and practitioners conducted research studies on the load distribution behavior of these new bridge systems. The live load distribution formulas recommended in some research studies were adopted by the subsequent AASHTO Standard Bridge Design Specifications.

In the period from 1964 to 1969, a comprehensive research program was performed by the Department of Civil Engineering at Lehigh University to investigate the lateral load distribution behavior of prestressed concrete spread box beam bridges, for example Albert and David (1967); Chen and VanHorn (1970); Douglas and Vanhorn (1966); Guilford (1967); Guilford and VanHorn (1967); Guilford and VanHorn (1968); Lin and VanHorn (1968); Motarjemi and VanHorn (1969); and VanHorn (1969). The study work included field testing of five in-service prestressed concrete spread box beam bridges in Pennsylvania and a theoretical analysis of the structural responses. It is stated that number of traffic lanes is an important factor to determine wheel load fraction factor values and the following equation was recommended to determine bending moment values of interior beams for a spread box beam bridge system.

$$DF = \frac{2N_L}{N_B} + k\frac{S}{L} \tag{2.2}$$

where DF = fraction of the wheel load; N_L = number of design lanes; N_B = number of beams ($4 \le N_B \le 10$); S = average beam spacing, ft ($6.75 \le S \le 11.00$); L = span length, ft; $k = 0.07W - N_L\left(0.10N_L - 0.26\right) - 0.20N_B - 0.12$; W = roadway width, ft ($32 \le W \le 66$). The moment demands for the exterior beams were determined using the lever rule, but the fraction factor should not be less than $2N_L/N_B$.

Sanders and Elleby (1970) investigated the distribution of wheel loads on multi-beam precast concrete bridges. It was suggested that significant changes should be made on the denominator, "*D*", value of the simple "*S*-over" formula in the AASHTO Standard Specifications. The live load bending moments could be determined by the fraction factor shown in Equation (2.3).

$$DF = \frac{S}{D} \tag{2.3}$$

where $D = 5 + \frac{N_L}{10} + \left(3 - 2\frac{N_L}{7}\right)\left(1 - \frac{C}{3}\right)^2$ in ft when $C \le 3$; $D = 5 + \frac{N_L}{10}$ in ft when $C > 3$; C = stiffness parameter depending on bridge type, bridge geometry, and material properties in US customary units.

The AASHTO Standard Bridge Design Specifications adopted these two research achievements to broaden the applicable range of the code-specified LDF formulas (AASHTO 1965; 1977). It can be seen that more parameters were introduced in these

formulas for new bridge types, considering the effects of more bridge geometric information, such as: span length, numbers of beams, number of lanes, bridge width, etc. This trend could make the code formulas predict LDF values more accurately, but more complicated for practical design usage.

The LDF formulas described above were used with minor changes by the subsequent AASHTO Standard Bridge Design specifications until the 17th edition (AASHTO 2002), and the simple "*S*-over" LDF formulas still covered a majority of bridge types except multi-beam precast concrete bridges (AASHTO Article 3.23.4), prestressed concrete spread box beam bridges (AASHTO Article 3.28) and steel box girder bridges (AASHTO Article 10.39.2). Table 2.2 shows the "*S*-over" expressions in US customary units for the majority of bridge types in the latest version of AASHTO Standard Bridge Design Specifications (AASHTO 2002).

The "*S*-over" LDF formulas specified in the AASHTO Standard Bridge Design Specifications has been successfully utilized by bridge engineers for more than 70 years due to the straight-forward philosophy and simple format. However, some changes have taken placed in the bridge design overtime, leading to inconsistencies in the load distribution criteria, such as: reduction in multiple-lane load intensity, change in live load model and modification in lane width, etc. Thus, the applicability and reliability of the historic "*S*-over" formulas under the new design criteria needs further evaluation. In this dissertation, new design models similar with a "*S/D*" format are proposed for the purpose of providing bridge engineers a more straight-forward option to determine the moment and shear demands in the service load design phase. The applicability of the proposed

design models to slab on prestressed concrete girder bridges widely used in Texas and elsewhere will be evaluated on the basis of new design criteria.

2.3.2 Background and Development of the AASHTO LRFD LDF Formulas

2.3.2.1 General

In 1994, AASHTO adopted the LRFD Bridge Design Specifications as an alternative reference for bridge design. The first edition of the AASHTO LRFD Bridge Design Specifications (AASHTO 1994) recommended power function formulas to calculate LDF values. These new empirical LDF formulas can be applied in the specified range of bridge types and geometries. Table 2.3 lists typical bridge superstructures commonly used in Texas and elsewhere. The LDF formulas and the ranges of applicability are shown in Table 2.4.

As described in Section 2.3.1, the historic "*S*-over" method in the AASHTO Standard Bridge Design Specifications has been modified and updated as new research achievements made by many scholars were available in different time periods. Conversely, the empirical LDF formulas specified in the AASHTO LRFD Bridge Design Specifications were developed mainly based on the research work completed in National Cooperative Highway Research Program (NCHRP) research project 12-26, reported by Zokaie et al. (1991), and no changes have been made on these formulas since 1994. A thorough description about the development of the LDF formulas in NCHRP project 12-26 will be given in the next section.

Table 2.2. Distribution of Wheel Loads in Longitudinal Beams (AASHTO 2002).

	Kind of Floor		One Lane	Multiple Lanes
Timber Floor	Plank		*S/4.0*	*S/3.75*
	Nail laminated	4 in. thick or multiple layer floor over 5 in. thick	*S/4.5*	*S/4.0*
		6 in. or more thick	*S/5.0* *S* > 5 ft*	*S/4.0* *S* > 6.5 ft*
	Glued laminated panels on glued laminated stringers	4 in. thick	*S/4.5*	*S/4.0*
		6 in. or more thick	*S/6.0* *S* > 6 ft*	*S/5.0* *S* > 7.5 ft*
	On steel stringers	4 in. thick	*S/4.5*	*S/4.0*
		6 in. or more thick	*S*/5.25 *S* > 5.5 ft*	*S*/4.5 *S* > 7.5 ft*
Concrete Floor	On steel I-beam stringers and prestressed concrete girders		*S/7.0* *S* > 10 ft*	*S/5.5* *S* > 14 ft*
	On concrete T-beams		*S/6.5* *S* > 6 ft*	*S/6.0* *S* > 10 ft*
	On timber stringers		*S/6.0* *S* > 6 ft*	*S/5.0* *S* > 10 ft*
	Concrete box girders		*S/8.0* *S* > 12 ft*	*S/7.0* *S* > 16 ft*
	On steel box girders		See Article 10.39.2	
	On prestressed concrete spread box beams		See Article 3.28	
Steel Floor	Steel grid	Less than 4 in. thick	*S/4.5*	*S/4.0*
		6 in. or more thick	*S/6.0* *S* > 6 ft*	*S/5.0* *S* > 10.5 ft*
	Steel bridge corrugated plank (2 in. min. depth)		*S/5.5*	*S/4.5*

*: in this case the load on each stringer shall be the reaction of the wheel loads, assuming the flooring between the stringers to act as a simple beam.

Note: *S* is expressed in feet, 1 inch = 25.4 mm, 1 feet = 304.8 mm

Table 2.3. Common Bridge Deck Superstructures (AASHTO 2012).

Supporting Components	Type of Deck	Typical Cross-Section
Steel Beam	Cast-in-place concrete slab, precast concrete slab, steel grid, glued/spiked panels, stressed wood	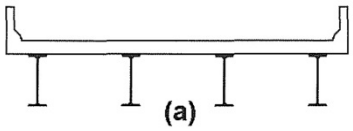
Close Steel or Precast Concrete Boxes	Cast-in-place concrete slab	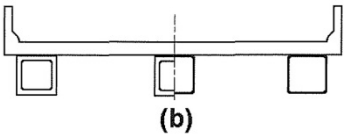
Open Steel or Precast Concrete Boxes	Cast-in-place concrete slab, precast concrete deck slab	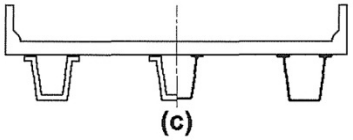
Precast Concrete Tee Section with Shear Keys and with or without Transverse Post-tensioning	Integral concrete	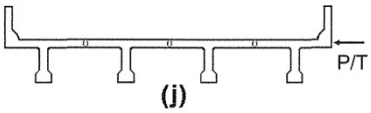
Precast Concrete I or Bulb-Tee Sections	Cast-in-place concrete, precast concrete	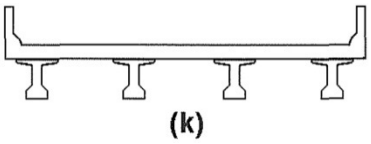

Table 2.4. Moment LDF Formulas for Interior Beams Specified in AASHTO LRFD Bridge Design Specifications (AASHTO 2012).

Type of Beams	Applicable Cross-Section from Table 4.6.2.2.1-1	Distribution Factors	Range of Applicability
Wood Deck on Wood or Steel Beams	a, l	See Table 4.6.2.2.2a-1	
Concrete Deck on Wood Beams	l	One Design Lane Loaded: $S/3700$ Two or More Design Lanes Loaded: $S/3000$	$S \le 1800$
Concrete Deck, Filled Grid, Partially Filled Grid, or Unfilled Grid Deck Composite with Reinforced Concrete Slab on Steel or Concrete Beams; Concrete T-Beams, T- and Double T-Sections	a, e, k and also i, j if sufficiently connected to act as a unit	One Design Lane Loaded: $0.06+\left(\frac{S}{4300}\right)^{0.4}\left(\frac{S}{L}\right)^{0.3}\left(\frac{K_g}{Lt_s^3}\right)^{0.1}$ Two or More Design Lanes Loaded: $0.075+\left(\frac{S}{2900}\right)^{0.6}\left(\frac{S}{L}\right)^{0.2}\left(\frac{K_g}{Lt_s^3}\right)^{0.1}$	$1100 \le S \le 4900$ $110 \le t_s \le 300$ $6000 \le L \le 73\,000$ $N_b \ge 4$ $4\times10^9 \le K_g \le 3\times10^{12}$
		use lesser of the values obtained from the equation above with $N_b = 3$ or the lever rule	$N_b = 3$
Cast-in-Place Concrete Multicell Box	d	One Design Lane Loaded: $\left(1.75+\frac{S}{1100}\right)\left(\frac{300}{L}\right)^{0.35}\left(\frac{1}{N_c}\right)^{0.45}$ Two or More Design Lanes Loaded: $\left(\frac{13}{N_c}\right)^{0.3}\left(\frac{S}{430}\right)\left(\frac{1}{L}\right)^{0.25}$	$2100 \le S \le 4000$ $18\,000 \le L \le 73\,000$ $N_c \ge 3$ If $N_c > 8$ use $N_c = 8$
Concrete Deck on Concrete Spread Box Beams	b, c	One Design Lane Loaded: $\left(\frac{S}{910}\right)^{0.35}\left(\frac{Sd}{L^2}\right)^{0.25}$ Two or More Design Lanes Loaded: $\left(\frac{S}{1900}\right)^{0.6}\left(\frac{Sd}{L^2}\right)^{0.125}$	$1800 \le S \le 5500$ $6000 \le L \le 43\,000$ $450 \le d \le 1700$ $N_b \ge 3$
		Use Lever Rule	$S > 5500$
Concrete Beams used in Multibeam Decks	f	One Design Lane Loaded: $k\left(\frac{b}{2.8L}\right)^{0.5}\left(\frac{I}{J}\right)^{0.25}$ where: $k = 2.5(N_b)^{-0.2} \ge 1.5$	$900 \le b \le 1500$ $6000 \le L \le 37\,000$ $5 \le N_b \le 20$
	g if sufficiently connected to act as a unit	Two or More Design Lanes Loaded: $k\left(\frac{b}{7600}\right)^{0.6}\left(\frac{b}{L}\right)^{0.2}\left(\frac{I}{J}\right)^{0.06}$	

2.3.2.2 LDF Formula Development in NCHRP Project 12-26

The NCHRP research project 12-26, "Distribution of Wheel Loads on Highway Bridges", was conducted by Zokaie et al. (1991) in order to investigate wheel load distribution behavior in highway bridge structures. As one significant achievement in this project, a complete and consistent set of formulas were developed to calculate LDF values for commonly used bridge types. These equations provided consistently conservative results for the bridge structures with the specified ranges of geometric characteristics.

A variety of bridge types were considered in the study, including slab bridge, slab-on-beam bridge; multi-cell bridge, multi-box beam bridge and spread box beam bridge. In order to cover most bridge types commonly used in the United States, over three hundred existing bridges were selected from a national bridge database, the National Bridge Inventory File (NBIF). These selected bridge configurations were utilized to determine the common values of the design parameters (girder spacing, span length, overhang, slab thickness, etc.). Hypothetical bridges having the average geometric properties were established for different bridge types, and they were named "average bridges."

In order to identify the importance of different parameters for the live LDF values, a sensitivity study was performed on the "average bridges". Finite element models of "average bridges" were developed to investigate load distribution behavior for both moment and shear actions under AASHTO HS20 truck loading. In the sensitivity study process, only one parameter was varied while other parameters were kept unchanged, and the LDF values for each parameter were obtained. Figure 2.4 presents the effect of different parameters on the live load distribution factor (Zokaie 2000). It is shown that

girder spacing plays the most significant role on the LDF determination, but span length, slab thickness and girder stiffness also have some effect. These four geometric properties would be considered in the further parametric study to develop design formulas.

The bridge database described above was utilized to determine representative values of those four geometric parameters. In summary, bridge configurations in the parametric study covered the following geometric range: span length (8.9-45.7 m), girder spacing (0.46-3.99 m), slab thickness (112-305 mm) and girder stiffness (0.024-0.56 m^4). Refined analysis was conducted on these bridge configurations to determine moment and shear LDF values, which provided a basis to develop LDF formulas.

Several assumptions were made by Zokaie (2000) in order to systematically study the live LDFs. The effect of each parameter was considered to be independent and a set of equations with consistent power-function format, shown in Equation (2.4), were assumed in the development of new LDF formulas. The power, b_i, represented the effect of each parameter and could be determined based on the variation of LDF values when only that parameter was varied. The coefficient, a, would be determined after all powers of each parameter were obtained.

$$g = a(L)^{b_1}(S)^{b_2}(d)^{b_3}(\cdots) \tag{2.4}$$

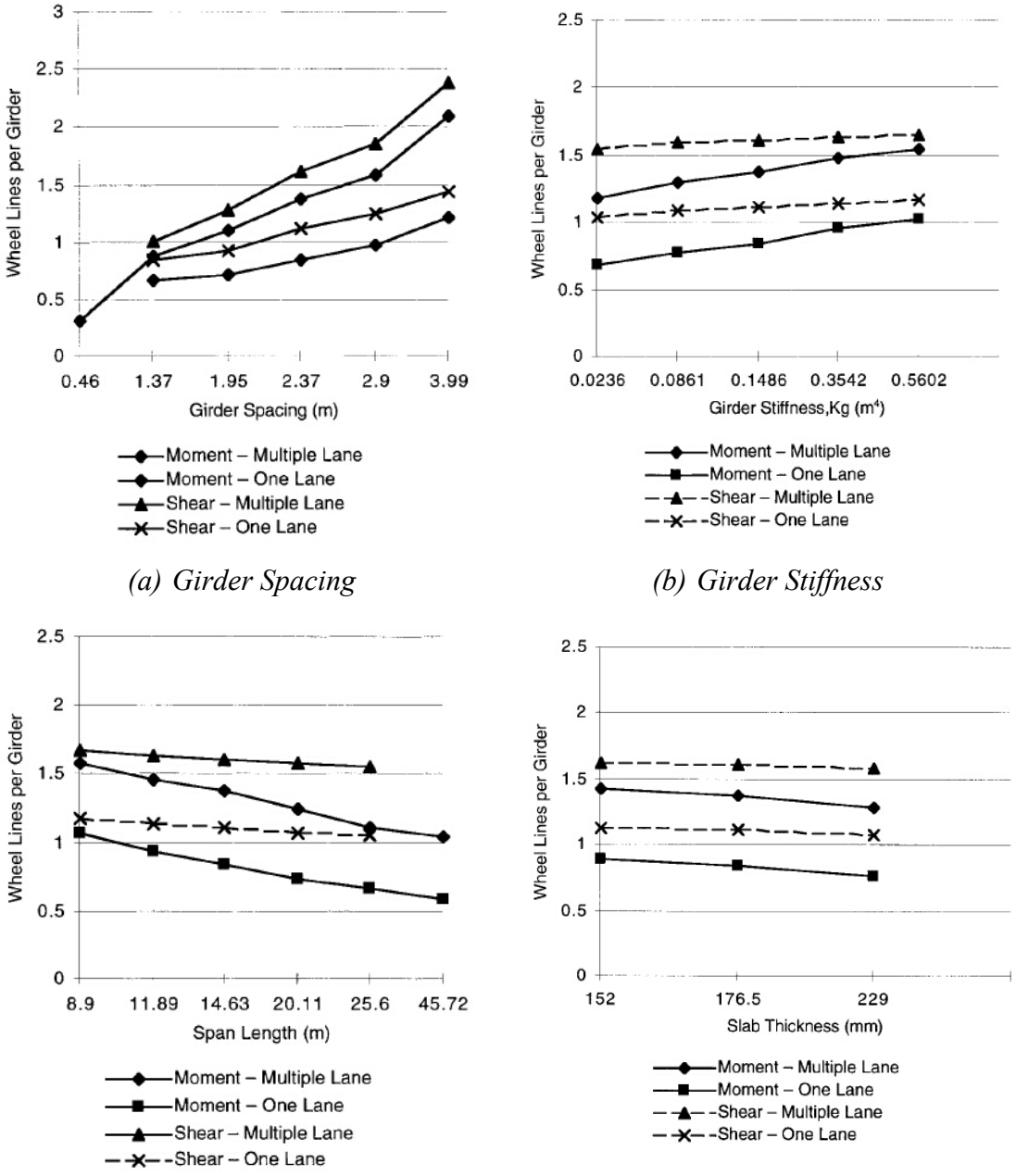

Figure 2.4. Sensitivity of Wheel Load Distribution Factors to Different Parameters (Zokaie 2000).

New empirical formulas were then developed to calculate moment LDF values necessary for girder design. Equation (2.5) shows the moment LDF formulas when multiple design lanes are loaded (Zokaie 2000).

$$LDF = 0.15 + \left(\frac{S}{914}\right)^{0.6}\left(\frac{S}{L}\right)^{0.2}\left(\frac{I + Ae^2}{Lt_s^3}\right)^{0.1} \tag{2.5}$$

where L = span length, mm.; I = moment of inertia of the transformed girder section, mm^4; A = area of the transformed girder section, mm^2; e = distance between the girder centroid and deck slab centroid, mm; t_s = thickness of deck slab, mm. The proposed equations were modified slightly and incorporated in the first edition of the AASHTO LRFD Bridge Design Specifications (AASHTO 1994).

2.3.2.3 Extension of the Research Work in NCHRP Project 12-26

In order to promote the usage of the new LDF formulas specified in the AASHTO LRFD Bridge Design Specifications, Zokaie (2000) discussed the accuracy of the historic "*S*-over" method and LRFD formulas by comparisons with FEM analysis results. Figure 2.5 shows the histogram of two approaches. The ratio of LDF obtained from the formula to the FEM value, *g*-ratio, was used to compare the accuracy of the historic "*S*-over" method and proposed equations. It is concluded that the standard deviation and accuracy of the proposed approach is improved as compared to the historic "*S*-over" method.

The continuity and skew effects were also evaluated using FEM analysis to extend the applicable range of new LDF formulas. It was found that the LDF values for

continuous bridge cases are slightly higher than those in simply-supported bridges. For the positive moments, the difference between them is less than 5%; but for negative moments, the discrepancies could reach up to 10%. The load path was changed slightly by the skewed support. Because the load is transferred to the end supports in the shortest span, the moment values became smaller and the shear forces at the obtuse end are larger as compared to a non-skew bridge with the same length.

Zokaie (2000) stated that the new LDF formulas were complicated because they consider the effects of more parameters. Especially for the term, K_g, existing in some formulas, an iterative procedure is needed because the member size is unknown initially. All these factors made new formulas more complex for the designers as compared to the historic "*S*-over" method. It may not be obvious whether the increased complexity could provide corresponding added accuracy for the engineers. Many research studies evaluating the "*S*-over" method and LRFD formulas are described in the following sections.

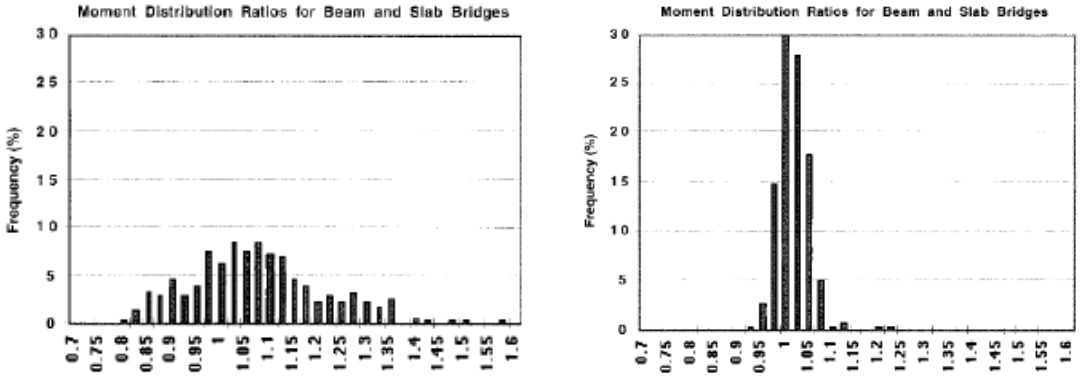

(a) "S-over" Method *(b) Proposed Formulas*

Figure 2.5. Comparison of Simple Formulas with FEM Analysis (Zokaie 2000).

2.3.3 Evaluation of AASHTO "*S*-over" Method and LRFD LDF Formulas

2.3.3.1 Research Studies Evaluating AASHTO "S-over" Method (1931-1991)

Since the AASHTO Standard Bridge Design Specifications introduced the "*S*-over" method for the bridge design in 1931, many research studies have been accomplished to evaluate the accuracy of this simple formula. Considering the limitation of the computational capacities in the early period, experimental tests and theoretical analysis were mainly utilized by the scholars.

Hindman and Vandegrift (1945) performed a field test on a steel I-beam bridge in Ohio. The tested bridge was continuous with two equal spans of 26.8 m. The bridge structure was loaded by a hydraulic jack, and the LDF value of each girder was determined based on measured deflections. The maximum measured moment distribution factor was 1.05, smaller than the code-specified value (1.26). Other field tests on steel I-beam were conducted by Holcomb (1956) in Iowa, and White and Purnell (1957) in Texas. Strain values were measured in both two bridges to determine the experimental distribution factors. All these test results showed that "*S*-over" formulas in the AASHTO Standard Bridge Design Specifications proved to be conservative and reliable for bridge design.

Fritz laboratory at Lehigh University performed field studies on five in-service spread box beam bridges in Pennsylvania (VanHorn 1969). The experimental distribution factors were determined based on the strain gage measurements, and then compared with the design values from the AASHTO Standard Bridge Design Specifications. Figure 2.6 shows the comparisons between experimentally developed distribution factors and design values for tested spread box beam bridges. Note that design LDFs of interior beams were

obtained from "*S*-over" formulas while the lever rule was utilized to determine LDFs for exterior beams. It is seen that the code-specified LDF values for all interior girders were higher than the experimental results in all tested bridges. Conversely, the design LDFs for all exterior girders were somewhat lower than the experimental values. VanHorn (1969) stated that the curb and parapet composited with the exterior girders made great contributions to the flexural stiffness of the bridge superstructure, resulting in higher LDF values for exterior girders than expected. However, when interior and exterior girders were treated equally and the most critical load effects were considered for design purpose, the "*S*-over" method still proved to be conservative and reliable as shown in Figure 2.6.

As a parallel research project with the earlier investigation of spread box beam bridge superstructures, two field studies on the lateral load distribution behavior of prestressed concrete I-beam bridges were conducted by Fritz laboratory at Lehigh University (Chen and VanHorn 1971; VanHorn and Chen 1971). The strain values were measured to determine the experimental distribution factors. Figure 2.7 shows the comparisons between experimental distribution factors and design values for two tested prestressed concrete I-beam bridges. Similar experimental results with spread box beam bridge investigation were observed in these two field tests: it was found that the code-specified LDF values were slightly greater than the test results for interior beams. Conversely, the design LDFs of exterior beams from the lever rule were less than the observed values, which could also be explained by the existence of the curbs and parapet. From Figure 2.7, it is also evident that the "*S*-over" method provide conservative values for design as compared to the most adverse load effects across the bridge cross section.

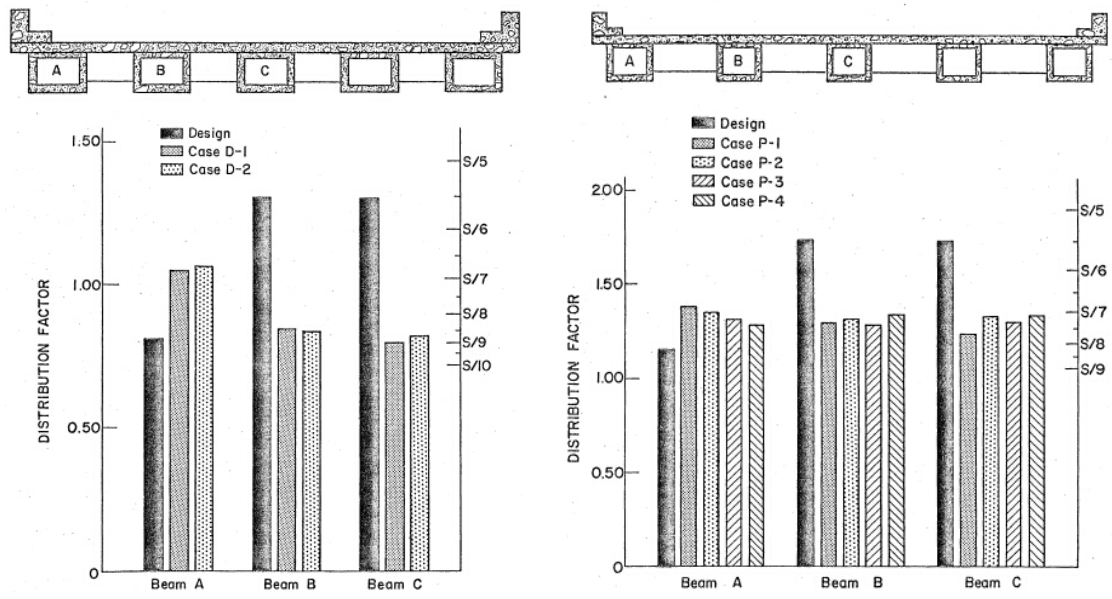

(a) Drehersville Bridge

(b) Philadelphia Bridge

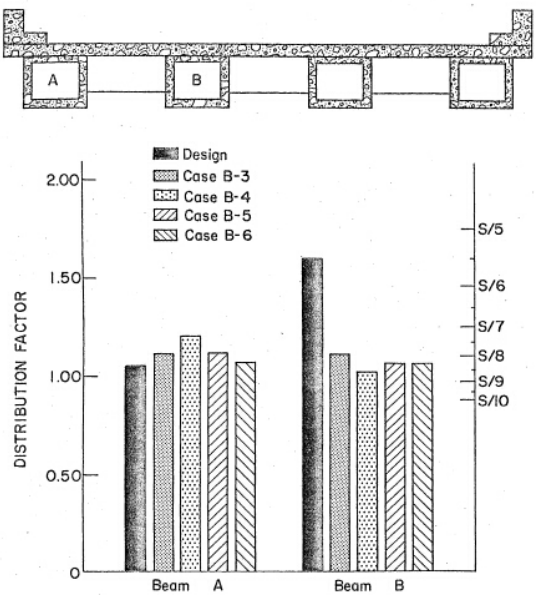

(c) Berwick Bridge

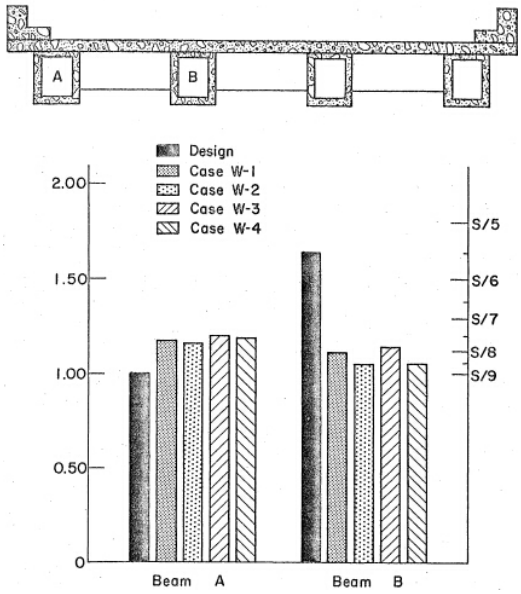

(d) White Haven Bridge

Figure 2.6. Comparisons between Experimentally Developed Distribution Factors and Design Values for Spread Box Beam Bridges (VanHorn 1969).

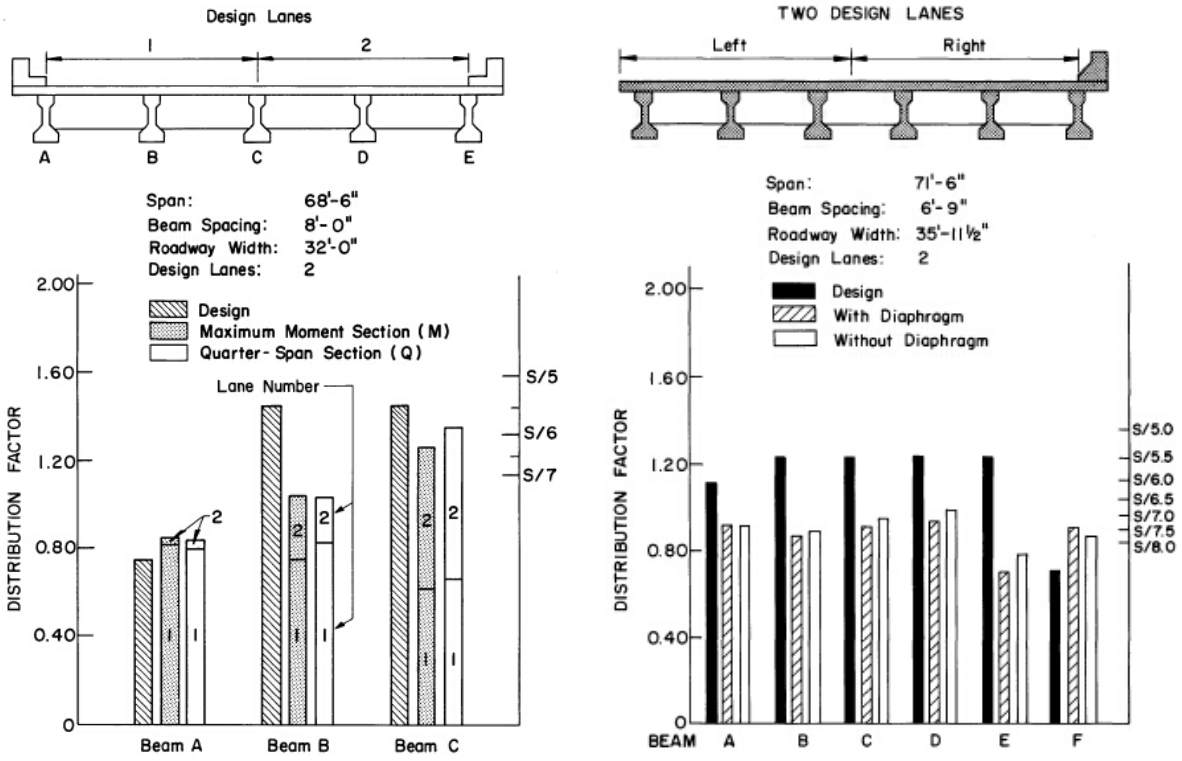

(a) Bartonsville Bridge *(b) Lehighton Bridge*

Note: 1 inch = 25.4 mm, 1 feet = 304.8 mm

Figure 2.7. Comparisons between Experimental Distribution Factors and Design Values for I-Beam Bridges (Chen and VanHorn 1971; VanHorn and Chen 1971).

Since 1980s, computer program using grillage and FEM techniques became popular in bridge engineering due to the rapid development of the computational capacity. Many scholars and practitioners began to utilize this power tool to analyze the bridge structures and investigate the load distribution behavior. Field experimental tests still played an important role in the research studies because it reflects the bridge structural behavior in the actual situation and the test results could be used for the validation of the computational models.

Hays Jr et al. (1986) developed a FEM program, SALOD, to evaluate the flexure load distribution behavior of simple span bridges, including steel girder, prestressed concrete girder, T-beam and flat-slab bridge. The span length was found to have a considerable influence on flexure LDF values, but cause few effects for shear actions. By comparisons between code-specified values and computational results, it is shown that AASHTO Standard "*S*-over" formulas provided slightly unconservative LDF values for short-span bridges, but overconservative results for longer spans.

Marx et al. (1986) conducted a parametric study by analyzing over 100 simply supported steel I-beam and prestressed concrete girder bridges with the aid of FEM program. The bridge configurations ranged the girder spacing from 1.83 to 2.74 m and the span length from 12.2 to 24.4 m. The parametric study results showed that the AASHTO "*S/5.5*" formula provided the LDF value for interior beams between 12% unconservative and 32% on the safe side. For the exterior girders of steel I-beam bridge structure, the wheel load distribution factors based on the AASHTO formula were overconservative for

design. Besides, Marx et al. (1986) pointed out that the LDF values decreased as the span length increased if the girder spacing was kept unchanged.

On the basis of the literature described above, a well-established finding that girder spacing plays the most significant role in determining LDF value was confirmed. The historic "*S*-over" method represents this fundamental concept with the simple format, thus it has been extensively utilized by bridge engineers since its inception. In particular, when the most adverse load effects amongst different girders were considered for the design purposes, the "*S*-over" method generally provided conservative and reliable LDF values.

The major weakness of the "*S*-over" formula stated by many researchers was neglecting the effects of other design parameters, like span length, skew angle, girder stiffness and secondary elements. In order to predict more accurate LDF values, some scholars recommended developing new LDF formulas with considering parameters other than girder spacing. However, it may not be obvious whether the increased complexity could provide corresponding added accuracy for the engineers. It is worth mentioning that for the bridge cases with common range of design parameters, "*S*-over" formulas still provided an easy and reliable option for the preliminary design of bridge structures.

2.3.3.2 Research Studies Evaluating AASHTO –specified LDF Formulas (1991-2014)

LDF determination for bridge structures has received significant attention in recent years as the historic "*S*-over" method in the AASHTO Standard Bridge Design Specifications was transited to the power function empirical approach proposed by Zokaie et al. (1991) and adopted in the AASHTO LRFD Bridge Design Specifications. Many scholars and

practitioners have conducted significant research studies on this topic and various methods were utilized to evaluate the applicability and reliability of both AASHTO "*S*-over" method and LRFD empirical approach. The investigation strategies mainly focus on field experimental tests and computational analysis.

In order to support the development of the new LRFD empirical formulas, Nowak (1993) conducted FEM analysis to investigate moment distribution factors of bridge superstructures under two lane loading. The range of two key parameters, girder spacing and span length, performed in FEM models were 1.2 to 3.6 m. and 9 to 60 m, respectively. All girder distribution factors determined from FEM analysis were compared with the values calculated based on the AASHTO Standard "*S*-over" method and formulas recommended by Zokaie et al. (1991). The comparative results indicated that the AASHTO Standard "*S*-over" formulas tended to provide unconservative LDF values for bridges with smaller girder spacing and span length, but yielded overconservative values when girder spacing and span length are relatively large. Conversely, the computational results were found to show a good agreement with the values obtained from Zokaie's formulas since the effects of span length, girder stiffness and deck thickness were also considered.

Although it is stated that AASHTO LRFD empirical LDF formulas could provide more accurate results as compared with AASHTO Standard "*S*-over" method, their complex format were criticized by researchers and practitioners. In particular, the longitudinal stiffness parameter, K_g, included in the formulas were unknown in the early design stage, thus the iteration procedure is often needed (Huo et al. 2004; Zokaie 2000).

Even if new LRFD formulas could be used to calculate the LDF values relative easily with the aid of design program or spreadsheet, they cannot provide a direct concept of each parameter's influence. Conversely, the historic "*S*-over" method represented a better form and provided an obvious concept to designers that the LDF values decrease when the girder spacing is becoming smaller (Suksawang et al. 2013). In addition, limited ranges of applicability were considered as another weakness of the LRFD empirical LDF formulas. When the bridge configuration is beyond the applicable ranges, more refined analysis is mandated by the AASHTO LRFD Bridge Design Specifications.

Shahawy and Huang (2001) modeled a total of 645 prestressed concrete bridges with one or multiple lanes using three-dimensional FEM techniques for the purpose of evaluating the accuracy of the AASHTO LRFD moment distribution factor formulas. It was concluded that the AASHTO LRFD code-specified LDF values for multiple design lanes loaded cases were satisfactory when the deck overhang and girder spacing were smaller than 0.92 and 2.44 m, respectively. However, if the limits were exceeded, LRFD empirical LDF formulas would result in up to 30% errors.

Kocsis (2004) developed a new computer program, SECAN, based on the semi-continuum method (only continuum in the longitudinal direction) to calculate the LDFs of I-girder bridges. The LDF values of over 50 bridge configurations, covering various girder spacing (1.75-3.05 m) with different girder numbers (3, 4 and 5), and with span lengths varying from 3 to 100 m, were determined by SECAN program and compared with AASHTO "*S*-over" formula values. It is shown that the AASHTO Standard "*S*-over" formulas provide accurate live load distribution factors under AASHTO truck loading.

Kocsis stated that the computer program could be used for LDF calculation, but it is easier to use the AASHTO Standard "*S*-over" formulas because only a calculator is needed.

Although new LRFD empirical formulas considered more geometric properties than the historic "*S*-over" method did, some researchers argued that some other design parameters were still neglected. They made great effects to investigate the influence of skew angle, diaphragm, continuity and parapet on the load distribution behavior with intentions of testing the applicable limits of current AASHTO LRFD LDF formulas.

Chen and Aswad (1996) conducted a parametric study using FEM analysis to compute LDF values of prestressed concrete I-girder and spread box beam bridges with wide girder spacing and long span length. The parametric study results indicated that the refined analysis reduced the moment values at midspan by 18-23% for interior I-girders, and 4-12% for exterior girders as compared to the values calculated from the AASHTO LRFD empirical formulas. Similarly, for spread box beam, FEM solutions were 6-12% lower than the code-specified values. In particular, FEM analysis may reduce the moment values as much as 30% for exterior girders when the midspan diaphragms existed.

Barr et al. (2001) utilized the FEM technique to analyze 24 bridges with various geometric configurations to investigate the effects of lifts, diaphragms, skew angle, continuity and load type on the live load distribution behavior. FEM solutions revealed that the existence of lifts, skew angles and end diaphragms reduced the flexure LDF values significantly. As for load type, flexure LDF values under truck loading were consistently around 10% higher than those obtained under lane loading. By adding continuity, flexure LDF values increased slightly in some cases and reduced in others. By comparing the

FEM solutions with the code-specified values, it is evident that AASHTO LRFD empirical formulas provided conservative flexure LDF values for all 24 bridge cases.

Cai et al. (2002) performed field tests on six bridges to evaluate the influence of intermediate diaphragm and skew angles. With comparisons between experimental results and code-specified values, it was shown that both AASHTO Standard "*S*-over" and LRFD empirical approach generated overconservative (up to 40%) LDF values for design. The maximum girder strains would be reduced significantly by considering the stiffness of intermediate diaphragms in FEM analysis. The LDF values rose with the increase of skew angles for the bridge cases with intermediate diaphragms.

Sotelino et al. (2004) conducted a comprehensive research project to develop simplified equations with no need of iterative procedure for steel and prestressed concrete girder bridges (Chung et al. 2005; Phuvoravan et al. 2004). As part of the research, the effects of several bridge features not considered in the AASHTO LRFD formulas, such as parapets, cross bracing diaphragms and deck cracking were also investigated. It was found that the LDF values determined by the AASHTO LRFD formulas would be reduced by up to 40 percent when the secondary elements including parapets and cross bracing diaphragms existed. As for the cracking effects, it was shown that the longitudinal cracking increase the LDF values by up to 17 percent while the transverse cracking caused no effects.

From the literature described above, it is shown that many other design parameters also have influences on the load distribution behavior of bridge superstructures. However, if all these effects were taken into account to pursue a higher degree of accuracy, the

increased complexity would make the LDF formulas not user-friendly for design purpose, especially for the preliminary design stage.

Significant research studies on the moment distribution factor have been conducted by scholars and practitioners (Barr et al. 2001; Chen and Aswad 1996; Eom and Nowak 2001; Huo et al. 2004), but very few work have been accomplished on the shear distribution factor, although shear force may control the bridge design in some situations (Al-Mahaidi et al. 2000).

Barr and Amin (2006) analyzed over 200 simply supported bridge cases to investigate the effects of different bridge parameters, including girder spacing, span length and skew angle, on the shear LDFs of slab-on-girder bridges. It was found that the girder spacing had the most significant influence on shear LDF values. The skew angles increased the shear distribution factors of exterior girders, but decreased the values of interior girders. The LDF values determined from FEM analysis were also compared with those calculated based on AASHTO LRFD formulas, it was found that shear LDF values determined from the AASHTO empirical formulas was unconservative for exterior girders in some bridge cases. Also, LRFD-specified shear LDF values were overconservative for interior girder of bridges with high skew angles.

Nowadays, some new bridge systems were developed and it is meaningful to check whether the current code LDF formulas were still applicable. Harris et al. (2010) conducted a parametric study using FEM modeling strategy on the lateral load distribution behavior of a new bridge deck system consisting of a rigid polyurethane core and two steel plates bonded at both sides, known as the sandwich plate system (SPS). The FEM model

was validated by a field experimental test and then 75 bridge models were developed to investigate the effect of the deck thickness on the live load distribution behavior. It was found that a thinner deck thickness in SPS bridge yields 20% larger moment LDF values as compared to the traditional reinforced concrete deck bridge. Additional comparisons were also made between the LDF values calculated from AASHTO LRFD empirical LDF formulas and FEM analysis. It was shown that LRFD formulas provide conservative values for all bridge cases and it is reliable to use current AASHTO LRFD methods to predict lateral load distribution factor of SPS bridge system.

On the basis of the literature described above, some findings about AASHTO Standard "*S*-over" method and LRFD empirical LDF formulas were summarized as follows:

1. In general, both AASHTO Standard "*S*-over" method and LRFD empirical approach provide conservative LDF values for the bridge design. LRFD formulas are claimed to predict more accurate distribution factors than "*S*-over" method since more design parameters are considered.
2. AASHTO LRFD empirical formulas are complex for bridge engineers and cannot provide a direct concept of each parameter's influence as compared to AASHTO Standard "*S*-over" method. Besides, iteration procedure is needed in the early design stage for the reason that some unknown parameters are included in the LRFD empirical formulas.

3. AASHTO LRFD empirical approach specifies the range of applicability. When the bridges are beyond the applicable range, more refined analysis is mandated in the design process because LRFD empirical formulas may result in significant errors.
4. Some other parameters (overhang, skew, continuity, diaphragm, etc.) not included in AASHTO LRFD formula have influences on the load distribution behavior of bridge superstructures. If these effects were incorporated to pursue a higher degree of accuracy, the LDF formulas would become too complicated for design usage, especially for the service load design phase.

2.3.4 Other LDF Methods

2.3.4.1 Code Specifications Other than AASHTO

The live LDF concept is also used in the Canadian bridge design codes. The Ontario Highway Bridge Code (1991) adopted "*S*-over" formatted LDF formula similar as the AASHTO Standard Bridge Design Specifications. The denominator value was determined based on the research work done by Bakht et al. (1979) and Bakht and Moses (1988). In the Canadian Highway Bridge Design Code (2006), distribution factors for moment and shear actions are based on the design traffic lanes divided by girder numbers. Modification factors developed from orthotropic plate theory are then applied to the moment and shear distribution expressions.

The bridge design codes in Japan and European countries generally do not use the simplified LDF method to determine lateral load distribution characteristics of bridge

superstructures. Rather, refined analysis methods are typically utilized in the bridge design process (JRA 1996; Nutt 1988).

2.3.4.2 Simplified Methods Proposed by Other Scholars

In the past decades, many researchers made great efforts to develop new LDF formulas or propose modification factors for existing code formulas in order to further increase the accuracy of the LDF determination. Those proposed formulas were claimed by developers to be conservative and reliable for design usage even though some of them were more complicated than LRFD empirical equations.

Some new formulas were developed based on AASHTO Standard "*S*-over" method, only changing the expressions of the denominator "*D*". The "*S*-over" method is still very popular because its simple format represents the fundamental concept of load distribution factor.

Huo et al. (2004) introduced modified Henry's method to calculate moment LDF values. In this simplified method, only basic bridge information (bridge width and beam numbers) was required and both interior and exterior beams were treated equally. The calculation process of Henry's method is listed in Equations (2.6) and (2.7).

$$n_l = \frac{W}{3050} \tag{2.6}$$

$$g_M = k_1 k_2 \frac{n_l}{n_b} \tag{2.7}$$

where W = roadway width, mm; n_l = fractional number of traffic lanes; n_b = beam numbers; k_1 = multiple-presence factor, it is obtained from a linear interpolation for the traffic lane numbers, n_l; for two-lane bridges, $k_1 = 1.0$; for three-lane bridges, $k_1 = 0.9$; for four-or-more lane bridges, $k_1 = 0.75$; k_2 = modification factor on type of deck superstructures; for cast-in-place (CIP) concrete T-beams, $k_2 = 0.95$; for precast concrete I- or bulb-tee sections, $k_2 = 1.1$; for CIP concrete multi-cell box beams, $k_2 = 1.1$; for other types, $k_2 = 1.0$.

By comparing the LDF values determined from FEM analysis, AASHTO LRFD formulas and modified Henry's method for 24 bridges of six different superstructure types, it was found that the LDF values from the proposed method were slight higher than FEM solutions, but stayed in close range with AASHTO LRFD values. It was concluded that reasonable and reliable moment LDF values can be determined from the modified Henry's method. However, this modified Henry's method didn't provide calculation options for shear LDF, which is also critical in bridge design process.

Suksawang et al. (2013) conducted a FEM parametric study on 30 bridge configurations with different girder spacing (1.22-4.88 m.) and span length (6.1-61.0 m) in order to develop new "*S*-over" formatted shear LDF formulas for steel and prestressed concrete I-girder bridges. On the basis of the findings from parametric study, it was stated that the girder spacing had the most critical influence on the shear LDF and no significant variations in shear LDF values were observed with respect to span length and girder stiffness. The author argued that the proposed "*S*-over" shear distribution formulas

represented a better approach than AASHTO LRFD equation for the bridge designer for the reason that they took a more rational form than the power function. The proposed shear LDF formula is shown in Equation (2.8). Although the lowest sum of square errors is achieved, many LDF values specified by the proposed formulas are unconservative as compared with FEM solutions.

$$(LDF)_V = \frac{S}{D_V} \tag{2.8}$$

where $S =$ girder spacing, mm; for one lane loaded case, $D_V = 2286 + \frac{S}{579}$; for two or more lanes loaded case, $D_V = 2286 + \frac{S}{914}$.

Some researchers proposed new empirical LDF formulas using other formats, including power function similar with AASHTO LRFD empirical LDF equations. Tarhini and Frederick (1992) developed a new load distribution formula (in US customary unit) based on FEM analysis results, as shown in Equation (2.9). This quadratic equation accounts the effects of girder spacing and span length, whose importance was demonstrated by a parametric study. It was stated that the new formula predicted realistic load distribution behavior and could be applied in the design of both simple span and continuous bridges.

$$LDF = 0.00013L^2 - 0.021L + 1.25\sqrt{S} - \frac{(S+7)}{10} \tag{2.9}$$

Phuvoravan et al. (2004) developed a new simplified formula based on the AASHTO LRFD method to determine the moment LDF values of concrete slab-on-steel

girder bridges. Two most influential parameters, girder spacing and span length, were kept in the new proposed formula based on the sensitivity study. Another two parameters, the deck slab thickness, t_s, and the longitudinal stiffness parameter, K_g, were implicitly embedded in the equation, thus the iteration procedure needed for AASHTO LRFD method could be eliminated. Equations (2.10) and (2.11) provide expressions for basic LDF formula and skew correction factor. $(k)_\theta$ is a coefficient representing the effects of skew angles. Units of S and L are mm in the equations.

$$(LDF)_M = 0.15 + 0.042\frac{S^{0.8}}{L^{0.3}}e^{\left(\frac{L}{180,000}\right)} \tag{2.10}$$

$$(k)_\theta = 1 - 2.5 \cdot \frac{S^{0.5}}{L^{0.75}} \cdot (\tan\theta)^{1.5} \cdot e^{\left(\frac{L}{72,000}\right)} \tag{2.11}$$

Forty-three "Indiana representative steel bridges" covering a specific range of bridge parameters were selected and analyzed using FEM models to determine "exact" LDF values. By comparisons with the values determined from AASHTO Standard "*S*-over" method, AASHTO LRFD formula and FEM analysis, it was found that the new simplified formula always provided conservative LDF values. The applicable range of the new proposed LDF formula is listed as follows: girder spacing (1.22-3.05 m), span length (13.4-37.2 m), slab thickness (200 mm) and skew angle (0-45º).

The applicability of the new simplified LDF formula (Phuvoravan et al. 2004) to the prestressed concrete girder bridges were investigated by Chung et al. (2005). A total of 17 "Indiana representative prestressed concrete girder bridges" were selected and

analyzed with FEM analysis. By comparing with the LDF values calculated using AASHTO LRFD formulas and the "exact" FEM solutions, it is concluded that the new simplified formula always provide conservative results and is applicable for prestressed concrete girder bridges. However, this research only provided the method for moment distribution factor calculation and the shear aspect were not touched at all.

Tanbsh and Tabatabai (2001) investigated the effects of oversized trucks on the live load distribution in bridge structures. The LDF values specified by the AASHTO LRFD empirical formulas are determined based on specific truck geometries and load configurations. However, there are some cases where trucks with larger gauge widths, axle spacing, or loads are used. Through a parametric study involving FEM analysis, the author found that the LDFs for oversized loads were less than those found using the AASHTO LRFD equations (AASHTO 1994). The main overload parameter, truck gauge width, was shown to have a greater influence on the shear distribution than the flexural distribution between girders. To make this process easier Tanbsh and Tabatabai (2001) proposed modification factors for the LRFD formulas to account for these overload situations and thus make it possible to design for these events. The expressions for the moment and shear modification factors are shown in Equations (2.12) and (2.13).

$$\alpha_M = \left[\frac{2.95 + 3.33\sqrt{S}}{6.14 + S}\right]^{\left[(G-1.83)/1.22\right]} \tag{2.12}$$

$$\alpha_V = \left[0.13S^2 - 0.66S + 1.54\right]^{\left[(G-1.83)/1.22\right]} \tag{2.13}$$

where S = girder spacing, m; G = truck gauge width, m.

Table 2.5. Representative LDF formulas.

	Reference	Expression	Restriction	Unit System
"S/D" formula	Newmark and Siess (1942)	$D = 4.4 + 0.42\frac{L}{10\sqrt{H}}$	Load is more than 2 ft from an edge beam	US
		$D = 4.4 + 0.21\frac{L}{10\sqrt{H}}$	Load is close to an edge beam and $S \le 6$ ft	US
	Sanders and Elleby (1970)	$D = 5 + \frac{N_L}{10} + \left(3 - \frac{2N_L}{7}\right)\left(1 - \frac{C}{3}\right)^2$	$C < 3$	US
		$D = 5 + \frac{N_L}{10}$	$C > 3$	US
	Suksawang et al. (2013)	$D_V = 2286 + \frac{S}{579}$	One lane	SI
		$D_V = 2286 + \frac{S}{914}$	Multiple lanes	SI
Other Format Formulas	Tarhini and Frederick (1992)	$0.00013L^2 - 0.021L + 1.25\sqrt{S} - \frac{(S+7)}{10}$		US
	Tanbsh and Tabatabai (2001)	$\alpha_M = \left[\frac{2.95 + 3.33\sqrt{S}}{6.14 + S}\right]^{[(G-1.83)/1.22]}$		SI
		$\alpha_V = \left[0.13S^2 - 0.66S + 1.54\right]^{[(G-1.83)/1.22]}$		SI
	Phuvoravan et al. (2004)	$0.15 + 0.042\frac{S^{0.8}}{L^{0.3}}e^{\left(\frac{L}{180,000}\right)}$		SI
	Huo et al. (2004)	$g_M = k_1 k_2 \frac{n_l}{n_b}$		SI

For completeness, some representative LDF formulas proposed by researchers and practitioners are listed in Table 2.5.

2.3.5 Summary

A thorough literature review of the development of the AASHTO Standard "*S*-over" method and AASHTO LRFD empirical approach is described in this section. The historic "*S*-over" method has been extensively used by bridge engineers since it is adopted by the AASHTO Standard Bridge Design Specifications in 1930's. It accounts for the effects of girder spacing, which was confirmed to play the most significant role in the load distribution behavior. However, the "*S*-over" method was considered to generate conservative LDF values, particularly for the bridges with long span. Thus, new power function LDF equations based on FEM analysis were developed as part of NCHRP project 12-26 (Zokaie et al. 1991). The new empirical formulas took other parameters into account, such as span length, deck slab thickness and girder stiffness. It was quickly adopted by the AASHTO LRFD Bridge Design Specifications (AASHTO 1994) and later evaluated by many other researchers using field tests and numerical analysis strategies (Barr et al. 2001; Barr et al. 2006; Chen and Aswad 1996; Eamon and Nowak 2002; Schwarz and Laman 2001). It was found that the LRFD empirical approach provided more accurate LDF vales as compared to the "*S*-over" method. However, the LRFD power function formulas were criticized by practitioners for the complex format and limited ranges of applicability. Especially for the stiffness term K_g, an iterative procedure is needed since the member size is not known in the early design stage. It may not be obvious whether the increased complexity could provide corresponding added accuracy for the

engineers. Although computer software becomes available to determine the LDFs more easily, the LRFD formulas cannot provide a direct concept of each parameter's influence to designers. Thus it is necessary to develop more fundamental approaches for bridge engineers to determine reliable design loads in the service load stage.

Conservatism, simplicity and accuracy are considered as three major criteria to evaluate a new formula for design purpose. There may be a tradeoff between the latter two characteristics under the actual circumstances. For the preliminary design, only basic bridge information (bridge width and beam numbers) is available, simpler-formatted LDF formulas are more easily accepted by practitioners. Moreover, the focus of prestressed concrete girder bridge structure designs remains on service loads and the associated allowable material tensile and compressive stress limits. While wide variation of the material strength, especially for concrete, exists for on-site applications, there seems little advantage in seeking a particularly accurate formula to determine the design moment and shear demands for individual girders when the material strength is highly variable.

New design models using similar format with "*S*-over" method are proposed in this dissertation to determine the critical moment and shear LDF values for service load design. Their applicability to a variety of prestressed concrete girder bridges commonly used in Texas and elsewhere is evaluated with FEM analysis.

2.4 EXPERIMENTAL STUDIES ON BRIDGE SUPERSTRUCTURES

Experimental test is a powerful tool for researchers to investigate the structural behavior of bridges in the actual situation. Various types of instruments, like strain gage, string potentiometer, load cell, accelerometer, etc., are utilized by researchers to measure the bridge responses in static and dynamic tests. The observed results are not only necessary to get a knowledge of the structural performance, but also useful to validate the computational models. Several representative experimental studies on the structural performance in general and live load distribution behavior in particular of bridge superstructures are introduced in this section. The bridge types include prestressed concrete spread box beam bridge, steel girder bridge, solid slab bridge and prestressed concrete I-girder bridge.

Prestressed concrete spread box beam bridge was thoroughly investigated by Fritz laboratory at Lehigh University in the 1960's. Five in-services bridges in Pennsylvania were tested under static and dynamic vehicle loads to determine the load distribution behavior (VanHorn 1969). Figure 2.8 shows the elevation and cross section of Dreherville Bridge, which is the first test bridge in this research project. Strain gages and deflectometers were installed in the bridge superstructure to record the responses of different girders in static and dynamic tests. The vehicle was parked at critical locations in the static test to generate the most adverse moment values. In the dynamic test, timer and lateral position indicators were utilized to determine the vehicle speed and location. The dynamic loads were applied by driving one or two trucks at various speeds (16-55 km/h) along different lanes. Based on the data recorded, moment distribution factors and

impact factors were determined. From the test results, it was concluded that: 1) the magnitudes of moment distribution factors are relatively insensitive to the vehicle speed; 2) the experimental moment distribution factors were considerably less than code specified values for interior girders; 3) due to the extra stiffness contributions from the curb and parapet, the observed moment LDFs for exterior girders were larger than code specified values; 4) compared with the bridge response under crawling speed (3.2 km/h) trucks, the amplification factor induced by moving loads is smaller than the code specified value. This bridge test served as a pilot study, from which reliable instrumentation, load pattern and test procedure were determined and then applied to other bridge tests. Schaffer and VanHorn (1967) and Lin and VanHorn (1968) studied the effects of skew and diaphragms on the load distribution behavior of spread box beam bridges by conducting similar field tests on Brookville Bridge and Philadelphia Bridge, respectively.

Kim and Nowak (1997) investigated the load distribution behavior of steel girder bridges by conducting experimental tests on two simply-supported bridges in Michigan. For both bridges, the strain transducers were attached on the bottom flanges of steel I-girders at midspan location to measure the bridge responses under normal traffic loads without lane closure for two consecutive days. The girder LDF values and impact factors were determined by processing the recorded strain data. It was found that the effects of closely spaced diaphragms were negligible. Measured LDF values of the bridge with more sparsely spaced girders were more uniformly distributed than the other bridge. In terms of impact factors, the test data indicated that the increasing strain values reduced the impact factor and the measured values for large strains were smaller than the code specified value.

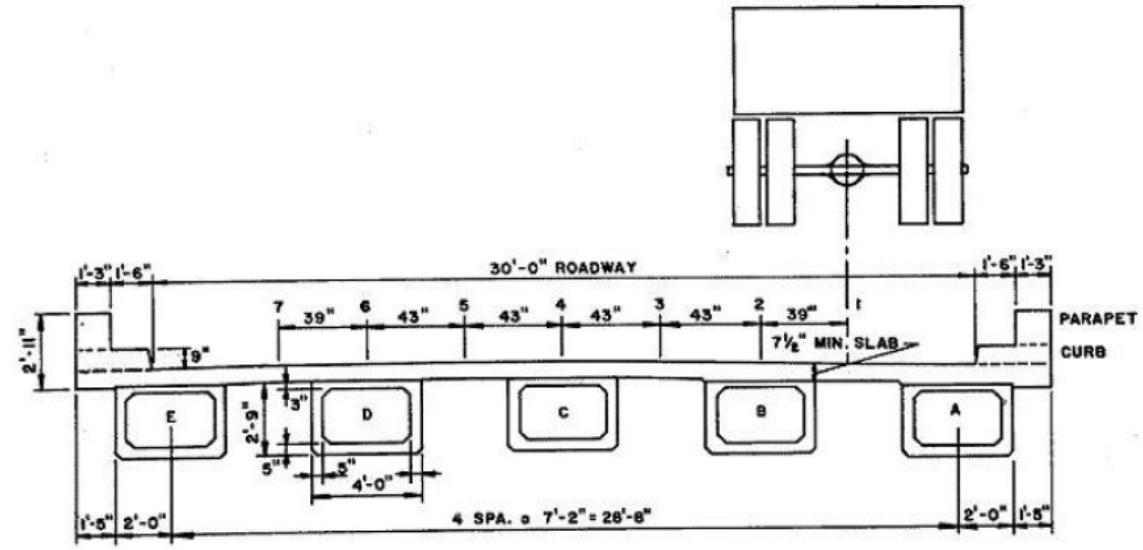

(a) Transverse Section

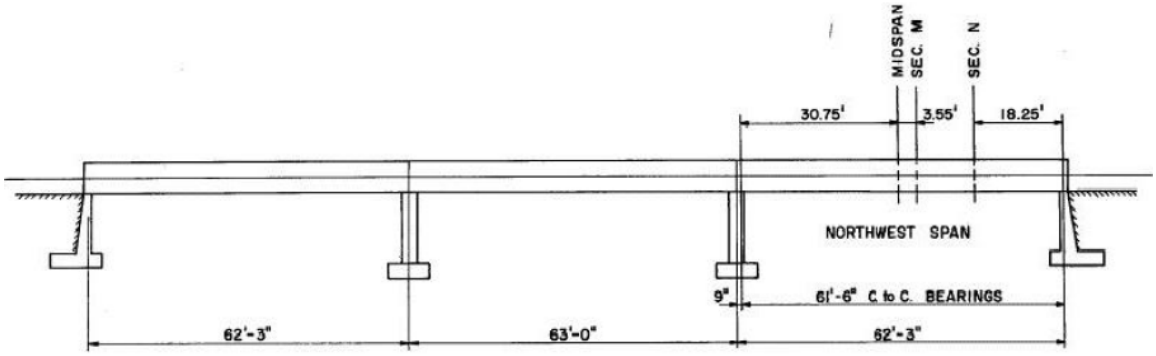

(b) Elevation View

Note: 1 inch = 25.4 mm, 1 feet = 304.8 mm

Figure 2.8. Transverse Section and Elevation View of Drehersville Bridge in Pennsylvania (Douglas and Vanhorn 1966).

Eom and Nowak (2001) carried out an experimental research project on evaluating the conditions of existing bridges by testing 20 steel girder bridges. The strain gages were used to record bridge responses and further infer the experimental moment LDF values. It was found that the values specified by AASHTO LRFD Bridge Design Specifications (AASHTO 1998) and AASHTO Standard Bridge Design Specifications (AASHTO 1996) were always conservative as compared to test results. It was also noted that the existence of secondary components, such as sidewalk, railing and parapet, cause effects on the load distribution behavior due to the extra stiffness.

Amer et al. (1999) conducted experimental tests on three short-span solid slab bridges to investigate the equivalent width and load capacity of existing slab bridges. The strain gages were installed at critical locations to measure the bridge response. The moment values were determined by multiplying the strain values with the section modulus and concrete elastic modulus. It was found that the depth of edge beams had significant effects on the equivalent width because the edge beam moment raised with an increase of the moment of inertia. Conversely, observed results showed that the variation of slab thickness caused very little influence on the equivalent width. It was also noted that for bridge structures with considerable cracks, test results based on measured strains may not be realistic if the material nonlinearity is not taken into account.

Schwarz and Laman (2001) conducted field tests on three prestressed concrete I-girder bridges, with span lengths of 10.2, 23.3 and 31.1 m, to investigate the lateral load distribution behavior and the dynamic amplification factor. Strain gages were installed underside of each girder at the midspan of bridges to measure the strain values and further

determine the moment LDF values. This arrangement is consistent with previous experimental work done by many researchers (Kim and Nowak 1997); (Laman et al. 1999); (O'Connor and pritchard 1985); (Paultre et al. 1995). By comparing with the values calculated from AASHTO Standard and AASHTO LRFD formulas, it was found that the code-specified LDF values were greater than those measured in the test for both one and two lanes loaded, thus the code equations are conservative for design usage. In terms of dynamic effects, the test results indicated that the amplification factor decreases with the increasing stress. With the increase of the vehicle speed, it was observed that the amplification factor increases.

From the literature described above, it is shown that the strain gage was normally utilized to measure the bridge response in the field tests and the strain value was the major parameter to determine the girder moments and further infer experimental LDF values. Most research work focused on the moment actions while very few studies dealt with the shear force measurements.

In order to investigate the shear distribution behavior of slab-on-girder bridge structures, Barr and Amin (2006) carried out a static load test on a full-scale steel I-girder bridge. This simply-supported bridge had a span length of 12.2 m with three steel I-girders. Three load cells were installed between the girders and supports at one end to measure the reaction forces under externally applied load. Based on the data recorded by load cells, the shear LDF values of steel I-girders were further determined.

Hughs and Idriss (2006) adopted embedded fiber-optic sensors to investigate moment and shear load distribution behavior for a prestressed concrete spread box-girder

bridge. The sensors were arranged in different topologies to measure various structural responses. Crossed topology is used to measure the shear forces while the parallel topology is for bending moments, as shown in Figure 2.9(a). The elevation view and plan view of sensor layout for the test bridge are shown in Figure 2.9(b) and Figure 2.9(c). By comparing test results with those calculated from the AASHTO LRFD empirical formulas, it is found that the LRFD empirical formula would yield safe design values, although the distribution factors of exterior girders would be overconservative.

In this dissertation, an in-service spread slab beam bridge was tested to investigate the load distribution behavior of this new bridge system. A creative method that using bearing pad deformations to infer the shear LDF values was developed in the test process. Besides, the effects of the secondary elements (guardrail and sidewalk) and amplification factors were also evaluated based on the test results.

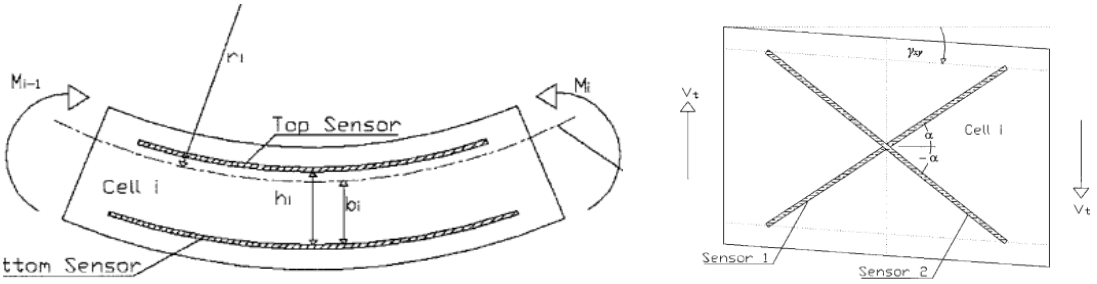

Parallel Topology *Crossed Topology*

(a) Parallel and Crossed Topology for Moment and Shear Measurement

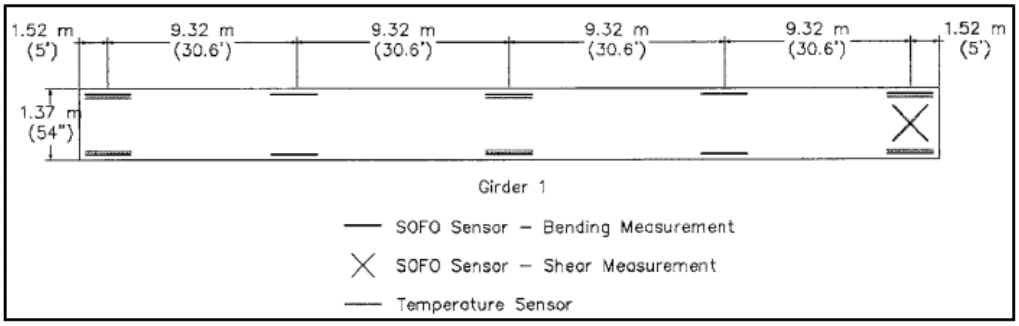

(b) Elevation View of Sensor Layout for Girder 1

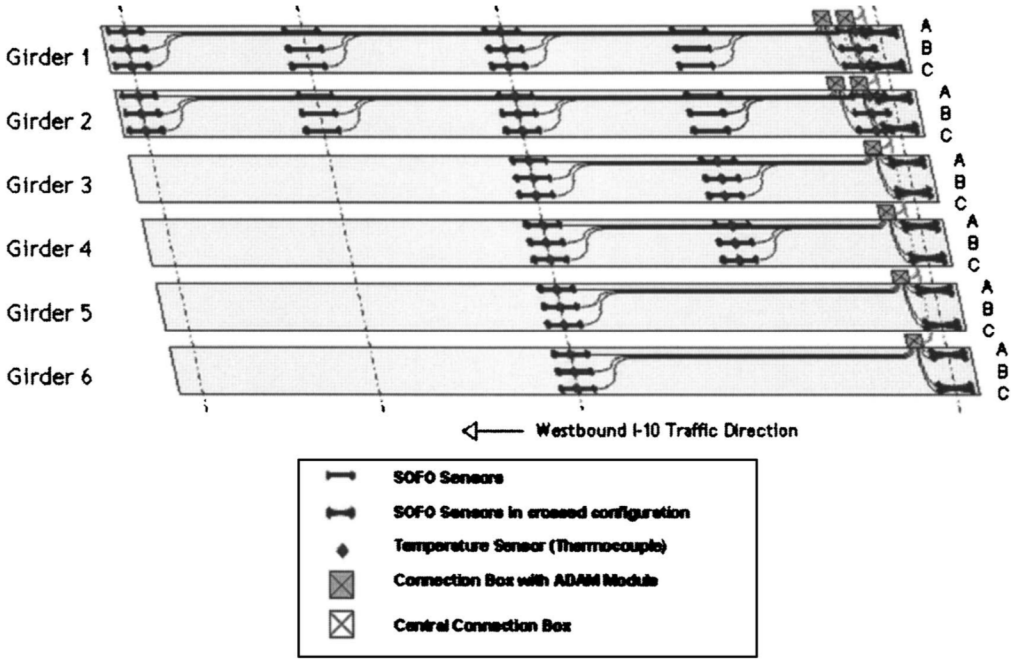

(c) Plan View of Sensor Layout

Figure 2.9. Sensor Layout for Bridge Monitoring (Hughs and Idriss 2006).

2.5 COMPUTATIONAL ANALYSIS FOR BRIDGE SUPERSTRUCTURES

2.5.1 Introduction

The concept of load distribution factor has been widely used in the bridge design because it provides structural engineers a simple option to determine the moment and shear demands with no need of high-level structural analysis. However, when bridge geometries are beyond the applicable range of LDF formulas, refined analysis becomes mandated in the design process based on the requirements in the AASHTO LRFD Bridge Design Specifications. Thus, it is still necessary for practitioners to get a knowledge of computational analysis techniques. There are several major analysis methods for bridge structures, including the grillage analogy method, orthotropic plate theories, the finite-strip method, the finite difference method (FDM) and the finite element method (FEM). In particular, grillage and FEM techniques are two methods mostly adopted by bridge engineers nowadays. The historic grillage method is the simplest approach of analysis in which the girders and the deck in bridge superstructure are assumed to be a mesh of beam elements in two orthogonal directions. As for the FEM technique, the fewest simplifying assumptions were required and most variables governing the structural behavior are considered. It is capable of modeling and combining several different mathematical models to better represent the practical behavior and boundary conditions of a complex bridge structure. These two methods were adopted to analyze bridge superstructures in this research study and their accuracy will be verified by comparison with measured test data. This section presents instructions and recommendations for developing

computational models using grillage and FEM methods. Literature about previous computational analysis work on live load distribution factors is also included.

2.5.2 Grillage Analysis

The grillage analogy method is one of the most basic and simplest types of modeling technique. By modeling the bridge superstructure as equivalent grillage of connected beams at discrete nodes, the numbers of degrees of freedom within bridge system are dramatically reduced and the loading transfer mechanism is simplified. Also, the simplification could lower computational complexity and decrease the time needed for modeling and calculation. Several journal articles, books and manuals (Hambly 1976; Hueste et al. 2006; Lightfoot and Sawko 1959; Ryall et al. 2000; Schwarz and Laman 2001; Surana and Agrawal 1998) provide guidelines for developing grillage models.

Lightfoot and Sawko (1959) pioneered the grillage method of analysis by making programing to solve the grid framework problem. Since then, this approach has become very popular to bridge engineers for the simple concept that bridge deck can be divided into several equivalent grillage members in longitudinal and transverse direction. The accuracy was also improved with the development of the computational capacity.

Hambly (1976) discussed the grillage method application in various types of bridge superstructures and provided guidelines for developing accurate grillage configuration, including grillage mesh generation, grillage member properties determination, load application, etc. It was suggested that the spacing in transverse and longitudinal directions should be similar and the grillage members be assigned the same stiffness parameters as the original bridge section. For slab-on-girder bridges, the

longitudinal grillage members are normally arranged coincide with the girder centerlines to reflect the actual longitudinal stiffness and cross-beams are used at appropriate spacing to represent the deck. Once the grillage mesh is generated and appropriate parameters are assigned, the grillage model needs to be loaded in specific patterns. Point and line loads are often utilized in the grillage analysis to represent actual external loads. If the intended load position lies between grillage beams rather than at the nodes. The point or line loads could be split to the nearest grillage members using the lever rule, making the resultant force of the new forces has the same magnitude and at the same location with the originally external loads. Figure 2.10 represents the grillage idealizations for different bridge superstructures.

Chen and Aswad (1996) summarized several guidelines for grillage analysis method: 1). each beam span should be divided with at least nine nodes per beam span; 2). the aspect ratio of grid panels should be less than 5.0; for better accuracy, it's better to reduce the ratio to 2.0; 3). the magnitude and position of nodal loads need to be equivalent to the actual external loads; 4). composite section properties should be taken into account and appropriate torsional constant, *J*, needs to be determined .

Surana and Agrawal (1998) discussed the application of the grillage method in different situations. Despite the grillage method is less complex than other computational approaches, the grillage method could accurately analyze numerous bridge types, even complicated bridge configurations with unusual support conditions, large skew angles and edge stiffening beams. Therefore, the grillage analogy method is considered as a power analysis tool in the design of bridge structures.

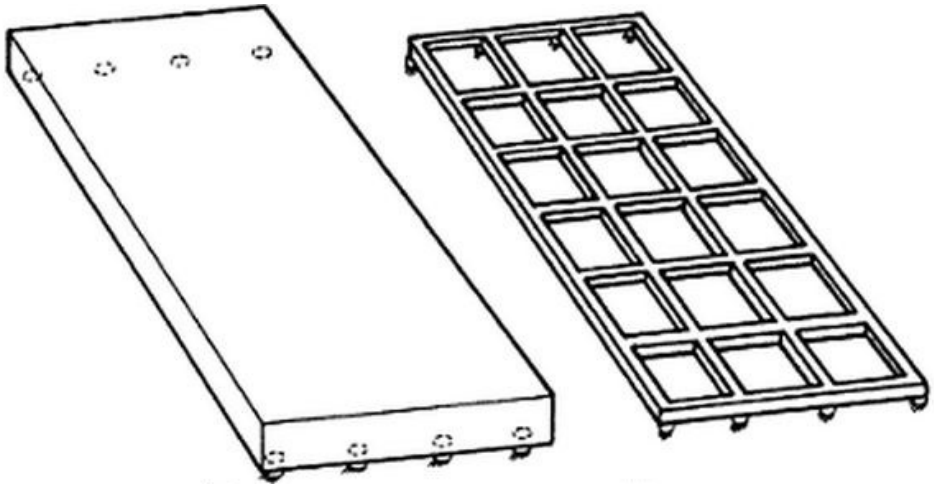

(a) Slab Bridge Deck (Hambly 1991)

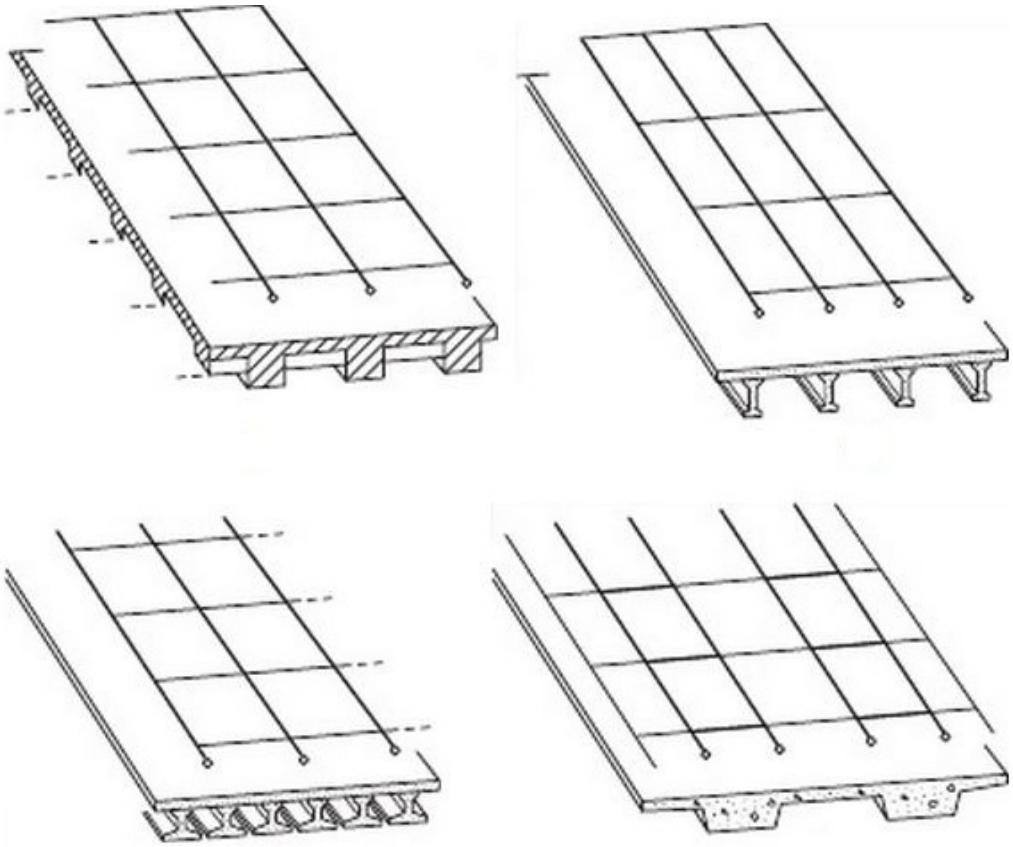

(b) Waffle, Spaced I-Girder, Adjacent I-Girder, and Solid Box Beam Bridge Decks (Parke and Hewson 2008)

Figure 2.10. Grillage Idealizations of Typical Bridge Superstructures.

Schwarz and Laman (2001) developed grillage models for three prestressed concrete I-girder bridges to predict the LDF values in each. In the development of grillage models, well-established guidelines were followed and several different grillage characteristics were tried. The transverse grillage members were placed in the spacing of about 1/10 of span length. Although the midspan diaphragms existed in the second and third bridges, both grillage models with and without midspan diaphragms were developed to assess the effects of these members. The diaphragms were modeled perpendicular to the longitudinal direction in the second bridge due to small skew angle, while these members were perpendicular to the girders in the third bridge model for the consistency with the actual construction situation. The computational LDF values were compared with experimental data from field testing. It was found that the numerical grillage model provided LDF values in close agreement with test results and more accurate results could be obtained with neglecting the diaphragms in the grillage model development, particularly for shorter spans.

Hueste et al. (2006) evaluated the accuracy of the LRFD LDF formulas for the bridge configurations beyond the ranges of applicability by conducting a parametric study. The grillage analysis technique was utilized in the parametric study to investigate the load distribution behavior of bridges cases with over 42.7 m span length and 60 degree skew. The grillage models were developed using the program SAP2000, and validated with more advanced finite element analysis. The distribution factors determined from the grillage analysis were compared with code-specified values. It was concluded that the LRFD empirical formula generated conservative LDF values, and they are overconservative in

some cases; however it was recommended by Hueste et al. (2006) that grillage analysis be confirmed by a higher analysis method before it was applied to extensive usage.

Parke and Hewson (2008) provided some grillage analysis examples using a structural engineering software package. Some concerns were arisen about the grillage analysis of the slab structure. Despite the grillage method of analysis attempts to take all properties of a real bridge into account, it still simplifies the bridge structure and some physical aspects are lost in the model development process. Although force equilibrium equivalence between the grillage model and bridge deck are easy to capture accurately, the main drawback is the lack of displacement compatibility between cross beams. However, it is shown that the real bridge behavior can be approached if the grillage mesh is sufficiently refined. Another concern brought up by the author is that the moment in a grillage member is only proportional to the curvature in that beam, while the curvature in both longitudinal and transverse directions affects the moment values in the real bridge.

2.5.3 Finite Element Analysis

2.5.3.1 General

The finite element method (FEM) is a general and powerful tool to analyze the real engineering problems involving complicated geometry and boundary conditions. In the FEM analysis process, a given domain is divided into a number of subdomains and the physical governing equations are developed over each subdomain (Reddy 1993). The concept of FEM was brought up in aerospace engineering for aircraft structural analysis in 1940's (Courant 1943). Since the formal "finite element" term was introduced later by

Clough (1960), this powerful tool has been widely used in various research areas including civil engineering, and many commercial software packages were developed for engineering application, such as: SAP2000, ANASYS, Abaqus, etc.

The bridge superstructure analysis is a highly complex problem for engineers to obtain the "exact" theoretical solution. The FEM technique provides an easier option for the bridge engineers to accurately investigate the structural behavior. In terms of slab-on-girder bridges, there are two different ways to idealize the bridge system: two-dimensional (2D) or three-dimensional (3D) models. The 2D idealization contains fewer degrees of freedom and requires less computational cost due to underlying simplifications. Conversely, 3D model accurately represents the real physical geometry with additional degrees of freedom and a higher level of refinement, thus gives better results for bridge structures. Based on element types used for different structural components, 3D FEM analysis of bridges can be classified into several categories: eccentric beam model, detailed beam model and solid deck model. Instructions and recommendations for properly developing FEM models can also be found in multitudes of scholarly articles and books (Barker and Puckett 2007; Puckett et al. 2005; Ryall et al. 2000; Zokaie et al. 1991). Literature about previous FEM analysis on bridge superstructures is also included in this section.

2.5.3.2 Two-dimensional Finite Element Modeling

In 2D FEM analysis of bridge superstructures, the centroid of girder element is coincided with that of the slab element, making all the nodes in the same plane. Mabsout et al. (1997) adopted this modeling technique to investigate the load distribution behavior of concrete-

slab-on-steel-girder bridges. The steel girder was idealized with space frame element while quadrilateral shell elements were used to model the concrete deck slab, as shown in Figure 2.11(a). By comparing the FEM solutions with test results and code-specified values, it is concluded that the 2D finite element modeling could be applied in the design of straight girder bridges with no complex structural components. However, this method does not reflect the girder eccentricity from the deck slab, thus the section stiffness property cannot be accurately modeled.

2.5.3.3 Three-dimensional (3D) Finite Element Modeling

Wegmuller and Kostem (1973) introduced the eccentric beam model to analyze the slab-on-girder bridge superstructure. The bridge deck was idealized with shell elements and girders were modeled as two node beam elements and eccentrically connected to shell elements with rigid links, as shown in Figure 2.11(b). This approach could reduce the computational complexity, but reflect the actual interaction of deck slab and girders. The accuracy was verified by comparison with the test results.

Some practitioners criticized that the beam element in eccentric beam model cannot accurately reflect the behavior the bridge girder, especially for those with wide webs. Brockenbrough (1986) utilized a detailed beam model to idealize the I-girder bridge superstructures. The girder flanges and webs were modeled with beam and shell elements respectively, as shown in Figure 2.11(c). Rigid links were used to connect the deck shell elements and top flange elements. It was concluded that the use of shell elements for girder webs could realistically modeled the lateral bending stiffness, thus give better results.

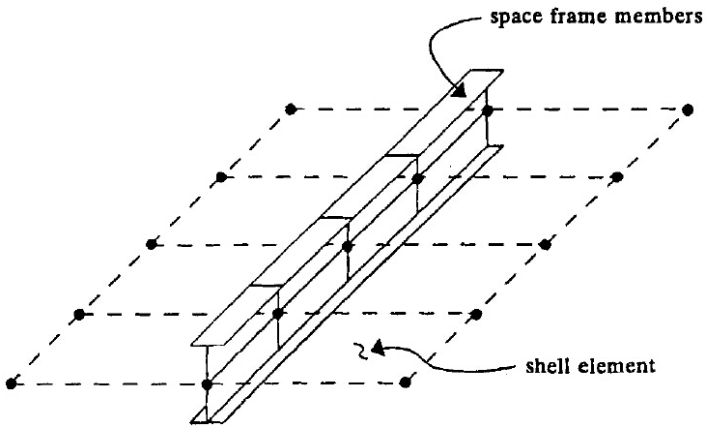

(a) 2D FEM Model for Steel Girder Bridge (Mabsout et al. 1997)

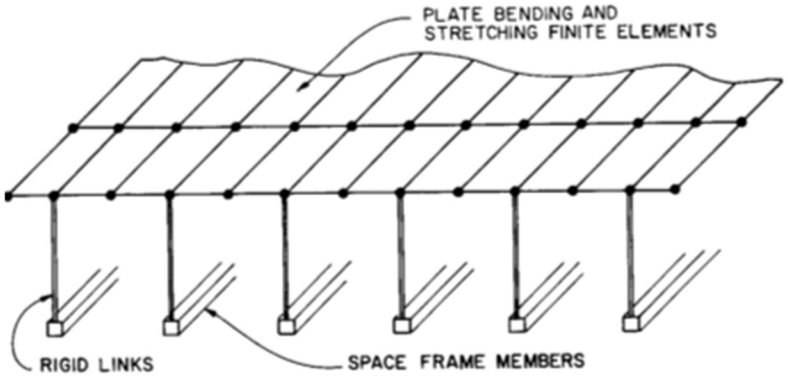

(b) 3D Eccentric Beam Model (Wegmuller 1973)

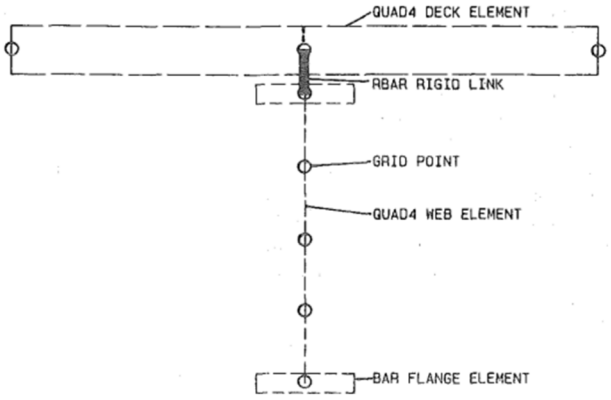

(c) 3D Detailed Beam Model (Brockenbrough 1986)

Figure 2.11. FEM Models for Slab on Steel Girder Bridges.

Tarhini and Frederick (1992) conducted a comprehensive FEM study to investigate the load distribution behavior of I-girder bridges. The FEM models were generated to adequately describe bridge geometric properties. The steel girders were idealized with quadrilateral shell elements and the concrete deck slab was idealized as isotropic solid elements, thus this model is called solid deck model. Two types of elements were connected with interface nodes to make sure no slip occurs. It was concluded that this finite element idealization to model slab-on-girder bridges yielded good results.

Barr and Amin (2006) used three different FEM modeling schemes to stimulate steel I-girder bridge. All three models were developed using the commercial software, SAP2000. Frame and shell elements were used to model the steel girder and the concrete deck respectively in the first model; the second scheme used shell element for both bridge deck and girders; the last one use solid elements and frame elements to model the deck and girders. With comparisons to test results, it was concluded that all three FE modeling strategies could closely reproduced the measured values.

The boundary condition is a major concern to realistically represent the bridge structures in the FEM modeling process. Eom and Nowak (2001) developed 3D FEM models of bridges with Abaqus program and experimental results were used to calibrate the model. Three different boundary conditions (roller-hinge, hinge-hinge and partially fixed supports) were considered in the analysis process. By comparing with the test results, it is found that the strain values predicted by FEM analysis are always larger than the observed ones and partial fixity of support due to corrosion or accumulation of debris was considered to be one of the major reasons. FEM solutions indicated that the girder moment

distribution was most uniform under ideally simply supported boundary conditions; when some degree of partial fixity existed at supports, the strain values would decrease considerably. It was concluded that these refined analysis was complicated for actual use in bridge design procedure and inconsistency existed in these methods due to different assumptions made by engineers.

2.6 ULTIMATE STRENGTH ANALYSIS OF SLAB-ON-BEAM BRIDGES

2.6.1 Plastic Analysis Methods

The prediction of the ultimate load capacity is necessary for the design safety check of bridge superstructures. The research work on strength analysis of bridge decks has evolved along two lines: the yield line theory analysis and grillage analysis utilizing the plastic hinge concept (Sawko and Saha 1967). The latter is akin to the historic strip method used for slab design.

Hillerborg (1956) first introduced the strip method for the design of concrete slab structures in Sweden. The method divides the structure into “strips” in the two orthogonal directions and then uses equilibrium alone to assess the load carried by each strip, the summation of all strip loads gives the capacity of the slab. This straight-forward method is very amenable for design and was adopted by British code of practice for the structural design of reinforce concrete slabs (BSI 1972).

Since the advent of plastic methods of analysis in the 1950’s, the yield line method (Johansen 1962) and the strip method (Hillerborg 1956) have seen widespread use for the design of reinforced concrete floor systems in structures. In the 1950’s and 60’s, the field

of plastic methods of analysis in structures matured quickly, but it has not progressed markedly over the decades since, due to the ascendancy of computational solutions provided by the finite element method (FEM). The FEM approach remains relatively difficult to apply to design situations in the ultimate limit state, whereas yield line theory has been shown to provide structural engineers with relatively accurate predictions with simple calculations (Park and Gamble 2000; Sawko and Saha 1967).

Not withstanding the historical development with a focus on hand calculations, Middleton (1997; 2008) has conducted comprehensive research on the plastic analysis of bridge decks. A computer program, COBRAS, was developed at Cambridge University to perform yield line analysis of short-span reinforced concrete bridges. Various failure mechanisms are predefined in the program for users to select. The solution iterates on a large number of possible geometric tries and a systematic search is made for the lowest, and hence critical, failure mode. The validity of the program has been confirmed by comparison with test results. Over 20 concrete bridges were reassessed using this program and higher flexural capacities were found when plastic, rather than elastic, analysis was used for assessment.

Hazell (1999) tested a simple span scale model of reinforced concrete slab-on-beam bridge with two patch loads applied by mechanical jacks to determine the collapse load. With using yield line theory analysis, Hazell (1999), Lowe (1999) and Jackson and Middleton (2013) predicted ultimate load capacity accurately as compared to the test results.

T. J. Mander et al. (2010b) recently adapted and modified yield line theory for the bridge deck slabs consisting of bottom stay-in-place (SIP) precast prestressed concrete panels and topping CIP reinforced concrete deck slabs, respectively. Full-scale experimental tests were also conducted by T. J. Mander et al. (2010a; 2010c) to identify the ultimate load capacity of the interior spans and overhangs. For the interior spans, a compound shear-flexure failure mechanism was proposed to reflect the observed failure mode in the test. Capacities determined from yield line theory compare well with experimental observations.

Following the above work of T. J. Mander et al., Pirayeh Gar et al. (2014) applied yield line theory to determine the ultimate load capacity of bridge deck slab with precast panels prestressed with fiber reinforced polymer (FRP) bars. By comparison with experimental test results, it was confirmed that the yield line theory is applicable to this new bridge deck system and it was able to predict collapse loads within 3 percent of the observed test results.

2.6.2 Nonlinear Computational Analysis

The strip method described in the previous section is also akin to the grillage method where a bridge deck is modelled as a "grillage" of beams in two orthogonal directions. The grillage method has historically been widely used to perform linear elastic analysis of bridge superstructures due to the simplicity. Its application to nonlinear analyses for bridge structures in in the inelastic range up to the ultimate limit state was investigated by a few scholars with utilizing the nonlinear static analysis strategy (Ghosn et al. 1996; Ghosn and Moses 1998).

The nonlinear static analysis, also known as pushdown analysis, is a popular approach to track the nonlinear relationship between load and deformation of the bridge structure and finally evaluate the ultimate strength and maximum displacement. The structure is loaded monotonically from initial elastic condition till collapse. In the implementation of pushdown analysis, plastic hinges with predefined hinge properties were assigned in the longitudinal and transverse grillage elements to capture the behavior at the ultimate limit state.

The software SAP2000 (Computers and Structures 2013) is considered as the most common software package to perform nonlinear static analysis for bridge superstructures. Ghosn et al. (2014) utilized this software to conduct nonlinear grillage analysis of spread box girder and I-girder bridge superstructures for the purpose of investigating the design redundancy of these bridge types. Deng et al. (2001) used a special program NONBAN (Nonlinear Bridge Analysis) to perform nonlinear grillage analysis of prestressed concrete girder bridges. It was claimed that the nonlinear grillage approach has a high potential for use in bridge engineering practice due to its simplicity.

Some researchers utilized FEM technique to analyze the bridge behavior at ultimate state by considering the material nonlinearity.

Razaqpur and Nofal (1990) developed a nonlinear FEM program NONLACS (Nonlinear Analysis of Concrete and Steel) to investigate the effects of steel yield and concrete nonlinearity on load distribution behavior of composite concrete slab-steel beam bridges. Fifty bridges were analyzed over the entire loading range up to failure. The parameters studied included number of loaded lanes, number of girders, bridge width, slab

thickness, truck position and existence of diaphragms. The moment distribution factors at different load levels were obtained and compared with the corresponding elastic LDFs calculated from AASHTO LRFD empirical formulas. The study revealed that only the number of loaded lanes and the bridge width significantly affect transverse moment redistribution at ultimate limit state. Based on the FEM analysis results, as the bridge traverses from the elastic state to the ultimate state, the internal girder LDFs increased from zero to 54% (on average 32%) compared to its value at the elastic state, while the external girder LDF decreased from zero to 42%, with an average reduction of 19%.

Cheung et al. (1987) used the commercial software package, ANASYS, to carry out a nonlinear FE analysis on a small scale six girder bridge model. Both elastic and inelastic behavior of the steel beams of the bridge was taken into consideration in the finite element idealization. It is reported that load redistribution in bridge girders is insignificant before the formation of the first plastic hinge. However, a considerable reduction of load distribution factors is observed between linear elastic and first yielding.

Since the nonlinear FEM analysis requires extensive computational costs and this approach remains relatively complicated for the design usage at the ultimate limit state. Thus plastic analysis methods and nonlinear grillage model was utilized in this dissertation to predict the overstrength capacity of slab-on-beam bridge decks at the ultimate collapse load.

2.7 CLOSURE

In light of the foregoing survey of the open literature the following research questions arise:

What is the structural performance in general and the load distribution behavior in particular of the in-service spread slab beam bridge system?

Extensive experimental work has been conducted on various different types of bridge structures to investigate the structural behavior. In particular, bridges superstructure consists of prestressed concrete I-girders, prestressed concrete spread box beams, steel I-girders, etc., to name a few. To date, no field testing has been conducted on the new class of spread slab beam bridge deck system. Therefore, there is a need to explore the experimental structural performance of this new class of bridge. In this present research, an in-service spread slab beam bridge is instrumented and tested to investigate the structural performance in general, and the load distribution behavior in particular, of one as-built in-service structure.

How can one effectively and efficiently experimentally infer from field observations the load distribution factors for shear in an in-service bridge structure?

Based on the literature review presented in this section, it was shown that most experimental studies on bridge structures focused on the distribution of moments amongst beams. Only a few experimental investigation dealt with the shear force measurements. Some scholars conducted girder tests in the laboratory and used load cells to measure reaction forces. However, it is difficult to temporarily install load cells during field testing, therefore the issue remains on how expediently measure the shear force and then infer the

shear LDF values for an in-service bridge. In this research, a creative method that uses the bearing pad deformations to infer the shear LDF values is developed and validated as part of the experimental process; bearing pad deformations are measured with LVDTs attached beneath the slab beams close to the support.

What contemporary method of computational modeling is most appropriate for an accurate analysis of a slab-on-beam bridge? And how do these temporary methods compare with the historical grillage approach used in the AASHTO LRFD code development?

Extensive publications present computational model development for bridge structures with different methods. Nowadays, finite element method (FEM) is the most common technique utilized by practitioners to accurately analyze the slab-on-beam bridges because the fewest simplifying assumptions were required and most variables governing the structural behavior are considered. In this research, FEM technique was adopted to model the new class of spread slab beam bridge and the accuracy was evaluated be comparisons with observed test data. Moreover, the historic grillage approach was also used to analyze the tested bridges. It is evident that with carefully developing the models, the historic grillage method could also predict fairly accurate moment and shear force values.

Is there a more straightforward way to determine the moment and shear demands for both simply supported and continuous slab-on-beam bridges?

Current AASHTO LRFD LDF formulas are criticized by practitioners for their complex format. Moreover, some parameters within the LDF equations are unknown at the preliminary stage of a design, thus an iterative procedure may often be needed. Therefore,

there is a need to develop more straightforward and simpler models to determine the moment and shear demands under live and impact loads at the preliminary stage of design. In this way the bridge designers has the freedom to explore more options within an allotted time and select the best candidate for bidding. In this research, new design models with a "*S/D*" format are developed and their applicability to slab-on-beam bridges are verified by comparison with rigorous FEM results.

For checking the reserve strength capacity of slab-on-beam bridges (especially for the new class of spread slab beam bridge), are the classical plastic analysis methods applicable?

There is a general understanding from literature, the plastic methods, including the upper bound yield line theory and lower bound strip methods, are appropriate for the design and analysis of structural concrete slab system. Only a few scholars have attempted to adopt these methods to predict failure modes of bridge decks that include both slabs and beams. The question is, is it both expedient and prudent to use plastic analysis methods to evaluate the reserve strength capacity of a slab-on-beam bridge system. In this research work, different limit state behavior modes are considered for slab-on-beam bridge structures to investigate the hierarchy of failure mechanisms. Particularly, classical plastic overstrength analyses are conducted on two spread slab beam bridges and important information regarding the "balance" of designs for slab and beam with respect to the hierarchy of failure mechanisms are provided.

3 EXPERIMENTAL STUDY OF AN IN-SERVICE SPREAD SLAB BEAM BRIDGE

3.1 SUMMARY

A new class of spread slab beam bridges has recently been developed and implemented in Texas. Due to the absence of appropriate design guidelines, moment and shear design actions have been based on those used for spread box beam bridges; however, their applicability remains in question. To develop new criteria, the load distribution behavior of this new bridge system is investigated. Comprehensive static and dynamic tests are performed on an in-service spread slab beam bridge, the US 69 Bridge located in the City of Denison, Texas. Various experimental methods are used to infer the moments and shears resisted by individual beams that arise from a heavily loaded truck. The experimental test results indicate that the existence of a sidewalk and guardrail markedly stiffens the structure leading to higher than expected moment values. The observed bridge responses under moving dynamic loads exceed the present design specifications impact factor of 33 percent. Thus, for service load design it is recommended the allowable tensile stress be slightly reduced.

3.2 INTRODUCTION

Prestressed concrete slab beam bridges have been used in Texas and elsewhere as an effective low profile solution for simply supported spans up to 15 m. However, design experience shows that slab beam bridges cost more when compared with the more common traditional prestressed concrete I-girder bridges. In order to explore an economical and practical design solution for short-span bridges with a shallow depth, a new bridge type, known as a spread slab beam bridge, was recently developed by the Texas Department of Transportation (TxDOT). Due to the absence of specific guidelines TxDOT considered the same concepts and design criteria adopted for spread box beam bridges. It remains unknown whether the load distribution factors (LDFs) in particular are valid for spread slab beam bridges. Therefore, a dual experimental and computational investigation has been conducted to explore the experimental performance of spread slab beam bridges in general, and load distribution behavior in particular. This section focuses on the experimental performance evaluation of an in-service spread slab beam bridge.

The analysis for slab-on-girder bridges is a complex problem due to a high degree of indeterminacy in the structure. Since the 1930's, the concept of LDFs was utilized by bridge engineers to determine the moment and shear force of an individual girder, which is necessary for new bridge design or existing bridge evaluation. In 1991, Zokaie et al. (1991) developed power function formulas to calculate live LDF values for specified types of bridge structures and they were quickly adopted by AASHTO LRFD Bridge Design Specifications (AASHTO 1994). As there are currently no LDF equations for the spread slab beam class of bridge, designers need to resort to LDF formulas for a similar bridge

type such as the spread box beam bridge (AASHTO 2012) but their applicability is unknown.

When developing design criteria, it is highly desirable to conduct experimental tests for validation purposes. Previously, field experiments have been conducted on a limited number of bridges. Experimental determination of moment LDF values for different bridge types has been conducted that include spread box beam bridges (VanHorn 1969), steel girder bridges (Kim 1997), solid slab bridges (Amer et al. 1999) and prestressed concrete I-girder bridges (Barr et al. 2001; Schwarz and Laman 2001).

This section describes the comprehensive static and dynamic tests performed on the spread slab beam portion of the US 69 highway located in Denison, Texas. The load distribution behavior and dynamic amplification effects of the spread slab beam bridge system are evaluated on the basis of the recorded data.

3.3 BRIDGE DESCRIPTION

Figure 3.1 presents the bridge investigated herein that is part of US 69 highway located in Denison, Texas. The US 69 Bridge consists of 18 spans, and the first three spans near the south abutment consist of spread slab beams. The third span passes over Day Street (Figure 3.1(a)). To improve clearance of the Day Street roadway the designers selected a low-profile bridge deck that consists of six spread slab beams, as shown in Figure 3.1(b). The tested spread slab span over Day Street is 15.2 m long and 11.5 m wide (Figure 3.1(c)). Overall, the five-lane US 69 Bridge has been constructed as two similar side-by-side symmetric structures, with one structure for the northbound lanes and the other structure for the southbound lanes; a 25 mm joint exists between the two halves of

the bridge. The bridge was instrumented at the locations as shown in Figure 3.1(c). The span length between the centerlines of bearing pads of the simply-supported bridge is 14.8 m as shown in Figures 3(d) and 3(e). The slab beams are precast pretensioned 5SB15 concrete sections, which are 1.52 m (5 ft) wide and 381 mm (15 in.) deep. The structural drawings indicate that the thickness of the reinforced concrete deck on the top of the slab beams is 305 mm. Because the spacing is relatively small between slab beams (406 mm), corrugated steel sheets were used as stay-in-place forms between the slab beams to support the 203 mm thick cast-in-place (CIP) deck slab. However, due to the camber of the pretensioned slab beams, the deck thickness at midspan is around 254 mm based on site observations. The specified minimum 28-day concrete compressive strength for the 5SB15 slab beams and the CIP deck was 37 MPa and 28 MPa, respectively.

3.4 EXPERIMENTAL METHODOLOGY

3.4.1 Instrumentation

Figure 3.1(c) depicts the plan view of instrumentation layout for the tested span of the US 69 Bridge. The comprehensive static and dynamic tests were conducted on the US 69 Bridge spread slab beam deck span over Day Street to evaluate the general in-service performance and specifically investigate the moment and shear distributions amongst the slab beams of the bridge system.

(a) Location of US 69 Bridge (Google Maps 2014)

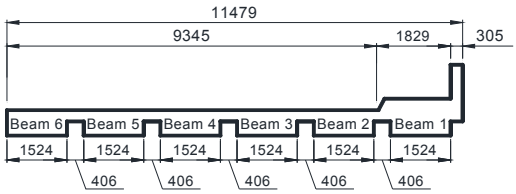

(b) Transverse Section

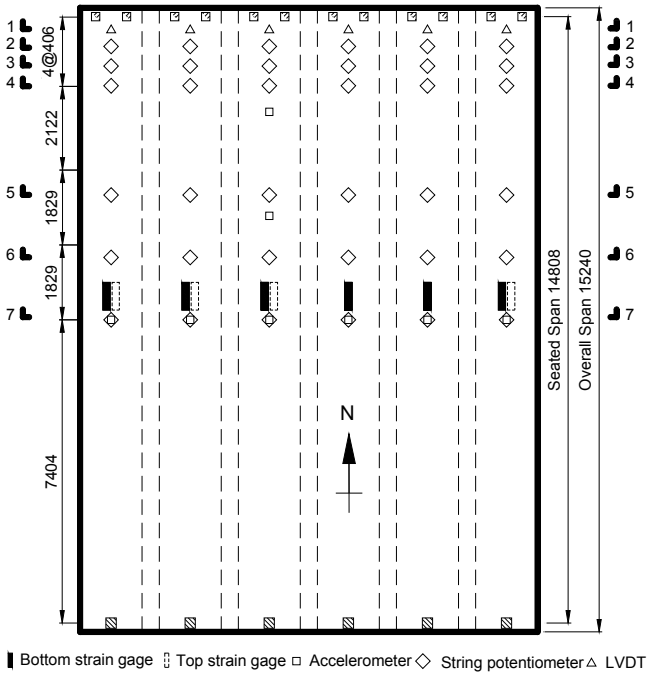

(c) Instrumentation Layout

(d) US 69 Bridge Looking West along Day Street, Denison, Texas

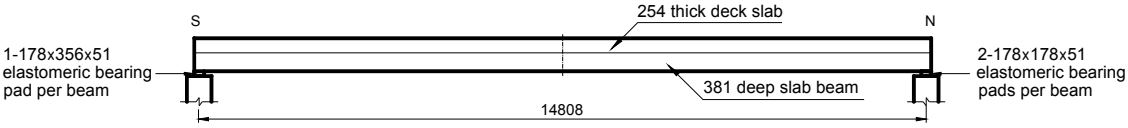

(e) Side Elevation of US 69 Bridge

Figure 3.1. US 69 Northbound Bridge at Denison, TX.

Twelve strain gauges (TML PL-60-11-3LT) were installed at the midspan of the bridge to infer moment LDFs under vehicular loading: six of them attached on the soffit surface of each slab beam, three attached on the top surface of Beams 4 to 6, and the other three installed on the surface of the sidewalk and guardrail (Figure 3.1(c)). LVDTs were attached to the surface of the north bent cap close to each bearing pad at the north support under the slab beams to measure their deformations and thereby infer shear LDFs. Additionally, 36 string potentiometers were installed at six stations distributed between the north pier support and midspan to obtain the bridge deflection field for that half span. To capture mode shapes and natural frequencies of the bridge under moving truck loads, a total of eight accelerometers were affixed to the soffit of the slab beams; six were located at the midspan location of each slab beam, the remaining two were attached to Beam 4 between the midspan and the north support. A 62-channel data acquisition system was utilized during the field test.

3.4.2 Static Tests

Details of the static load 'tests' are listed in Table 3.1. The static tests were applied by a calibrated dump truck along various alignments on the span as shown in Figure 3.2. The fully loaded dump truck, provided by the TxDOT Sherman Area Office, was loaded with an asphalt base material. Individual axle loads were measured at the nearby Denison weigh station on US 75; Figure 3.2(a) shows the measured axle spacing and axle loads of the test dump truck.

Figures 3.2(b) and (c) show the vehicle positions during the critical moment and shear load cases. For the purpose of investigating moment and shear LDFs of exterior and

interior slab beams, a series of static tests including two longitudinal positions and five transverse alignments were conducted. In the longitudinal direction, the maximum bending moment was observed when the resultant load and the axle load closest to the resultant load were placed at an equal distance from midspan. Guided by St. Venant's principle, the maximum shear force was observed when the last axle load was placed at a distance equal to the beam depth (0.6 m) to the center of bearing pad.

In accordance with AASHTO (2012), for the transverse direction the critical moments and shears were taken when the possibility of two side-by-side vehicles exist with a minimum distance between vehicles of 1.2 m. Given that only one dump truck was available during the field test, the vehicle was parked at different transverse alignments and the superposition method was utilized during the data analysis to calculate two-lane loaded reactions.

The most critical position for the exterior slab beam is when the two trucks are parked as close as possible to the bridge's west edge (Alignments 1 and 2). However, the existence of the diagonal median (Figure 3.2) inhibited the test vehicle from straddling the bridge center, therefore Alignment 1 for moment is slightly different from Alignments 2 to 5 as shown in Figure 3.2(b).

For the interior slab beams, two vehicles were loaded in Alignments 3 and 4 to explore potential possible maximum LDF values. Alignment 5, where the vehicle was parked as close as possible to the sidewalk curb, was taken into consideration in order to investigate the composite action between the deck, sidewalk, and guardrail.

Table 3.1. Static Load Test Protocol.

Test Number	Vehicle position	Purpose
-	Initial Alignment 5	Composite Action
1	Center Alignment 5	
2	North Alignment 5	
-	Initial Alignment 4	Interior Beam Critical
3	Center Alignment 4	
4	North Alignment 4	
-	Initial Alignment 3	Interior Beam Critical
5	Center Alignment 3	
6	North Alignment 3	
-	Initial Alignment 2	Exterior Beam Critical
7	Center Alignment 2	
8	North Alignment 2	
-	Initial Alignment 1	Exterior Beam Critical
9	Center Alignment 1	
10	North Alignment 1	

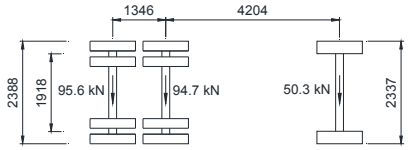

(a) Test Vehicle Axle Loads and Wheel Spacing

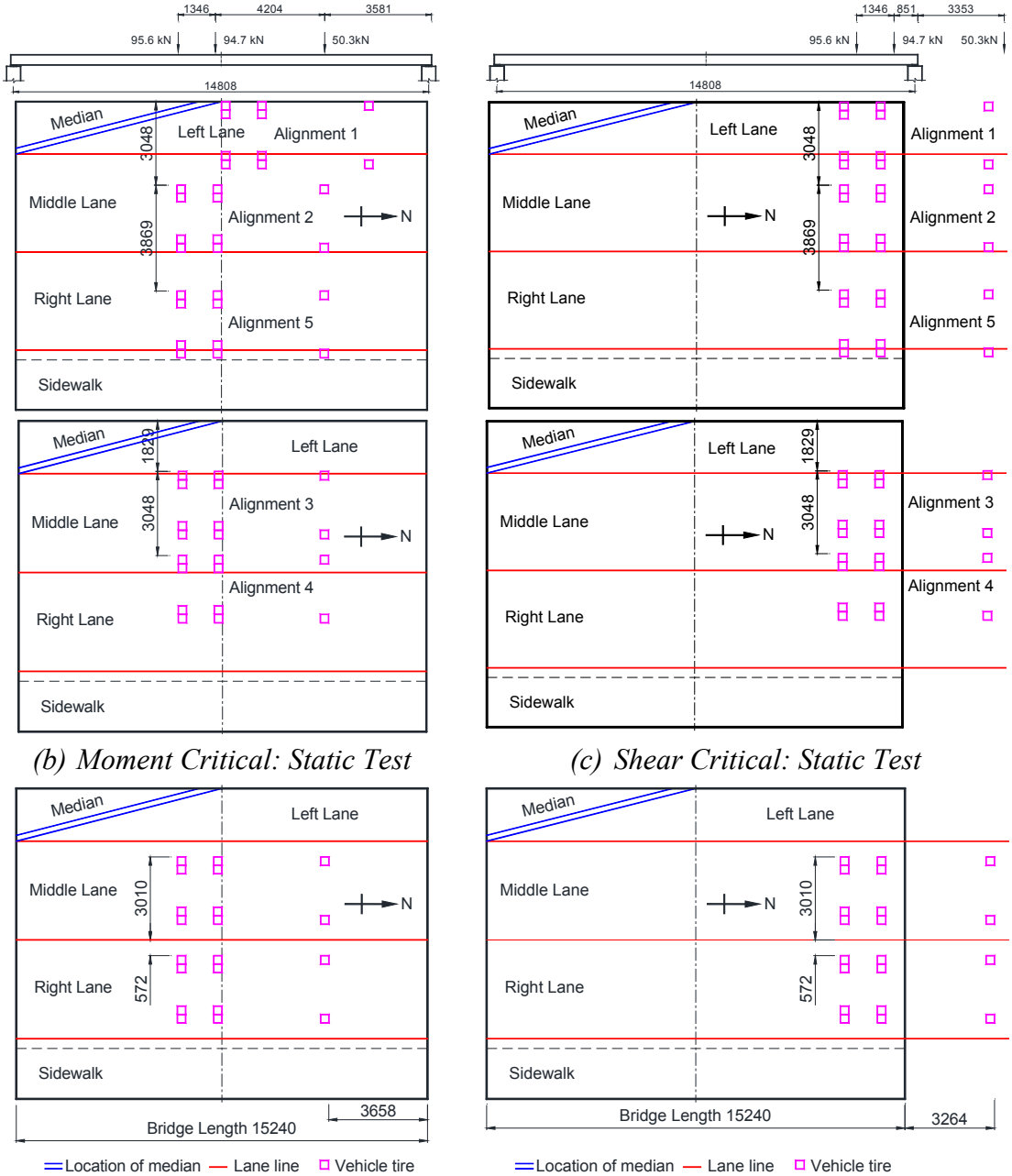

(b) Moment Critical: Static Test

(c) Shear Critical: Static Test

(d) Moment Critical: Dynamic Test

(e) Shear Critical: Dynamic Test

Figure 3.2. Applied Vehicle Loads and Locations

3.4.3 Controlled Dynamic Test

The individual tests to assess dynamic effects are listed in Table 3.2. The right and middle lane locations are shown in Figure 3.2. Controlled dynamic load tests were conducted to determine the dynamic amplification effects when the vehicle passed over the bridge at different speeds. These tests were also useful in obtaining natural frequencies and mode shapes of the bridge. The dump truck was driven along each of the two lanes at specific speeds during the controlled dynamic load tests. Before conducting the dynamic tests, the strain gauge cables on the deck surface were removed and the remaining instruments were kept on the bridge to record the structural responses. With the purpose of comparing the bridge static and dynamic responses, reference static load cases with the vehicle parked at the moment and shear critical position along the two different lanes were also conducted. A radar gun was utilized to measure the vehicle speed when passing over the bridge. The moment and shear critical positions aligned with the two different lanes for the reference static load cases are shown in Figure 3.2(d) and Figure 3.2(e).

Table 3.2. Controlled Dynamic Load Test Protocol.

Test Number	Observed Speed (km/h)	Lane
1	0	Middle (Center)
2	0	Middle (North End)
3	0	Right (Center)
4	0	Right (North End)
5	27	Middle
6	40	Right
7	56	Middle
8	64	Right

3.4.4 Analysis Methods for Experimental Observations

A load distribution factor (LDF), *g*, is defined as the ratio of a general moment or shear action created on each bridge girder due to vehicular loading to that created on an isolated beam element due to the same loading and is given by

$$g_i = \frac{F_i}{F_{1D-Girder}} = \frac{F_i}{\sum F_i} \tag{3.1}$$

where F_i represents the moment or shear action of the i^{th} beam, and $F_{1D-Girder}$ represents the corresponding action on a single beam.

The moment of each slab beam is normally determined based on measured strain values and then the experimental LDF values would be obtained by comparing the moment distribution for each beam.

$$g_{Mi} = \frac{M_i}{\sum M_i} = \frac{E\,\varepsilon_{bi} I_i / c_{bi}}{\sum E\,\varepsilon_{bi} I_i / c_{bi}} = \frac{\varepsilon_{bi} I_i / c_{bi}}{\sum \varepsilon_{bi} I_i / c_{bi}} = \frac{\varepsilon_{bi} S_i}{\sum \varepsilon_{bi} S_i} \tag{3.2}$$

where ε_{bi} = concrete strain on the bottom surface of the i^{th} beam; M_i = moment of the i^{th} beam; I_i = moment of inertia for the i^{th} beam; c_{bi} = distance between the neutral axis and bottom face of the beam section; E = Young's modulus; and $S_{bi} = I_i / c_{bi}$ denotes the section modulus of the i^{th} beam.

The procedure used is similar to approaches utilized by Ghosn et al. (1986) and Kim (1997) to determine the moment distribution factors while assuming the section modulus to be the same for all girders, such that the LDF is equal to the ratio of the strain values. However, due to the existence of edge stiffening members including the sidewalk and guardrail, the Beam 1 section modulus is greater than the value for the other regular beam sections; this difference is considered herein.

The experimental identification of the neutral axis for the beam members is presented in Figure 3.3. For Beams 2 to 6 the neutral axis location was identified as 295 mm from the beam soffit based on the top and bottom surface strain gage readings as shown in Figure 3.3(b). A transformed section analysis based on expected concrete strengths for the CIP deck and precast beams confirms this result.

To identify the system behavior in the vicinity of Beam 1, four strain gages were installed on the surface of the beam, sidewalk and guardrail to investigate the extent of composite action behavior (Figure 3.3(c)). The results derived from strain gages when the truck was positioned along Alignment 5 are also presented in Figure 3.3(c), where the strain gage values do not appear to exhibit plane section behavior. According to the design drawings, reinforcing bars were utilized at the surface between the sidewalk and guardrail to provide interface shear resistance. It is inferred that the deck, sidewalk, and guardrail are fully composite with each other.

A series of static and dynamic tests on an elastomeric bearing pad has been conducted in the laboratory. The measured load-deformation curve shows that some hysteretic behavior is exhibited due to viscoelastic effects although within the operational range the pads behave in essentially an elastic fashion (Hueste et al. 2015). The bearing pads were thus utilized as surrogate load cells whereby the pad deformations were used to infer shear LDFs. During the field test, six LVDTs were attached to the surface of the bent cap close to the bearing pads at the north support under each slab beam to measure their deformations. The LDF for the i^{th} beam in shear is given by the following:

$$g_{Vi} = \frac{V_i}{\sum V_i} = \frac{K\delta_i}{\sum K\delta_i} = \frac{\delta_i}{\sum \delta_i} \tag{3.3}$$

where $V_i =$ reaction (shear force) of the i^{th} slab beam; $K =$ bearing pad stiffness; and $\delta_i =$ bearing pad deformation for the i^{th} slab beam.

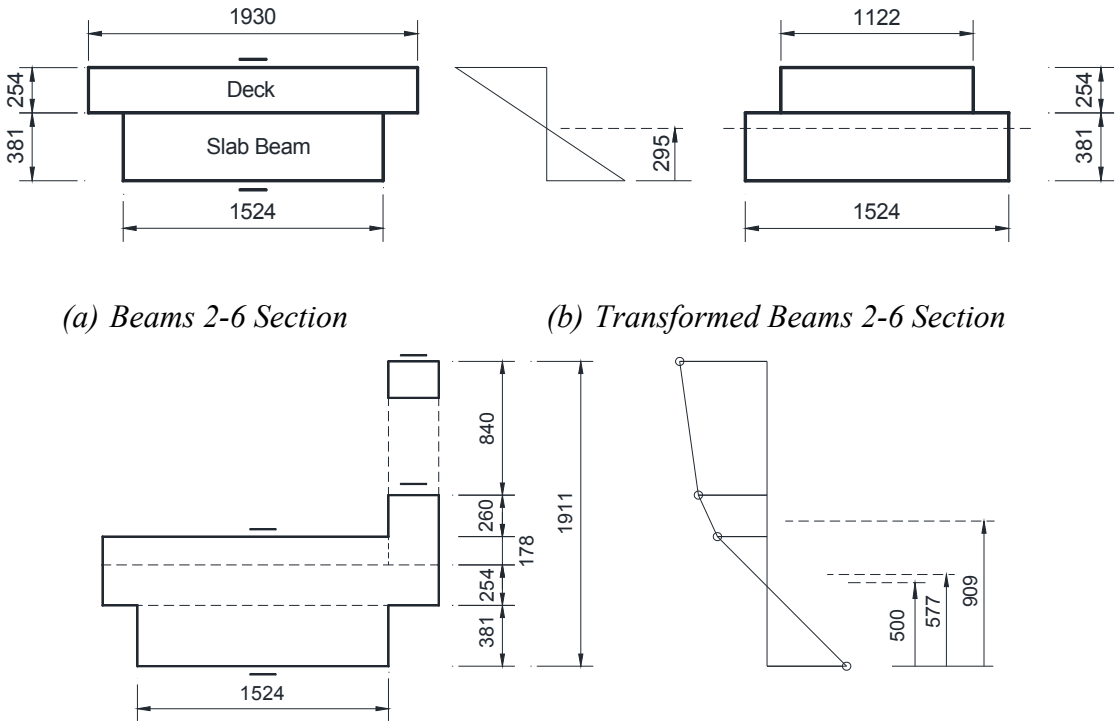

(a) Beams 2-6 Section *(b) Transformed Beams 2-6 Section*

(c) Beam 1 Section with Sidewalk and Guardrail

Figure 3.3. Measured Neutral Axis of Beam Sections on US 69 Bridge.

3.5 TEST RESULTS

A total of ten moment and shear critical load cases were conducted with the TxDOT dump truck during the static load tests to determine the moment and shear LDFs of the exterior and interior slab beams. As for controlled dynamic tests, the vehicle was driven along two different lanes with various speeds and dynamic amplification effects were investigated.

3.5.1 Load Distribution Factors

Figure 3.4 presents (a) the maximum moment and shears inferred from the experimental values; and (b) the moment and shear LDFs derived from Equations (3.2) and (3.3), respectively. Alignment 1 was used to load exterior Beam 6 to impose the greatest load on that beam, whereas Alignment 3 was used to create the most adverse loading on Beam 5. LDF values for all alignments are presented in Tables 3.3 and 3.4 for moments and shears, respectively. It is shown that the distribution of moments and shear values amongst the beams changes when the truck was positioned at different locations on the bridge. The value of one specific beam is higher if the alignment location is close to the beam.

The composite effect due to the existence of the sidewalk and guardrail led to a marked increase in stiffness of Beam 1. Not surprisingly when Alignment 5 was loaded additional moment was resisted by Beam 1, also leading to a greater LDF (g_M = 0.488). However, no effects on the shear distribution behavior were caused by the additional stiffening.

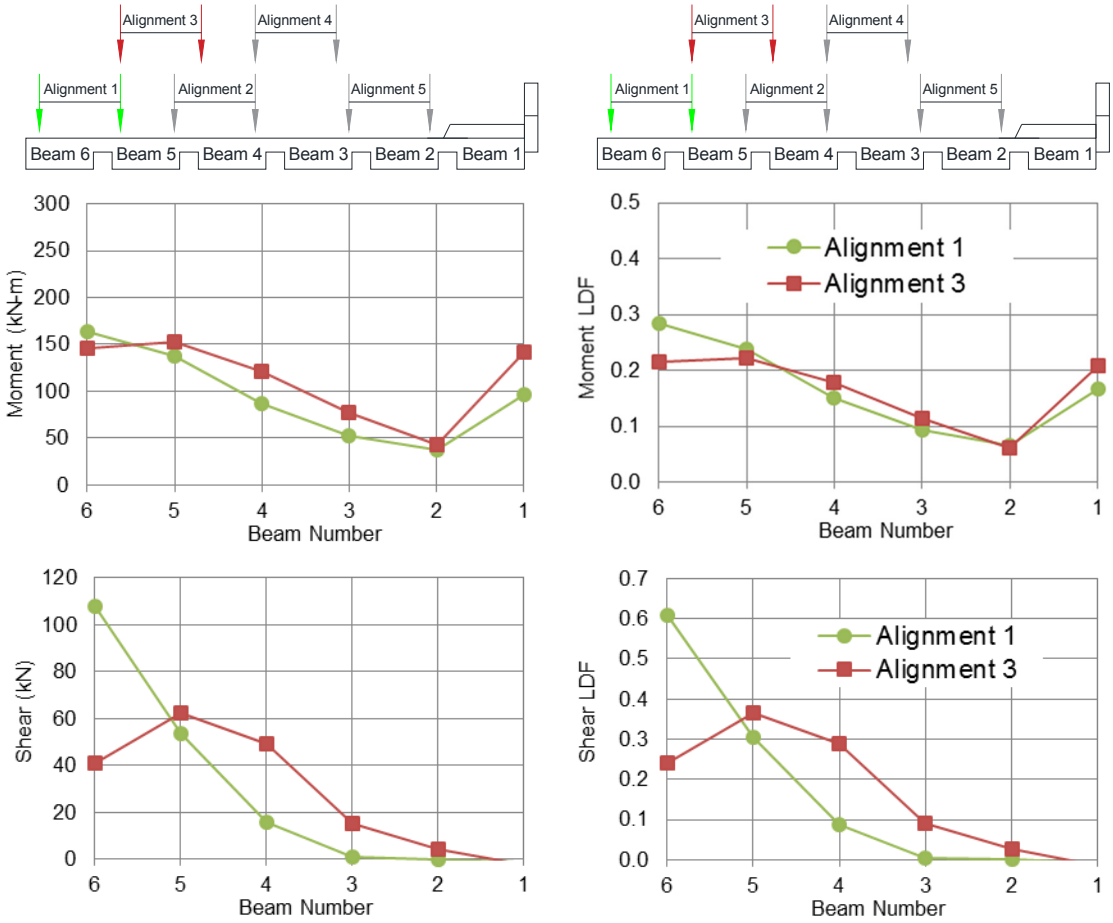

(a) Moment and Shears *(b) LDFs for Moments and Shears*

Figure 3.4. LDF Results for Critical Static Load Cases. Alignments 1 and 3 give the maximum moments and shears for exterior and interior slab beams, respectively.

Table 3.3. Moment Distribution Factors Based on Strain Gauge Data.

Load Case	West Edge					East Edge
	Beam 6	**Beam 5**	**Beam 4**	**Beam 3**	**Beam 2**	**Beam 1**
Alignment 1	**0.284**	**0.239**	0.151	0.093	0.066	0.167
Alignment 2	0.165	0.209	0.217	0.150	0.090	0.169
Alignment 3	0.215	**0.223**	0.178	0.114	0.062	0.209
Alignment 4	0.106	0.131	0.158	0.164	0.117	0.325
Alignment 5	0.061	0.072	0.098	0.136	0.145	**0.488**

Table 3.4. Experimental Shear LDFs Based on Bearing Pad Deformation.

Load Case	West Edge					East Edge
	Beam 6	**Beam 5**	**Beam 4**	**Beam 3**	**Beam 2**	**Beam 1**
Alignment 1	**0.609**	0.304	0.088	0.006	0.001	-0.007
Alignment 2	0.093	0.276	0.356	0.200	0.075	0.000
Alignment 3	0.242	**0.366**	0.289	0.090	0.026	-0.013
Alignment 4	0.031	0.125	0.271	0.328	0.193	0.052
Alignment 5	0.000	0.035	0.117	0.298	0.358	0.192

3.5.2 Dynamic Amplification Effects

In the controlled dynamic load tests, the structural responses were recorded by several types of sensors when the vehicle passed over the bridge for the considered load cases, including two different lanes at various truck speeds. Also, the reference static moment and shear critical lane-load cases were conducted during the test process. By comparing the results for both the static and dynamic load responses, it is possible to evaluate dynamic amplification effects.

Figure 3.5 shows a comparison of bridge behavior under static and dynamic loads. Strain values measured at the midspan soffit, bearing pad deformations at the north support, and deflection values at midspan were used to infer moment and shear LDFs. The left column shows the results when the truck was driven along the middle lane while the right column shows the results when the truck was driven along the right lane. It is evident that as truck speed increases the observed resistance to the moving load also increases, particularly for those beams resisting the maximum moments (given by both strain and deflection) and the maximum shear (given by bearing pad deformations). It is noted however, that while there are modest differences in the resulting LDFs, in essence the LDFs do not markedly change with vehicle speed. This is consistent with present design philosophy where dynamic effects are treated as a magnification of the applied static load. AASHTO (2012) applies a uniform magnification of 33 percent to account for dynamic effects which is independent of vehicle speed. From the results presented in Figure 3.5 it is evident that dynamic magnification of moments and shears increases with velocity for this class of spread slab beam bridges. This aspect is considered further in what follows.

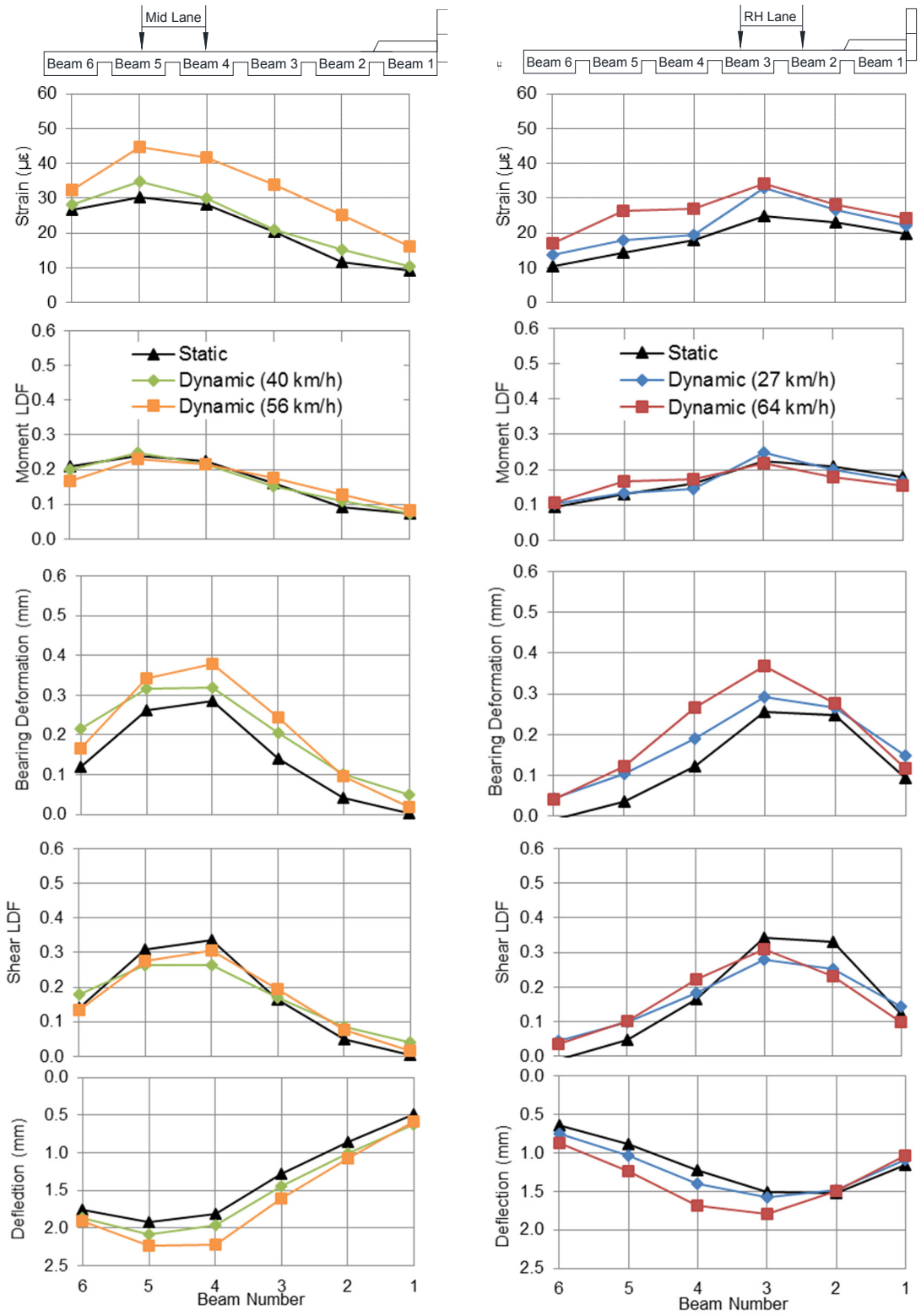

Figure 3.5. Comparative Results for Static and Controlled Dynamic Test.

3.6 DISCUSSION

Based on the 9.3 m roadway width for the tested bridge, AASHTO (2012) design requirements classify the span as a two-lane bridge. Therefore, herein the critical effects of two-lane loading are considered. The moment and shear LDF curves when two trucks are loaded simultaneously are shown in Figure 3.6(a) and (b), respectively. The red dashed line represents the LDF values specified by the AASHTO LRFD formulas for a spread box beam bridge with the same geometric properties. From Figure 3.6(a) and (b) it is evident that the combination of Alignments 1 and 2 loaded provides the largest moment and shear design demands for both the exterior Beam 6 and interior Beam 5. The exception to this is due to the stiffening effect of the sidewalk and guardrail at Beam 1. The bar graphs in Figure 3.6 show critical combinations for (c) moments and (d) shears in the exterior and interior beams compared to the AASHTO formulas. Evidently, the AASHTO spread box beam formulas are somewhat conservative for assessing design moments and unconservative for edge beam shear forces.

The existence of supplemental sidewalk and guardrail elements not only stiffens the edge Beam 1, but markedly increases the moment demand. This is not effectively accounted for in the AASHTO bridge design process. On the other hand, in terms of shear action, the code-specified value for the stiffened beam section is much larger than experimental values and it shows that the secondary elements relieve the shear demand. Clearly the AASHTO design formulas have been derived for a “clean” bridge with no additional stiffening effects. It is evident that when the presence of a thicker slab

(sidewalk) or an edge stiffening element (either median or guardrail) the normal design process should be handled with caution.

Figure 3.7 shows the dynamic amplification effects with different vehicle speeds. The AASHTO impact factor (1.33) is represented by black horizontal dashed line. The moment, shear, and deflection data points were determined with measurements from strain gages, string potentiometers, and LVDTs, respectively. It is evident that as the vehicle speed increases, so do the dynamic moment and shear demands. It is of concern that the code-based uniform impact is unconservative for a normal operating speed above 50 km/h for this bridge, which is common for most bridges. It is suggested that until this aspect of vehicle-structure interaction is better understood for this class of short span bridges, a more conservative approach to the service load design be adopted. For example, it is suggested that the allowable tensile stress for a no-crack design criteria be reduced from $f_t = 0.625\sqrt{f_c'}$ (MPa) and restricted to $f_t = 0.5\sqrt{f_c'}$ (MPa).

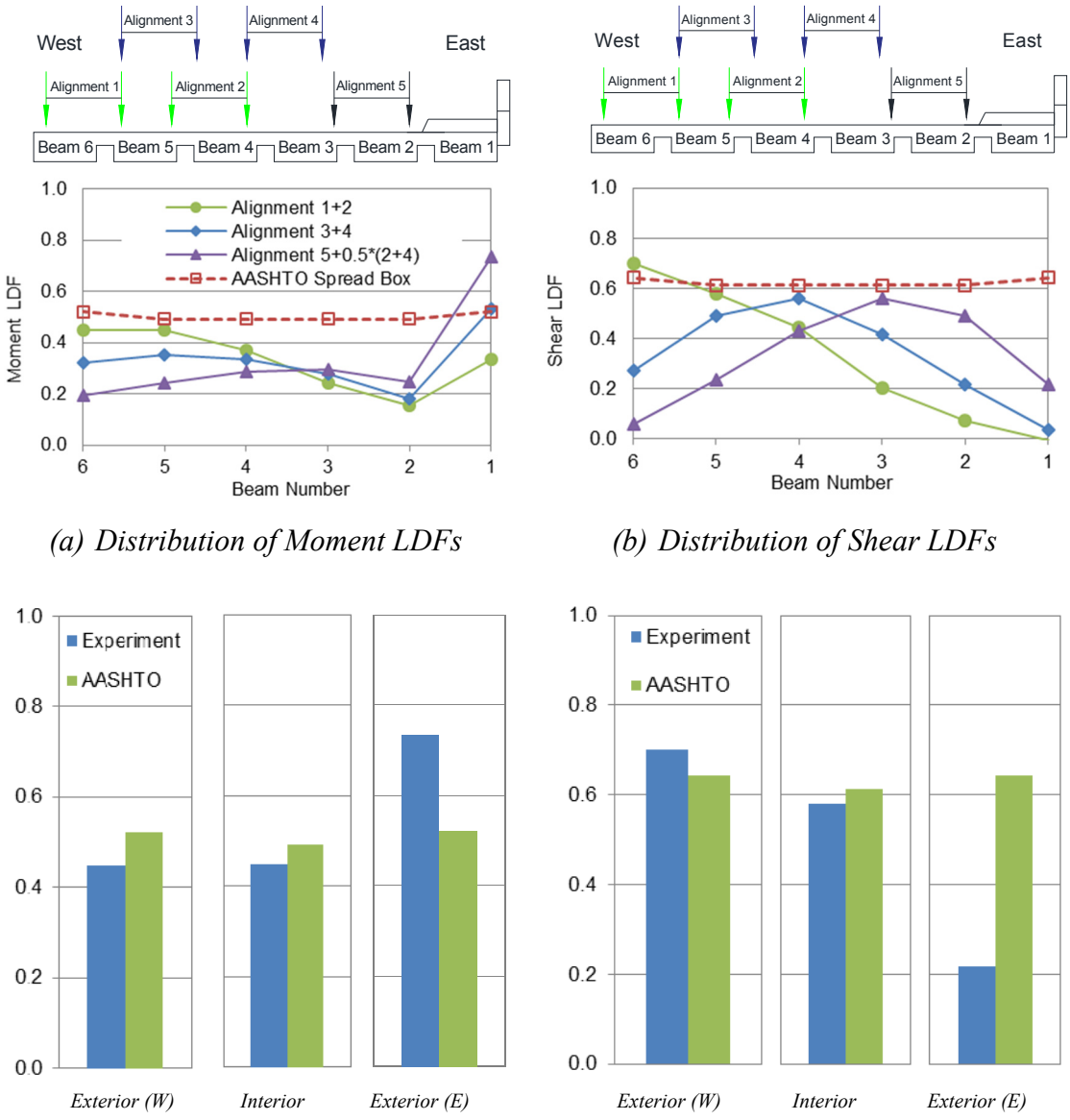

(a) Distribution of Moment LDFs

(b) Distribution of Shear LDFs

(c) Critical Moment LDF

(d) Critical Shear LDF

Figure 3.6. Combined Load Cases for Critical Moment and Shear LDFs.

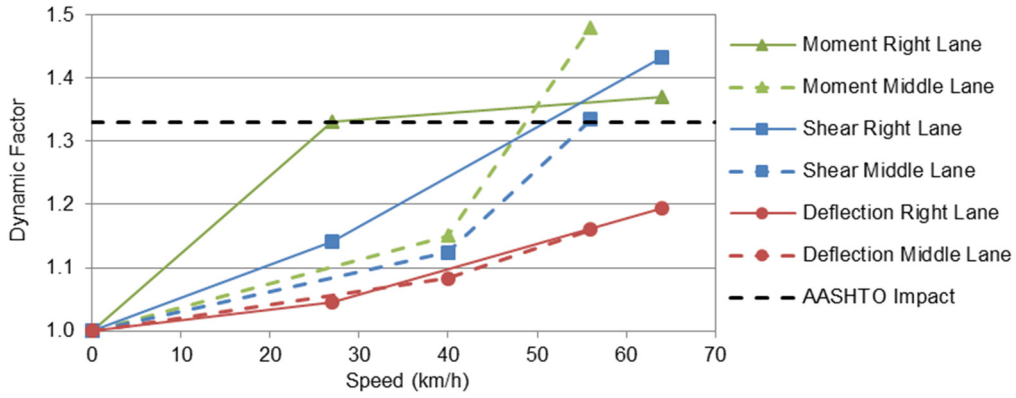

Figure 3.7. Dynamic Amplification Factors with Various Instrument Measurements.

3.7 CLOSURE AND KEY FINDINGS

Comprehensive static and dynamic tests were conducted on the US 69 northbound bridge over Day Street in Denison, Texas, to investigate the in-service performance and load distribution behavior of the spread slab beam bridge system. Several types of instruments (strain gages, LVDTs, string potentiometers, and accelerometers) were installed on the bridge to measure the structural responses under static and dynamic vehicular loading. By analyzing the data collected from all tests, the following findings are achieved for this specific bridge geometry.

1. From the experimental tests conducted, it was shown that the presently used design methods are conservative for moment LDFs and unconservative for shear LDFs for the edge beams in particular.

2. The existence of integrally cast sidewalk and guardrail elements not only stiffens the edge beam, but markedly increases the moment demand for such beams. This is not effectively accounted for in the AASHTO bridge design process. In terms of shear action, the secondary elements relieve the shear demand. With the presence of a thicker slab (sidewalk) or an edge stiffening element (either median or guardrails) the normal design process should be handled with caution.
3. As the vehicle speed increases, so do the dynamic moment and shear demands while the LDFs do not markedly change with the vehicle speed. It is shown that the code-based uniform impact factor of 1.33 was unconservative for the tested bridge at speeds above 50 km/h. Until this aspect of vehicle-structure interaction is better understood, a more conservative approach to the service load design is recommended for this class of short span bridge. For example, it is suggested that the allowable tensile stress for a no-crack design criteria be restricted to $f_t = 0.5\sqrt{f_c'}$ (MPa).

4 COMPUTATIONAL ANALYSIS OF SPREAD SLAB BEAM BRIDGES

4.1 SUMMARY

In order to computationally model the moment and shear design actions and hence investigate the load distribution behavior for this new class of spread slab beam bridge system, several modeling strategies are explored in this section. The different computational techniques considered in this research include the historic grillage analysis and the more computationally rigorous finite element method (FEM). Comparative accuracy with physical test results is examined for a similar class spread box beam bridge (Drehersville Bridge) tested in 1966, and the tested spread slab beam bridge described in Section 3. Based on comparisons between experimental and computational results, it is shown that while each considered method is arguably valid, improved accuracy is achieved when a higher level of computational rigor is used. In the analysis process, given the ease of developing and applying advanced computational solutions, bridge engineers should use the best available analysis tools.

4.2 INTRODUCTION

A new class of low profile short-span bridges has been developed by the Texas Department of Transportation (TxDOT). Known as a spread slab beam bridge system, this new bridge type has been developed as an economical and practical design and construction alternative to box beams used in short spans. An in-service prestressed concrete spread slab beam bridge has been instrumented and recently tested. The experimental findings provide valuable information on load distribution behavior, structural performance and construction requirements (Hueste et al. 2015). Due to the absence of specific guidelines in the AASHTO LRFD Bridge Design Specifications (2012), the most appropriate class of load distribution factors for design remain ill defined. Therefore, a computational study has been conducted to investigate the load distribution behavior by utilizing different computational modeling techniques, including grillage and finite element analysis.

The grillage method is a simplified method of analysis in which the girders and deck slab of the bridge structure are assumed to be a mesh of beam elements in two orthogonal directions. This is the most basic computational modeling approach for long and wide structures that are loaded out-of-plane. By modeling the bridge superstructure as an equivalent grillage of rigidly connected beams at discrete nodes, the number of degrees of freedom within a single bridge span is quite small, and the load transfer mechanism of the span is somewhat simplified. This simplified method of analysis lowers computational complexity and decreases the time and effort needed for modeling and computation. Lightfoot and Sawko (1959) pioneered the grillage method of analysis by writing

computer programs to solve the grid framework problem. Hambly (1976) provided guidelines for developing an accurate grillage configuration for bridge superstructures, including grillage mesh generation, grillage member properties determination and load application. Over the years, the grillage method has been popularized and its application expanded to various bridge types including steel and prestressed concrete I-girder bridges, and box girder bridges (Hueste et al. 2006; Schwarz and Laman 2001).

In contrast to the historical method for establishing load distribution factors using a grillage analysis, the finite element method (FEM) is a more exacting approach where fewer approximations and simplifications are necessary. The FEM permits the bridge engineer to accurately investigate structural behavior in a more direct fashion. For slab-on-girder bridges, full three-dimensional (3D) analyses require significantly more degrees of freedom and a higher level of refinement to realistically represent normal bridge geometries. The FEM technique has been widely applied in the design and analysis of bridge superstructures. A large number of element types are available based on different element degrees-of-freedom and relevant characteristics such as beam element, shell element and isoparametric brick elements. Naturally, the choice of element depends on the actual disposition of the bridge topology (Barr and Amin 2006; Eom and Nowak 2001; Tarhini and Frederick 1992). Abundant recommendations and guidelines for properly developing 3D FEM models for normal bridge types may be found in the literature (Barker and Puckett 2013; Puckett et al. 2005; Zokaie et al. 1991).

In this section, two contemporary commercial FEM software packages are used and the results are compared herein. Abaqus (Version 6.13) (Dassault Systemes 2013) is

a general purpose FEM code used for solving a broad range of advanced problems in various fields of engineering. CSiBridge (Version 15) (Computers and Structures 2013), which is from a similar software suite to SAP2000, is more specific for bridge engineering.

It should be noted that both tested spread slab beam bridges (Riverside and US 69 Bridges) in Project 0-6722 were modeled with grillage and FEM approaches (Hueste et al. 2015). The modeling techniques were validated and improved by comparisons with test results. This section emphasizes on the computational modeling and results analysis of the US 69 Bridge

4.3 VERIFICATION OF COMPUTATIONAL TECHNIQUES

Prior to developing computational solutions for the tested spread slab beam bridge described in Section 3, it is considered prudent to conduct methodological verification analyses on known test data provided from other independent historic research work. Grillage and FEM models were developed for the Drehersville Bridge, a spread box beam structure located in Pennsylvania crossing the Little Schuylkill River. The Drehersville Bridge was instrumented and tested in 1966 as part of a Lehigh University research project to investigate the transverse distribution of static loads (Douglas and VanHorn 1966), and test data is available to validate the results of computational models developed herein.

4.3.1 Background

Figure 4.1 presents the transverse section and elevation view of the Drehersville Bridge. The superstructure consists of three simply supported spans with no skew angle. The right end span was instrumented and tested. This span has a length of 18.8 m from center to center of the bearing pads and a roadway width of 9.1 m. The structural components for the Drehersville Bridge include five prestressed concrete box-beam girders in a spread configuration, a reinforced concrete deck, sidewalks and parapets on both sides, and diaphragms at midspan and both ends. The box-beam girders have an overall depth of 838 mm and an overall width of 1219 mm with a web thickness of 127 mm. The bridge deck is specified as 191 mm thick and the diaphragms are 254 mm thick and as deep as the box beams. The elastic modulus for the box beam concrete was experimentally obtained as $E_b = 47$ GPa. The deck strength was assumed to be $f_c^{'} = 35$ MPa and the calculated elastic modulus was $E_d = 40$ GPa. These values were adopted in the grillage and FEM analyses for this bridge.

The transverse location of the axle loads was determined in a test-alignment format as shown in Figure 4.1(a), where there were seven possible transverse stations. Figure 4.1(b) shows the longitudinal location of the applied truck loads, in which the vehicle was placed with their central axles at the location of Section M during the test process to create the maximum moment.

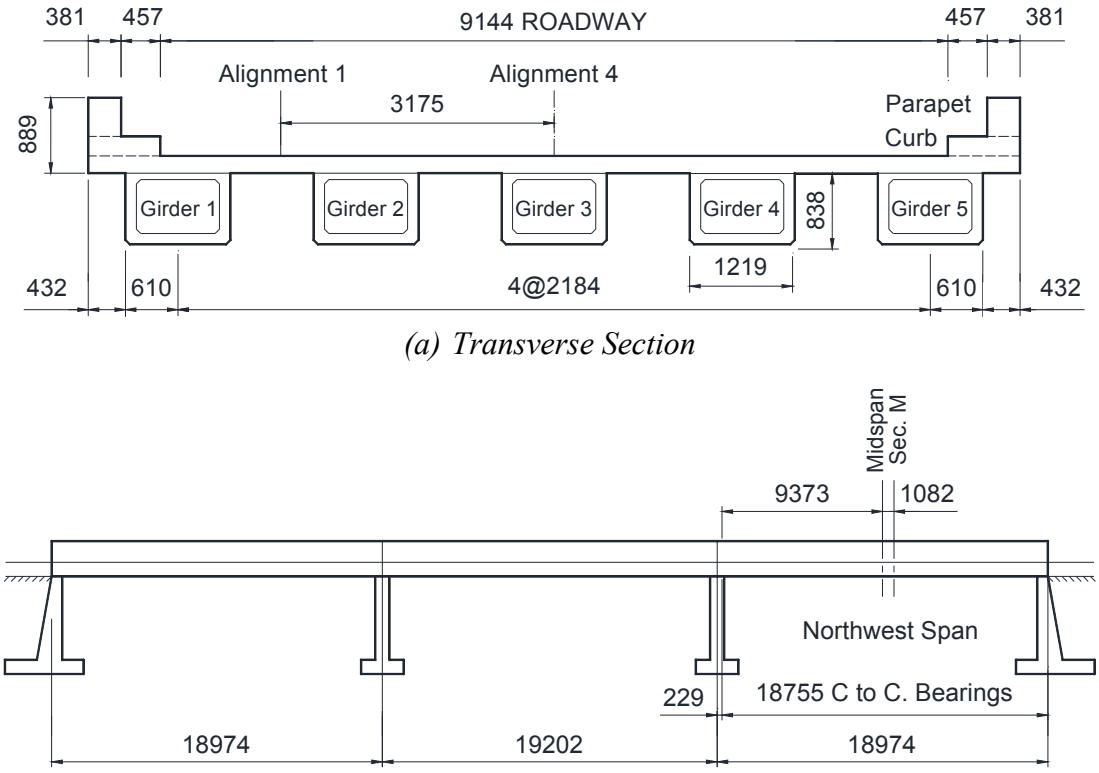

(a) Transverse Section

(b) Elevation View

Figure 4.1. Geometric Information for the Drehersville Bridge (Adapted from Douglas and VanHorn 1966).

4.3.2 Computational Modeling and Results

The grillage model was set up with frame elements using the commercial software SAP2000. There were five longitudinal grillage members representing each prestressed box beam and 11 grillage members in the transverse direction. The finite element method (FEM) model was developed with solid brick elements using the commercial software Abaqus (Dassault Systemes 2013). Another finite element model developed by Hueste et al. (2015) using CSiBridge is also described herein for comparison purpose. Figure 4.2 depicts the grillage and FEM models for the Drehersville Bridge. It is noted that the guardrail was also modeled with the Abaqus software while the CSiBridge model didn't consider its effect.

Results of only two load cases are discussed herein for the sake of brevity. The Alignment 4 load case is a central load, thus computational moment results are symmetric about the longitudinal centerline of the bridge. The Alignment 1 plus Alignment 4 load case provides the maximum exterior girder moment due to eccentric vehicle load. Figure 4.3 depicts the final comparison between different modeled moment results and the experimental values as a graphical representation. It is shown from Figure 4.3(a) that both grillage and FEM solutions give reasonably accurate moment results when the vehicle was loaded on Alignment 4. The FEM solution, especially the Abaqus model, gives more accurate LDFs for both the exterior and interior box beams when compared to the test results. However, for the case when both Alignments 1 and 4 were loaded simultaneously, it is evident from Figure 4.3(b) that the grillage model more accurately captured the girder moments and LDFs than the FEM solutions. Especially for exterior girder 1, the LDFs

determined from FEM are around 30 percent lower than the test results, which is an unconservative outcome. In addition, it is shown that while the errors of the absolute force values may be significant in some cases, the LDF errors are smaller.

4.4 COMPUTATIONAL MODELING OF THE US 69 BRIDGE

4.4.1 Grillage Model

As described in Section 3, comprehensive static and dynamic tests were performed on the US 69 Bridge to investigate the structural performance in general and the load distribution behavior in particular for this new class of spread slab beam bridges. Various experimental methods were used to infer the moments and shear forces resisted by individual beams that arise from a heavily loaded truck. During the field test, no major cracking or reduction in the overall stiffness of the bridge superstructure was observed for the US 69 Bridge. Because the tested bridge remained in its linear elastic range of behavior, elastic analyses utilizing both grillage and finite element methods were conducted to replicate the actual applied loading during the field tests.

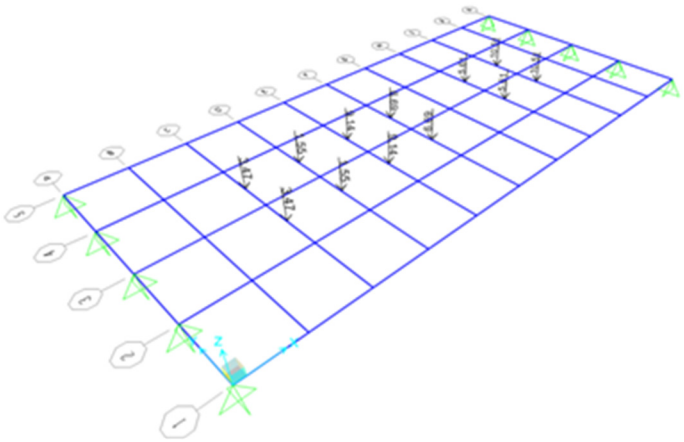

(a) Grillage Model

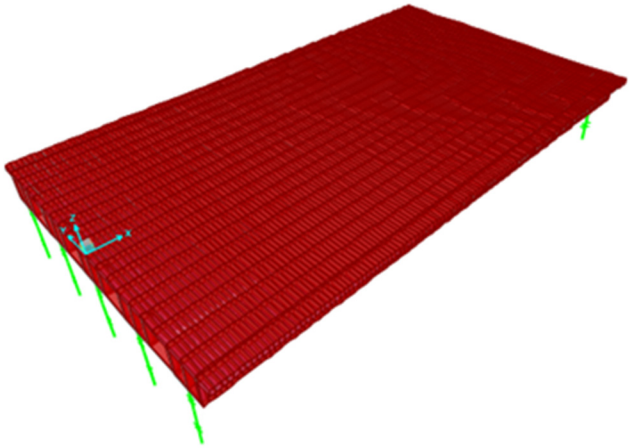

(b) CSiBridge FEM Model (Hueste et al. 2015)

(c) Abaqus FEM Model

Figure 4.2. Grillage and Finite Element Models for Drehersville Bridge.

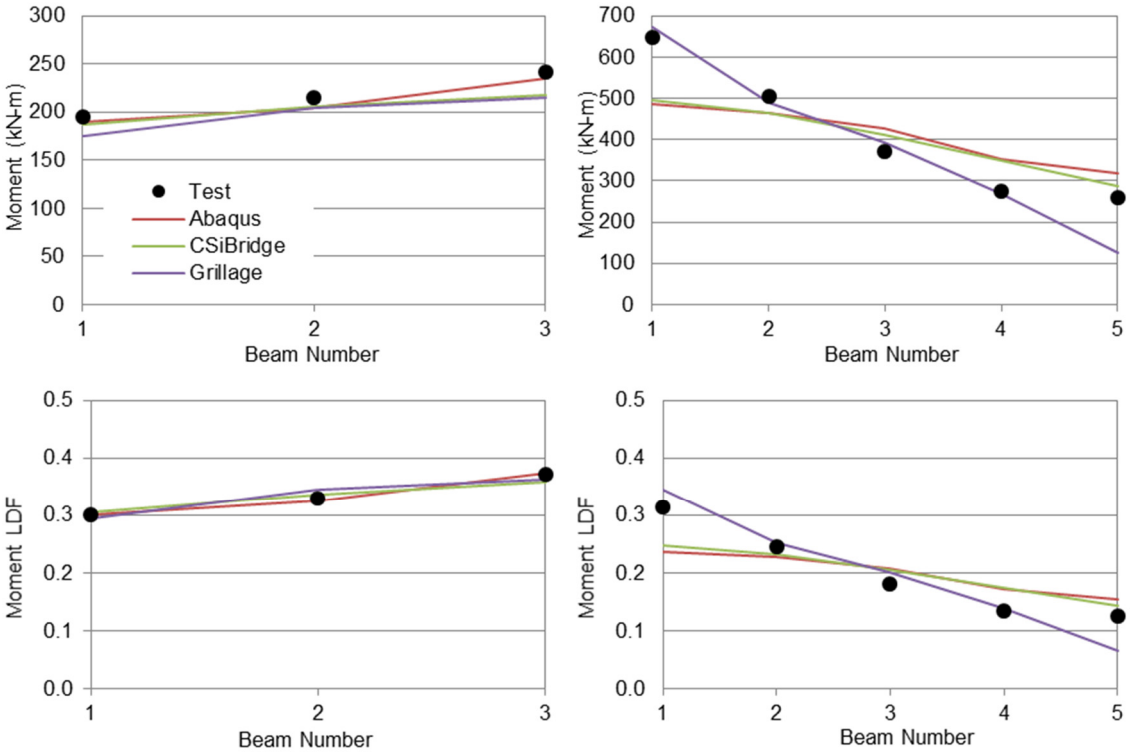

(a) Alignment 4 Loaded *(b) Alignments 1 and 4 Loaded*

Figure 4.3. Drehersville Bridge Moment and Moment LDF Comparison.

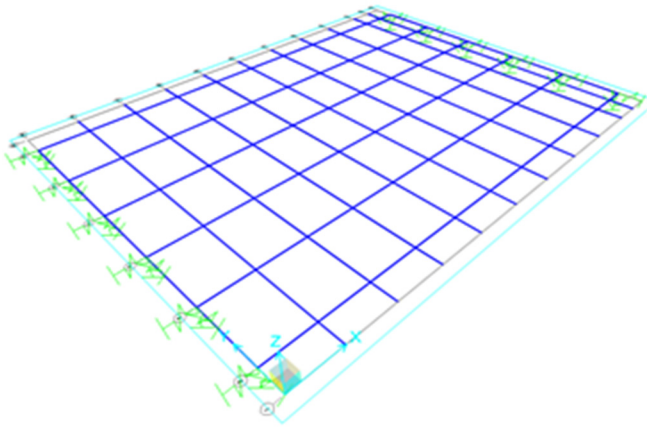

(a) Grillage Model

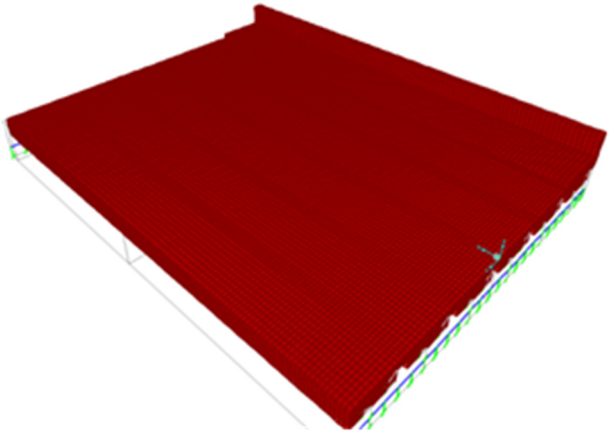

(b) CSiBridge FEM Model

(c) Abaqus FEM Model

Figure 4.4. Grillage and Finite Element Models for US 69 Bridge.

Figure 4.4(a) presents the grillage topology for modeling the US 69 Bridge. For the spread slab beam bridge superstructure, one longitudinal member was used to represent each slab beam girder, regardless of the spacing of the girders. Longitudinal grillage members were modeled as a composite T-beam section including the slab beam and deck. The section designer function in SAP2000 was used to correctly reflect actual section properties. In the transverse direction, grillage members were placed to distribute the applied bridge deck loads such that the spacing between transverse grillage members was less than 10 percent of the overall span length. The transverse grillage members were modeled as rectangular sections representing the 254 mm thick deck. The tributary width of the interior transverse member section was taken as the center-to-center spacing of each transverse grillage member, while for the end two transverse beam sections 50 percent of the spacing was used as the section width. It should be noted that the sidewalk and guardrail were considered to be fully composite with the deck thus forming a stiffer edge section along the east edge of the US 69 bridge.

Elastomeric bearing pads were placed between the soffit of the slab beams and the top surface of the abutments or piers. A series of tests that were conducted on this standard bearing pads in the laboratory showed that the pads performed in an essentially linear fashion over the applied vehicular loading range (Hueste et al. 2015). In the modeling process, the bearing pads were considered as linear springs in three dimensions to simulate the field conditions of the test bridge. Rotational restraints were released in the model.

The locations of the applied loads for the grillage models were taken to be the same as the positions of the truck wheels in the different load cases. However, the actual applied

test loads were often not concentric with the grillage nodes or members. To accomplish the same loading in the grillage model as on the physical bridge test, the actual loads were proportionally distributed to the nearest surrounding grillage members by use of the lever rule to give the equivalent net effect. In particular, an additional transverse grillage beam member was placed at the last rear tire location, 0.6 m away from the span end, in order to apply the vehicle load directly in the shear-critical location. It is evident from a sensitivity study that this arrangement could successfully improve the modeling accuracy. Given that it was necessary to apply wheel loads external to the centerline of the exterior slab beam in some load cases, near-rigid transverse grillage member extensions were added to apply wheel loads at the same locations with the physical structure.

4.4.2 Finite Element Model

The three-dimensional brick element was adopted in modeling the US 69 Bridge with the FEM technique. In the Abaqus commercial software, the C3D8R element is a general purpose linear eight-node brick element with three degrees of freedom at each node. This element type was used to model both the slab beams and deck slabs of the tested bridge. For the CSiBridge software, the eight-node isotropic solid element having three degrees of freedom at each node was available to model the different components of the tested bridge. Based on the mesh sensitivity study results, the mesh of each model was generated with 6 in. evenly spaced nodes. The effects of the secondary members (sidewalk and guardrail) were also taken into consideration in the analysis procedure. Figure 4.4(b) and (c) illustrate the CSiBridge and Abaqus finite element models for the tested bridge.

Wheel loads were applied on the deck surface based on the actual vehicle positions during the test. Small areas similar to the tire contact surface were defined in the FEM models to place the vehicle loads uniformly. As mentioned previously, bearing pads at both ends were modeled as vertical and horizontal springs. Three-dimensional FEM solutions were developed based on the design drawings and actual on-site conditions for the tested bridge using the well-known general purpose commercial software Abaqus and the more industry specific software CSiBridge. In the modeling, the sidewalk and guardrail were modeled and considered to be fully composite with the reinforced concrete deck. The deck and slab beam concrete are defined as elastic material in the finite element models. Based on the early concrete strength measured at the plant of $f_c^{'} = 79$ MPa, the age-adjusted modulus for the slab beam concrete is estimated as $E_b = 54$ GPa. Similarly the deck concrete modulus is estimated as $E_d = 35$ GPa. These values were adopted in the analysis for the US 69 Bridge.

4.5 COMPUTATIONAL RESULTS FOR THE US 69 BRIDGE

4.5.1 Static and Dynamic Properties

Figure 4.5 shows the comparison of the experimental and computational deflection profiles for all slab beams under critical static load cases. The numbering of the slab beams is provided in Figure 3.1. Deflections were directly obtained from string potentiometer measurements beneath the bridge deck as represented with open symbols in Figure 4.5. The FEM values computed from Abaqus and CSiBridge are represented as solid and dash lines. The small deflection values measured near the north end show some random

variations with the computed deflections. These deviations are attributed to the measurement quality and accuracy. The resolution of the string potentiometer measurements is around 0.2 mm. Overall, it is evident that the FEM solution provides reasonable agreement with the measured deflection field; differences are generally less than 0.3 mm for most load cases.

Perhaps more challenging than capturing the deflection field is to accurately model the dynamic properties of the bridge. Table 4.1 lists a comparison of experimental and FEM computed first three natural frequency values (f_1, f_2, and f_3) for the bridge span. Experimentally observed natural frequencies and mode shapes were identified from accelerometer readings during the controlled dynamic tests. It is shown that the computed natural frequency values show promise as compared to the observed data. In particular, the first and second natural frequencies predicted by Abaqus and CSiBridge are close to each other, but some differences exist for the third natural frequency. Figure 4.6 presents a comparison between the FEM computed and experimentally derived first three mode shapes. Note that Abaqus solutions are shown here with solid lines as representative of FEM results. It is evident that satisfactory agreement is achieved. In summary, it is concluded that because satisfactory agreement exists between the measured deflection field as well as the dynamic mode shapes and natural frequencies and the developed FEM model, the model is therefore valid for use in other computational comparisons of the moment and shear actions and the corresponding LDF values.

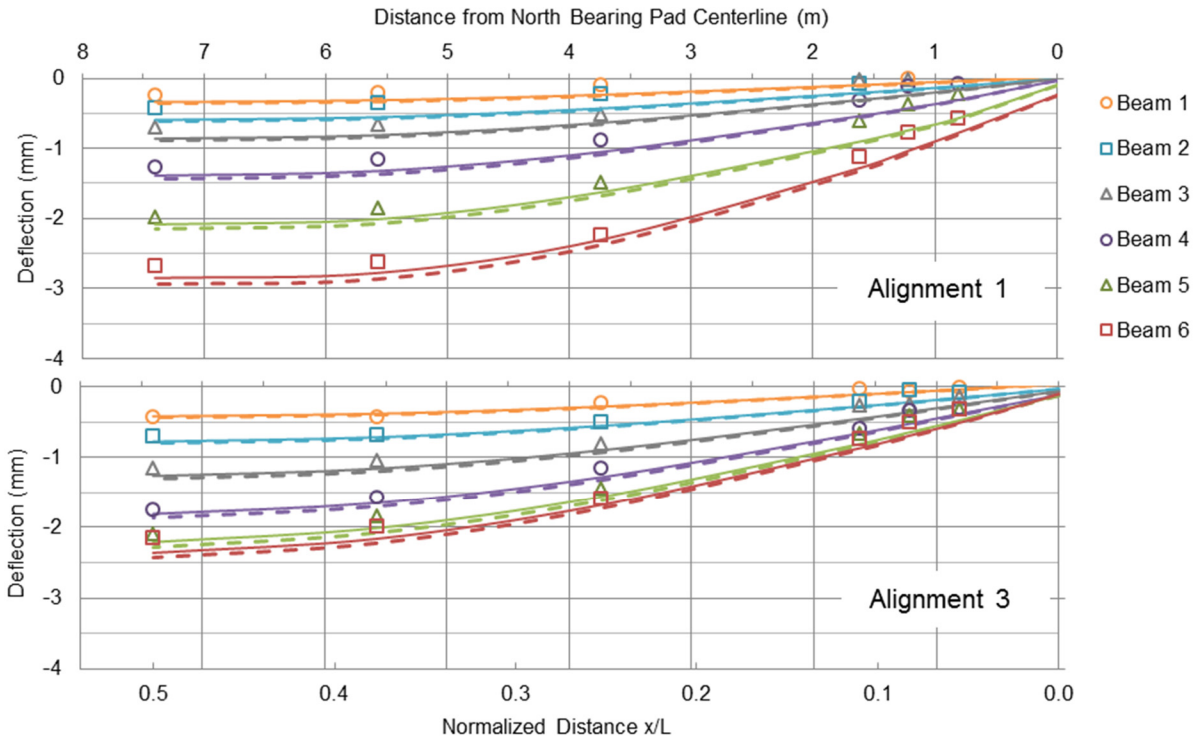

Figure 4.5. Static Deflection Curves for Moment Critical Load Cases.

Table 4.1. Comparison of the Experimental Observed and Computational Natural Frequencies.

Lane	Speed (km/h)	f_1 (Hz)	f_2 (Hz)	f_3 (Hz)
1	27	6.35	9.28	14.7
2	40	5.86	9.28	15.1
3	56	6.10	9.28	14.8
4	64	6.10	9.16	14.9
Average	-	6.10	9.25	14.9
FEM (Abaqus)		6.07	8.54	13.3
Ratio = Abaqus/Test		0.99	0.92	0.89
FEM (CSiBridge)		5.92	8.38	15.2
Ratio = CSiBridge/Test		0.97	0.90	1.02

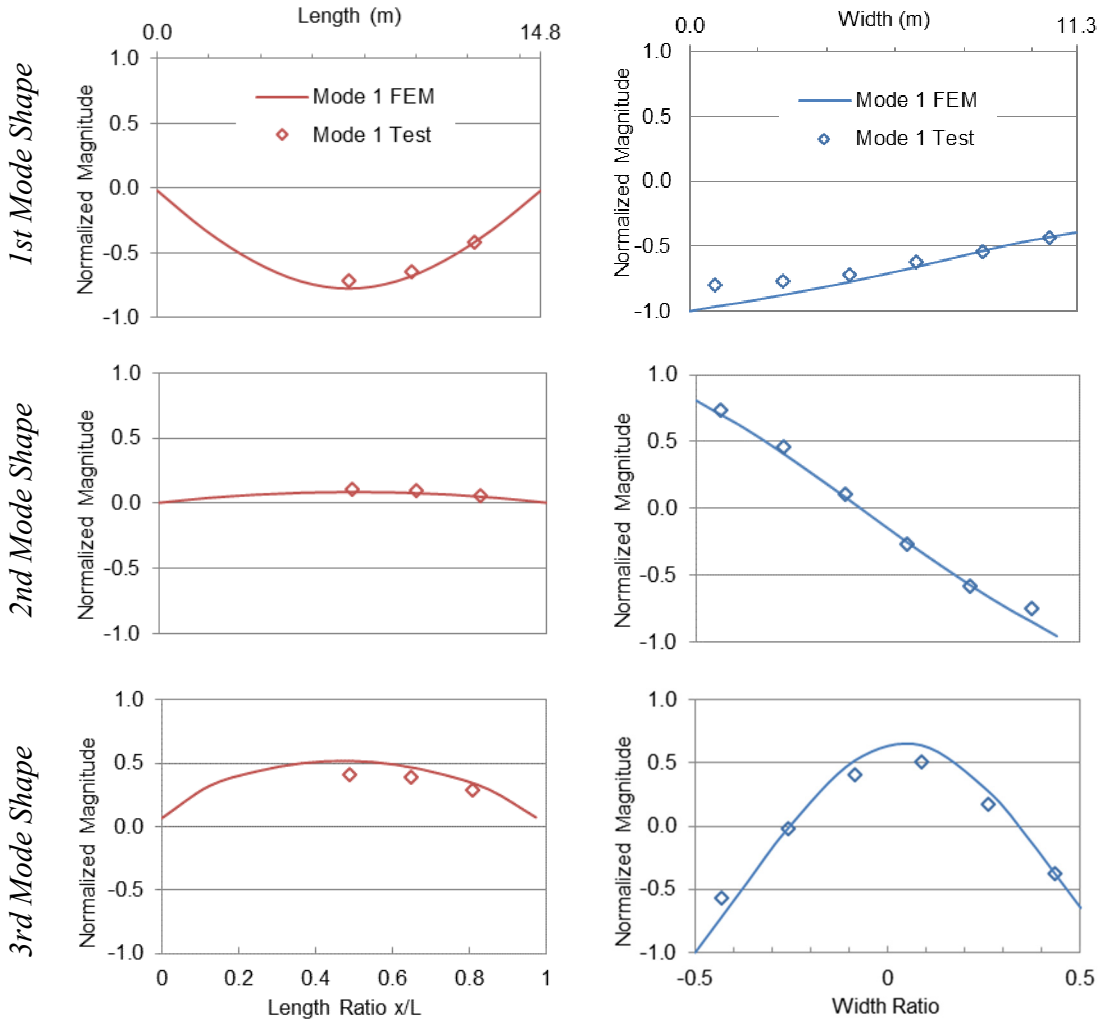

(a) Longitudinal Direction *(b) Transverse Direction*

Figure 4.6. First Three Mode Shapes in Longitudinal and Transverse Directions.

4.5.2 Moment, Shear and LDF Results

Figure 4.7 depicts the comparison of moment and the companion LDF curves determined from field test and computational analysis. It is evident that FEM solutions show promise when compared with the observed field test results, and the moment distribution curve obtained from two different FEM codes (Abaqus and CSiBridge) are close. While some differences exist between the grillage model and observed test values, especially in the moment-critical load case when the dump truck was parked along Alignment 5, the LDFs from the grillage model are unconservative for the exterior beam composite with sidewalk and guardrail. The shear force and LDF curves calculated from grillage and FEM models are close to experimentally observed values as shown in Figure 4.8. In general, the computed solutions agree quite well when compared with shear forces and inferred LDFs based on the experimental field test results. The shear force curves determined from grillage models are closer to experimental observations for the three different load cases.

Table 4.2 provides critical maximum moment and shear values for both exterior and interior slab beams for the US 69 Bridge; the companion LDF values are listed in Table 4.3. It is evident from Table 4.3 that the FEM LDF results are similar to the test results in most load cases. However, for the east exterior slab beam that has the sidewalk and guardrail, the CSiBridge predicts a somewhat (+40%) higher value than the test result. For the grillage model, the moment LDF for the east exterior beam is unconservative (-10%) compared with the experimental value. By comparing the difference in the values listed in Tables 4.2 and 4.3, it is shown that while the errors of the absolute values may be significant in some cases, the LDF errors are smaller.

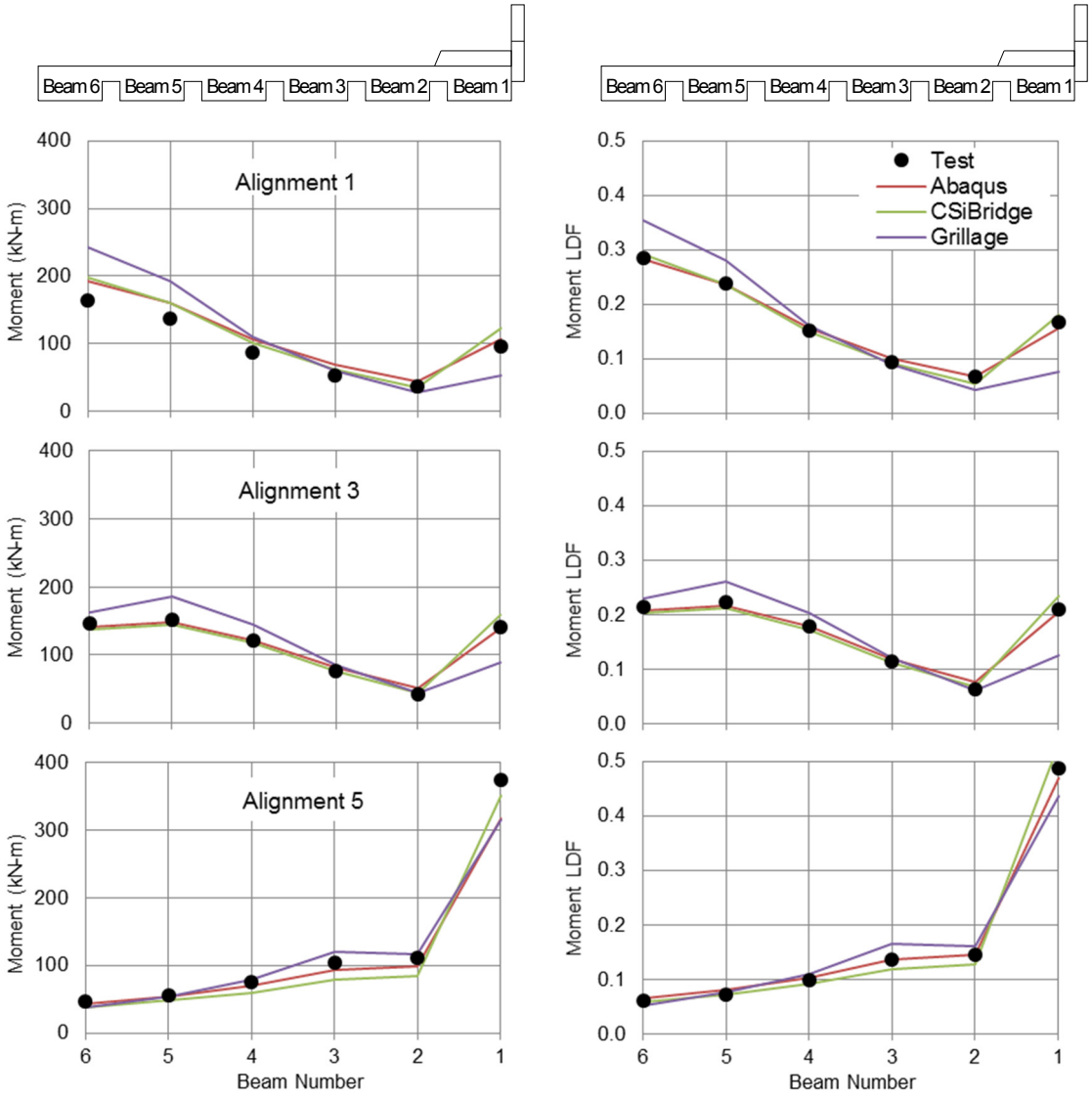

(a) Moment Values *(b) Moment LDF Values*

Figure 4.7. Comparison of Experimental and Numerical Moment Values and Moment LDFs.

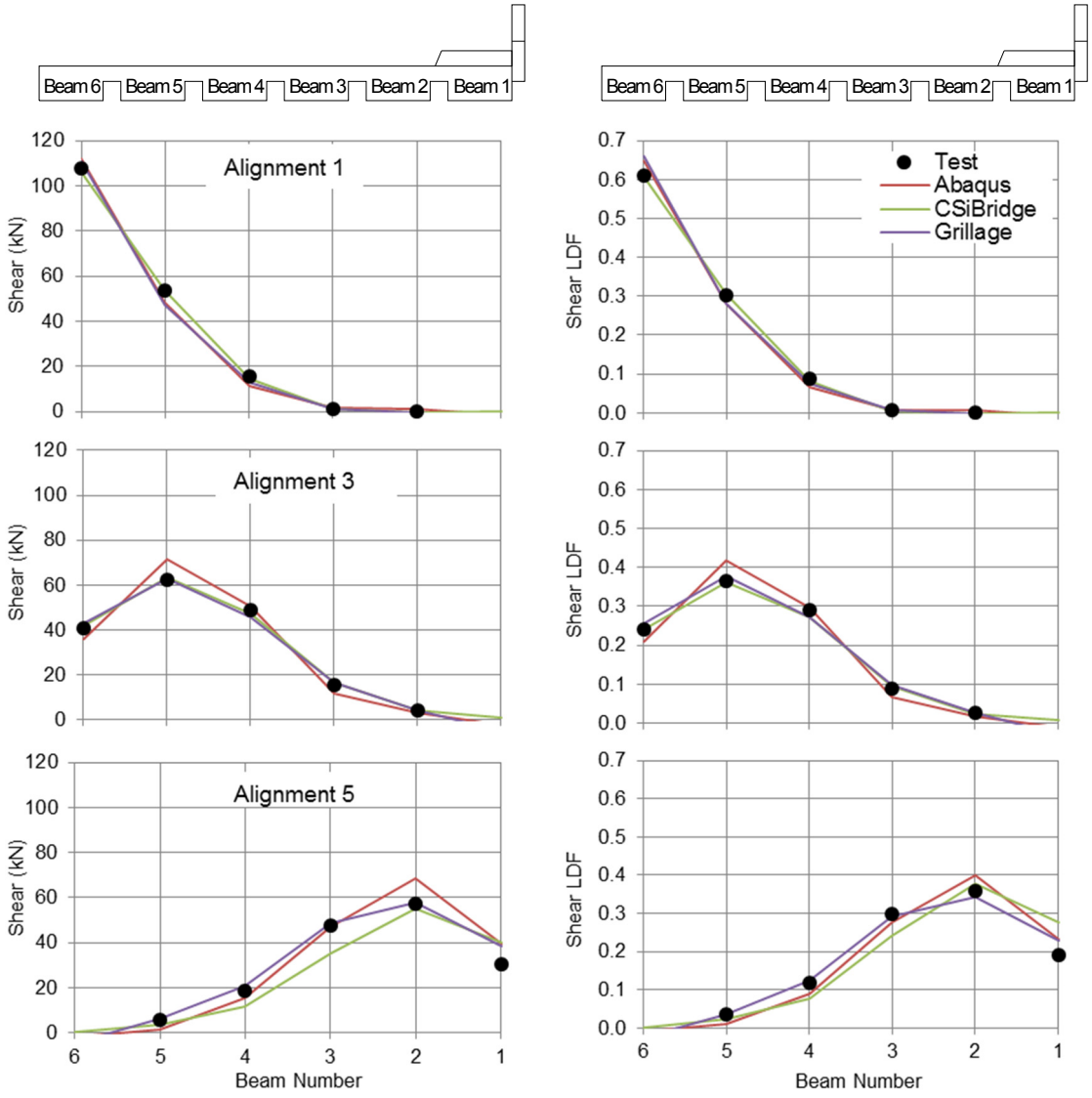

(a) Shear Values *(b) Shear LDFs*

Figure 4.8. Comparison of Experimental and Numerical Shear Values and Shear LDFs.

Table 4.2. Summary of Key Moment and Shear Values

Load	Beam	Item	Test	Abaqus	CSi	Grillage
Moment Critical	Exterior (West Edge)	Moment (kN-m)	163.7	192.3	197.7	243.6
		Difference	-	+17%	+21%	+49%
	Interior	Moment (kN-m)	137.4	161.2	160.2	192.4
		Difference	-	+17%	+17%	+40%
	Exterior (East Edge)	Moment (kN-m)	374.0	317.8	351.1	315.1
		Difference	-	-15%	-6%	-16%
Shear Critical	Exterior (West Edge)	Shear (kN)	107.7	111.8	106.0	110.8
		Difference	-	+4%	-2%	+3%
	Interior	Shear (kN)	62.2	71.3	63.3	63.1
		Difference	-	+15%	+2%	+1%
	Exterior (East Edge)	Shear (kN)	30.5	39.6	40.3	38.3
		Difference	-	+30%	+32%	+26%

Table 4.3. Summary of Key LDF Results.

Load	Beam	Item	Test	Abaqus	CSi	Grillage
Moment Critical	Exterior (West Edge)	LDF	0.28	0.28	0.29	0.35
		Difference	-	0%	+4%	+25%
	Interior	LDF	0.24	0.24	0.24	0.28
		Difference	-	0%	0%	+17%
	Exterior (East Edge)	LDF	0.49	0.47	0.53	0.44
		Difference	-	-4%	+8%	-10%
Shear Critical	Exterior (West Edge)	LDF	0.61	0.64	0.61	0.66
		Difference	-	+5%	0%	+8%
	Interior	LDF	0.36	0.40	0.38	0.35
		Difference	-	+11%	+6%	-3%
	Exterior (East Edge)	LDF	0.20	0.23	0.28	0.23
		Difference	-	+15%	+40%	+15%

4.6 CLOSURE AND KEY FINDINGS

Computational models were developed for a spread box beam bridge (Drehersville Bridge) and the tested spread slab beam bridge (US 69 Bridges) by applying different analysis methods (grillage and FEM) and utilizing different commercial software. By comparing computational results with experimental values, the following conclusions may be drawn:

1. For the spread box beam bridge tested in the 1960s, the grillage model more accurately captured the girder moments and LDFs than the FEM solutions. It is reasonable to simplify this type of bridge as several major longitudinal grillage members due to the comparatively greater box beam depth.
2. In contrast, for the spread slab beam bridge tested as part of the present research, the FEM solutions provide moderately accurate deflections but given the small magnitude of deflection, it is difficult to discriminate where the errors arise; whether they are predominantly from measurement error or modeling simplifications.
3. The FEM LDFs for the tested spread slab beam bridge are similar to the observed test values in most load cases. However, for the east exterior slab beam that has the sidewalk and guardrail, the CSiBridge predicts a somewhat (+40%) higher value than the test result. For the grillage model, some differences exist between computation values and observed test results. In particular, for the exterior beam with sidewalk and guardrail in the US 69 Bridge, grillage analysis provided unconservative (-10%) moment LDFs compared with the experimental values.
4. By developing the models carefully, the historic grillage method could be utilized for

the analysis and design of the spread slab beam bridge. It is recommended that the spacing of transverse grillage member is less than 10 percent of the overall span length. Also, an additional transverse beam member at the loading position could help to improve the analysis accuracy.

5. The general conclusion from this dual experimental and computational study is: given the ease of developing and applying advanced computational FEM solutions, one should use the best available analysis tools. Regardless of the claimed accuracy, it remains prudent to validate results against realistic experimental evidence, if available.

5 LIVE LOAD MODELS FOR HIGHWAY BRIDGE DESIGN

5.1 SUMMARY

Applied live loads plus their dynamic impact effects are one of the major components for highway bridge design. Current HL-93 live load models specified in the AASHTO LRFD Bridge Design Specifications were developed as a notional representation for moments and shear forces generated by permitted vehicles based on truck-survey results. However, design experience indicates that the asymmetric HS20 truck load as part of HL-93 live load model brings inconvenience to determine the maximum moment value and critical load position. In this section, an alternative symmetric live load model is developed in an attempt to provide bridge engineers with a more direct and simpler option for rapid design. For the live load model, moment and shear force envelopes were calculated for a wide range of simple spans. To validate the load effects of the proposed live load model, the "exact" actions generated by the HL-93 live load model are compared.

5.2 INTRODUCTION

In the structural design of highway bridges, there are several major load components including dead load, live load, impact load and other environmental effects (temperature, wind and earthquake). The AASHTO LRFD Bridge Design Specifications designate the live load model as the superposition of the design truck/tandem load and a uniformly distributed lane load, called the HL-93 live load model. This live load model was developed as a notional representation of the load effects produced by permitted vehicles on highways under exclusions to weight laws (AASHTO 2012). The vehicles considered as representative of these exclusions were determined on the basis of a study conducted by the Transportation Research Board (Cohen 1990). The load model is called "notional" because it is not intended to exactly represent a particular truck.

Although it is claimed that the HL-93 live load model could represent the maximum moments and shear forces produced by highway traffic for certain time periods (Nowak and Hong 1991), the asymmetric HS20 truck load brings inconvenience when bridge engineers determine the most unfavorable loading position and the corresponding maximum bending moment values in highway bridge design. For the purpose of rapid analysis and design, a potential alternative symmetric live load model is developed in this section. The effect of live load on moment and shear design actions depends on many parameters including the span length, axle loads, axle configuration, and vehicle position on the bridge. The moment and shear effects of the proposed live load model are compared with those generated by the HL-93 live load model to validate its reliability for design practice.

5.3 CURRENT AASHTO LRFD LIVE LOAD MODELS

Figure 5.1 presents the live load models for highway bridge design. The axle load magnitude and axle spacing for different design trucks and tandems are listed in Table 5.1. The AASHTO LRFD Bridge Design Specifications designate HL-93 live load for the design of bridge superstructures. The most adverse combination using both the (i) HS20 design truck (where $P_1 = P_2 = 32$ kips ≈ 143 kN , and $P_3 = 8$ kips ≈ 36 kN), or (ii) tandem axle load (where $P_1 = P_2 = 25$ kips ≈ 110 kN , and $P_3 = 0$ kips $= 0$ kN), along with the uniformly distributed lane load (where $w = 0.64$ kips/ft $= 9.3$ kN/m) is used to define the maximum moment and shear demands. A dynamic allowance, normally taken as 33 percent, is added to the truck and tandem loads effects; the uniform lane load is not increased for dynamic effects.

In the design process, the truck or tandem axle loads may be considered as a series of concentrated loads moving across the bridge. Particularly for the truck load, previous design experience shows that more critical load effects are normally generated when the spacing of the rear-axle loads (32 kips ≈ 143 kN) are kept at their minimum value of (14 ft ≈ 4.3 m). In functional form, the moment and shear force at different sections of the simple span bridge under design truck or tandem plus impact load along with lane load may be expressed as follows.

$$\begin{aligned} M(x) = {} & \frac{(1+IM)\left[(P_1+P_2+P_3)(L-a)-(P_2+P_3)b-P_3c\right]}{L}x-(1+IM)P_1\langle x-a\rangle \\ & -(1+IM)P_2\langle x-a-b\rangle-(1+IM)P_3\langle x-a-b-c\rangle+\frac{w}{2}Lx-\frac{w}{2}x^2 \end{aligned} \tag{5.1}$$

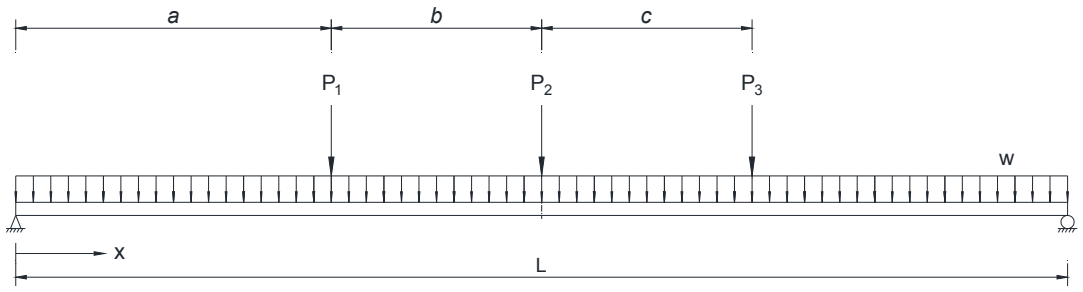

Figure 5.1. Live Load Models.

Table 5.1. Design Parameters for Design Trucks and Tandem.

Live Load Model	**Axle Loads (US Units)**			**Axle Spacing (US Units)**	
	P_1 (kips)	P_2 (kips)	P_3 (kips)	b (ft)	c (ft)
AASHTO HS20 Truck	32	32	8	14 - 30	14
AASHTO Tandem	25	25	-	4	-
Proposed Truck Load	25	25	25	10	10
Live Load Model	**Axle Loads (SI Units)**			**Axle Spacing (SI Units)**	
	P_1 (kN)	P_2 (kN)	P_3 (kN)	b (m)	c (m)
AASHTO HS20 Truck	143	143	36	4.3 – 9.1	4.3
AASHTO Tandem	110	110	-	1.2	-
Proposed Truck Load	110	110	110	3	3

$$V(x)=\frac{(1+IM)\left[(P_1+P_2+P_3)(L-a)-(P_2+P_3)b-P_3c\right]}{L}-(1+IM)P_1\langle x-a\rangle^0$$
$$-(1+IM)P_2\langle x-a-b\rangle^0-(1+IM)P_3\langle x-a-b-c\rangle^0+\frac{w}{2}L-wx \tag{5.2}$$

where a = the distance between the beam support and the front axle of the moveable truck or tandem load; b = the spacing between two rear axles; and c is the spacing between front and second axle, as shown in Figure 5.1. The impact factor IM = 33 percent. The envelop curves for the moment and shear force diagrams are determined by assigning various values for the parameter 'a'. In Equations (5.1) and (5.2), $\langle\bullet\rangle$ denotes the Macaulay brackets such that when $(x-a)<0$ then $\langle x-a\rangle=0$.

The maximum moment and shear force values of simple spans under the moveable tandem or truck plus impact load, along with lane load, are determined using the following equations.

$$M_{\max}=-\left[\frac{(1+IM)(P_1+P_2+P_3)}{L}+\frac{w}{2}\right]x^2$$
$$+\left[(1+IM)(P_1+P_2+P_3)+\frac{wL}{2}+\frac{(1+IM)(P_1-P_3)b}{L}\right]x-(1+IM)P_1b \tag{5.3}$$

$$V_{\max}=(1+IM)(P_1+P_2+P_3)-\frac{(1+IM)\left[P_2b+2P_3b\right]}{L}+\frac{wL}{2} \tag{5.4}$$

where the axle spacing is considered as a constant value, b. Note that as the axle loads are applied on a simple span bridge the maximum moment value occurs when $x=\frac{L}{2}+\frac{(1+IM)(P_1-P_3)b}{wL+2(1+IM)(P_1+P_2+P_3)}$. It is obvious that the maximum moment equation is

too complicated for engineering practice. However, some design guides provide the most critical position of HL-93 live load model for simple span bridges since it is a well-defined case.

By substituting the relevant values of P_1, P_2, P_3, b and IM value for the HL-93 live load model, the specific expressions for maximum moments and shear forces could be determined. Equations (5.5a) – (5.6b) present the maximum moments and shear forces in US customary and SI units when the HS20 truck load with impact factor plus uniform lane load is applied on the beam. The expressions for maximum moments and shear forces generated by tandem axle loads with impact factor plus uniform lane load are shown in Equations (5.7a) – (5.8b)

$$M_{\max} = \frac{\left(4L^2 + 1197L - 1862\right)\left(4L^2 + 1197L - 16758\right)}{50L\left(4L + 1197\right)} \text{ (kip-ft)} \tag{5.5a}$$

$$M_{\max} = \frac{\left(93L^2 + 8565L - 4060\right)\left(93L^2 + 8565L - 36890\right)}{80L\left(93L + 8565\right)} \text{ (kN-m)} \tag{5.5b}$$

$$V_{\max} = 0.32L - \frac{893.8}{L} + 95.8 \text{ (kips)} \tag{5.6a}$$

$$V_{\max} = 4.65L - \frac{1230}{L} + 428.3 \text{ (kN)} \tag{5.6b}$$

$$M_{\max} = \frac{\left(16L^2 + 3325L - 6650\right)^2}{200L\left(16L + 3325\right)} \text{ (kip-ft)} \tag{5.7a}$$

$$M_{\max} = \frac{\left(465L^2 + 29260L - 17556\right)^2}{2000L\left(93L + 5852\right)} \text{ (kN – m)} \tag{5.7b}$$

$$V_{\max} = 0.32L - \frac{133}{L} + 66.5 \text{ (kips)} \tag{5.8a}$$

$$V_{\max} = 4.65L - \frac{175.6}{L} + 292.6 \text{ (kN)} \tag{5.8b}$$

The maximum moment and shear forces for the AASHTO HS20 truck and tandem axle cases are plotted in Figure 5.2. By equating the maximum moment expressions for tandem and truck loads plus impact and lane load, it is found that when $L > 12.3$ m the HS20 truck plus lane load governs the design.

5.4 ALTERNATIVE LIVE LOAD LANE MODEL

Previous design experience shows that the asymmetric HS20 truck load brings inconvenience for the bridge engineers to determine the most unfavorable load position and the corresponding maximum bending moment values. While this is no longer a problem for computational modeling, for rapid hand analysis either for design purposes or checking computational solutions it is desirable that a more rapid solution can be dependably generated with ease.

An alternative symmetric truck load model is proposed herein in an attempt to more easily determine the most adverse moment effects. The axle loads and configuration of alternative truck loads are also listed in Table 5.1. The axle loads of the proposed truck model are such that $P = P_1 = P_2 = P_3$ (where $P = 25$ kips $= 110$ kN) and $b = c$ (where

$b = 10$ ft $= 3$ m). Because the alternative truck load is a symmetric three concentrated load series, the maximum moment value always occurs at the midspan location as follows.

$$M_{\max} = 3P(1+IM)\left(\frac{L}{4}-\frac{b}{3}\right)+\frac{wL^2}{8} \tag{5.9}$$

$$V_{\max} = 3P(1+IM)\left(1-\frac{b}{L}\right)+\frac{wL}{2} \tag{5.10}$$

By substituting the relevant values of P, b and IM value for the alternative symmetric live load model, the specific expressions for maximum moments and shear forces could be determined as follows.

$$M_{\max} = 0.08L^2 + 24.9L - 332.5 \text{ (kip-ft)} \tag{5.11a}$$

$$M_{\max} = 1.16L^2 + 109.7L - 438.9 \text{ (kN-m)} \tag{5.11b}$$

$$V_{\max} = 0.32L - \frac{997.5}{L} + 99.8 \text{ (kips)} \tag{5.12a}$$

$$V_{\max} = 4.65L - \frac{1316.7}{L} + 438.9 \text{ (kN)} \tag{5.12b}$$

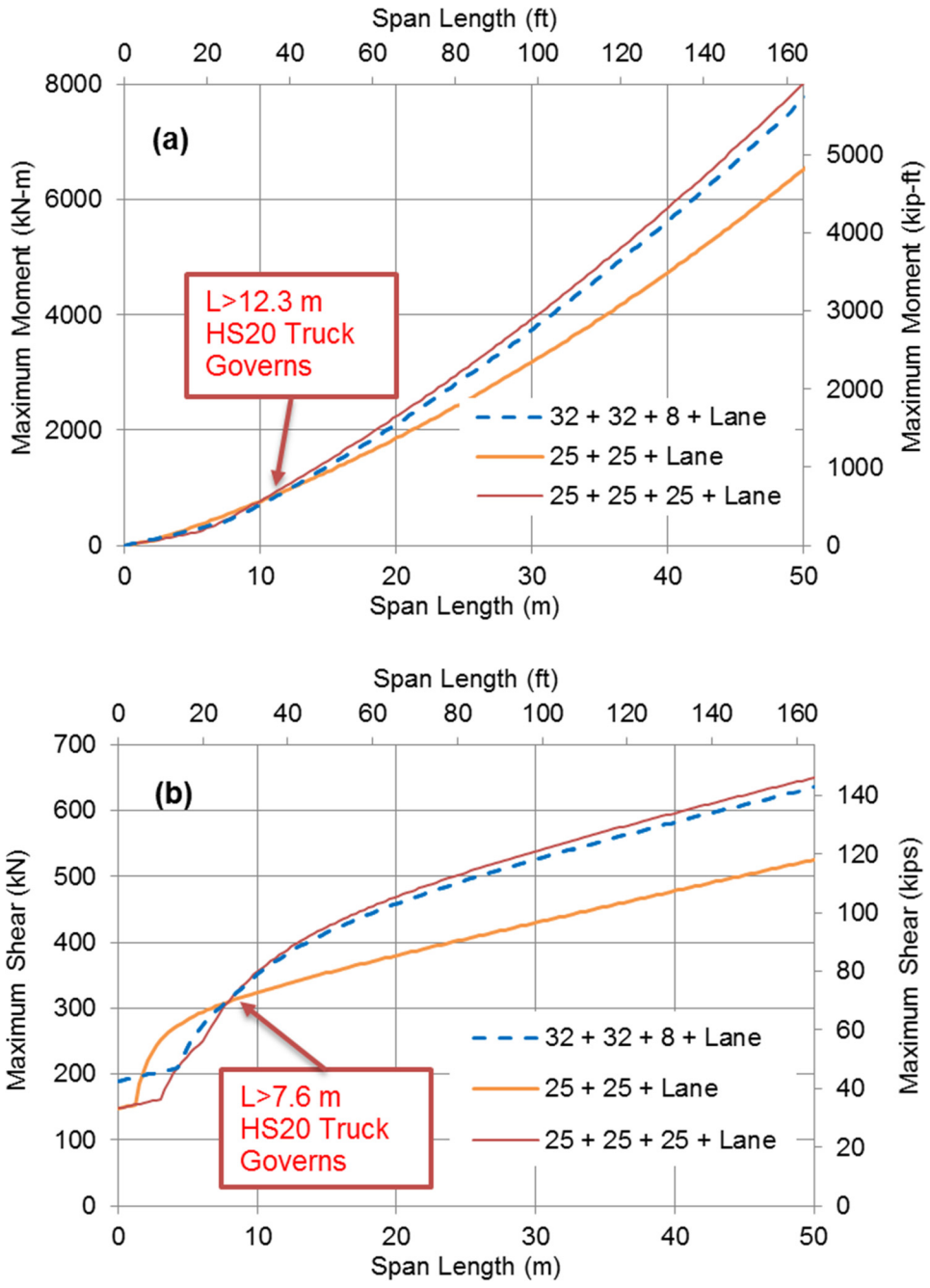

Figure 5.2. Design Actions for (a) Moment and (b) Shear Values under Various Live Load Models.

5.5 COMPARISONS AMONG DIFFERENT LIVE LOAD MODELS

Figure 5.2 shows the comparison amongst maximum moment and shear values under different live load models. When L > 12.3 m., more critical moment values are produced by the design truck load rather than the tandem axles, which confirms the theoretical derivation results. It is evident that the proposed alternative live load produce slightly more conservative maximum moment values than the HL-93 live load does in the region where the truck load governs the design, which demonstrates that the alternative truck load may be utilized to determine moment effects of simply supported bridges in the design process. As for the shear action, it is shown from Figure 5.2(b) that the design truck load generates a more critical design shear force value than the tandem load when L > 7.6 m. In this span range, the maximum shear design values provided by the proposed live load are slightly conservative when compared to the values generated by HS20 truck along with lane load.

Figure 5.3(a) shows the moment envelope curves of simply supported beams with different span lengths when various moveable truck or tandem loads plus impact and lane loads are applied. The blue dash and orange solid lines represent the respective maximum moment envelopes produced by the HS20 truck load and tandem axle load along with lane load. The moment envelope generated by the proposed live load model is represented with red solid line, from which it can be found that the maximum moment always occurs at the midspan location. This characteristic makes the bridge analysis or design more direct. By comparing the moment envelopes from different live load models, it is evident that the tandem load generate more critical moment values for short span beams. Thus the tandem axles should be used for the analysis and design of short spans.

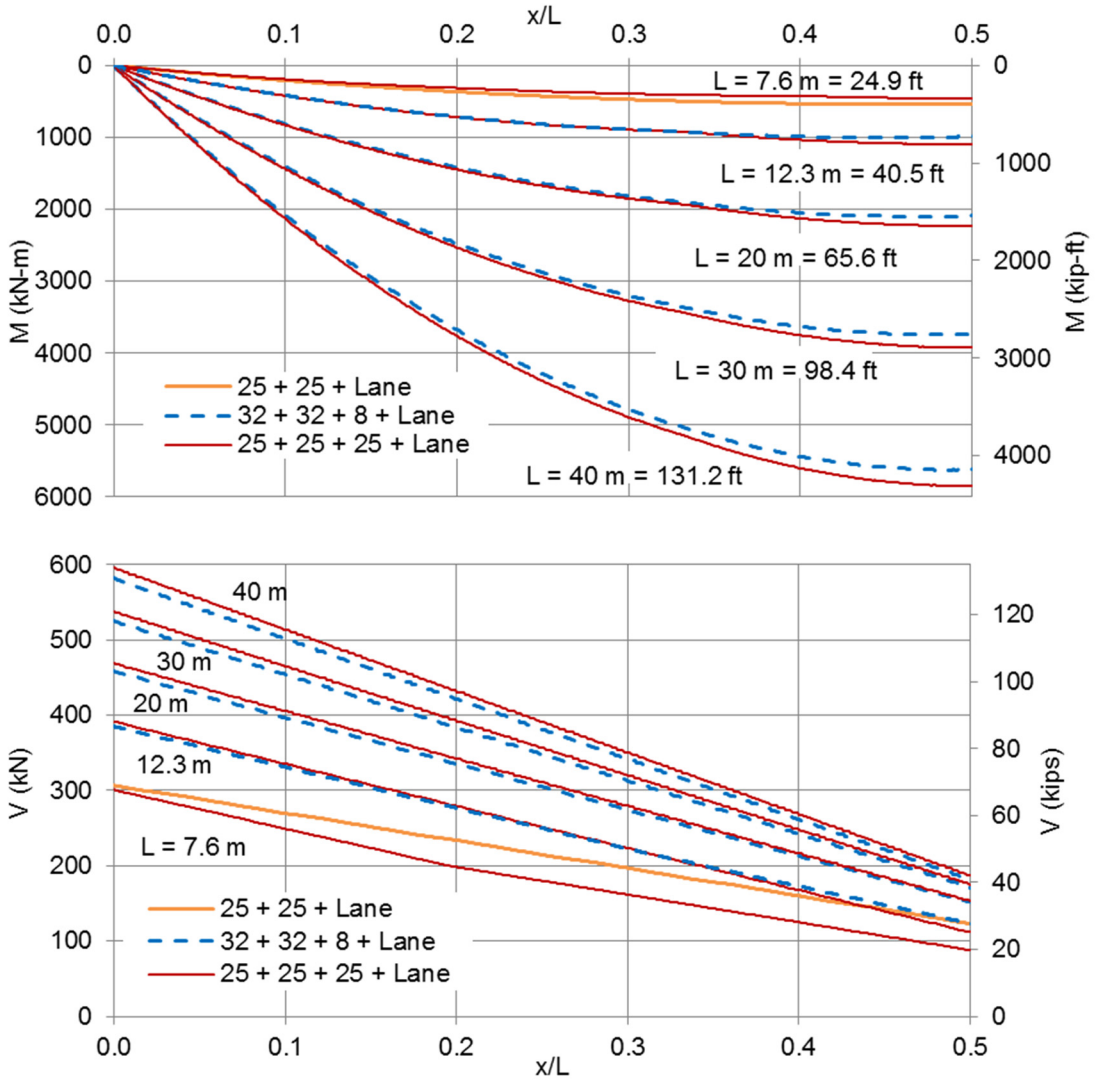

Figure 5.3. Moment and Shear Envelopes of Simple Span Beams under Various Types of Live Loads Plus Lane Load.

Figure 5.3(b) represents the shear force envelope for simple span beams under various live load models. It is shown that for short spans the tandem load produces a more critical shear envelope due to the closer axle spacing ($b = 4$ ft $= 1.2$ m). When compared to the shear effects caused by the HS20 truck along with lane load, the proposed live load generates slightly conservative shear force values, which may be utilized for rapid analysis or design of bridge spans.

5.6 CLOSURE AND KEY FINDINGS

A symmetric live load model was developed in an attempt to provide bridge engineers a more direct and simpler approach to design. The moment and shear effects of simple spans under the proposed live load model were evaluated and compared with those produced by the AASHTO LRFD HL-93 live model. The following conclusions may be drawn:

1. When the span length is over 12.3 m, more critical moment values are produced by the HS20 truck load rather that the tandem load. Similarly, the HS20 truck load generates more critical shear forces when the span length is larger than 7.6 m.
2. The proposed alternative truck load produces similar but slightly conservative moment and shear envelope curves as compared to the AASHTO HS20 truck load. Due to the symmetric arrangement, the maximum moment generated by alternative truck load always occurs at the midspan location.
3. It is recommended to use a live load pattern as one of the following combinations for rapid design, whichever produce maximum force effects. The impact factor (33%) is only applied to the design truck or tandem load when the dynamic allowance is considered in the design.

- Alternative design truck plus lane load: $P = P_1 = P_2 = P_3 = 25 \text{ kips} = 110 \text{ kN}$, $b = c = 10 \text{ ft} = 3 \text{ m}$, $w = 0.64 \text{ kips/ft} = 9.3 \text{ kN/m}$.
- Design tandem load plus lane load: $P_1 = P_2 = 25 \text{ kips} = 110 \text{ kN}$, $b = c = 4 \text{ ft} = 1.2 \text{ m}$, $w = 0.64 \text{ kips/ft} = 9.3 \text{ kN/m}$.

6 DESIGN MODELS FOR SIMPLY SUPPORTED PRESTRESSED CONCRETE GIRDER BRIDGES

6.1 SUMMARY

Structural analysis for the design of bridge deck structures can be a complex problem due to the high degree of indeterminacy in the structure. To simplify design, the historic AASHO bridge design specifications introduced the concept of load sharing amongst girders and provided a "*S*-over" method for defining the load distribution factor (LDF). The "*S*-over" formula has been extensively utilized by bridge engineers due to its straight-forward concept and simple format. Since the advent of the AASHTO LRFD Bridge Design Specifications in 1994, empirically derived power functions have been adopted. Although the LRFD formulas may have generated slightly more accurate design values for bridge structures within the range of the specified geometric characteristics, they were criticized by practitioners for the limited range of applicability, and their undue complexity sometimes requiring an iterative design procedure. New design models with a "*S/D*" format are proposed in this section for the purpose of providing bridge engineers a more straight-forward option to determine the moment and shear demands in the service load design phase. The applicability of the proposed design models for the prestressed concrete girder bridges commonly used in Texas and elsewhere is evaluated by comparing to finite element method (FEM) analysis results. Comparative results show that the proposed design formulas are mostly conservative for these bridge types.

6.2 INTRODUCTION

The complexity of calculating the design moment and shear force for an individual bridge girder member under imposed live plus impact loads necessitates simplified analysis methods. The historic concept of load distribution factor (LDF) was introduced to the structural design of bridge decks in the first edition of the American Association of State Highway Bridge Standard Design Specifications (AASHO 1931). That code and the following updates allowed bridge designers to uncouple the transverse and longitudinal effects of the wheel loads and then transform those effects to calculate the maximum internal design actions as part of a single one-dimensional beam analysis. The scaling factors were given in the form of a "*S*-over" formulation where S is defined as the beam spacing in feet. A typical denominator value for commonly used bridge configurations was taken as 5.5; the resulting scalar was multiplied by the wheel load to give the effective beam load. Thus since its inception the LDF concept and "$S/5.5$" formulation were extensively utilized by bridge engineers in the design of highway bridges due to the straight-forward philosophy and simple format. However, some researchers argued that the AASHTO "*S*-over" formulation was simplistic and not particularly accurate in predicting the moment and shear force values. It has been contended that the AASHTO "*S*-over" design values are too conservative for long span bridges, potentially making the design uneconomical (Nowak 1993; Zokaie et al. 1991).

Zokaie et al. (1991) developed a consistent set of power function formulas to calculate LDF values for commonly used bridge types. In addition to the girder spacing, these empirical equations also accounted for more design parameters including span

length, slab thickness, girder stiffness, etc. Studies demonstrated that the new formulas provided consistently conservative results for bridge structures within a specified range of geometric characteristics. With the advent of the new AASHTO LRFD Bridge Design Specifications (AASHTO 1994) these LDF formulas were adopted with some slight modifications to replace the historic "*S*-over" method.

Although it is claimed that the LRFD method could provide more accurate results as compared with the AASHTO Standard "*S*-over" formula, its limited range of applicability and complex format were criticized by researchers and practitioners. In particular, the longitudinal stiffness parameter, K_g, included in the formulas is unknown in the early design stage, thus an iterative procedure is often needed (Chung et al. 2005; Zokaie 2000). Even if new LRFD formulas could be used to calculate the LDF values more directly, or with the aid of software, they cannot directly provide a connection between each parameter's influence and potential design actions. In contrast, in spite of its simplicity the "*S*-over" method provides a very transparent connection between the applied loads and the required resistance. Moreover, the focus of prestressed concrete girder bridge structure designs remains on service loads and the associated allowable material tensile and compressive stress limits. While a wide variation of the material strength, especially for concrete, exists for on-site applications, there seems little advantage in seeking a particularly accurate formula to determine the design moment and shear demands for individual girders when the material strength is highly variable. It is contended that for such design purposes it seems appropriate to envoke Elms' (1992)

"principle of consistent crudeness". The principle of consistent crudeness deals with the connumdrum of accuracy versus expediency.

Certain researchers have developed alternative LDF formulas in an attempt to overcome the shortcomings of the AASHTO LRFD method and provide simpler options for highway bridge design. Sotelino et al. (2004) developed simplified LDF Equations with no need of an iterative procedure for steel and prestressed concrete girder bridges. The span length and girder spacing were incorporated in the proposed equations with proper power exponents. Although the equations generated reliable design values as compared to computational solutions, the power function format cannot directly reflect the influence of different parameters.

Huo et al. (2004) introduced the method in use at the Tennessee Department of Transportation, called Henry's method, which they modify to calculate moment LDF values. In this simplified method akin to the earlier AASHO/AASHTO *S*-over formulation; only the bridge width and number of beams are required – both interior and exterior beams are treated similarly. This method normally generates conservative design values for different types of bridges and its simplicity makes it popular amongst bridge engineers in Tennessee.

Suksawang et al. (2013) developed a new "*S*-over" equation to determine the shear LDF for steel and prestressed concrete I-girder bridges, but many LDF values specified by the proposed formulas are unconservative as compared with FEM solutions although the lowest sum of square errors is achieved.

In light of the above, new design models with a "*S/D*" format are proposed in this section for the purpose of providing bridge design engineers a more straight-forward option to determine the moment and shear demands particularly for the preliminary design phase. Naturally, more exacting analyses can be conducted once a preliminary design is completed.

The applicability of the proposed LDFs for prestressed concrete girder bridges commonly used in Texas and elsewhere is evaluated by comparing the models to more exacting finite element method (FEM) analysis results. This section focuses on developing the simplified design methods for simply supported bridge spans. Its extension to continuous bridge spans will be described in the follow up section.

6.3 CURRENT AASHTO LRFD DESIGN METHOD

Figure 6.1 presents the current design HL-93 live load for bridge decks in the United States, in accordance with the AASHTO LRFD Bridge Design Specifications (AASHTO 2012). The most adverse combination using both the (i) design truck or (ii) tandem axle load, along with a uniformly distributed lane load is used to define the maximum moment and shear demands. A dynamic allowance, normally taken as 33 percent is added to the truck and tandem loads effects for all limit states except the fatigue limit state; the uniform lane load is not increased for dynamic effects.

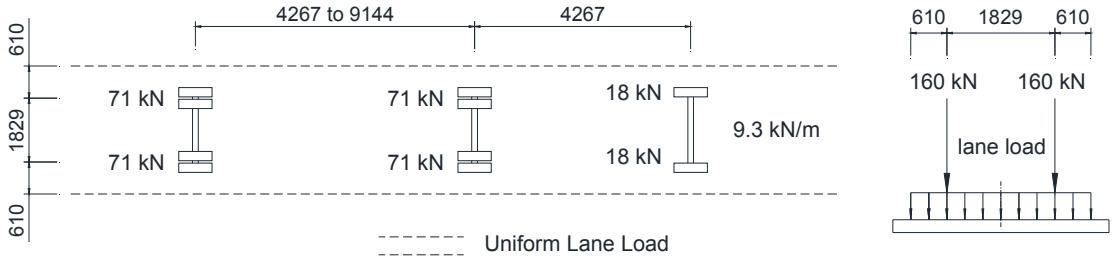

(a) Plan and End Views of Design Truck Plus Lane Load

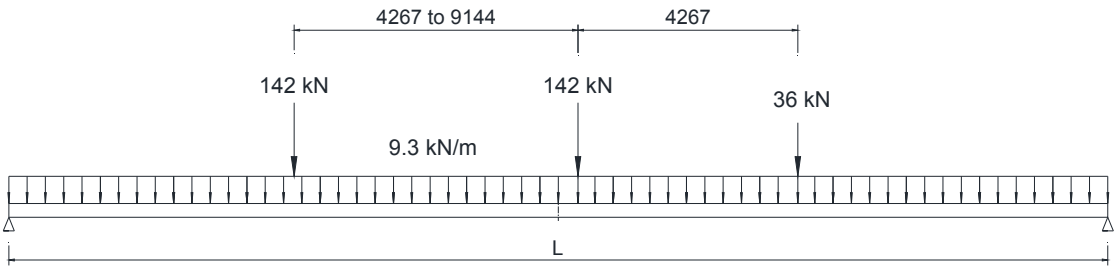

(b) Side View of Design Truck Load Plus Lane Load

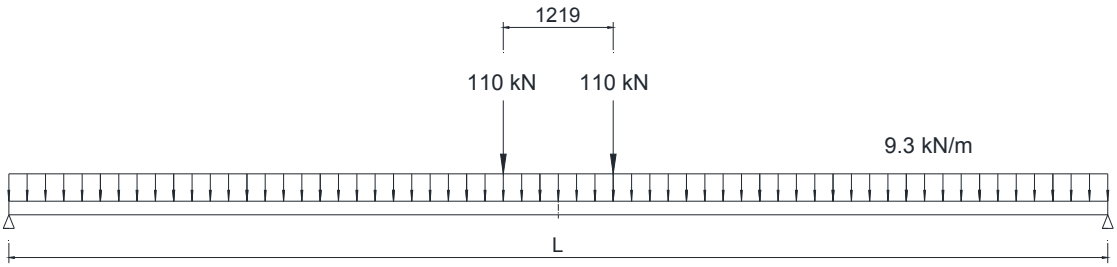

(c) Side View of Design Tandem Axle Load Plus Lane Load

Figure 6.1. AASHTO LRFD HL-93 Live Load Models.

The lane width is designated as 3.66 m (12 ft) in the AASHTO LRFD Specifications. The transverse wheel spacing of the design truck and tandem is 1.83 m (6 ft), while the width of the uniform design lane load is 3 m (10 ft). The live loads are assumed to occupy each design lane to produce the most adverse combination. A truck is to be positioned no closer than 0.61 m (2 ft) from the edge of the design lane.

The AASHTO LRFD Bridge Design Specifications provide empirical LDF formulas for various types of bridge superstructures, which have simplified the analysis of the three-dimensional bridge structure to an one-dimensional beam problem. The moment and shear demands of individual girders in the bridge superstructure could be determined by multiplying the corresponding forces created in an isolated beam element with the LDF value. Common practice is to design all the girders the same with a critical girder under the most adverse load effects.

$$F_i = \left(LDF\right)_i F_{1D-Girder} \tag{6.1}$$

where F_i represents the moment or shear force of beam *i*, and $F_{1D-Girder}$ represents the moment or shear force values on a single beam under the HL-93 live load model.

There are no side-by-side slab beam and spread slab beam configurations defined in AASHTO LRFD Bridge Design Specifications (AASHTO 2012). However, LDF formulas for both exterior and interior girders of prestressed concrete I-girder bridges and spread box beam bridges are provided in the specifications, as shown in Table 6.1. The latter bridge type is very similar to the spread slab beam bridge recently introduced by TxDOT. The applicability of the AASHTO formulas are evaluated in this section along with proposed design models described in what follows.

Table 6.1. AASHTO LRFD LDF Formulas for Prestressed Concrete I-girder Bridge and Spread Box Beam Bridge.

Item			Moment LDF	Shear LDF
I-girder Bridge	Interior Girder	One Lane Loaded	$0.06+\left(\frac{S}{4300}\right)^{0.4}\left(\frac{S}{L}\right)^{0.3}\left(\frac{K_g}{Lt_s^3}\right)^{0.1}$	$0.36+\frac{S}{7600}$
		Multiple Lanes Loaded	$0.075+\left(\frac{S}{2900}\right)^{0.6}\left(\frac{S}{L}\right)^{0.2}\left(\frac{K_g}{Lt_s^3}\right)^{0.1}$	$0.2+\frac{S}{3600}-\left(\frac{S}{10700}\right)^{2.0}$
	Exterior Girder	One Lane Loaded	Lever Rule	Lever Rule
		Multiple Lanes Loaded	$g_{ext}=e\cdot g_{\text{int}}$ $e=0.77+\frac{d_e}{2800}$	$g_{ext}=e\cdot g_{\text{int}}$ $e=0.6+\frac{d_e}{3000}$
Spread Box Beam Bridge	Interior Girder	One Lane Loaded	$\left(\frac{S}{910}\right)^{0.35}\left(\frac{Sd}{L^2}\right)^{0.25}$	$\left(\frac{S}{3050}\right)^{0.6}\left(\frac{d}{L}\right)^{0.1}$
		Multiple Lanes Loaded	$\left(\frac{S}{1900}\right)^{0.6}\left(\frac{Sd}{L^2}\right)^{0.125}$	$\left(\frac{S}{2250}\right)^{0.8}\left(\frac{d}{L}\right)^{0.1}$
	Exterior Girder	One Lane Loaded	Lever Rule	Lever Rule
		Multiple Lanes Loaded	$g_{ext}=e\cdot g_{\text{int}}$ $e=0.97+\frac{d_e}{8700}$	$g_{ext}=e\cdot g_{\text{int}}$ $e=0.8+\frac{d_e}{3050}$

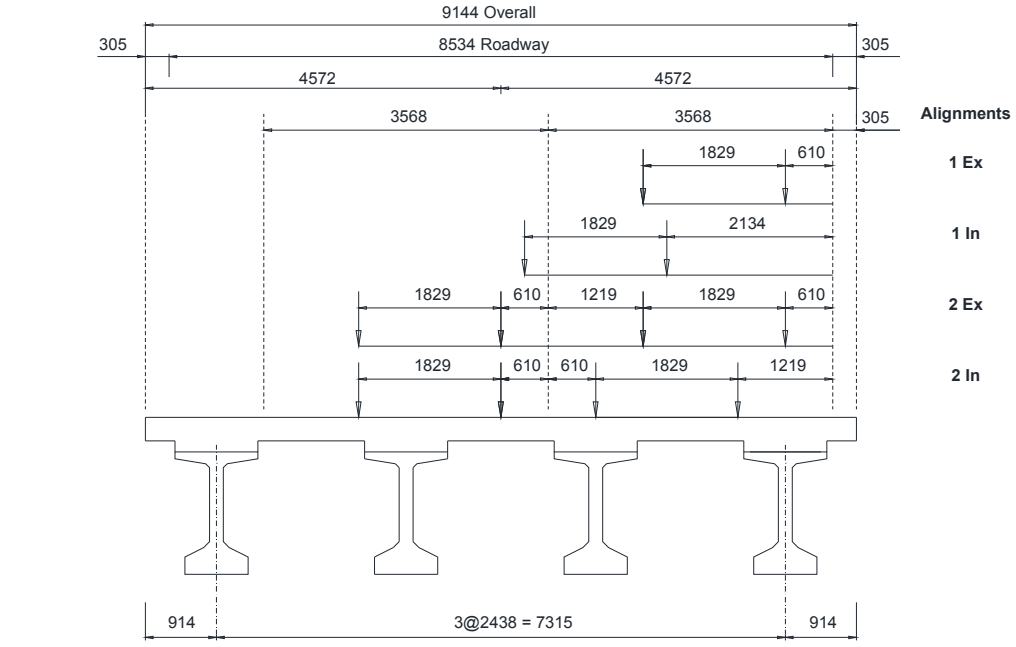

(a) Two-Lane I-girder Bridge

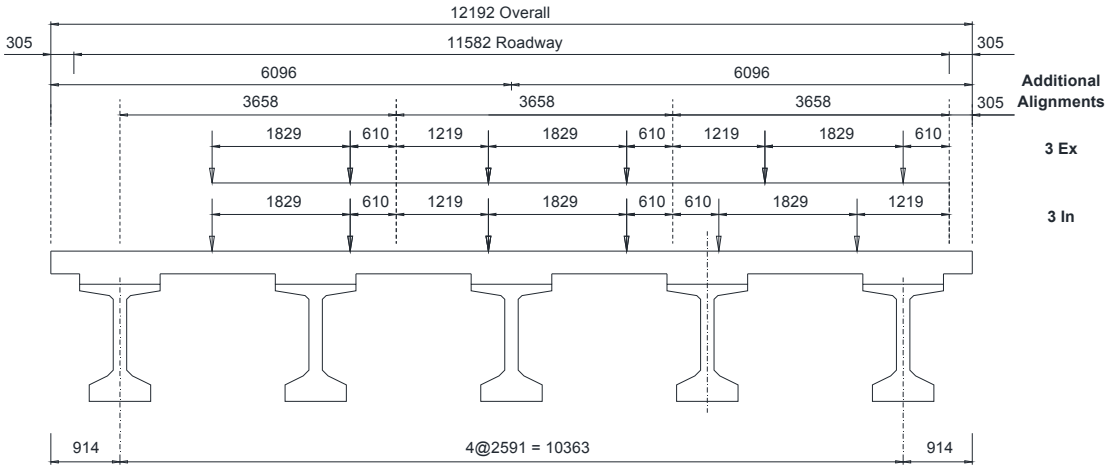

(b) Three-Lane I-girder Bridge

Figure 6.2. Transverse Load Positions for Representative Two-Lane and Three-Lane Prestressed Concrete I-girder Bridges.

6.4 PROPOSED DESIGN MODELS

For multiple-lane bridges, the vehicle is normally allowed to occupy its own lane and the lane width is specified as 3.66 m wide in the AASHTO LRFD Bridge Design Specifications (AASHTO 2012). Figure 6.2(b) presents the truck load position of a prestressed concrete I-girder bridge with 11.6 m roadway width. It is obvious that the live load magnitude for each lane is constant, but the girder numbers per lane are variable for different bridge configurations. Therefore, new design methods are proposed to determine the design moment and shear demands of each girder based on the live load effects and lane numbers occupied by each girder. Note that the design loads determined from the proposed methods represent the maximum values amongst all girders across the bridge section. The exterior and interior girders will be treated equally in the design process.

For flexural and shear actions, design moments and shears for each girder are determined by proportion of the lane moments and shears as follows.

$$M_g = k_M \frac{S}{D_M} M_L \tag{6.2}$$

$$V_g = k_V \frac{S}{D_V} V_L \tag{6.3}$$

in which M_g and V_g are the respective girder moment and shear demands; M_L and V_L are the lane moments and shears over the prescribed lane width; S = girder spacing in feet; The denominators $D_M = 12 \text{ ft} = 3.66 \text{ m}$ and $D_V = 10 \text{ ft} = 3 \text{ m}$, representing the overall lane width and the distributed lane load width, respectively, as shown in

Figure 6.1(a). Parameters k_M and k_V are the respective correction factors that are calibrated herein. It should also be noted that the correction factors normally take the values of $k_M = 1.0$ and $k_V = 1.0$ unless otherwise verified through rigorous analysis.

6.5 EVALUATION OF CORRECTION FACTORS FOR SIMPLY SUPPORTED PRESTRESSED CONCRETE GIRDER BRIDGES

The applicability of the proposed design models is evaluated in this section for slab on prestressed concrete girder bridges commonly used in Texas and elsewhere, including prestressed concrete I-girder bridges, prestressed concrete slab beam bridges and prestressed concrete spread slab beam bridges. For each bridge type, a number of bridge configurations covering different girder spacings, span lengths, bridge widths and number of lanes were analyzed using the finite element method (FEM) approach. In the FEM models, trucks were placed in numerous locations to obtain the most adverse live load combination for exterior and interior girders. Both single lane and multiple lanes loaded cases were considered in the analysis process. Thus, for each bridge configuration a pair of "exact" maximum girder moment and shear force values was obtained using the FEM solutions.

For each bridge configuration, the design moment and shear demands were calculated based on the proposed design models plus the formulas available in the present AASHTO LRFD Specifications. The comparison between the design values and computational solutions are made to verify the applicability of the proposed design models. Through conducting a statistical study on the comparative values, the statistical parameters, including median values, standard deviations and cumulative distribution probabilities, were calculated to evaluate the reliability of the proposed design models. If needed, the correction factors in the proposed design models are adjusted so that there is approximately a non-exceedance probability of 5 percent, so the final design formulas are at least 95 percent conservative.

6.6 EVALUATION OF PROPOSED DESIGN MODELS FOR SIMPLY SUPPORTED PRESTRESSED CONCRETE I-GIRDER BRIDGES

As an effective and economical solution for short to medium spans, prestressed concrete I-girder bridges have been extensively used in Texas and elsewhere. Therefore, the Texas Department of Transportation (TxDOT) has released standard drawings online to provide design details to bridge engineers. Based on the information provided by TxDOT standard drawings, representative bridge configurations covering various girder spacings, span lengths, bridge widths and number of lanes were selected. The “exact” values for moment and shear actions were evaluated for selected bridge geometries using the results computed with FEM analysis. These moments and shear forces were then compared with the design values obtained from proposed models to evaluate their applicability.

Table 6.2. Simply Supported I-girder Bridge Geometries.

No.	Bridge Width, *B* (m)	Roadway Width, *W* (m)	Girder Spacing, *S* (m)	No. of Girders	No. of Lanes	Span Length, *L* (m)	Girder Type
1	7.9	7.3	2.0	4	2	21.3	Tx54
2	7.9	7.3	2.0	4	2	30.5	Tx62
3	7.9	7.3	2.0	4	2	36.6	Tx70
4	9.1	8.5	2.4	4	2	21.3	Tx54
5	9.1	8.5	2.4	4	2	30.5	Tx62
6	9.1	8.5	2.4	4	2	36.6	Tx70
7	10.4	9.8	2.8	4	2	21.3	Tx54
8	10.4	9.8	2.8	4	2	30.5	Tx54
9	10.4	9.8	2.8	4	2	30.5	Tx62
10	10.4	9.8	2.8	4	2	30.5	Tx70
11	10.4	9.8	2.8	4	2	36.6	Tx62
12	10.4	9.8	2.8	4	2	36.6	Tx70
13	10.4	9.8	2.8	4	2	42.7	Tx70
14	12.2	11.6	2.6	5	3	21.3	Tx54
15	12.2	11.6	2.6	5	3	30.5	Tx62
16	12.2	11.6	2.6	5	3	36.6	Tx70
17	14.0	13.4	2.4	6	3	21.3	Tx54
18	14.0	13.4	2.4	6	3	30.5	Tx54
19	14.0	13.4	2.4	6	3	30.5	Tx62
20	14.0	13.4	2.4	6	3	30.5	Tx70
21	14.0	13.4	2.4	6	3	36.6	Tx62
22	14.0	13.4	2.4	6	3	36.6	Tx70
23	14.0	13.4	2.4	6	3	42.7	Tx70

6.6.1 Bridge Superstructure Geometries Considered

Five different bridge roadway widths (7.9, 9.1, 10.4, 12.2 and 14.0 m), and three common girder types (Tx54, Tx62 and Tx70) were selected for all bridge configurations to account for a wide range of girder spacing, lane number and span length. Table 6.2 presents the geometric information of the chosen simply supported prestressed concrete I-girder bridge configurations.

6.6.2 FEM Analysis Strategies

All 23 simply supported prestressed concrete I-girder bridge cases were modeled using a detailed FEM analysis and the maximum girder moment and shear force values were obtained for each bridge case. The FEM analysis was performed using CSiBridge (Computers and Structures 2013) software package. The frame and brick elements were utilized to model I-girder and deck slab. Figure 6.3(a) shows a representative FEM model for prestressed concrete I-girder bridges.

Figure 6.2 presents the transverse load alignments adopted for the FEM analysis of prestressed concrete I-girder bridge superstructures. The alignment labels #Ex and #In in Figure 6.2 represent the load cases critical for exterior and interior girders where # is the number of lanes loaded simultaneously. These alignments were arranged in such a fashion that the most adverse combination of load effects would be captured through rigorous analysis. The transverse positions were selected based on the allowable travel distances specified by the code and engineering judgment. Transverse positions of the lanes were defined by dividing the bridge roadway into as many 3.66 m (12 ft) wide lanes

as possible. Vehicles and lane loads were then allowed to move within their own lane for multiple lane loaded cases. The 1.83 m (6 ft) wide truck load is to be positioned no closer than 0.61 m (2 ft) from the edge of the design lane and uniform lane load (9.3 kN/m (0.64 kips/ft)) is applied over a 3 m (10 ft) width in the transverse direction for each loaded design lane. For the one lane loaded case, the vehicle was permitted to pass between lanes. Therefore, a transverse load position crossing the design lane could be defined for the single lane loaded case to achieve the most critical loading for an interior girder.

Many load cases were investigated using the AASHTO (2012) HS20 design truck plus uniform lane loading. The CSiBridge software simulates the design truck load as a series of movable concentrated loads passing over the bridge and gives the maximum moment or shear force values for each girder. Thus, there was no need to define critical positions in the longitudinal direction. In the analysis, the AASHTO multiple presence factor and dynamic allowance are considered. The values of multiple presence factors for one-, two- and three-lane loaded cases are 1.2, 1.0, and 0.85; respectively. The impact factor is taken as 33 percent and applied only to the truck or tandem load.

6.6.3 Analysis Results Evaluation for Simply Supported I-girder Bridges

The computational results of the critical moment and shear force values for 23 simply supported prestressed concrete I-girder bridge configurations are listed in the Appendix Table A1.1. It is seen that the critical shear force values were obtained on an interior I-girder when multiple lanes are loaded simultaneously for all bridge configurations, but no consistent pattern was found for critical moment values. All critical cases are highlighted in Table A1.1.

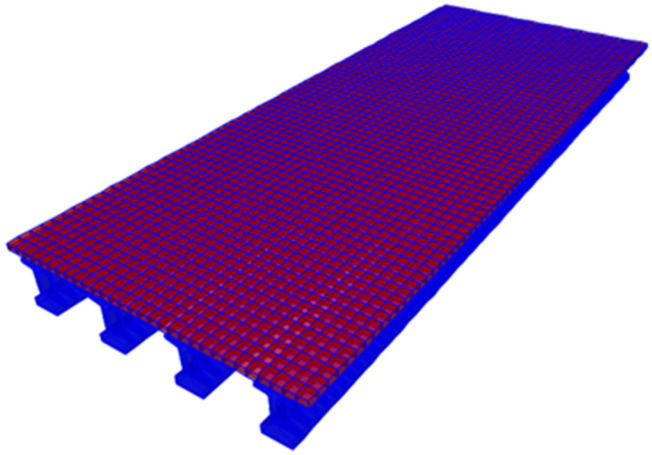

(a) I-girder Bridge

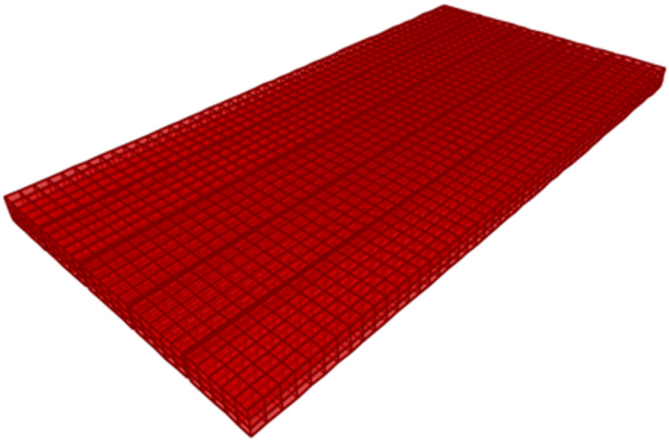

(b) Slab Beam Bridge

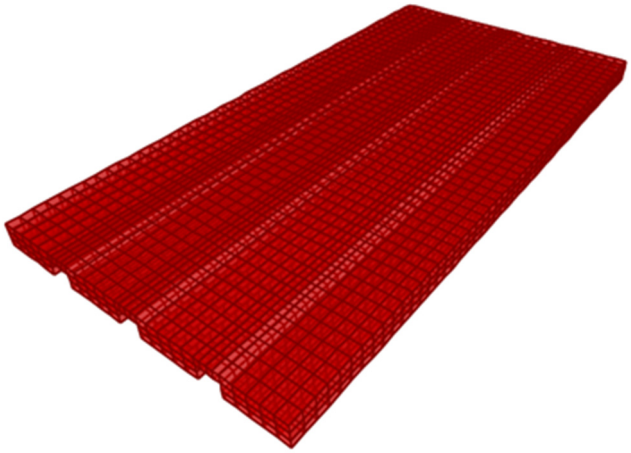

(c) Spread Slab Beam Bridge

Figure 6.3. Finite Element Models for Prestressed Concrete Girder Bridges.

According to the proposed design models developed in the previous section, the design moments and shear forces for the girders of the 23 bridge configurations could be determined. Table A1.2 lists the critical moment and shear force values calculated from FEM analysis and the proposed design models. The median values of the ratios (Model/FEM) show that the design models provide about 10 percent conservative moment and 6 percent conservative shear force values as compared to computational solutions. In addition, the AASHTO LRFD Bridge Design Specifications provide empirical LDF formulas to calculate the most adverse girder moments and shear forces as listed in Table A1.3. It is seen that similar degree of conservatism was obtained from code-specified values.

Figure 6.4 presents the comparisons of the critical moment and shear force values determined from the proposed models, AASHTO LRFD empirical formulas and FEM analysis. It is evident from Figure 6.4(a) that both proposed models and AASHTO LRFD empirical formulas generally produce conservative moment and shear force values for design. The cumulative probabilities of the moment and shear ratios (Model/FEM and AASHTO/FEM) are also plotted in Figure 6.4(b) to better visualize the distribution of each data point and their probability of occurrence. The solid green and blue lines represent the lognormal model curves for the proposed design models and AASHTO LRFD Specifications method. The model curve is a curve that the same lognormal standard deviation and median as the ratios of the proposed models or AASHTO LRFD Specifications method. It is seen that the dispersion of moment values determined from proposed models is greater than the code-specified values, while the dispersion of shear

values based on proposed models is slightly smaller than AASHTO LRFD values. For moment action, the lognormal model curve for the proposed design models (solid green line) crosses the ratio 1.0 at 5 percent probability, which indicates that for at least 95 percent of all design cases the proposed model remains conservative. The blue curve shows that the AASHTO LRFD formula provides conservative moment design values for all bridge configurations without exception. In terms of shear action, the design values determined from the proposed models are higher than FEM solutions for all bridge configurations. From the statistical comparative results above, it can be concluded that the proposed models are sufficiently reliable for the design of the simply-supported I-girder bridges and the correction factors do not need to be adjusted.

6.7 EVALUATION OF PROPOSED DESIGN MODELS FOR SIMPLY SUPPORTED PRESTRESSED CONCRETE SLAB BEAM BRIDGES

As an effective solution for short spans in low-clearance locations, prestressed concrete slab beam bridges have been extensively used in Texas and elsewhere. TxDOT provides online standard drawings to promote their application, in which the geometric boundaries of this bridge superstructure type are specified. Based on the information provided by TxDOT standard drawings, representative bridge configurations covering various beam spacings, span lengths, bridge widths and number of lanes were selected. The “exact” values for moment and shear actions were evaluated for selected bridge geometries, using the results computed with FEM analysis. These moments and shear forces were then compared with the design values determined by the proposed design models to evaluate their applicability.

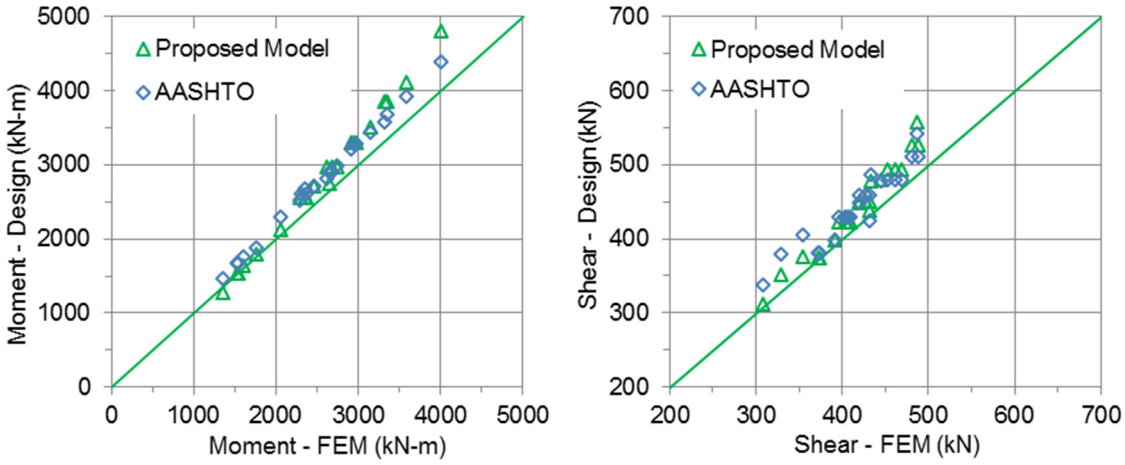

(a) CompariSons between Design and FEM Values

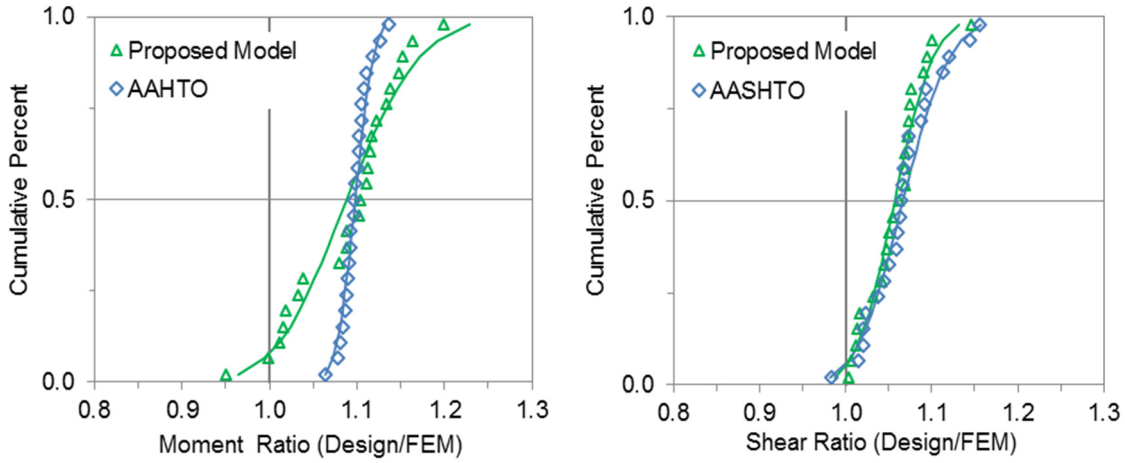

(b) Cumulative Distribution Probabilities of Moment and Shear Ratios

Figure 6.4. Comparisons of Design Moment and Shear Force Values and FEM Solutions for Simply Supported I-girder Bridges.

6.7.1 Bridge Superstructure Geometries Considered

Three different bridge roadway widths (7.3, 8.5 and 9.1 m) are specified by TxDOT standard drawings and the applicable range of span length is 7.6 to 15.2 m, which shows that the prestressed concrete slab beam bridge is normally used for simply supported short-span two-lane bridges. Table 6.3 presents the geometric information for selected simply supported slab beam bridge configurations, which includes the most adverse design parameters.

6.7.2 FEM Analysis Strategies

Similar with prestressed concrete I-girder bridge analysis described previously, all 12 simply supported prestressed concrete slab beam bridge cases were modeled using CSiBridge (Computers and Structures 2013) software package and maximum moment and shear force values of slab beams were obtained for each bridge configuration. The eight-node linear solid element having three degrees of freedom at each node was utilized to model both the slab beam and deck. Figure 6.3(b) shows a representative FEM model for a prestressed concrete slab beam bridge. Values of the design parameters were chosen in accordance with TxDOT standard design drawings.

The transverse alignments adopted for the FEM analysis of prestressed concrete slab beam bridge superstructures were arranged in a similar fashion with the analysis of prestressed concrete I-girder bridges so that the most adverse combination of load effects would be captured. In the analysis process, the multiple presence factor and dynamic allowance were also considered.

Table 6.3. Simply Supported Slab Beam Bridge Geometries.

No.	Bridge Width, *B* (m)	Roadway Width, *W* (m)	Beam Spacing, *S* (m)	No. of Beams	No. of Lanes	Span Length, *L* (m)	Girder Type
1	7.9	7.3	1.6	5	2	7.6	5SB15
2	7.9	7.3	1.6	5	2	9.1	5SB15
3	7.9	7.3	1.6	5	2	10.7	5SB15
4	7.9	7.3	1.6	5	2	12.2	5SB15
5	7.9	7.3	1.6	5	2	13.7	5SB15
6	7.9	7.3	1.6	5	2	15.2	5SB15
7	9.8	9.1	1.2	8	2	7.6	4SB15
8	9.8	9.1	1.2	8	2	9.1	4SB15
9	9.8	9.1	1.2	8	2	10.7	4SB15
10	9.8	9.1	1.2	8	2	12.2	4SB15
11	9.8	9.1	1.2	8	2	13.7	4SB15
12	9.8	9.1	1.2	8	2	15.2	4SB15

6.7.3 Analysis Results Evaluation for Simply Supported Slab Beam Bridges

The computational results of the critical moment and shear force values for 12 simply supported slab beam bridge configurations are listed in the Appendix Table A1.4. For 7.9 m wide slab beam bridges (Cases 1-6), the most critical moments and shear forces were obtained from the two lanes loaded interior beam cases. When the bridge width increases to 9.8 m (Cases 7-12), the critical moment values occurred in the two lanes loaded exterior beam cases, but no consistent pattern was found for critical shear forces. All critical cases are highlighted in Table A1.4.

The design moment and shear forces for the slab beams of the 12 bridge configurations were calculated according to the proposed design models. Table A1.5 lists the critical moment and shear force values calculated from FEM analysis and proposed design models. The median values show that that the design models provide about 5 percent conservative moment and shear values as compared to the computational results.

Figure 6.5(c) presents the comparisons of moment and shear force values determined from the proposed models and FEM analysis. It is evident that the proposed models normally generate slightly conservative load values for design. The cumulative probabilities of the moment and shear ratios, in which design loads determined from proposed models are divided by FEM values, are shown in Figure 6.5(d). It is seen from Figure 6.5(d) that there is less than 5 percent chance that the ratios of the proposed model to the FEM values are below 1.0 for both moment and shear actions. Based on the statistical results, it can be concluded that the proposed models are suitably reliable for design without further modification for simply supported slab beam bridges.

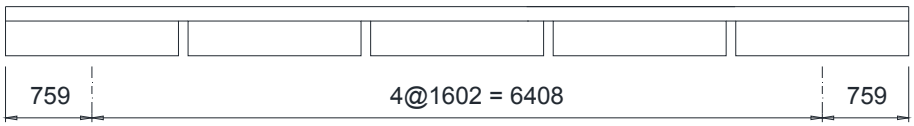

(a) Example of a Five-beam Slab Beam Bridge Deck Striped for Two Lanes

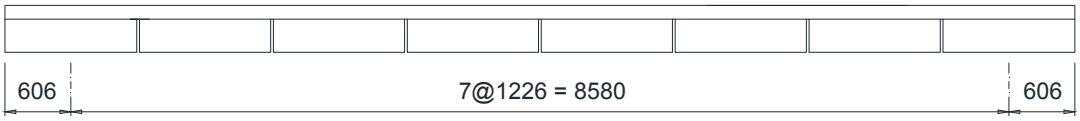

(b) Example of a Eight-beam Slab Beam Bridge Deck Striped for Three Lanes

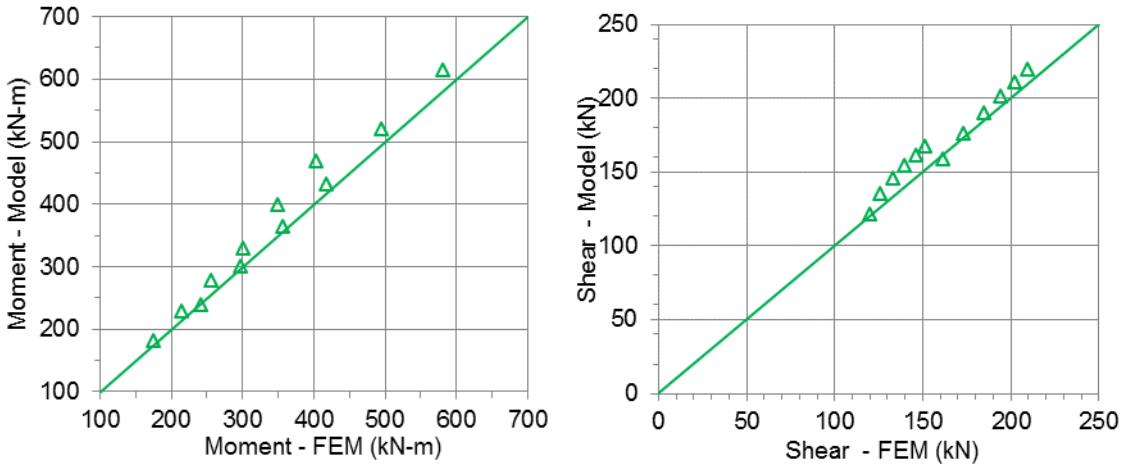

(c) Comparisons between S/D Model and FEM Values

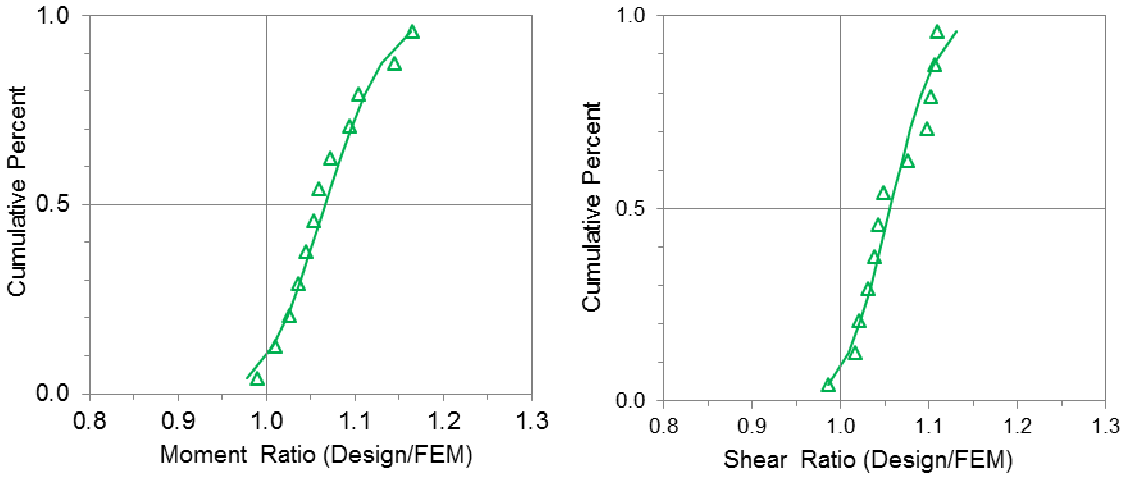

(d) Cumulative Distribution Probabilities of Moment and Shear Ratios

Figure 6.5. Comparisons of Design Moment and Shear Force Values and FEM Solutions for Simply Supported Slab Beam Bridge.

6.8 EVALUATION OF PROPOSED DESIGN MODELS FOR SIMPLY SUPPORTED PRESTRESSED CONCRETE SPREAD SLAB BEAM BRIDGES

As a new class of bridges, prestressed concrete spread slab beam bridges were developed by TxDOT recently and implemented in Texas. Based on the research findings from TxDOT Project 0-6722 (Hueste et al. 2015), representative spread slab beam bridge configurations covering various beam spacings, span lengths, bridge widths and numbers of lane were selected to conduct evaluation work. The "exact" moment and shear force values for selected bridge geometries were determined using FEM analysis. These moments and shear forces were then compared with the design values obtained from the proposed models and AASHTO LRFD formulas to evaluate the applicability of both methods.

6.8.1 Bridge Superstructure Geometries Considered

Six different bridge roadway widths (7.9, 9.1, 10.4, 11.6, 12.8 and 14.0 m) were selected for all bridge configurations to account for a wide range of beam spacings and different number of lanes. The feasible span length and beam spacing of simply supported bridge cases were determined based on the parametric study completed by Hueste et al. (2015). In general, bridge configurations with a closer beam spacing could lead to a greater span length. Table 6.4 presents the geometric information of 26 simply supported spread slab beam bridge configurations, which includes the most adverse design parameters.

Table 6.4. Simply Supported Spread Slab Beam Bridge Geometries.

No.	Bridge Width, *B* (m)	Roadway Width, *W* (m)	Girder Spacing, *S* (m)	No. of Girders	No. of Lanes	Span Length, *L* (m)	Girder Type
1	7.9	7.3	2.1	4	2	9.1	5SB15
2	7.9	7.3	2.1	4	2	10.7	5SB15
3	7.9	7.3	2.1	4	2	12.2	5SB15
4	7.9	7.3	2.1	4	2	13.7	5SB15
5	7.9	7.3	2.1	4	2	15.2	5SB15
6	9.1	8.5	2.5	4	2	9.1	5SB15
7	9.1	8.5	2.5	4	2	10.7	5SB15
8	9.1	8.5	2.5	4	2	12.2	5SB15
9	9.1	8.5	2.5	4	2	13.7	5SB15
10	9.1	8.5	2.5	4	2	15.2	5SB15
11	10.4	9.8	2.9	4	2	9.1	5SB15
12	10.4	9.8	2.9	4	2	10.7	5SB15
13	10.4	9.8	2.9	4	2	12.2	5SB15
14	10.4	9.8	2.9	4	2	13.7	5SB15
15	11.6	11.0	3.4	4	3	9.1	5SB15
16	11.6	11.0	3.4	4	3	10.7	5SB15
17	11.6	11.0	3.4	4	3	12.2	5SB15
18	11.6	11.0	3.4	4	3	13.7	5SB15
19	12.8	12.2	2.8	5	3	9.1	5SB15
20	12.8	12.2	2.8	5	3	10.7	5SB15
21	12.8	12.2	2.8	5	3	12.2	5SB15
22	12.8	12.2	2.8	5	3	13.7	5SB15
23	14.0	13.4	3.1	5	3	9.1	5SB15
24	14.0	13.4	3.1	5	3	10.7	5SB15
25	14.0	13.4	3.1	5	3	12.2	5SB15
26	14.0	13.4	3.1	5	3	13.7	5SB15

6.8.2 FEM Analysis Strategies

Similar with prestressed concrete slab beam bridge analysis, all 26 spread slab beam bridge cases were modeled using the CSiBridge (Computers and Structures 2013) software package. The eight-node linear solid element having three degrees of freedom at each node was utilized to model both slab beam and deck, as shown in Figure 6.3(c). The alignments adopted for the FEM analysis of multiple-lane prestressed concrete spread slab beam bridge superstructures were arranged in a similar fashion with the previous two bridge types so that the most adverse combination of load effects would be captured through rigorous analysis. Values of the design parameters were chosen in accordance with TxDOT standard design drawings.

6.8.3 Analysis Results Evaluation for Simply Supported Spread Slab Beam Bridges

Table A1.6 lists the computational results of the critical moment and shear force values for 26 simply supported spread slab beam bridge configurations. It is seen that the critical moment and shear force values were obtained on the interior slab beam when multiple lanes are loaded simultaneously for all bridge configurations. All critical cases are highlighted in Table A1.6.

According to the proposed design models described previously, the design moment and shear demands for the slab beams of the 26 simply supported bridges were calculated. Table A1.7 lists the critical moment and shear force values determined from FEM analysis and proposed design models. Through comparison with the “exact” FEM solutions, it is

found that the proposed design models provide 16 percent conservative moments and 2 percent conservative shear forces. In order to achieve a reasonable degree of conservatism, the correction factors in the proposed design models were taken as 0.95 and 1.05 for moment and shear actions in spread slab beam bridge configurations.

The AASHTO LRFD Bridge Design Specifications provide empirical LDF formulas for both exterior and interior girders of the prestressed concrete spread box beam bridge, which is very similar with the spread slab beam bridge. Common practice for precast prestressed concrete bridges is to design all the girders the same as a critical girder. The FEM analysis results show that the moments and shear forces of the interior slab beam are dominating amongst all slab beams. Therefore, the design values will be determined based on two governing LDF equations for multiple-lane-loaded interior girders specified in the AASHTO LRFD Specifications:

For moments:
$$\left(\frac{S}{1900}\right)^{0.6}\left(\frac{Sd}{L^2}\right)^{0.125} \tag{6.4}$$

For shears:
$$\left(\frac{S}{2250}\right)^{0.8}\left(\frac{d}{L}\right)^{0.1} \tag{6.5}$$

Table A1.8 lists the design moment and shear force values calculated by the AASHTO LRFD formulas. The median values of the ratios (AASHTO/FEM) show that the AASHTO formulas provide 5 percent higher design moment values than FEM solutions while the median of code-specified shear forces are 6 percent unconservative as compared with FEM values.

Figure 6.6(c) presents the comparisons of moments and shear forces determined from the proposed models, AASHTO LRFD formulas and FEM analysis. The green and red points represent the design values with original and adjusted correction factors respectively. It is evident from Figure 6.6(c) that the proposed design model and AASHTO equation normally generate conservative moment values for design. As for the shear action, AASHTO-specified design values are unconservative as compared with FEM solutions. The cumulative distributions of the moment and shear ratios (Model/FEM and AASHTO/FEM) are shown in Figure 6.6(d). The solid lines represent the lognormal model curves for the proposed design models and AASHTO LRFD empirical equations. The median values show that that the design models with revised correction factors provide about 10 percent conservative moments and 7 percent higher shear forces as compared to FEM solutions. For moment action, the red and blue curves cross the ratio 1.0 at 5 percent probability, which indicates that there is only a 5 percent chance that the moment ratios (Model/FEM, AASHTO/FEM) are below 1.0. In terms of shear action, more than 95 percent of the results from the AASHTO LRFD spread box beam formulas are unconservative when compared to exact FEM solutions. The red solid line indicates that the proposed design model with adjusted correction factor provide conservative shear design values for all bridge configurations without exception. It may be concluded from the statistical analysis that the correction factors of 0.95 and 1.05 are appropriate for moment and shear actions for the design of the simply-supported spread slab beam bridges.

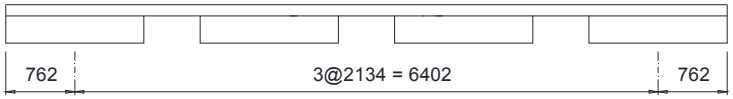

(a) Example of a Four-beam Spread Slab Beam Bridge Deck Striped for Two Lanes

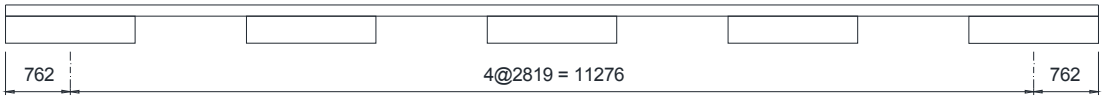

(b) Example of a Five-beam Spread Slab Beam Bridge Deck Striped for Three Lanes

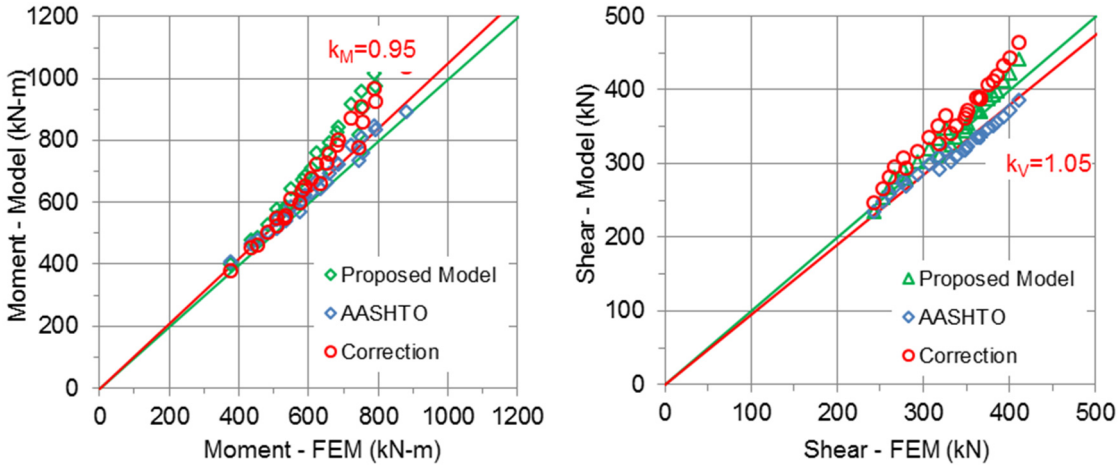

(c) Comparisons between Design and FEM Values

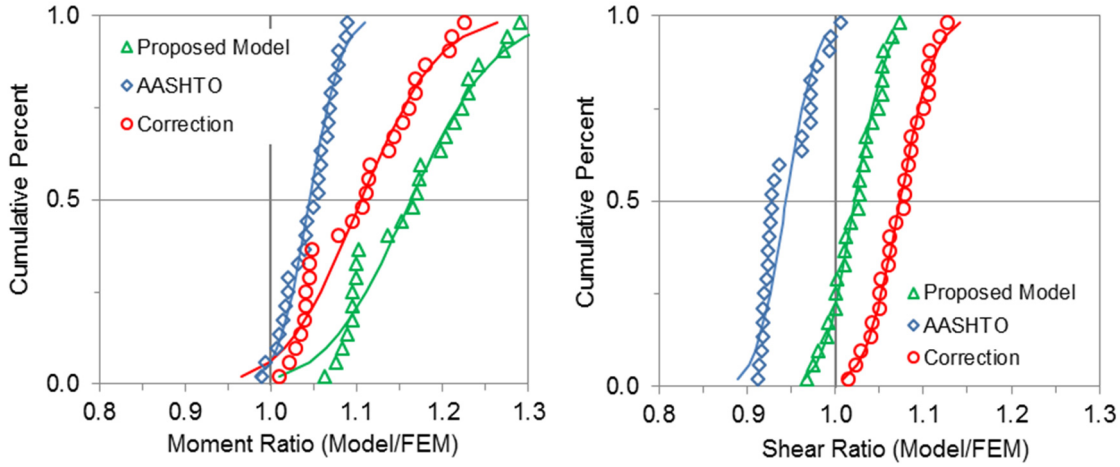

(d) Cumulative Distribution Probabilities of Moment and Shear Ratios

Figure 6.6. Comparisons of Design Moment and Shear Force Values and FEM Solutions for Simply Supported Spread Slab Beam Bridge.

6.9 CLOSURE AND KEY FINDINGS

The proposed design models are proposed for simply supported prestressed concrete girder bridges to determine the moment and shear demands in the service load design stage. A total of 61 bridge FEM models were developed and analyzed, with each bridge model having a different superstructure geometry, to determine the "exact" moment and shear force values which would be further utilized to evaluate the applicability of the proposed design models. Based on the comparative study conducted amongst design values from proposed models, FEM solutions and code-specified results, the following conclusions may be drawn:

1. For simply supported prestressed concrete I-girder bridges, the design models provide 10 percent conservative moment and 6 percent conservative shear force values as compared to computational results. A similar degree of conservatism was obtained from the values specified by the AASHTO LRFD formulas.
2. For simply supported prestressed concrete slab beam bridge decks, the proposed design models provide about 5 percent conservative moment and shear values when compared to computational solutions.
3. For simply supported prestressed concrete spread slab beam bridge, the AASHTO LRFD spread box beam formulas provide unconservative shear design values as compared to exact FEM solutions, which indicates that AASHTO shear equations are not applicable for this new bridge class.
4. For simply supported prestressed concrete spread slab beam bridges, the proposed design models provide about 16 percent conservative moments and 2 percent shear

forces when compared to computational results. For this specific bridge type, it is suggested to adjust the correction factors in the proposed models with 0.95 and 1.05 for moment and shear actions respectively.

5. Generally, the proposed design models provide conservative design values for moment and shear actions, which could be used for service load design of the simply supported prestressed concrete girder bridges. The two recommended equations for moment and shear force demands are:

   For moments: $M_g = k_M \frac{S}{D_M} M_l$

   For shears: $V_g = k_V \frac{S}{D_V} V_l$

   where $D_M = 12 \text{ ft} = 3.66 \text{ m}$; $D_V = 10 \text{ ft} = 3 \text{ m}$; k_M and k_V are normally taken as unity, however for spread slab beam bridges $k_M = 0.95$ and $k_V = 1.05$.

7 DESIGN MODELS FOR CONTINUOUS PRESTRESSED CONCRETE GIRDER BRIDGES

7.1 SUMMARY

Current AASHTO LRFD Bridge Design Specifications provide empirical LDF formulas to determine the moment and shear demands of individual girders in the design of such bridge types. The equations were mainly derived for simply supported bridge configurations and the applicability for continuous bridges has not been fully validated. Practitioners have been critical of equations for the limited range of applicability and the undue complexity that often necessitates an iterative design procedure is required. New design models with a "*S/D*" format are proposed in Section 6 and their applicability are assessed for the continuous bridge configurations in this section. Comparisons are made with present AASHTO methods. An extensive parametric study in which 38 continuous bridge prototypes are analyzed using the finite element method (FEM) is conducted to obtain "exact" girder moments and shear forces. It is shown that the proposed design formulas compare well with FEM solutions and are marginally conservative for continuous bridges.

7.2 INTRODUCTION

Structural analysis for continuous bridge structures can be a complex problem due to the high degree of indeterminacy. For new bridge design or existing bridge evaluation, it is important to determine the maximum positive and negative girder moments, and maximum girder shear forces at critical locations of the continuous bridge structures subjected to live plus impact loads. In the past century, codes of practice adopted the concept of load distribution factor (LDF) to simplify the structural analysis and determine the moment and shear demands. The AASHO Bridge Standard Design Specifications (AASHO 1931) and following updates provided the "*S/5.5*" formulation, which was widely used until the advent of new AASHTO LRFD specifications in the 1990s.

The AASHTO LRFD Bridge Design Specifications (AASHTO 1994) provided a consistent set of power function formulas to calculate LDF values for commonly used bridge types, which accounted for more design parameters. These formulas were mainly derived for simply supported bridge configurations, and the applicability was directly extended to continuous bridges based on Zokaie's findings about continuity effects. Zokaie (2000) claimed that the load distribution factors in continuous bridges are slightly higher than the simply supported cases and this effect could be cancelled by the moment redistribution. A similar commentary is given in Article 4.6 of the AASHTO LRFD Bridge Design Specifications that the lateral load distribution obtained for simple spans is also considered applicable to continuous structures.

Some research work was performed to evaluate the applicability of the code based formulas for continuous bridge configurations. Newmark (1949) carried out several

experimental tests to validate the applicability of the "*S/5.5*" formula for continuous I-girder beam bridges. Samaan (2002) conducted a parametric study to investigate the effect of continuity on the load distribution behavior in composite concrete-steel multi-spine box girder bridges. It was revealed that the use of the formulas proposed by Zokaie et al. (1991) can lead to highly conservative or highly unconservative LDFs for the design of continuous bridges. Mabsout et al. (1998) also evaluated the reliability of the current code method for the design of steel girder bridges. The research findings recommended the use of AASHTO LRFD empirical LDF formulas and AASHTO Standard "*S/5.5*" method with respective reductions of 5% and 15% for multi-span continuous steel girder bridges.

The current AASHTO LRFD method was criticized by researchers and practitioners for its limited range of applicability and complex format as mentioned in Section 6.2. New design models with a "*S/D*" format were developed in the previous section for the purpose of providing bridge design engineers a more straight-forward option to determine the moment and shear demands, particular for the preliminary design phase. Naturally, more precise analyses can be conducted for checking purposes once a preliminary design is completed.

The applicability of the proposed LDFs for prestressed concrete girder bridges commonly used in Texas and elsewhere is evaluated by comparing the proposed design models to more exacting finite element method (FEM) analysis results. This section focuses on evaluating the applicability of the proposed design methods for continuous bridge configurations.

7.3 CURRENT AASHTO DESIGN METHODS FOR CONTINUOUS BRIDGES

The AASHTO LRFD Bridge Design Specifications (AASHTO 2012) designated the HL-93 live load model for the design of bridge decks in the United States. Detailed information about potential loads combination and dynamic allowance requirements are described in Section 6.3.

When applying the HL-93 live load model in the design of the continuous bridges, more complicated load placement schemes need to be considered to determine the maximum moment and shear demands. According to AASHTO LRFD Bridge Design Specifications Section 3.6.1, only one vehicle per lane is allowed on the bridge at a time when determining live load moments in the regions of positive flexure (CALTRANS 2014). For computing the negative moment between points of contraflexure, a second design truck or tandem load is added in combinations with the design lane load (Article 3.6.1.3.1). The two design trucks/tandems shall be placed in adjacent spans and the most adverse force values are calculated as the larger of the following two loading cases (Grubb and Schmidt 2012):

- 90 percent of the effect (two design truck loads + design lane load).
- 100 percent of the effect (two design tandems + design lane load).

Figure 7.1 shows the live load models for the determination of negative moments. The minimum spacing between the lead axle of the second truck and the rear axle of the first truck is specified to be 15.2 m. The distance between the two 143 kN rear axles of

each of the design trucks is to be kept at a constant of 4.3 m. Similarly, the two design tandems are spaced from 7.9 m to 12.2 m apart.

The AASHTO LRFD Bridge Design Specifications (AASHTO 2012) provide empirical LDF formulas for various types of bridge superstructures. These formulas were derived for single spans, but the applicability can be extended to continuous bridge configurations. It is noted that the span length used for the calculation of negative moment demand be the average of the adjacent spans. Table 7.1 lists the definition of span length, L, used for the continuous bridge design.

There are no side-by-side slab beam and spread slab beam configurations defined in the AASHTO LRFD Bridge Design Specifications. However, empirical LDF formulas for both exterior and interior girders of prestressed concrete I-girder bridge and spread box beam bridge are provided in the code. The latter bridge type is very similar to the spread slab beam bridge developed recently by TxDOT.

New design methods are proposed in Section 6.3 to determine the critical design moment and shear demands of bridge girders. For flexural and shear actions, design moments and shears for each girder are determined with Equations (6.2) and (6.3). The correction factors typically take the value of unity. The remainder of this section tests the veracity of Equations (6.2) and (6.3), and then goes on to evaluate correction factors for k_M and k_V, as necessary for continuous bridges.

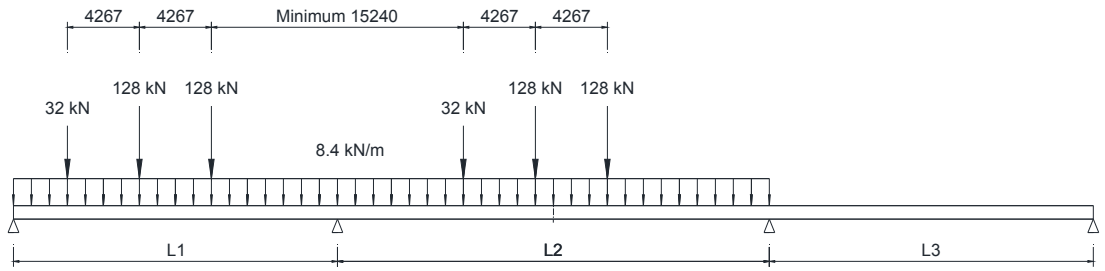

(a) Two Trucks Plus Lane Load

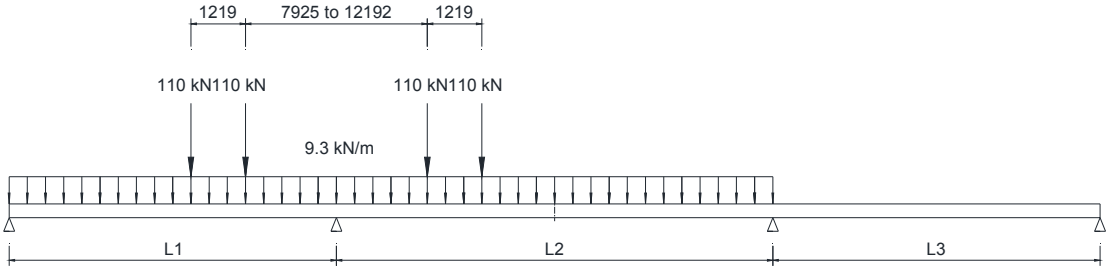

(b) Two Tandem Axle Loads Plus Lane Load

Figure 7.1. Live Load Pattern of Continuous Bridge Configurations to Determine Negative Moment at Supports.

Table 7.1. L for Use in AASHTO LRFD Live LDF Equations (AASHTO 2012).

Force Effect	***L***	
Positive moment	The length of the span for which moment is being calculated	End Span L_1
		Middle Span L_2
Negative moment near interior supports of continuous spans from point of contraflexure to point of contraflexure	The average length of the two adjacent spans	Interior Support: L=0.5*(L_1+L_2)
Shear	The length of the span for which shear is being calculated	End Span L_1
		Middle Span L_2
Interior reaction of continuous span	The average length of the two adjacent spans	Interior Support: L=0.5*(L_1+L_2)

7.4 EVALUATION OF PROPOSED DESIGN MODELS FOR CONTINUOUS PRESTRESSED CONCRETE I-GIRDER BRIDGES

7.4.1 Bridge Superstructure Geometries Considered

Three different bridge roadway widths (10.4, 12.2 and 14.0 m) were selected for all bridge configurations to account for a wide range of girder spacings, number of lanes and span lengths. Based on design experience, a new girder type, Tx82, is also included to reach greater span lengths. Table 7.2 presents the geometric information of the selected simply supported prestressed concrete I-girder bridge configurations.

7.4.2 FEM Analysis Strategies

All 14 continuous prestressed concrete I-girder bridge cases were modeled using a detailed FEM analysis and the maximum girder moment and shear force values were obtained for each bridge case. The FEM analysis was performed using the CSiBridge (Computers and Structures 2013) software package.

The transverse load alignments were arranged in the same fashion with the simply supported bridge analysis described in Section 6.4.2 so that the most adverse combination of load effects would be captured. Through the rigorous FEM analysis, the "exact" internal force values at critical sections of continuous bridge, such as: moment at mid-spans and shear forces at supports, could be determined for the future comparison. It is worth mentioning that vehicle class consisting of two truck/tandems was defined in the FEM models to determine the critical negative moment values. The AASHTO multiple presence factor and dynamic allowance were also considered in the analysis.

Table 7.2. Continuous I-girder Bridge Geometries.

No.	Bridge Width, *B* (m)	Roadway Width, *W* (m)	Girder Spacing, *S* (m)	No. of Girders	No. of Lanes	Span Length, *L* (m)	Girder Type
1	10.4	9.8	2.8	4	2	45.7 – 61.0 – 45.7	Tx70
2	10.4	9.8	2.8	4	2	45.7 – 61.0 – 45.7	Tx82
3	10.4	9.8	2.8	4	2	57.9 – 73.2 – 57.9	Tx70
4	10.4	9.8	2.8	4	2	57.9 – 73.2 – 57.9	Tx82
5	12.2	11.6	2.6	5	3	45.7 – 61.0 – 45.7	Tx70
6	12.2	11.6	2.6	5	3	45.7 – 61.0 – 45.7	Tx82
7	12.2	11.6	2.6	5	3	57.9 – 73.2 – 57.9	Tx70
8	12.2	11.6	2.6	5	3	57.9 – 73.2 – 57.9	Tx82
9	14.0	13.4	2.4	6	3	45.7 – 61.0 – 45.7	Tx70
10	14.0	13.4	2.4	6	3	45.7 – 61.0 – 45.7	Tx82
11	14.0	13.4	2.4	6	3	57.9 – 73.2 – 57.9	Tx70
12	14.0	13.4	2.4	6	3	57.9 – 73.2 – 57.9	Tx82
13	14.0	13.4	2.4	6	3	64.0 – 85.3 – 64.0	Tx70
14	14.0	13.4	2.4	6	3	64.0 – 85.3 – 64.0	Tx82

7.4.3 Analysis Results Evaluation for Continuous I-girder Bridges

Appendix Tables A2.1 and A2.2 list the computational results of the moment and shear force values for 14 continuous prestressed concrete I-girder bridge configurations when one lane or multiple lanes are loaded; all critical cases are highlighted in bold typeface within the tables. It is seen that that for all 14 bridges, the critical shear forces were obtained at interior girders when multiple lanes were loaded, while most critical moment values were captured on exterior girders when multiple lanes were loaded.

According to the proposed design models previously developed in Section 6.4, the design moment and shear forces at critical locations for the girders of the 14 continuous bridge configurations could be determined. Tables A2.3 and A2.4 list the critical moment and shear force values calculated from FEM analysis and proposed design models. The median values of the ratios (Model/FEM) show that the design models provide over 15 percent conservative moment and over 8 percent conservative shear force values as compared to computational results. In order to achieve a modest degree of conservatism for design moments and shears at all critical locations, a correction factor for proposed design models may be taken as $k_M = 0.9$ for the moment actions in prestressed concrete continuous I-girder bridge configurations.

The AASHTO LRFD Bridge Design Specifications provide empirical LDF formulas to calculate the most adverse girder moments and shear forces as listed in Tables A2.5 and A2.6. It is seen that similar degree of conservatism for shear force values was obtained from code-specified values. However, it is found that AASHTO LRFD LDF

formulas provide slightly unconservative design values for negative moment at interior support and positive moment at midspan as compared with FEM solutions.

Figure 7.2 presents the comparisons of the moment and shear force values at critical locations determined from the proposed model, AASHTO LRFD empirical formula and FEM analysis. The green and red points represent the design values with original and adjusted correction factors respectively. It is evident from Figure 7.2 that proposed models generate conservative moment and shear values for design while AASHTO LRFD empirical formulas provide slight lower negative moment at interior support and positive moment at midspan than FEM solutions. The cumulative probabilities of the moment and shear ratios (Model/FEM and AASHTO/FEM) are also plotted in Figure 7.3 to better visualize the distribution of each data point and their probability of occurrence. The solid lines represent the fitted lognormal cumulative distributions to the different design methods. The model curve is a curve that the same lognormal standard deviation and median as the ratios of the proposed models or AASHTO code method. It is seen that the dispersions of moment values determined from both proposed models and AASHTO LRFD formulas are quite small. The solid red lines show that the proposed design models with adjusted correction factors provide conservative design moment and shear force values for all bridge configurations without exception. The lognormal model curves for the AASHTO LRFD formulas (blue line) show that all LRFD specified values for negative moments at the interior support are unconservative, and for at least 70 percent of all design cases the AASHTO LRFD method remains unconservative for positive moments at the interior midspan location. In addition, the comparisons of moments and

shear forces at all critical locations and the corresponding cumulative distributions are represented in Figure 7.4 to get a general view of the performance of the proposed design models and AASHTO LRFD formulas on continuous slab beam configurations. From the statistical comparative results above, it can be concluded that the proposed models with suitable correction factors are adequate for the design of the continuous I-girder bridges.

7.5 EVALUATION OF PROPOSED DESIGN MODELS FOR CONTINUOUS PRESTRESSED CONCRETE SLAB BEAM BRIDGES

7.5.1 Bridge Superstructure Geometries Considered

Two different bridge roadway widths (7.3 and 9.1 m) specified by TxDOT standard drawings are utilized herein to conduct the parametric study. Short span prestressed concrete slab beam bridges are commonly used for simply supported cases and the applicable range of span length is 7.6 m to 15.2 m. However, previous design experience shows that this bridge type could be applied to continuous cases and the maximum span length could reach up to 21.3 m with the help of the post-tensioning technique. Table 7.3 presents the geometric information of selected continuous slab beam bridge configurations, which include the most adverse design parameters.

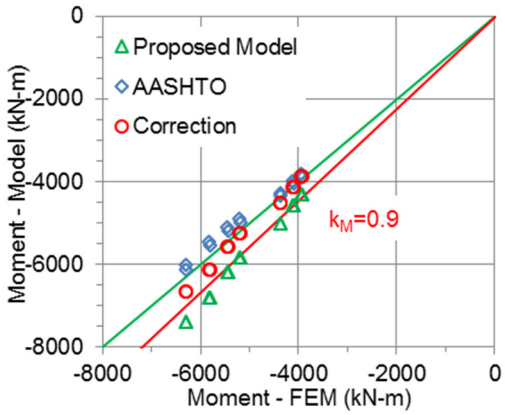

(a) Negative Moment (Continuous Support)

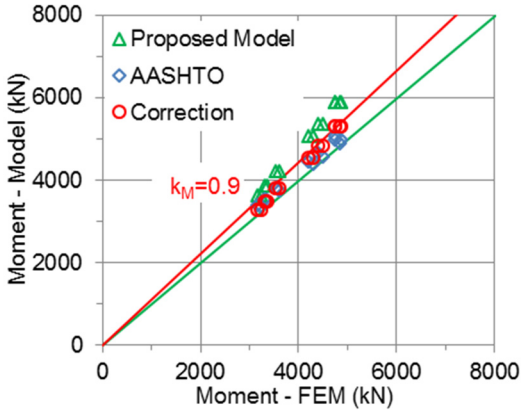

(b) Positive Moment (End Span)

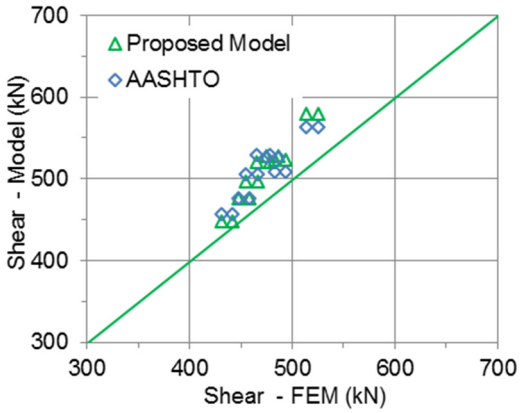

(c) Shear (End Support)

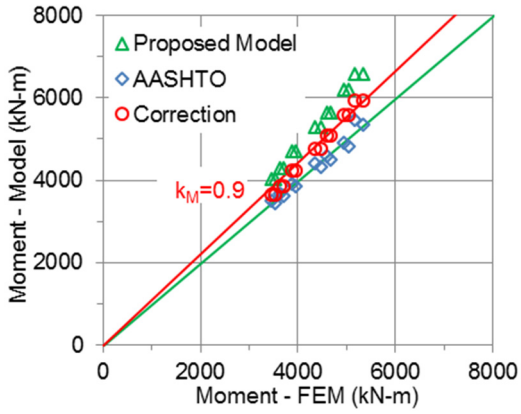

(d) Positive Moment (Interior Span)

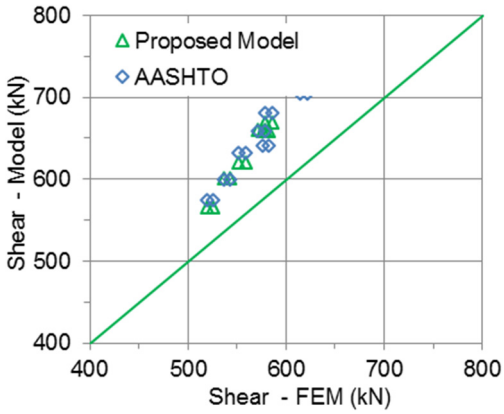

(e) Shear (Continuous Support)

Figure 7.2. Comparisons between Model and FEM Values (Continuous Prestressed Concrete I-girder Bridge).

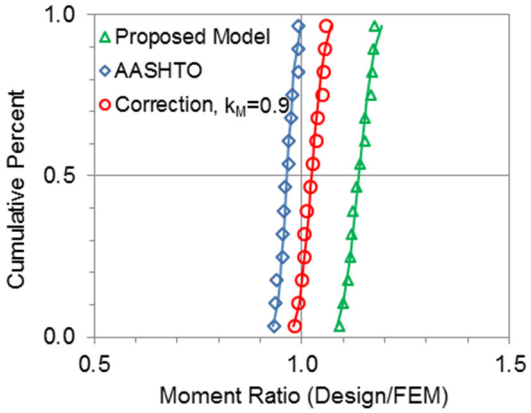

(a) Negative Moment (Continuous Support)

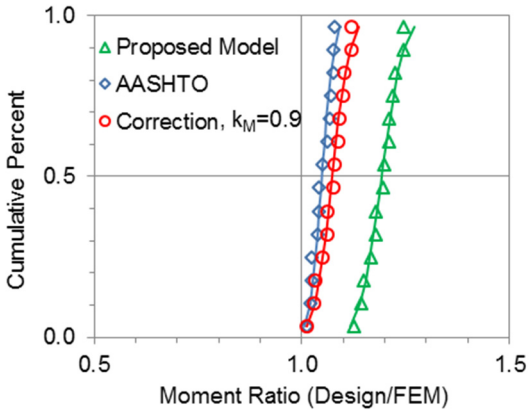

(b) Positive Moment (End Span)

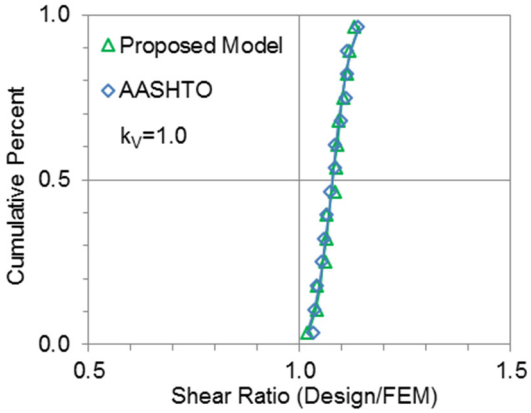

(c) Shear (End Support)

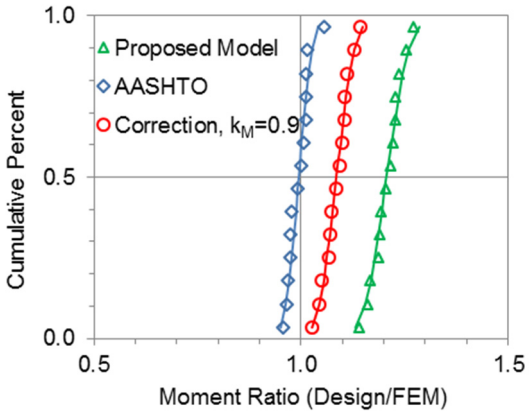

(d) Positive Moment (Interior Span)

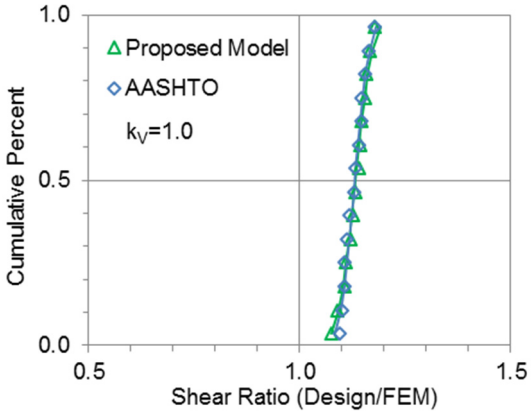

(e) Shear (Continuous Support)

Figure 7.3. Cumulative Distribution Probabilities of the Moment and Shear Ratios (Continuous Prestressed Concrete I-girder Bridge).

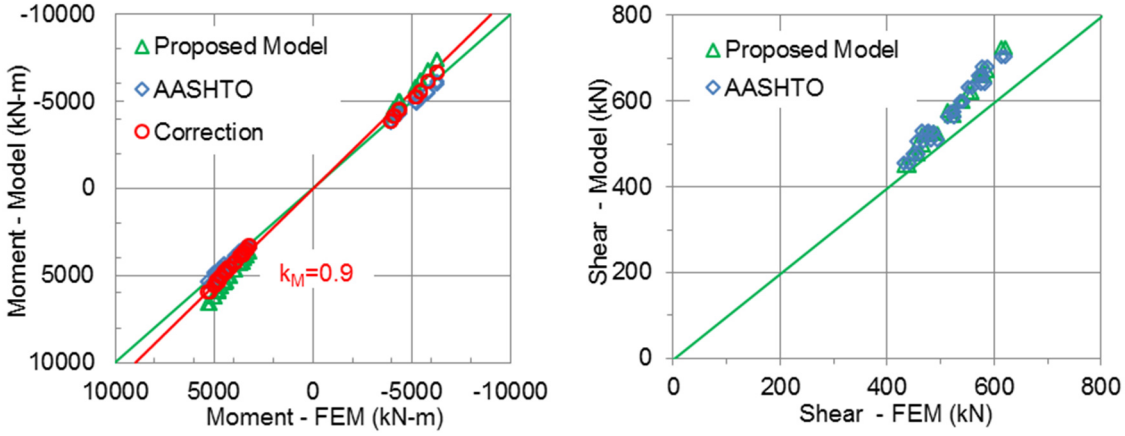

(a) Comparisons between Model and FEM Values

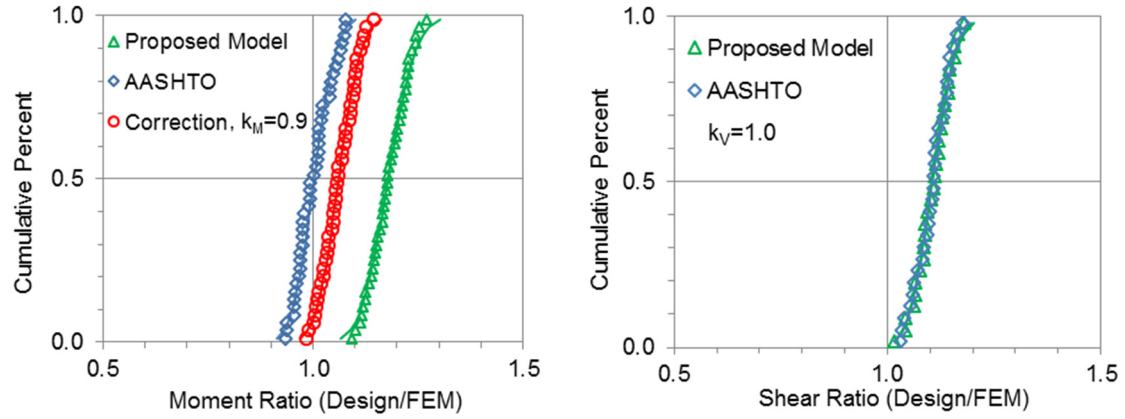

(b) Cumulative Distribution Probabilities of Moment and Shear Ratios

Figure 7.4. Comparisons of Design Moment and Shear Force Values and FEM Solutions for Continuous Prestressed Concrete I-girder Bridge: Including Moments and Shear Forces at All Critical Locations.

Table 7.3. Continuous Slab Beam Bridge Geometries.

No.	Bridge Width *B* (m)	Roadway Width, *W* (m)	Girder Spacing, *S* (m)	No. of Beams	No. of Lanes	Span Length, *L* (m)	Girder Type
1	7.9	7.3	1.6	5	2	13.7 – 18.3 – 13.7	5SB15
2	7.9	7.3	1.6	5	2	15.2 – 19.8 – 15.2	5SB15
3	7.9	7.3	1.6	5	2	16.8 – 21.3 – 16.8	5SB15
4	9.8	9.1	1.2	8	2	13.7 – 18.3 – 13.7	4SB15
5	9.8	9.1	1.2	8	2	15.2 – 19.8 – 15.2	4SB15
6	9.8	9.1	1.2	8	2	16.8 – 21.3 – 16.8	4SB15

7.5.2 FEM Analysis Strategies

Similar to prestressed concrete I-girder bridge analysis described previously, all six continuous prestressed concrete slab beam bridge cases were modeled using the CSiBridge software package and maximum moment and shear force values of slab beams were obtained for each bridge configuration. The eight-node linear solid element having three degrees of freedom at each node was utilized to model both slab beam and deck. The concrete compressive strength for beam and deck are specified as 59 MPa (8.5 ksi) and 28 MPa (4 ksi), respectively.

The alignments adopted for the FEM analysis of prestressed concrete slab beam bridge superstructures were arranged in a similar fashion with the analysis of prestressed concrete I-girder bridges so that the most adverse combination of load effects would be captured. In the analysis process, the multiple presence factor and dynamic allowance

were also considered. The "exact" internal force values at critical sections of each continuous bridge could be obtained from FEM analysis and further compared with the design values.

7.5.3 Analysis Results Evaluation for Continuous Slab Beam Bridges

Tables A2.7 and A2.8 list the FEM solutions of the moment and shear force values at critical locations for six continuous slab beam bridge configurations when one lane or two lanes are loaded; all critical cases are highlighted in the tables. It is seen that for all six bridges, the critical moments and shear forces were obtained when two lanes were loaded simultaneously except for the 9.8 m wide bridge configuration with the longest span length. No consistent pattern was found to show whether exterior or interior slab beam provide more critical moments and shear forces.

The design moment and shear forces at critical locations for the slab beams of the six continuous bridge configurations were calculated according to the proposed design models. Tables A2.9 and A2.10 list the moment and shear force values at critical locations calculated from FEM analysis and proposed design models. The median values show that the design models provide about 8 percent conservative positive moment values at both side and mid spans and 4 percent higher negative moment values at the interior support as compared to the computational results. In terms of shear forces, the proposed design values are more than 10 percent higher than FEM solutions. In order to achieve a reasonable degree of conservatism for design shear forces, the correction factors for the proposed design models were taken as 0.95 for shear action in prestressed concrete continuous slab beam bridge configurations.

Figure 7.5(c) shows the comparisons of moments and shear forces at all critical locations determined from the proposed models and FEM analysis. It is evident that the proposed models with adjusted correction factors normally generate slightly conservative design values for both moment and shear actions. The cumulative probabilities of the moment and shear ratios, in which design loads determined from proposed models are divided by FEM values, are shown in Figure 7.5(d). It is evident that the final formulas generate conservative design values for all bridge configurations. The standard deviations for the moment and shear ratios are lower than 0.05. Based on the statistical results, it can be concluded that the proposed models are reliable for design of the continuous slab beam bridges.

7.6 EVALUATION OF PROPOSED DESIGN MODELS FOR CONTINUOUS PRESTRESSED CONCRETE SPREAD SLAB BEAM BRIDGES

7.6.1 Bridge Superstructure Geometries Considered

Six different bridge roadway widths (7.9, 9.1, 10.4, 11.6, 12.8 and 14.0 m) were selected for all bridge configurations to account for a wide range of beam spacing and different lane numbers. The feasible span length and beam spacing of simply supported bridge cases are determined based on the parametric study completed by Hueste et al. (2015). Based on the previous design experience, the maximum span length can reach up to 21.3 m with the help of post-tensioning when the spread slab beam bridge configuration is applied to continuous cases. Table 7.4 presents the geometric information of selected continuous slab beam bridge configurations, which includes the most adverse design parameters.

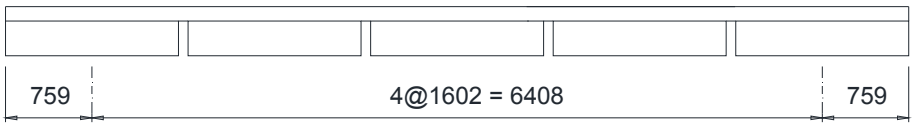

(a) An Example of A Four-beam Slab Beam Bridge Deck Striped for Two Lanes

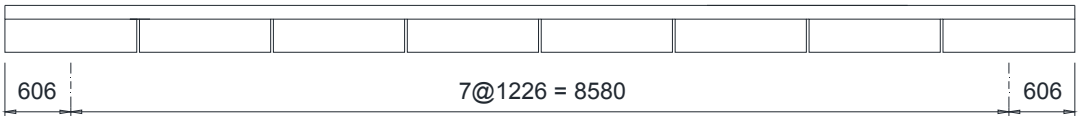

(b) An Example of A Five-beam Slab Beam Bridge Deck Striped for Three Lanes

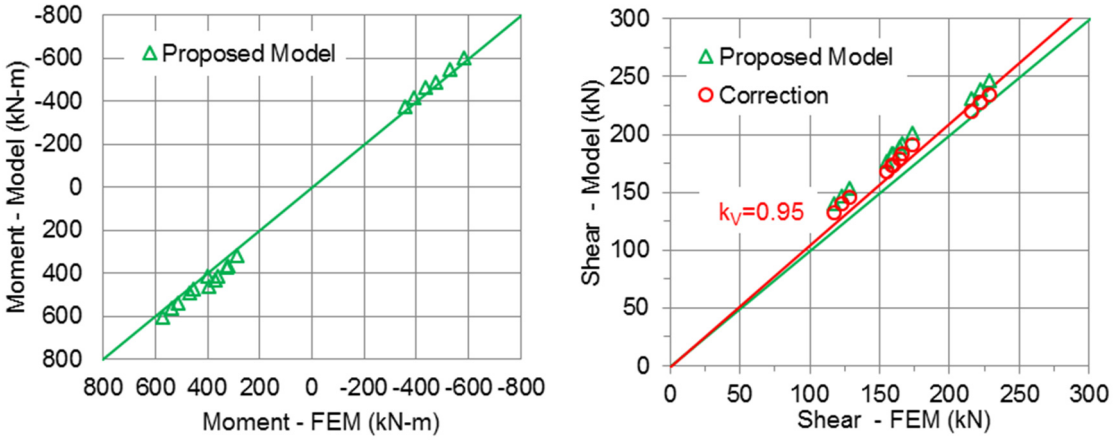

(c) Comparisons between Model and FEM Values

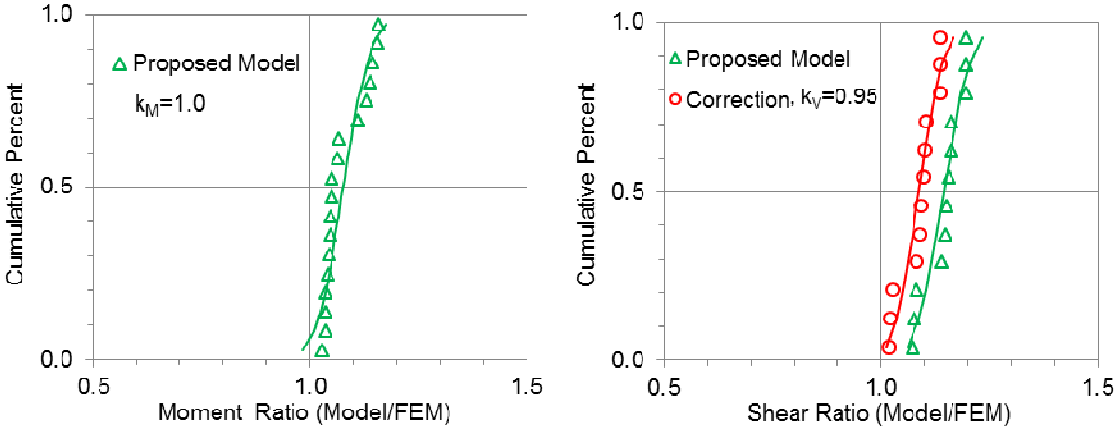

(d) Cumulative Distribution Probabilities of Moment and Shear Ratios

Figure 7.5. Comparisons of Design Moment and Shear Force Values and FEM Solutions for Continuous Prestressed Concrete Slab Beam Bridge: Including Moments and Shear Forces at All Critical Locations.

Table 7.4. Continuous Spread Slab Beam Bridge Geometries.

No.	Bridge Width, *B* (m)	Roadway Width, *W* (m)	Girder Spacing, *S* (m)	No. of Beams	No. of Lanes	Span Length, *L* (m)	Girder Type
1	7.9	7.3	2.1	4	2	13.7 – 18.3 – 13.7	5SB15
2	7.9	7.3	2.1	4	2	15.2 – 19.8 – 15.2	5SB15
3	7.9	7.3	2.1	4	2	16.8 – 21.3 – 16.8	5SB15
4	9.1	8.5	2.5	4	2	13.7 – 18.3 – 13.7	5SB15
5	9.1	8.5	2.5	4	2	15.2 – 19.8 – 15.2	5SB15
6	9.1	8.5	2.5	4	2	16.8 – 21.3 – 16.8	5SB15
7	10.4	9.8	2.9	4	2	13.7 – 18.3 – 13.7	5SB15
8	10.4	9.8	2.9	4	2	15.2 – 19.8 – 15.2	5SB15
9	10.4	9.8	2.9	4	2	16.8 – 21.3 – 16.8	5SB15
10	11.6	11.0	3.4	4	3	13.7 – 18.3 – 13.7	5SB15
11	11.6	11.0	3.4	4	3	15.2 – 19.8 – 15.2	5SB15
12	11.6	11.0	3.4	4	3	16.8 – 21.3 – 16.8	5SB15
13	12.8	12.2	2.8	5	3	13.7 – 18.3 – 13.7	5SB15
14	12.8	12.2	2.8	5	3	15.2 – 19.8 – 15.2	5SB15
15	12.8	12.2	2.8	5	3	16.8 – 21.3 – 16.8	5SB15
16	14.0	13.4	3.1	5	3	13.7 – 18.3 – 13.7	5SB15
17	14.0	13.4	3.1	5	3	15.2 – 19.8 – 15.2	5SB15
18	14.0	13.4	3.1	5	3	16.8 – 21.3 – 16.8	5SB15

7.6.2 FEM Analysis Strategies

Similar with prestressed concrete slab beam bridge analysis, all continuous spread slab beam bridge cases were modeled using solid element and maximum moment and shear force values of slab beams were obtained for each bridge case. The load alignments adopted for the FEM analysis of multiple-lane prestressed concrete spread slab beam bridge superstructures were arranged in a similar fashion with the previous two bridge types so that the most adverse combination of load effects would be captured through rigorous analysis.

7.6.3 Analysis Results Evaluation for Continuous Spread Slab Beam Bridges

Tables A2.11 and A2.12 list the FEM solutions of the moment and shear force values at critical locations for 18 continuous spread slab beam bridge cases when one lane and multiple lanes are loaded; all critical cases are highlighted in the tables. It is evident that for all 18 bridges, the critical moment and shear forces were obtained on interior slab beams when multiple lanes were loaded simultaneously.

The design moments and shear forces at critical locations for the slab beams of the 18 continuous bridge configurations could be determined on the basis of the proposed design models. Tables A2.13 and A2.14 list the moment and shear force values at critical locations calculated from FEM analysis and proposed design models. The median values shows that the proposed design models provide about 25 percent conservative positive moment values at both end and middle spans and 15 percent higher negative moment values at the interior supports as compared to computational results. In particular, the

degree of conservatism for the 26 ft wide bridges is smaller than other bridge cases. In terms of shear forces, the proposed design values are 9 percent higher at the end supports and 18 percent higher at interior piers than the FEM solutions. In order to achieve a reasonable degree of conservatism for design moments and shear forces at all critical locations, the correction factors in proposed design models were taken as 0.95 for moment and shear actions in prestressed concrete continuous spread slab beam bridge configurations.

The AASHTO LRFD Specifications provided empirical LDF formulas for both exterior and interior girders of the prestressed concrete spread box beam bridge, which is very similar with the spread slab beam bridge. Common practice for precast prestressed concrete bridges is to design all girders the same as a critical girder. The FEM analysis results show that the moments and shear forces of the interior slab beam are dominating amongst all slab beams for all continuous bridge configurations. Therefore, the design moment and shear force values will be determined based on two governing LDF equations (shown in (6.4) and (6.5)) for multiple-lane-loaded interior girders specified in the AASHTO LRFD Specification.

Tables A2.15 – A2.16 list the design moment and shear force demands at critical locations determined by AASHTO formulas. The median values of moment ratio (AASHTO/FEM) show that the design formulas provide about 5 percent higher positive moment values at the end spans as compared to FEM solutions. However the design values are unconservative for negative moment at the interior supports and positive moment at the middle span. In particular, the design values for negative moment are 7 percent smaller

than the “exact” FEM values. In terms of shear forces, the values specified by AASHTO formulas are slightly unconservative at the end supports, but slightly conservative at interior piers as compared to FEM solutions.

Figure 7.6 presents the comparisons of the moments and shear forces at critical locations determined from proposed models, AASHTO LRFD formulas and FEM analysis. It is evident that the proposed models normally generate conservative moment and shear force values for design. The degree of conservatism for the proposed models are higher than that for AASHTO LRFD formulas. In particular, the negative moments at interior support and shear forces at end support determined by those two equations are unconservative as compared with FEM solutions. The cumulative distribution of the moment and shear ratios (Model/FEM and AASHTO/FEM) is shown in Figure 7.7. The solid lines represents the lognormal model curves for the corresponding design methods. It is seen that the proposed design model with adjusted correction factors provide conservative positive moment and shear design values for all bridge configurations without exception. In terms of negative moment at interior support, at least 95 percent of the proposed design solutions are conservative. In contrast, the AASHTO equations are only reliable for the positive moment at end span. In addition, the comparisons of moments and shear forces at all critical locations and the corresponding cumulative distributions are represented in Figure 7.8 to get a general view of the performance of the proposed design models and AASHTO formulas on continuous spread slab beam configurations. It can be concluded from the statistical results that the proposed models are satisfactory for the design of the continuous slab beam bridges.

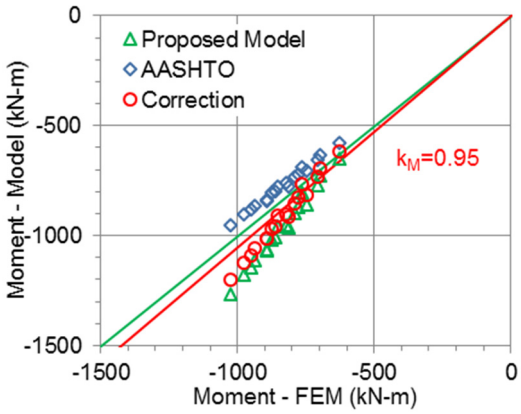

(a) Negative Moment (Continuous Support)

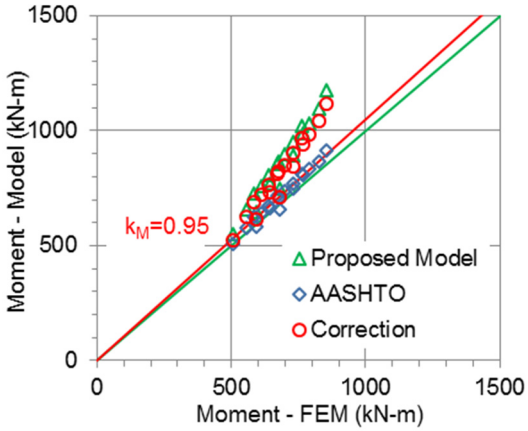

(b) Positive Moment (End Span)

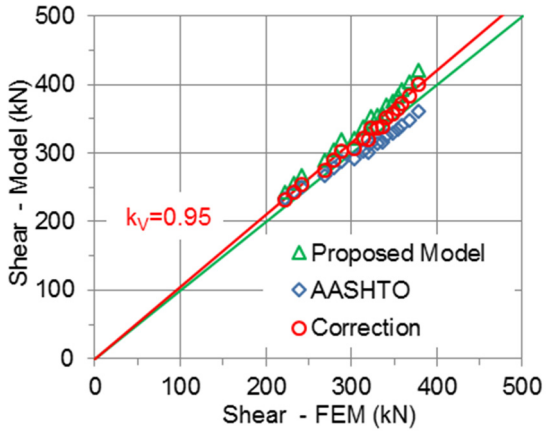

(c) Shear (End Support)

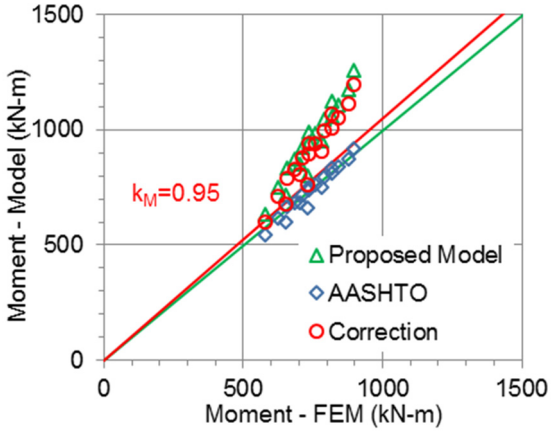

(d) Positive Moment (Interior Span)

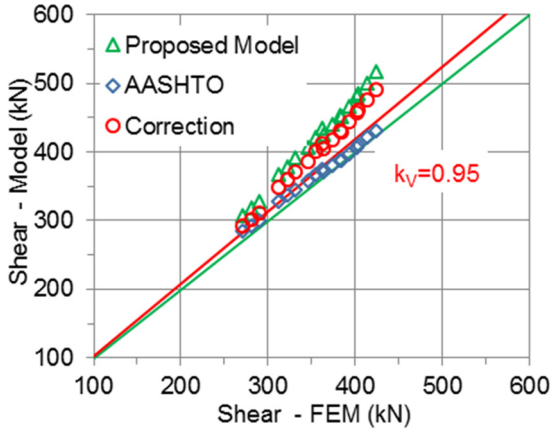

(e) Shear (Continuous Support)

Figure 7.6. Comparisons between Model and FEM Values for Continuous Spread Slab Beam Bridges.

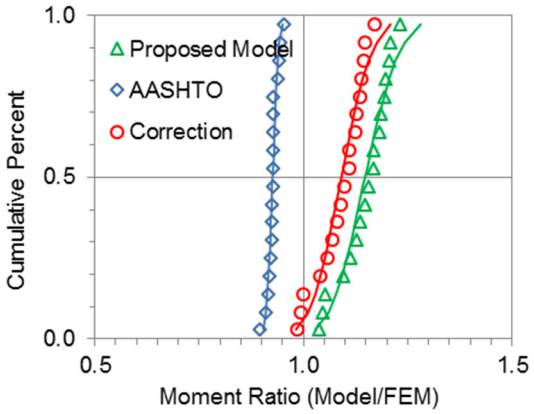

(a) Negative Moment (Continuous Support)

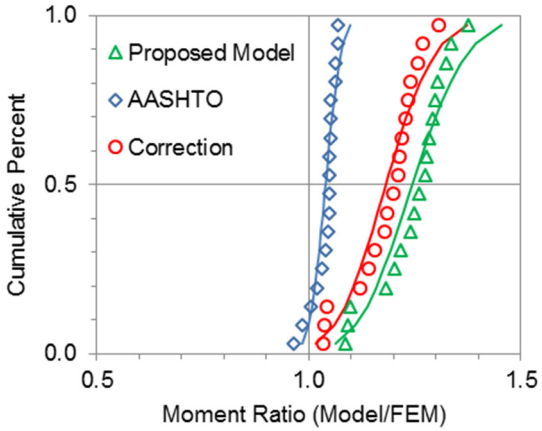

(b) Positive Moment (End Span)

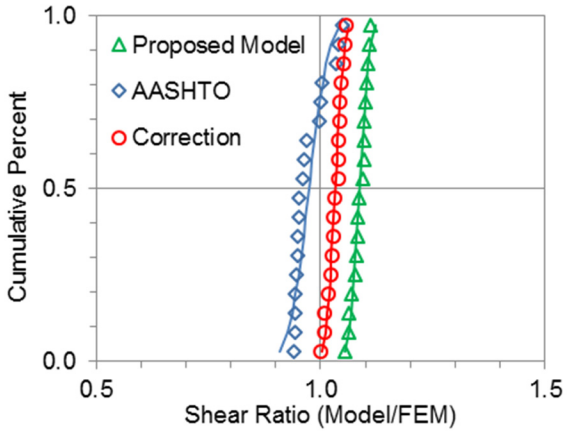

(c) Shear (End Support)

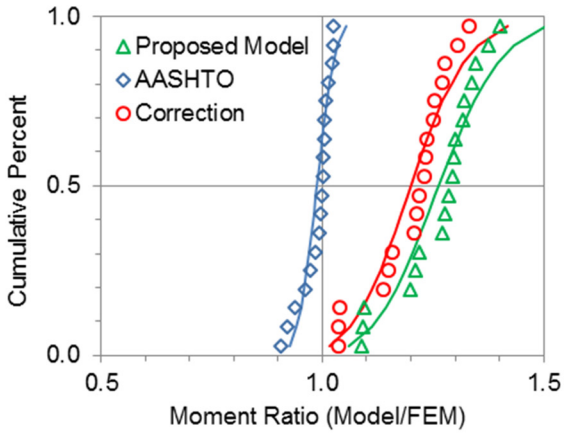

(d) Positive Moment (Interior Span)

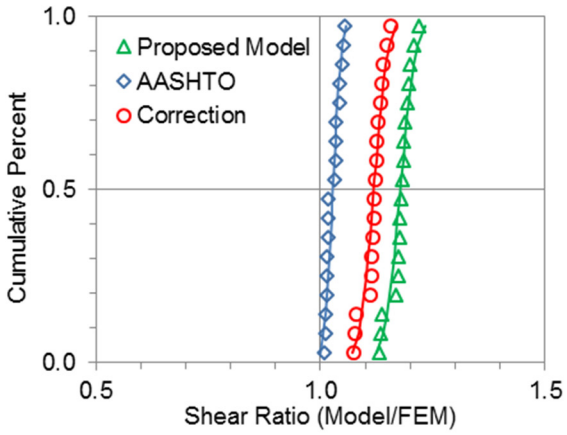

(e) Shear (Continuous Support)

Figure 7.7. Cumulative Distribution Probabilities of the Moment and Shear Ratios for Continuous Spread Slab Beam Bridges.

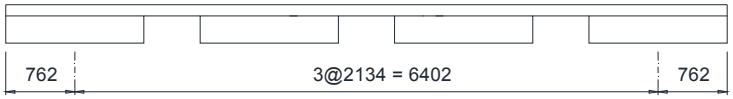

(a) An Example of A Four-beam Spread Slab Beam Bridge Deck for Two Lanes

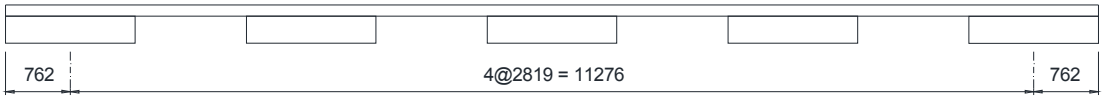

(b) An Example of A Five-beam Spread Slab Beam Bridge Deck for Three Lanes

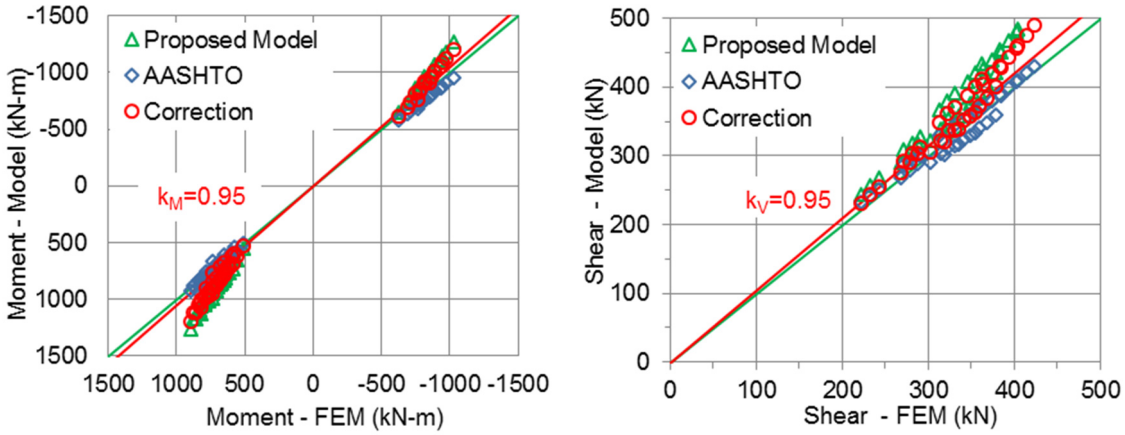

(c) Comparisons between Model and FEM Values

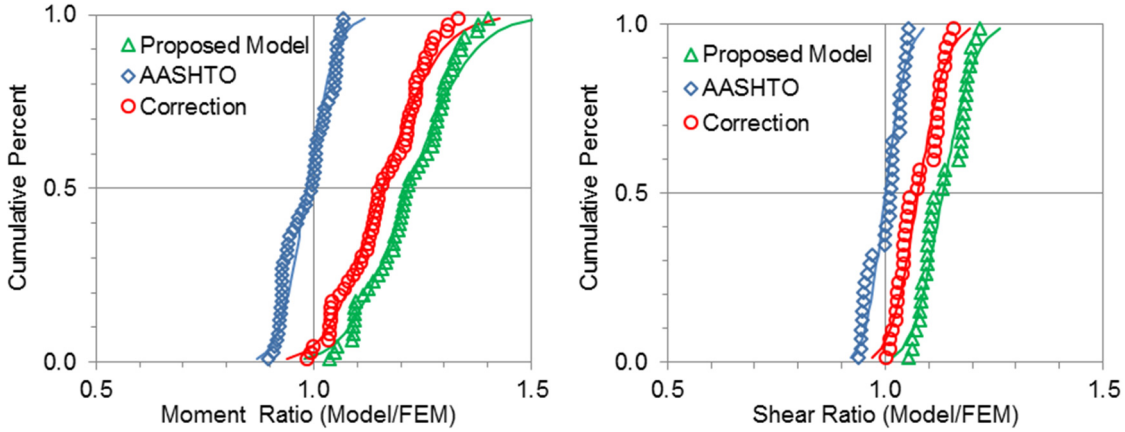

(d) Cumulative Distribution Probabilities of the Moment and Shear Ratios

Figure 7.8. Comparisons of Design Moment and Shear Force Values and FEM Solutions for Continuous Prestressed Concrete Spread Slab Beam Bridge: Including Moments and Shear Forces at All Critical Locations.

7.7 CLOSURE AND KEY FINDINGS

Design models were proposed for continuous prestressed concrete girder bridges to determine the moment and shear demands at the service load stage of design or for the rapid checking of computer output. A total of 38 bridge FEM models were developed and analyzed, with each bridge model having a different superstructure geometry, to determine the "exact" moment and shear force values which would be further utilized to evaluate the applicability of the proposed design models. Based on the comparative study conducted amongst design values from proposed models, FEM solutions and code-specified results, the following conclusions may be drawn:

1. For continuous prestressed concrete I-girder bridge decks, the design models with adjusted correction factors provide over 9 percent conservative moment and 8 percent conservative shear force values when compared to the "exact" computational results. It was also observed that AASHTO LRFD LDF formulas provide slightly unconservative design values for negative moment at continuous interior supports and positive moment at midspan of the middle span when compared with the "exact" FEM solutions.
2. For continuous prestressed concrete slab beam bridge cases, the final design formulas generate conservative moment and shear design values at critical locations and are suitably reliable for the service load phase of a design.
3. For continuous prestressed concrete spread slab beam bridges, the design models with adjusted correction factors provide over 15 percent conservative positive moment values at both end and middle spans and 8 percent higher negative moment values at

interior support as compared to computational results. In terms of shear forces, the proposed design values are 4 percent higher at end supports and over 10 percent higher at the interior piers than FEM solutions. Moreover, the AASHTO LRFD formulas generate unconservative design values for negative moments over continuous supports and shear forces at the simple end supports.

4. Generally, the proposed design models provide conservative design values for moment and shear actions, which could be used for service load design. It is also found that the continuity help to increase the conservatism of the proposed design models. The correction factors, k_M and k_V, in the two recommended Equations (6.2) and (6.3) for simply supported and continuous bridge configurations are tabulated in Table 7.5.

Table 7.5. Summary of Correction Factors.

Bridge Types	Simply Supported		Continuous	
	k_M	k_V	k_M	k_V
Prestressed Concrete I-girder	1.0	1.0	0.9	1.0
Slab Beam Bridge Deck	1.0	1.0	1.0	0.95
Spread Slab Beam Bridge Deck	0.95	1.05	0.95	0.95

8 PLASTIC OVERSTRENGTH ANALYSIS OF SLAB-ON-BEAM BRIDGES

8.1 SUMMARY

The evaluation of the ultimate load capacity of bridge superstructures is a necessary part of design checking. Since the 1950s, several plastic methods have been developed and successfully implemented for the design and analysis of structural concrete slabs, including yield line theory, strip methods, etc. In this section, plastic methods of analysis are utilized to predict the overstrength capacity of slab-on-beam bridge decks at the ultimate collapse load. Different limiting behavior modes are considered which include: slab-only mechanisms, a beam-only mechanism and mixed beam-slab mechanisms. Contrasting results are presented using upper bound yield line theory and lower bound strip methods. The limit analysis methods are applied to two realistic but contrasting spread slab beam bridge prototypes, the Riverside Bridge and the US 69 Bridge. By comparing the collapse loads from different yield-line patterns together with strip method solutions, the plastic overstrength factors for the two bridges are determined. It is demonstrated that the different analysis methods, when accurately applied are in agreement even though results are slightly different due to underlying assumptions. While it is evident that the two bridge designs are sufficiently safe at their ultimate limit states, the plastic overstrength analyses provide important information regarding the "balance" of each design with respect to the hierarchy of failure mechanisms. Local flexural failure is more likely when wheel loads are applied to the slab at the end of the bridge deck. To

remove this undesirable feature it is suggested to strengthen the end region of the deck slab by adding more reinforcing steel to rebalance the design.

8.2 INTRODUCTION

A necessary part of bridge deck design is to check the ultimate load capacity under critical flexure and shear conditions. Plastic methods of analysis have long been available for such design checks, although such limit methods are seldom used for analysis and design outside of Europe and Australasia. Limit analysis methods are useful in identifying the critical behavior modes, however they have seldom been used to investigate the possibility of mixed failure modes such as a mixed flexure and shear failure, or a mixed deck slab and beam failure.

This section considers the use of plastic methods of analysis to investigate the reserve strength capacity of a bridge deck. Both classic upper bound (yield line theory) and lower bound (strip methods) methods are utilized and extended to incorporate the possibility of mixed failure mechanisms. To investigate the sufficiency of a design a plastic overstrength factor is defined as:

$$\Omega = \frac{\phi R_n}{Q_u} \tag{8.1}$$

in which ϕ = critical mechanism-specific strength reduction factor; R_n = collapse load resistance based on nominal material properties; and Q_u = factored up demand loads such as those in the AASHTO LRFD Bridge Design Specifications (AASHTO 2012)

$1.25DL + 1.75(LL + IM)$, where DL, LL and IM represent dead load, live load and impact factor, respectively. Note the design is considered to be conservative when $\Omega \geq 1$.

Certain collapse mechanisms, such as flexure, are desirable as they are generally ductile, whereas shear mechanisms are undesirable as shear failures are generally brittle and such failures occur without warning. Thus, it is contended that it is desirable to investigate the hierarchy of failure mechanisms. As a consequence of knowing the failure mechanism hierarchy, it is possible to check the "balance" of a particular design. For example, if a shear mechanism governs the collapse load hierarchy, it may be a straightforward matter to avert this undesirable possibility by adding more steel to ensure a more ductile flexure mechanism governs the performance at the ultimate limit state.

In this section, the upper bound yield line theory, lower bound strip methods together with a computational grillage method are used to predict the overstrength capacity of slab-on-beam bridge decks at the ultimate collapse load. Three types of limiting behavior modes are considered in the analysis: slab-only mechanisms, a beam-only mechanism and mixed beam-slab mechanisms. The limit analysis methods are applied and the results discussed for a new class of spread slab beam bridge recently developed and implemented in Texas. Critical collapse mechanisms are identified and overstrength capacities are assessed for two prototype spread slab beam bridges: (i) the Riverside Bridge which has widely spaced slab beams and (ii) the US 69 Bridge which has narrow spaces between each slab beam.

8.3 LIMITING BEHAVIOR MODES AT ULTIMATE STRENGTH

Figure 8.1 shows the characterization of limit behavior modes for a slab-on-beam bridge deck. For a vulnerable deck slab, local slab failure mechanisms as shown in Figure 8.1(a) may occur due to high wheel loads applied within the deck slab at different locations. Conversely, when the connecting deck slab is sufficiently strong to successfully transfer the applied load from one beam to the neighboring beam without failure occurring on the deck slab, the global beam failure mechanism occurs as shown in Figure 8.1(b). A combination of beam and slab mechanisms may exist and this is referred to herein as mixed beam-slab mechanism as shown in Figure 8.1(c).

It is well known that yield line theory generally provides either the "correct" or an upper bound estimate to the "true" ultimate load. In order to identify the critical yield line mechanism, the analyst needs to postulate a wide variety of potential kinematically admissable yield line patterns; the lowest collapse load being the critical case.

The ultimate load corresponding to potential yield line collapse mechanisms may be determined using the components of virtual work formed by Park and Gamble (2000):

$$\sum W_u \Delta = \sum m_x \theta_x l_y + \sum m_y \theta_y l_x \tag{8.2}$$

where W_u = total load on a segment of the yield line pattern; Δ = movement of a segment's centroid; m_x, m_y = ultimate moment capacities per unit length in the x and y directions; θ_x, θ_y = plastic rotation angles in x and y directions; and l_x, l_y = length of yield lines in x and y directions, respectively.

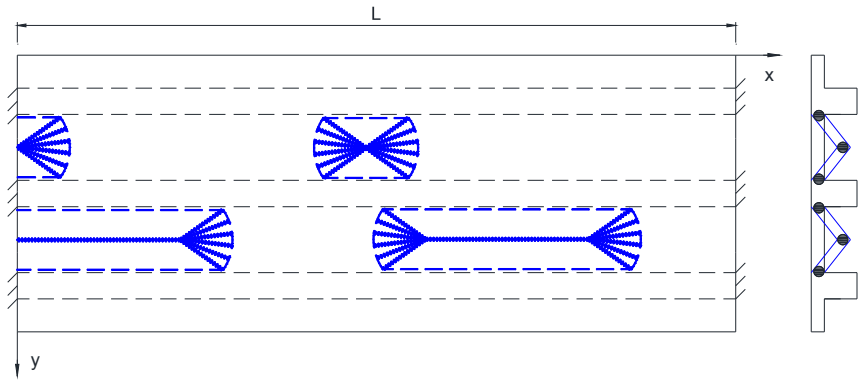

(a) Slab Yield Line Mechanism (Weak Slab – Strong Beam)

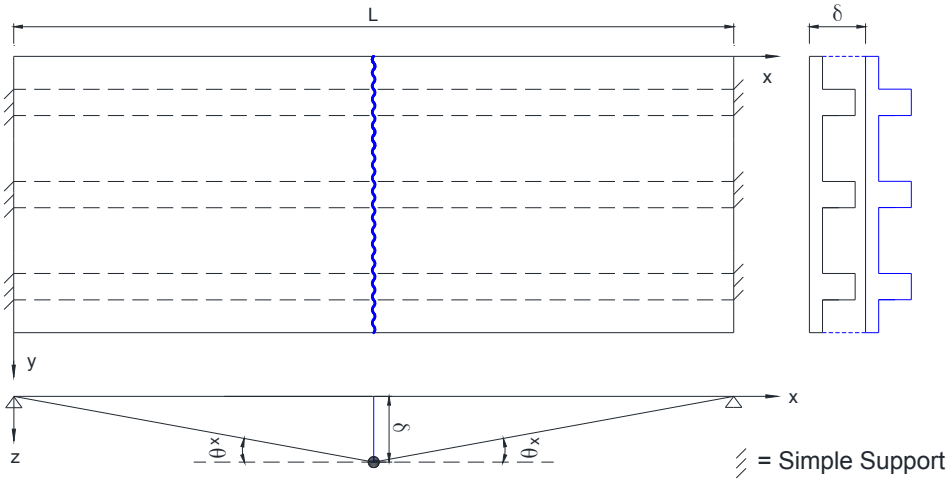

(b) Transverse Yield Line for Beam Mechanism (Strong Slab – Weak Beam)

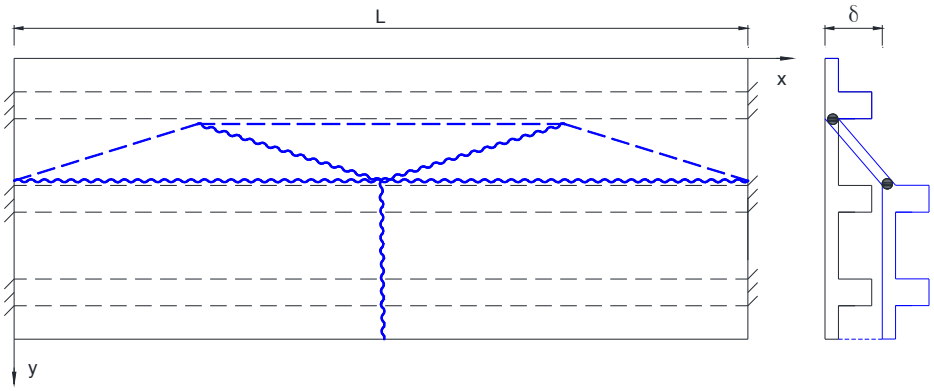

(c) Mixed Beam – Slab Mechanism Yield Lines

Figure 8.1. Characterization of Limit Behavior Modes for Slab-on-Beam Bridge Decks.

8.3.1 Slab Flexure Mechanisms

When truck wheel loads are applied within the connecting deck slab, a local flexure or shear failure may occur within the deck itself. If the bridge superstructure has a wide clear spacing between beams and the deck slab is relatively thin, then a flexural mechanism is possible. Figure 8.2 presents several admissible failure mechanisms of the deck slab under single or multiple wheel loads. The positive moments, compression on the top surface with tensile cracks appearing on the soffit, are represented in jagged blue solid lines while negative moments, tension cracks on the top surface, are shown in blue dashed lines. The collapse load values corresponding to various local flexure failure modes are determined based on the principle of the virtual work as follows:

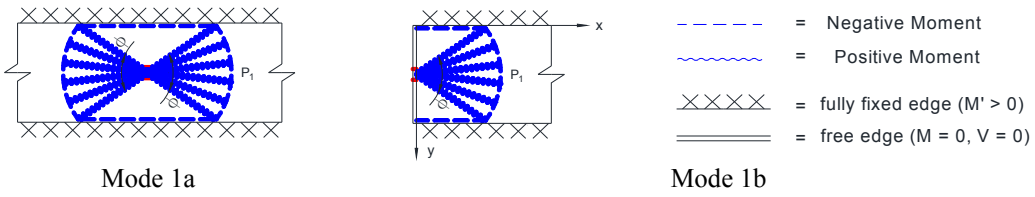

(a) Local Flexure Failure Mechanism Due to Single Wheel/Patch Load

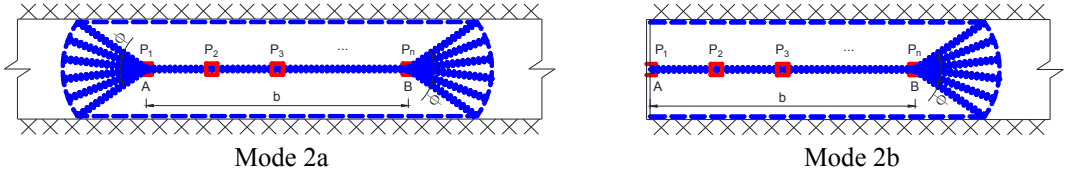

(b) Local Flexure Failure Mechanism Due to Multiple Wheel Loads

Figure 8.2. Weak Slab-Strong Beam Analysis of Slab-Only Mechanisms from Wheel Loads.

Mode 1a: $$P_1 = 2\varphi\left(m_d + m_d^{'}\right) + 4\left(m_{y,d} + m_{y,d}^{'}\right)\cot\frac{\varphi}{2} \tag{8.3}$$

Mode 1b: $$P_1 = \varphi\left(m_d + m_d^{'}\right) + 2\left(m_{y,d} + m_{y,d}^{'}\right)\cot\frac{\varphi}{2} \tag{8.4}$$

Mode 2a: $$\sum P_i = 2\varphi\left(m_d + m_d^{'}\right) + 4\left(m_{y,d} + m_{y,d}^{'}\right)\cot\frac{\varphi}{2} + 4\left(m_{y,d} + m_{y,d}^{'}\right)\frac{b}{b_d} \tag{8.5}$$

Mode 2b: $$\sum P_i = \varphi\left(m_d + m_d^{'}\right) + 2\left(m_{y,d} + m_{y,d}^{'}\right)\cot\frac{\varphi}{2} + 4\left(m_{y,d} + m_{y,d}^{'}\right)\frac{b}{b_d} \tag{8.6}$$

in which $\sum P_i$ = summation of the wheel loads applied on line AB shown in Figure 8.2(b); φ = central angle of the curved fan; b = spacing between the first and last wheel loads; m_d, $m_d^{'}$ = positive and negative moment capacities of a unit width of deck slab. To analyze an orthotropic plate, a solution may be found by applying the affinity theorem whereby the slab is transformed into an equivalent isotropic slab with equivalent positive and negative moment capacities (m_d, $m_d^{'}$) given by $m_d = \sqrt{m_{x,d} m_{y,d}}$ and $m_d^{'} = \sqrt{m_{x,d}^{'} m_{y,d}^{'}}$ (Park and Gamble 2000); where $m_{x,d}$, $m_{x,d}^{'}$, $m_{y,d}$ and $m_{y,d}^{'}$ represent positive and negative moment capacities of a unit deck slab in the x and y direction.

Failure modes in which the loads applied at the free end are more critical than the ones within the deck due to less internal virtual work done. By solving the differentiation equations, $\frac{dP_u}{d\varphi} = 0$, it is demonstrated that if $m_d + m_d^{'} \geq m_{y,d} + m_{y,d}^{'}$ the lowest collapse

loads for all the yield line patterns listed above are obtained when $\sin\frac{\varphi}{2}=\sqrt{\frac{m_{y,d}+m_{y,d}^{'}}{m_d+m_d^{'}}}$ and the central angle, φ, ranges from 0 to π. Otherwise, the minimum values are achieved when $\varphi=\pi$.

8.3.2 Slab Shear Mechanism

Punching-shear is a potential two-way shear failure mode for deck slabs that may occur when highly concentrated wheel loads are applied. The expression of punching-shear capacity may derived from the equilibrium equation of forces acting on the shear surface and listed as follows (Graddy et al. 2002; Mander et al. 2010c).

$$V_c = 2f_t'\left(b_1+b_2+2d\cot\theta\right)d\cot\theta \tag{8.7}$$

where V_c = punching-shear capacity; b_1, b_2 = short and long sides of the wheel/patch contact area; d = effective depth of the section; f_t' = diagonal tensile strength of concrete; and θ = angle between horizontal and assumed failure plane, where Graddy et al. (2002) suggested a value of 38 degrees. The AASHTO LRFD Bridge Design Specifications (AASHTO 2012) conservatively assumes a crack angle of $\theta=45$ degrees to determine punching shear capacity, thus

$$V_c = 2f_t'\left(b_1+b_2+2d\right)d \tag{8.8}$$

Modern bridge decks are normally constructed with a series of stay-in-place (SIP) precast prestressed panels (PCPs) topped with CIP reinforced concrete (RC) slabs. The

SIP PCPs are generally not connected and a seam exists between adjacent panels. Consequently, the punching shear failure mode may occur over the full SIP-CIP deck depth at one side but only topping CIP deck slab at the other side. Therefore, the length over which the shear area acts needs to be modified for two-way shear at a panel seam. The expression of punching shear capacity modified by Graddy et al. (2002) is.

$$V_c = f_t'\left(2b_1 + b_2 + 2d\right)d + f_t'\left(b_2 + d'\right)d' \tag{8.9}$$

where d = effective depth of the section; and d' = depth of the topping CIP deck slab.

8.3.3 Compound Shear – Flexure Slab Mechanism

For the bridge deck consisting of SIP PCPs between adjacent structural concrete beams, a potential compound shear-flexure failure, was identified by Mander et al. (2010b). A simple additive series model combining shear capacity in the topping CIP deck slab and the flexure capacity of the SIP PCP was developed by Mander et al. (2010b) to analyze the collapse load corresponding to the compound shear-flexure slab mechanism.

$$P_u = V_c + P_f \tag{8.10}$$

where P_u = ultimate failure load; V_c = shear capacity in the topping CIP deck slab; and P_f = flexural capacity of lower SIP PCPs.

8.3.4 Beam – Only Failure Mechanism

Figure 8.1(b) shows the flexure failure of a strong slab-weak beam system, in which the connecting deck slab is considered to be sufficiently strong enough to successfully transfer

the applied load from one beam to the neighboring beam without yield lines forming in the deck slab in the transverse direction. The collapse load, P_u, corresponding to this failure mechanism for a beam-slab-beam unit is.

$$P_u = \frac{8M_{x,b}}{L} \tag{8.11}$$

where $M_{x,b}$ = positive moment capacity of the composite T-beam section in the longitudinal direction and L = span length.

8.3.5 Mixed Beam – Slab Failure Mechanisms

Figure 8.3 presents potential failure mechanisms for a basic structural system consisting of two beams and an inter-connecting deck slab. When the beams are relatively widely spaced and the deck slab is relatively weak and not capable of transferring the applied load from one beam to the neighboring beam, a yield line mechanism may occur within the connecting deck slab as the beams also reach their plastic capacity. Figure 8.3(a) presents such a mixed beam-slab yield line mechanism. Using virtual work (See Appendix 3 for full derivation) the collapse load may be obtained from:

$$P_u = 4\frac{M_{x,b}}{L} + 4\frac{\left(m_{x,d} + m'_{x,d}\right)}{L}b_d + \left(\frac{m_{y,d} + m'_{y,d}}{b_d}\right)\left(1 - 2\frac{x}{L} + \frac{4x^2}{L^2}\right)L \tag{8.12}$$

where b_d = width of deck slab between two neighboring beams. Differentiating Equation (8.12) and solving $\frac{dP_u}{dx} = 0$ for x gives the lowest ultimate load achieved when $x = L/4$, thus:

$$P_u = 4\frac{M_{x,b}}{L} + 4\frac{\left(m_{x,d} + m'_{x,d}\right)b_d}{L} + \frac{3}{4}\frac{\left(m_{y,d} + m'_{y,d}\right)L}{b_d} \tag{8.13}$$

Such a slab-to-beam folded plate mechanism was observed in laboratory tests conducted in the aforementioned Cambridge tests (Hazell 1999; Jackson and Middleton 2013; Lowe 1999). Figure 8.4 shows the test model reinforced concrete slab-on-beam bridge loaded with wheels on two of its beams. The red and green lines represent the cracks observed from the top and bottom of the tested slab. The yield line pattern, based on dimensions calculated in Equation (8.13), are shown in blue lines. Two tested slabs failed at 69.0 and 68.7 kN. A simple yield line calculation based on the proposed mechanism predicts a collapse load of 73.3 kN, which validate the reliability of this yield line pattern.

For closely spaced beams where a weak slab-strong beam exists, a shear failure may occur in the connecting deck slab as shown in Figure 8.3(b) where the blue hatched lines represent the shear failure of the connecting deck slab. The ultimate load capacity, P_u, relates to the shear strength of the connecting deck slab. The magnitude of the collapse load may be determined as follows.

$$P_u = \frac{4M_{x,b}}{L} + \frac{V_p L}{2} \tag{8.14}$$

in which V_p = the unit shear capacity of unit deck slab (kN/m), $V_p = v_c d$, where v_c = the shear stress in concrete taken as $v_c = 0.33\sqrt{f'_{c,MPa}}$ and d = the effective depth of the deck slab.

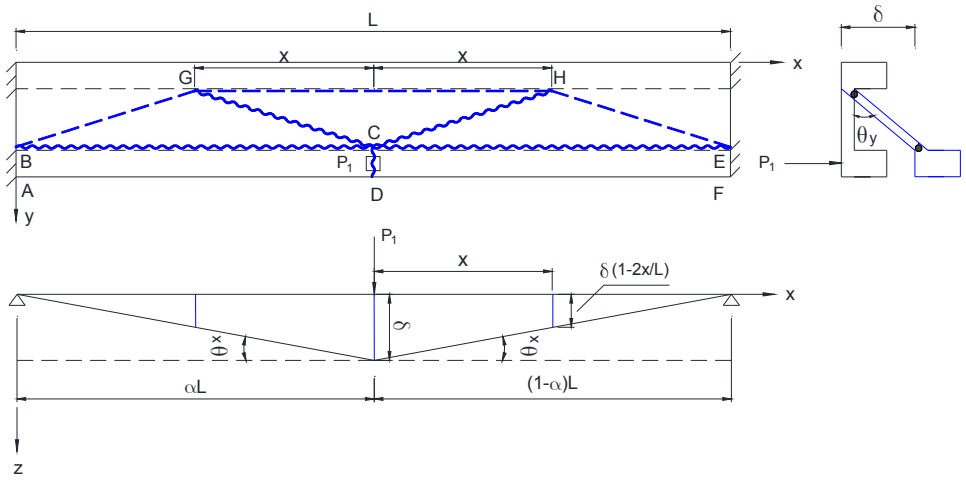

(a) Slab to Beam Folded Plate Mechanism

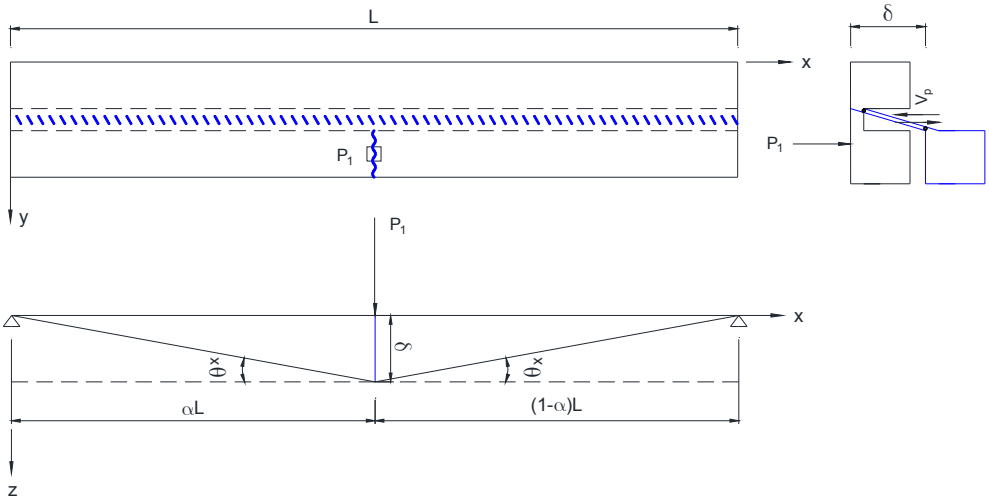

(b) Slab Shear Failure Mode

Figure 8.3. Mixed Beam and Slab Mechanisms.

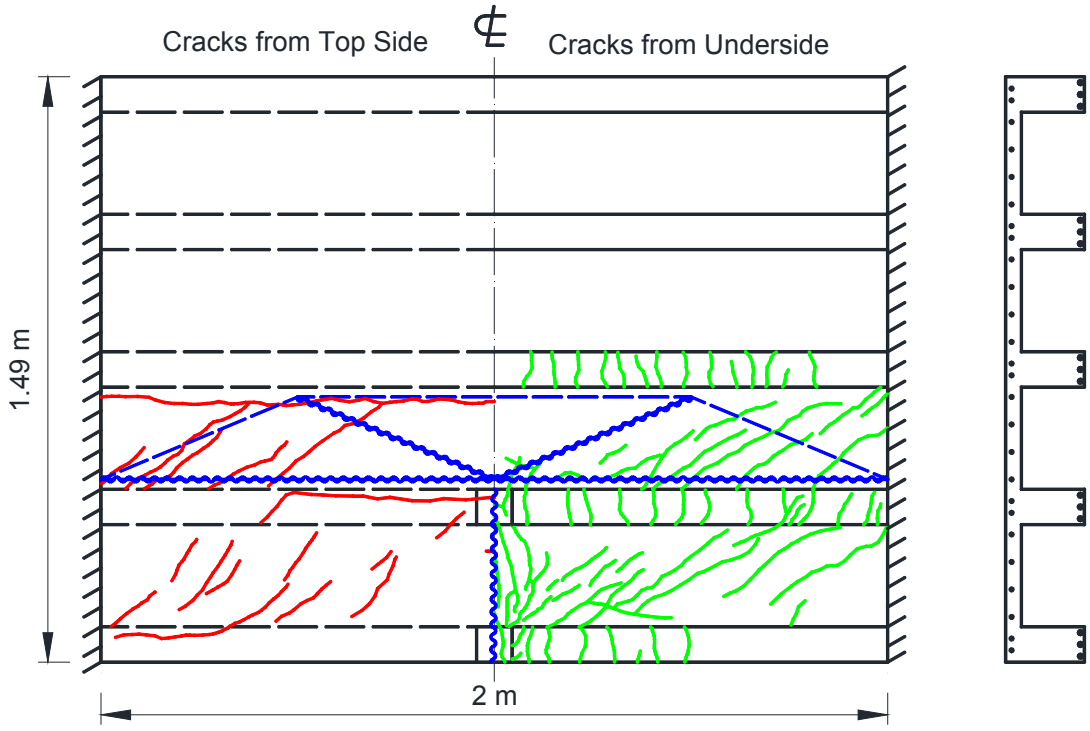

Figure 8.4. Model Reinforced Concrete Beam-and-Slab Bridge adapted from Jackson and Middleton (2013) Showing Observed Cracks as tested by Hazell (1999) with the Calculated Beam-Slab Collapse Mechanism Given by Equation (8.12).

For the beam-slab system, either a flexure or shear failure mechanism governs in the determination of the lowest collapse load. It is possible to make a simple judgement by comparing the shear force generated in the flexure failure mode, $V_f = \left(m_{y,d} + m'_{y,d}\right)\big/ b_d$, with the shear capacity, V_p. If $V_f < V_p$, the flexure failure mode is more likely to occur in the beam-slab system, otherwise shear failure will dominate.

8.4 THE STRIP METHOD - LOWER BOUND SOLUTION

The strip method is a lower bound method of limit analysis. The method is often preferred by engineers for its simplicity in application for design. Hillerborg (1956), who first championed this approach pointed out that the solution must have a moment field satisfying the governing equilibrium equation and boundary conditions for a specified set of external loads. For a general two-way slab the partial differential equation based on equilibrium requirements is (Park and Gamble 2000):

$$\frac{\partial^2 m_x}{\partial x^2} + \frac{\partial^2 m_{xy}}{\partial x \partial y} + \frac{\partial^2 m_y}{\partial y^2} = -q(x,y) \tag{8.15}$$

where m_x, m_y = bending moment per unit length in the x and y directions; m_{xy} = twisting moment per unit length and $q(x,y)$ = loading in the x, y space.

To reduce complexity while maintaining a lower bound solution it is common to simplify Equation (8.15) by neglecting the effect of the twisting moments, m_{xy}, thereby uncoupling the moment effects into "strips" running parallel to the reinforcement in the x

and y directions. The equilibrium equation of the slab may now be reduced to two independent ordinary differential equations:

$$q_x = -\frac{d^2 m_x}{dx^2} \tag{8.16}$$

$$q_y = -\frac{d^2 m_y}{dy^2} \tag{8.17}$$

such that for a lower bound design solution $q_x + q_y \geq q(x, y)$.

For the slab-on-beam bridge system, the magnitude of the collapse load may be determined by static limit equations for flexure and shear, as shown in Figure 8.5(a), and described as follows.

$$P_{pf} = P_x + P_{yf} = \frac{4M_{px}}{L} + 2\frac{m_y + m_y^{'}}{b_d} b_x \tag{8.18}$$

$$P_{ps} = P_x + P_{ys} = \frac{4M_{px}}{L} + 2V_{py} b_x \tag{8.19}$$

where P_{pf}, P_{ps} = collapse load due to flexure and shear failure respectively, the lower value is considered as the collapse load for the grillage system, M_{px} = moment capacity of the beam section in longitudinal direction; m_y and $m_y^{'}$ = positive and negative moment capacities of unit width deck slab in transverse direction; V_{py} = shear capacity of unit width deck slab in transverse direction; L = span length; b_d = length of connecting slab; and b_x = width of transverse slab.

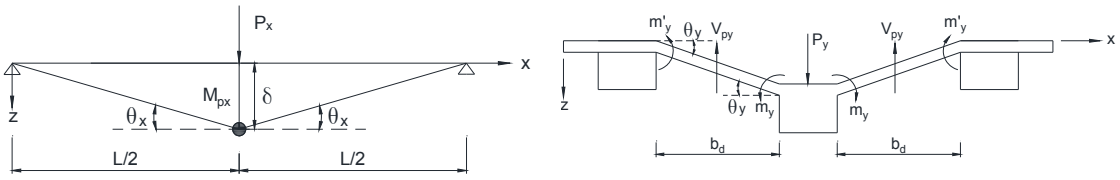

(a) Determination of Collapse Load in Longitudinal and Transverse Directions

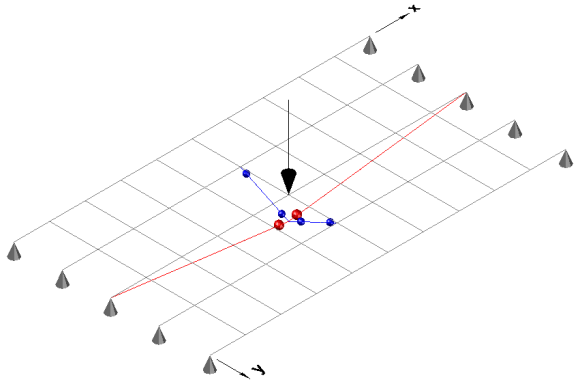

(b) Weak Slab – Strong Beam Mechanism (Lower Bound)

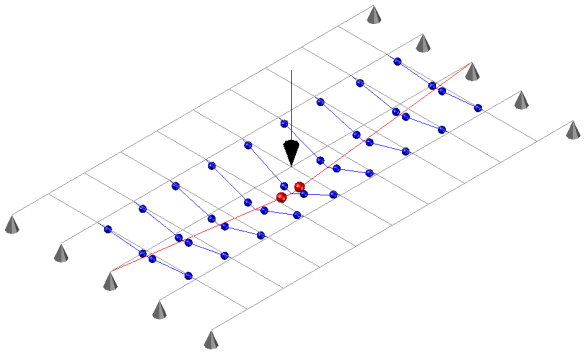

(c) Weak Slab – Strong Beam Mechanism (upper Bound)

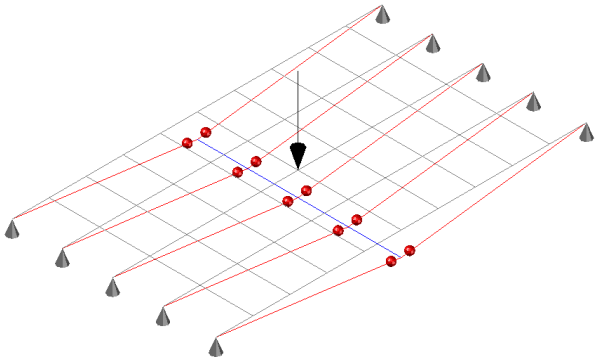

(d) Strong Slab – Weak Beam Mechanism (Beam Only)

Figure 8.5. Grillage Analysis Using the Strip Method at Ultimate Limit State.

The strip method is also akin to the grillage method where a bridge deck is modeled as a "grillage" of beams; the longitudinal grillage members are used to directly model the stringers/beams as T-beams and the transverse grillage members model the deck slab typically by dividing the deck into 10 or more "effective beam" segments. Although the grillage method has historically been used as an elastic solution in lieu of a full finite element method (FEM) analysis, there appears to be no reason to restrict the analysis to the elastic range. In this research, the viability of using the grillage method as a computational solution in the inelastic range up to the ultimate limit state is explored. Therefore, plastic hinges are included in the longitudinal and transverse grillage elements to capture the behavior at the ultimate limit state.

Figure 8.5 presents the hinge distribution of the grillage models for different limit behavior modes. For a weak slab-strong beam system, as the applied loading is increased initially a partial mechanism will form as shown in Figure 8.5(b). This provides a lower bound solution to the true collapse load. As the load is further increased more grillage members form plastic hinges until a limit load is achieved, in which plastic hinges occur in the longitudinal and transverse grillage elements close to the load position. For the strong slab-weak beam system, the hinges are considered to occur in the longitudinal beams only, as shown in Figure 8.5(d).

8.5 PLASTIC OVERSTRENGTH ANALYSIS FOR TWO SPREAD SLAB BEAM BRIDGES

The two prototype bridge structures shown in Figure 8.6 were tested as part of the present research, with full details of those bridges given in Hueste et al. (2015). A summary relevant to the analyses conducted herein follows.

The first bridge was a full-scale single span spread slab beam experimental structure that was constructed at the Texas A&M University Riverside Campus. Referred to herein as the Riverside Bridge, Figure 8.6 shows (a) the transverse section and (b) an elevation view of the bridge deck. The span length is 14.2 m (46 ft 7 in.) from the center-to-center of the bearing pads and the overall bridge deck width is 10.4 m (34 ft). The bridge superstructure has four standard TxDOT 5SB15 slab beams with a 1.4 m (56 in.) clear spacing. Precast prestressed concrete panels (PCPs) between the slab beams and seated on foamed bearing strips that were, on average, 51 mm (2 in.) thick. The PCPs served as 102 mm (4 in.) thick stay-in-place forms. A 102 mm (4 in.) thick reinforced topping slab was cast on the PCPs. The average deck-slab thickness on top of the slab beam is 254 mm (10 in.).

The second bridge, shown in Figure 8.6(c) and Figure 8.6(d), was an in-service spread slab beam structure that was designed by the TxDOT Bridge Division in 2010 and implemented in US 69 highway located in Denison, Texas. As shown in Figure 8.6(c), the US 69 Bridge has a low-profile bridge deck consisting of six standard TxDOT 5SB15 spread slab beams. The clear spacing between slab beams is 406 mm (16 in.). The span length between the centerlines of bearing pad seats is 14.8 m (48 ft 7 in.).

Note that the precast prestressed slab beams provided on both bridges were the same 5SB15 (1.5 m (5 ft) wide by 381 mm (15 in.) deep). The key difference is the Riverside Bridge has a wide 1.4 m (56 in.) clear spacing between beams, whereas the US 69 Bridge has a narrower 406 mm (16 in.) clear spacing.

Figure 8.6(e) presents the load application in the longitudinal direction. For a two-lane bridge structure, the two side-by-side HS20 trucks are positioned in a critical location while the dead load and lane load are uniformly distributed along the entire span length; the magnitudes of the factored applied ultimate loads follow:

$$P_{1u} = P_{2u} = N_l \times 1.75 \times 1.33 \times 32 \text{ kips} = 74.5N_l \text{ kips} = 331.3N_l \text{ kN} \tag{8.20}$$

$$P_{3u} = N_l \times 1.75 \times 1.33 \times 8 \text{ kips} = 18.6N_l \text{ kips} = 82.8N_l \text{ kN} \tag{8.21}$$

$$w_{lu} = N_l \times 1.75 \times \frac{0.64 \text{ kips/ft}}{10 \text{ ft}} = 0.112N_l \text{ ksf} = 5.36N_l \text{ kPa} \tag{8.22}$$

$$w_{du} = 1.25w_d \tag{8.23}$$

where N_l represents number of lanes.

Table 8.1 lists the moment or shear resistance capacities of structural components for the two spread slab beam bridges, which are used in the plastic overstrength analysis. When performing a plastic limit analysis all factored loads are multiplied by the overstrength scalar, Ω, to obtain the collapse load.

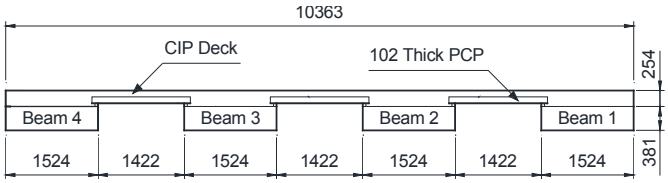

(a) Transverse Section of Riverside Bridge

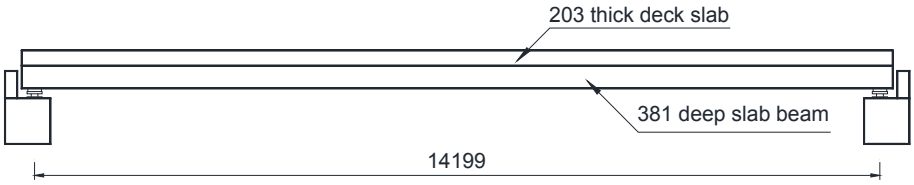

(b) Elevation View of Riverside Bridge

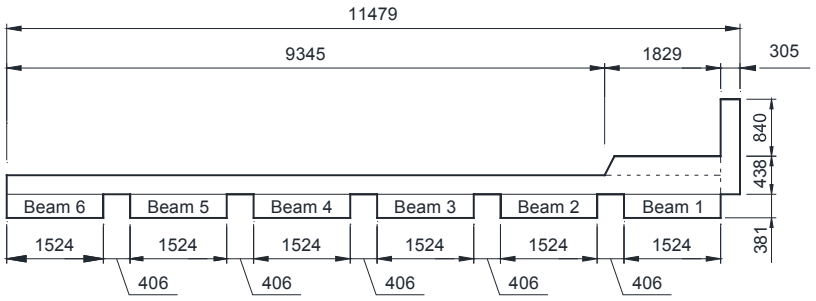

(c) Transverse Section of US 69 Bridge

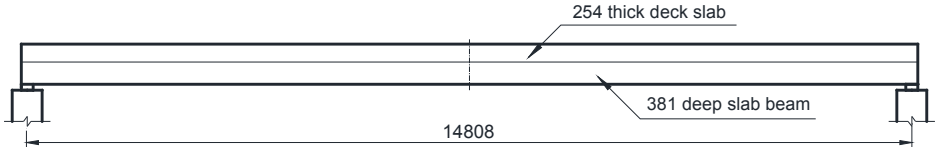

(d) Elevation View of US 69 Bridge

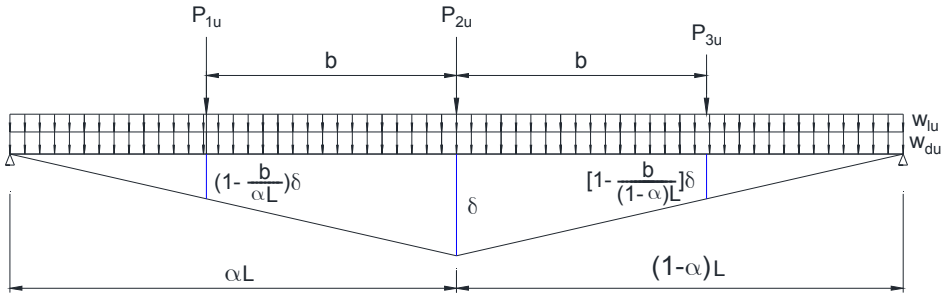

(e) Load Application in Longitudinal Direction Showing Displacements Used in Mechanism Analysis

Figure 8.6. Transverse Section and Elevation View of Riverside and US 69 Bridges.

Table 8.1. Capacities of Structural Components in Riverside and US 69 Bridges

Structural Components		Riverside Bridge	US 69 Bridge
Composite Beam	Exterior (kN-m)	$M_{x,be} = 4401$	$M_{x,be} = 4057$
	Interior (kN-m)	$M_{x,bi} = 4716$	$M_{x,bi} = 3937$
Deck Slab	Slab Flexure Capacities (kN-m/m)	$m_{x,d} = 11.3$	$m_{x,d} = 86.7$
		$m'_{x,d} = 25.9$	$m'_{x,d} = 86.7$
		$m_{y,d} = 29.8$	$m_{y,d} = 117$
		$m'_{y,d} = 70.3$	$m'_{y,d} = 117$
		$m_d = 18.4$	$m_d = 101$
		$m'_d = 42.7$	$m'_d = 101$
	Shear Capacities (kN/m)	$V_f = 70.5$ *	$V_f = 571$
		$V_P = 266$	$V_P = 244$ *
	$V_f = \frac{m_{y,d} + m'_{y,d}}{b_d}$	$b_d = 1.42$ m	$b_d = 0.41$ m

* Critical Case for Shear

Table 8.2. Overstrength Factors, (Ω), of Riverside and US 69 Bridges.

	Failure Mechanisms		Riverside Bridge	US 69 Bridge
Yield Line Analysis	Slab Flexure Mechanism (32 kips (142 kN) HS20 Truck Axle Load with 16 kips (71 kN) Wheel Load)	One Wheel at end	**1.04***	-
		One Wheel inside	2.09	-
		Two Wheels at end	3.87	-
		Two Wheels inside	4.48	-
		Three Wheels at end	6.34	-
		Three Wheels inside	6.88	-
	Slab Shear Mechanism		2.30	-
	Slab Compound Shear-Flexure Mechanism		3.50	-
	Beam – Only Failure Mechanism		2.04	2.24
	Mixed Beam – Slab Flexure Failure Mechanism		2.03† 2.36!	-
	Mixed Beam – Slab Shear Failure Mechanism		-	2.53
Plastic Hinge Analysis	Strip Method (lower bound)		1.81	1.86
	Grillage Computational Result		2.02	2.22

* Critical case without end-of-slab strengthening

† Critical case with end-of-slab strengthening

! Case with considering full transverse positive moment capacity of SIP-CIP Deck Slab

8.6 RESULTS OF PLASTIC OVERSTRENGTH ANALYSIS

8.6.1 Yield Line Theory Analysis

Table 8.2 lists plastic overstrength factors of the deck slab in the Riverside Bridge determined by yield line analysis for different slab-only failure mechanisms. Due to the narrow gap between slab beams, these slab-only failure mechanisms are not possible for the US 69 Bridge. For the yield-line pattern with curved fans caused by single wheel load, leading to a semi-circular shape at the free end of the slab as shown in Figure 8.7(a), an overstrength factor, $\Omega = 1.04$, was obtained. If the wheel load is applied away from the free end, the overstrength factor increases to give a full circular form with $\Omega = 2.09$. The overstrength values due to multiple wheel loads are larger than the value caused by a single wheel load. When considering the punching-shear and compound shear-flexure failure modes, it is found that the single truck wheel load caused the overstrength factors of $\Omega = 2.30$ and 3.50 respectively, indicating the shear failure are unlikely compared to the preferred flexure failure.

When the global beam failure mechanism occurs in the spread slab beam bridges, all slab beams reach their longitudinal moment capacities while no yielding occurs at the connecting deck slab in the transverse direction, as shown in Figure 8.7(b) and Figure 8.8(a) for Riverside and US 69 Bridges. Based on yield line theory analysis results, it is determined that the overstrength factors for the Riverside Bridge and US 69 Bridge are $\Omega = 2.04$ and $\Omega = 2.24$, respectively.

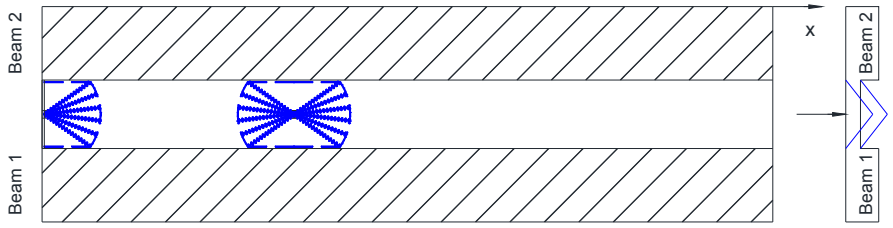

(a) Slab – Only Failure (Ω = 1.04 end wheel, Ω = 2.09 interior wheel)

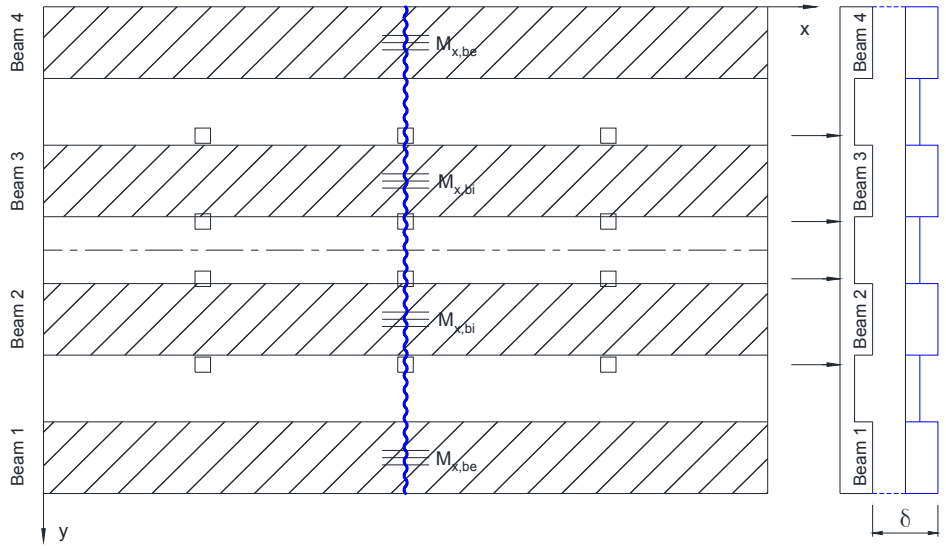

(b) Global Flexure Failure (Ω = 2.04)

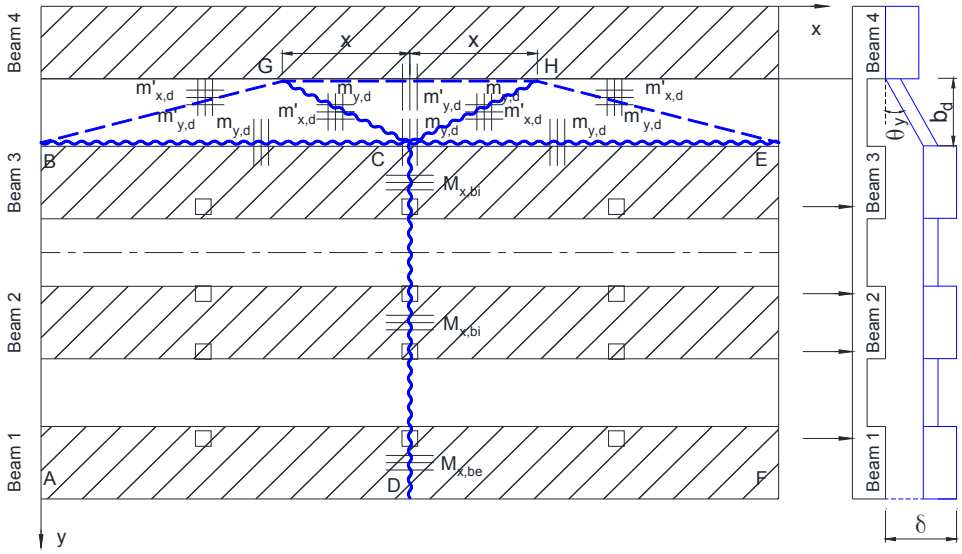

(c) Slab to Beam Folded Plate Mechanism (x = 0.249L, Ω = 2.03)

Figure 8.7. Failure Modes of Riverside Bridge.

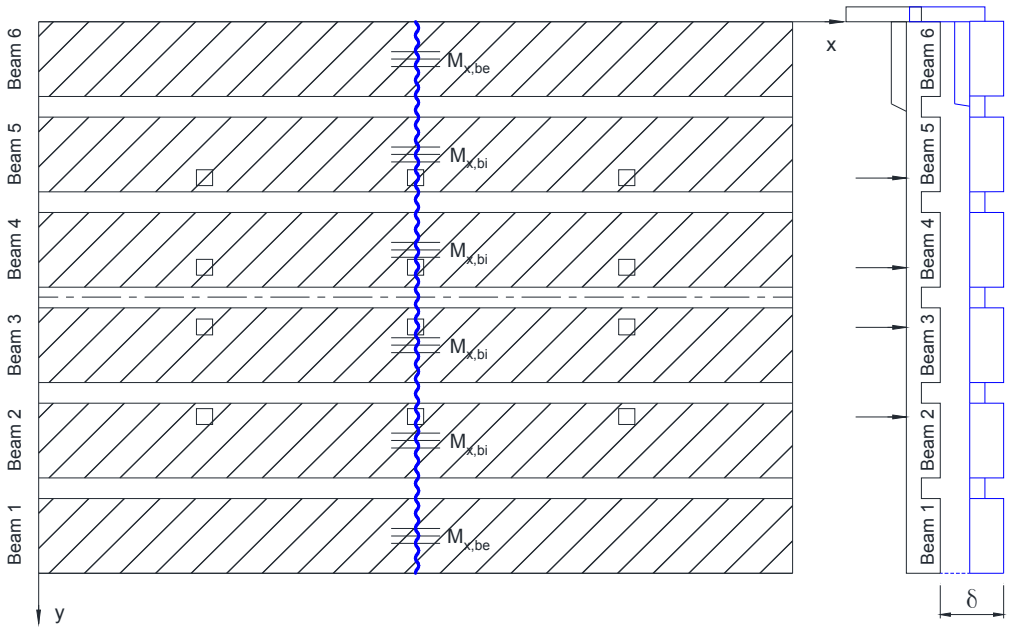

(a) Global Flexure Failure: Strong Slab – Weak Beam (Ω = 2.24)

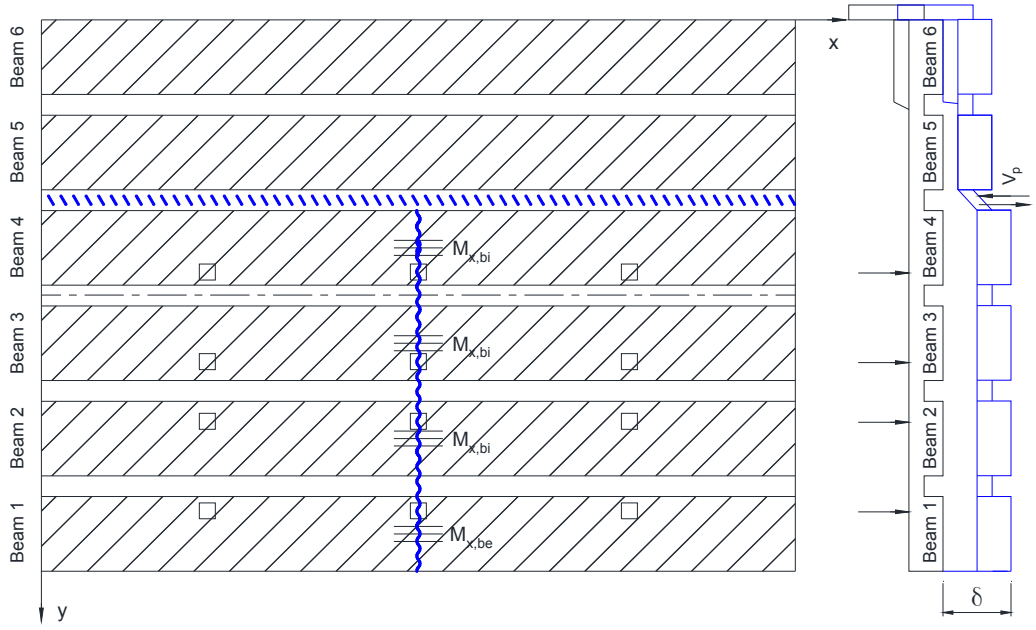

(b) Shear Failure of Beam-Slab System (Ω = 2.53)

Figure 8.8. Failure Modes of US 69 Bridge.

For mixed beam-slab mechanisms, it is inferred by comparing V_f and V_p that flexure failure is more likely to occur on the connecting deck slab of the Riverside Bridge while a shear failure is expected to dominate for the US 69 Bridge ultimate limit state behavior. Figure 8.7(c) shows the yield line pattern of the Riverside Bridge when the slab to beam folded plate mechanism occurs. A detailed yield line analysis is given in Appendix 3 to determine its collapse load. The shear failure yield line pattern for the US 69 Bridge is shown in Figure 8.8(c). The overstrength factors for the Riverside and US 69 bridges are $\Omega = 2.03$ and 2.53 for mixed beam-slab mechanisms.

8.6.2 Strip Method Analysis

Figure 8.9 presents the grillage topology for the two prototype bridges along with the most adverse vehicle load positions. Potential hinge locations corresponding to different limiting behavior modes are also depicted in Figure 8.9, where the hinges in longitudinal and transverse grillage members are represented with red and blue points. When the global beam failure mechanism occurs, the plastic overstrength factors for Riverside and US 69 Bridges are 2.03 and 2.33, respectively. If a mixed beam-slab mechanism happens, the plastic hinges may occur starting with the transverse grillage members close to the applied loads then progressing until all longitudinal beams reach their flexural capacities. When a limit load is achieved, the effective width, L_{eff}, of the transverse grillage members involved in the mixed beam-slab mechanism is between the length of the connecting deck slab, b_d and the span length, L; and it is referred to herein as a partial mixed beam-slab mechanism. Through simple hand calculations of the grillage system with hinges

distribution for partial mixed beam-slab mechanisms, the lower bound solutions to the overstrength factors for Riverside and US 69 Bridges are 1.81 and 1.86, respectively.

Nonlinear static analyses using SAP2000 (Computers and Structures 2013) were carried out for the grillage models of the two spread slab beam bridges to evaluate their ultimate strength. In the modeling process, flexural hinges were defined by moment-curvature relationships and assigned at both ends of the grillage members to indicate the status of nonlinearity throughout the loading procedure.

The moment-curvature curves implemented in the grillage model are determined by carrying out moment-curvature analysis of each element based on the cross-section and reinforcement details at the possible hinge locations. XTRACT is a powerful commercial software package available to carry out moment-curvature analysis. Based on the assumption of the linear strain distribution, it utilizes two dimensional discretization of a cross-section to determine strain, stress and moment by incrementally increasing the curvature applied to the cross-section. Three critical points were identified in the analysis to develop trilinear moment-curvature curves which were implemented in the nonlinear grillage models. These points represented different nonlinear status of the section, including cracking, yielding and ultimate points. The cracking point was defined when the tensile cracking strain (0.00022) is reached at the bottom of the concrete section; the yielding point occurred when the bottom prestress strands yield; and the. The ultimate point was identified as the compressive strain of the top fibre concrete reaches 0.005.

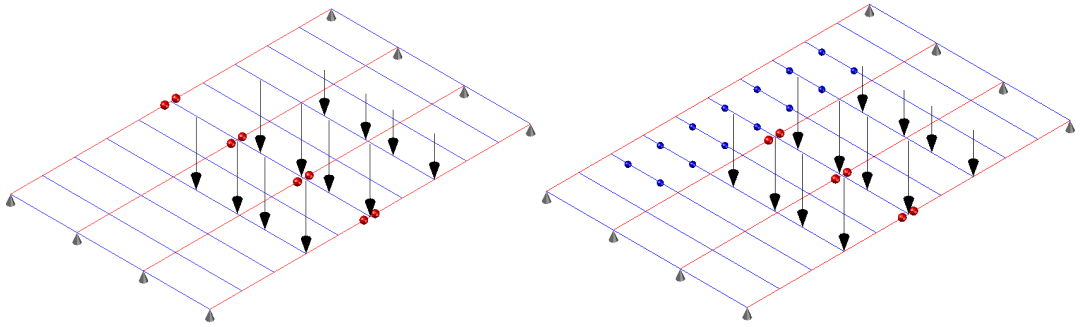

Global Mechanism ($\Omega = 2.03$) Partial Mixed Beam-Slab Mechanism ($1.81 \le \Omega \le 2.02$)

(a) Riverside Bridge

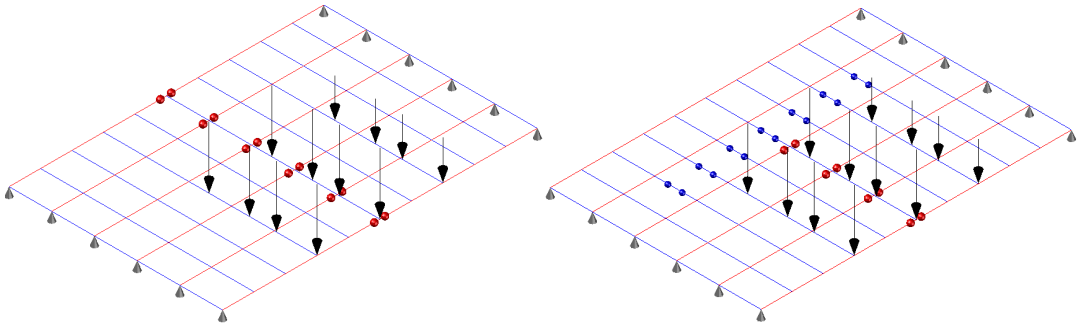

Global Mechanism ($\Omega = 2.23$) Parital Mixed Beam-Slab Mechanism ($1.86 \le \Omega \le 2.63$)

(b) US 69 Bridge

Figure 8.9. Strip Method Analysis of Two Spread Slab Beam Bridges.

Figure 8.10 shows the modified trilinear moment-curvature relations for longitudinal grillage members in the Riverside and US 69 bridges. Due to the pretension prestress effects, an initial negative curvature value exists in the moment-curvature relationships which SAP2000 cannot accommodate in the definition of the plastic hinge property. Therefore, appropriate modifications to the moment curvature relationships were made by shifting up the horizontal axis and applying a negative moment of a magnitude equal to the shift to account for the pretension prestress effects.

Figure 8.11 presents the mid-span deflections of each slab beam in the Riverside and US 69 bridges under monotonic loads from initial elastic conditions until collapse. The initial deflection value before applying the design load is negative due to the pretensioned prestress effect. When the scaled ultimate design load is applied in the bridge structure, all slab beams performed in a nonlinear fashion. The computed overstrength factors are 2.02 and 2.22 at failure in the Riverside and US 69 bridges, respectively. The values determined from the strip method and yield line analysis are also depicted by the black dashed lines in Figure 8.11. As expected, it is evident that the strip method provides a lower bound solution while the yield line theory gives an upper bound solution for a global mechanism. However, the overstrength factor determined from the local failure yield line pattern is lower than the computational value, which cannot be well predicted by the plastic hinge based grillage analysis.

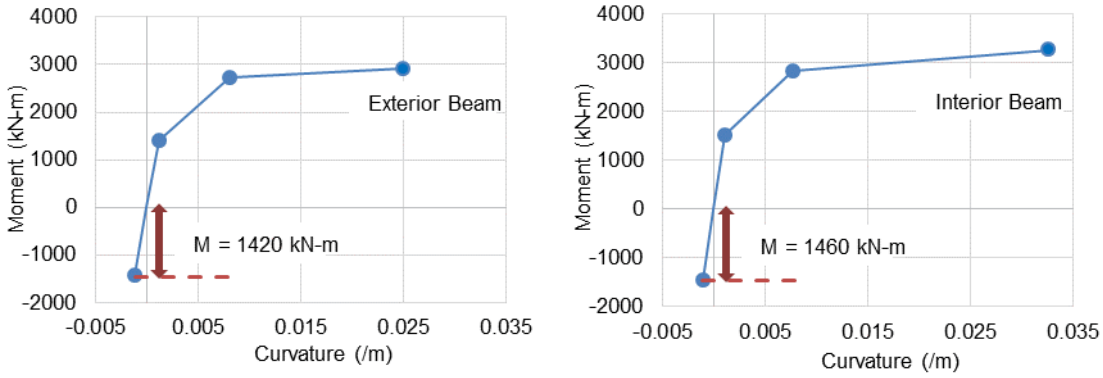

(a) Riverside Bridge

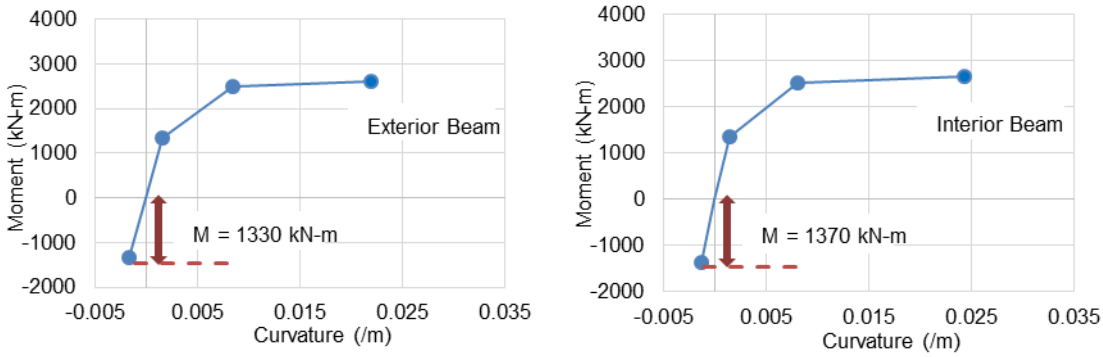

(b) US 69 Bridge

Figure 8.10. Modified Moment-Curvature Relationships for Longitudinal Grillage Members in Riverside and US 69 Bridges.

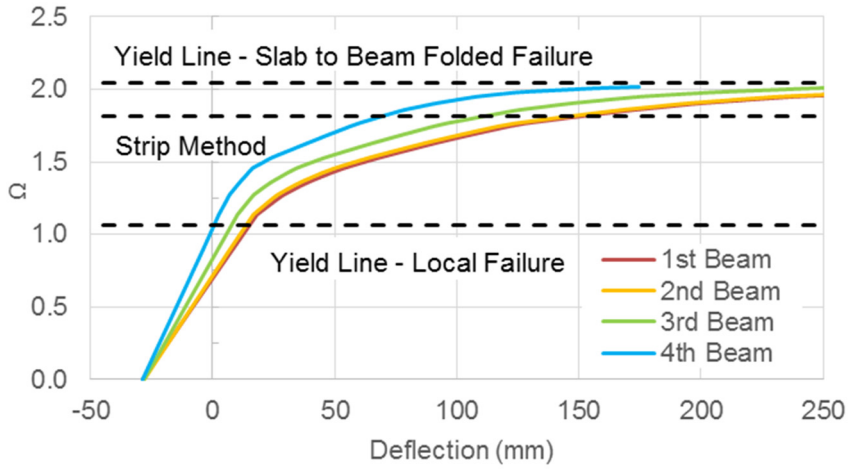

(a) Riverside Bridge

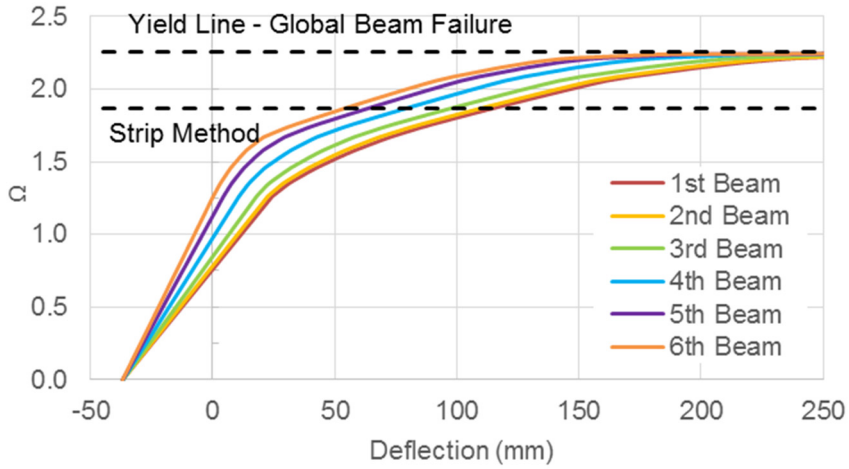

(b) US 69 Bridge

Figure 8.11. Beam Deflections due to Scaled Ultimate Design Loads.

8.7 DISCUSSION

The overstrength factors listed in Table 8.2 for the two spread slab beam bridge designs indicate the relative strength hierarchy by yield line analysis, the critical results being the lowest solution for each bridge. These overall yield line outcomes are independently corroborated by the alternative strip/grillage method of analysis. The different analysis methods reveal that the Riverside and US 69 bridges are sufficiently robust to resist ultimate design loads because the plastic overstrength factors are quite high ($\Omega \gg 1$). Apart from the slab-only failure mechanism, yield line theory generally provides upper bound solutions while strip methods generate lower bound results, and those values are similar to each other.

For the Riverside Bridge, the lowest overstrength factor, $\Omega = 1.04$, is achieved when a slab-only failure mechanism occurred due to a single wheel load loaded at the slab-end region. This issue may be simply addressed by placing a strong band of reinforcing slab steel parallel to the end-of-slab free edge. For the US 69 Bridge, the slab-only mechanism is not possible due to the narrow clear spacing between slab beams. According to the yield line theory analysis results, the most critical overstrength factor is obtained when the global beam failure occurs in the US 69 Bridge.

When the slab-end region in the Riverside Bridge is strengthened, the critical overstrength factor, $\Omega = 2.03$, is dominated by a mixed beam-slab flexural failure mechanism, which reveals that the slab design is relatively weaker than the slab beam. This is because the bottom SIP presressing strands in the SIP PCPs are not capable of providing the full positive flexural resistance at the slab-to-beam connection due to

insufficient tendon anchorage to the beam. It is evident from Table 8.2 that when full positive moment capacity of the SIP-CIP deck slab is taken into consideration, the overstrength factor for mixed beam-slab flexure failure mechanism increases to $\Omega = 2.36$, which becomes larger than the value for the global beam failure mechanism. Therefore, if the SIP strands or rebars are adequately anchored into the beam to provide full positive flexure resistance, a more desirable global beam failure mechanism would become the dominant failure mode for the Riverside Bridge.

Even though full transverse positive moment capacity of the SIP-CIP deck is obtained by anchoring the strands or rebars into the beam, the unstrengthened end-slab is still vulnerable due to the slab-only mechanism as compared to other mechanisms. This is attributed to the missing longitudinal positive moment capacity of the SIP-CIP deck due to the discontinuity between PCPs. In order to address this issue and achieve a stronger deck slab system, a new solution using PCPs with a longer span and thicker depth is developed in the next section. In short, the designs of slab and beam components in the bridge system need to be rebalanced so that the global beam failure remains the preferred failure mechanism.

8.8 CLOSURE AND KEY FINDINGS

In this section plastic limit methods of analysis have been used to define the overstrength capacity of bridge decks at the ultimate limit state collapse load. First, slab and beam mechanisms were considered separately. Then, combined beam and slab mechanisms were considered and validated for one particular case. Lower bound strip methods were

also analyzed and compared with the upper bound yield line method. The former is akin to grillage analysis, this was thus implemented in a nonlinear computational framework.

The limit analysis methods were applied to a new class of spread slab beam bridges. It was demonstrated that the different analysis methods, when accurately applied are in agreement even though results are slightly different due to underlying assumptions. Table 8.2 lists the overstrength factors of two spread slab beam bridges determined by yield line analysis and plastic hinge analysis. Based on the analysis results, the following bridge-type specific conclusions may be drawn:

1. Although all methods show that the plastic overstrength is adequate whereby $\Omega > 1$, the designs may not be "balanced" in the most appropriate way. More specifically, a deck-slab failure from a single wheel load at a slab-end region was indicated ($\Omega = 1.04$). This may be simply ameliorated by placing a strong band of reinforcing slab steel parallel to the end-of-slab free edge.
2. A mixed beam-slab flexure failure was found to be critical for the Riverside Bridge ($\Omega = 2.03$) which is close to a global beam failure ($\Omega = 2.04$). This is attributed to the CIP half-slab on the half-depth SIP panels where the bottom SIP prestressing strands cannot be depended on to provide full positive moment flexural resistance at the slab-to-beam connection. To increase the positive moment slab capacity, the SIP strand or rebar should be adequately anchored into the beam, in this way the design may be "rebalanced" such that the global beam failure remains the preferred failure mechanism.

3. In terms of beam-slab failure mechanism in the spread slab beam bridge system, wider clear spacing decreases the transverse flexure capacity of the connecting deck slab and the transverse flexure failure is more likely to occur in this situation. Conversely, shear failure tends to occur when the beams are closely spaced. Such performance potential is neither desirable nor recommended; beams should, ideally, be placed at a sufficiently wide spacing to lead to a secondary flexural failure in the deck slab, with the primary failure being beam flexure of the main spread slab beams.

9 PRELIMINARY DESIGN OF PRESTRESSED CONCRETE SPREAD SLAB BEAM BRIDGE

9.1 SUMMARY

A new class of spread slab beam bridges has recently been developed and implemented in Texas. The research questions addressed herein are: How long can such a low profile bridge system span in either a simply supported or continuous form? And, can construction operations be improved, by design? An effective way to extend the span length is to utilize post-tensioning and to make the bridge continuous over several spans. In order to explore the maximum span limit, the design of a multi-span prestressed concrete spread slab beam bridge is investigated in this section using the proposed live load model and companion load distribution factors. In addition, a new solution for precast prestressed concrete panels (PCPs) is proposed to facilitate accelerated bridge construction by removing one significant field operation: negating the need for field placement of any deck reinforcing steel. It is shown that the span length may be extended from 15 m to 21 m as a continuous shallow profile bridge. The design is verified for strength using the proposed plastic collapse mechanism analysis.

9.2 INTRODUCTION

The simply supported spread slab beam bridge configuration has been successfully designed for up to a 14.2 m long span. To date two viable examples have been implemented and constructed in Texas: (i) the Texas A&M University Riverside Campus experimental bridge, and (ii) the US 69 bridge in Denison, Texas (Hueste et al. 2015). The in-service performance and load distribution behavior of these two bridges has also been investigated through experimental testing and computational analysis.

However, the span limit of the continuous spread slab beam bridge configuration remains in question. While the two bridges have similar span lengths, the cross sections differ markedly. The TxDOT designed US 69 Bridge has six slab beams, whereas the Riverside Bridge only has beam slab beams. It was shown in Hueste et al. (2015) that for the latter case the design is at its limit for an eccentric pretensioned system – all viable prestressing tendon locations are used. Moreover, it was shown that this resulted in excessive camber, which remains problematic. Therefore, to further increase the span length several actions could be adapted:

1. Use harped prestress to overcome the end eccentricity and partially balance gravity loads.
2. Use supplemental post-tensioned prestress.
3. Use one or more additional slab beams in the cross section.
4. Make portions of the bridge continuous.

This section investigates the viability of (1) and (2) above in the context of continuity (4).

Nowadays, highway bridge deck systems in Texas are normally constructed with stay-in-place (SIP) precast prestressed concrete panels (PCPs) and a cast-in-place (CIP) topping. The Texas Department of Transportation (TxDOT) has provided PCP standard drawings for precaster usage, in which the geometric dimensions are specified as follows: panel length = 2438 mm (8'-0") maximum; width = 2896 mm (9'-6") maximum and depth = 102 mm (4"). Because the dimensions of the PCPs are relatively small, many extra CIP construction activities, specifically, formwork placement, reinforcing steel placement and concrete pouring are needed to complete the entire deck system. All these construction activities consume much site occupation time and at a considerable labor rate cost. Moreover, as described in the previous section, the bottom SIP reinforcement may not be depended upon to provide full resistance due to lack of anchorage at the continuity between the PCPs, which reduces the positive moment capacity of the deck slab. Therefore, a second key aim of this section is to investigate design improvements to speed up field operations. A thicker and longer PCP is developed herein that uses concentric pretensioned prestress to facilitate accelerated bridge construction.

As part of the design process in this section, the previously proposed symmetric live load model and the companion LDFs together with plastic overstrength analysis methods are applied to design an example multi-span spread slab beam bridge that consists of both simply supported and continuous spread slab beam portions. On the basis of the design results, the applicability of these proposed design methods is evaluated and the span limits of the spread slab beam bridge system is explored.

Full calculation sheets for the design are given in Appendix 4.

9.3 PROTOTYPE BRIDGE LAYOUT AND MATERIAL PROPERTIES

9.3.1 Bridge Geometry and Cross Section Properties

Figure 9.1(a) shows the overall bridge layout of the multi-span spread slab beam bridge. The spans at both ends are simply supported bridges with a span length of 14.2 m. The central three spans constitute a continuous spread slab beam bridge; and the span lengths of the end and middle spans are 16.8 m and 21.3 m, respectively. Figure 9.1(b) shows the cross section of the multi-span spread slab beam bridge, whose geometric dimensions are the same with the simply supported bridge investigated in Project 0-6722 (Hueste et al. 2015). The bridge has a total width of 10.4 m and a roadway width of 9.8 m, and is thus considered a two-lane bridge system. Throughout, the bridge superstructure consists of four 5SB15 slab beams with 2.95 m (9 ft-8 in.) center-to-center spacing. The width and depth of the 5SB15 slab beam is 1.5 m (5 ft) and 381 mm (15 in.) respectively. The total deck thickness is 203 mm (8 in.) between slab beams, but 254 mm (10 in.) on the top of beams due to the existence of 51 mm (2 in.) thick bedding strips. Two types of SIP PCPs were considered in the design process to evaluate their differences: (i) new 165 mm (6.5 in.) thick SIP PCPs plus a 38 mm (1.5 in.) CIP deck topping; (ii) conventional 102 mm (4 in.) thick SIP PCPs and 102 mm (4 in.) CIP deck topping. Accordingly, the steel rebar in the current design (left half portion) is arranged in different fashion with Hueste et al. (2015) design (right half portion) in order to facilitate accelerated bridge construction. The concrete bridge deck is designed to act in a composite fashion with the slab beams and the effective flange width is considered to be the center-to-center spacing of the neighboring beams.

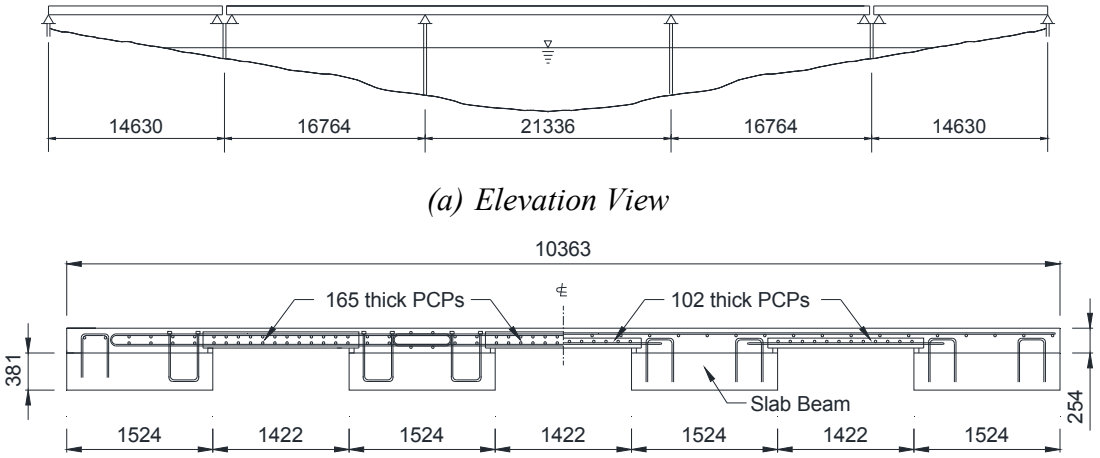

(a) Elevation View

(b) Cross Section

Figure 9.1. Multi-span Spread Slab Beam Bridge for Preliminary Design.

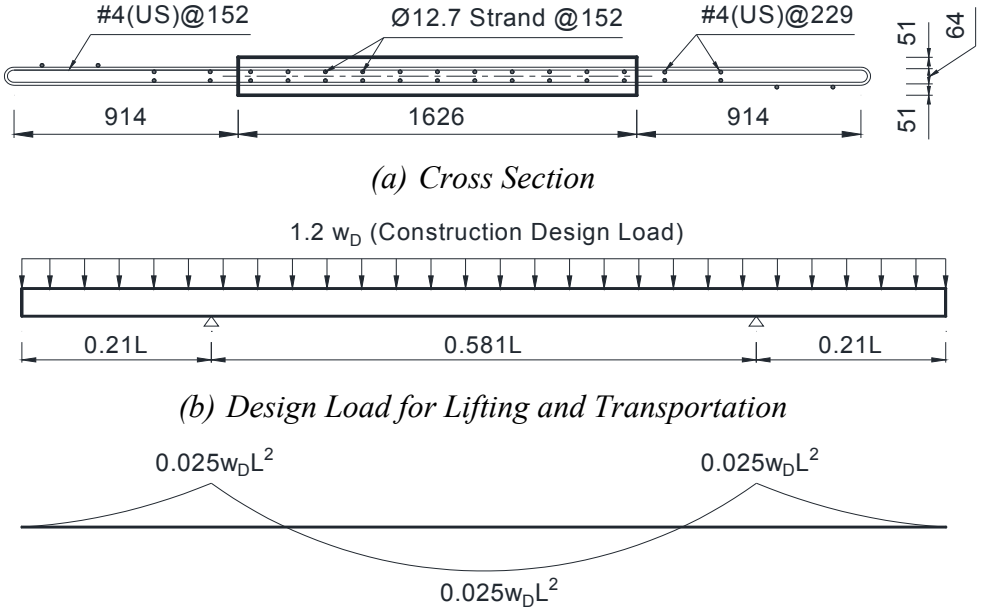

(a) Cross Section

(b) Design Load for Lifting and Transportation

(c) Bending Moment Diagram

Figure 9.2. Precast Prestressed Concrete Panel Design.

9.3.2 Material Properties

Design parameters for the spread slab beam bridge are based on the standard practice followed by TxDOT. The specified 28-day compressive strength for the deck concrete is 28 MPa. The compressive strengths of the slab beam concrete at release ($f_{ci}^{'}$) and service ($f_{c}^{'}$) are specified as 41 MPa and 59 MPa, respectively. The allowable stress limits and additional design parameters used for the preliminary design conforms to the AASHTO LRFD Bridge Design Specifications (2012).

The standard prestressing for the slab beams is 12.7 mm (0.5 in.) or 15.2 mm (0.6 in.) diameter low relaxation strands with ultimate strength, f_{pu}, of 1860 MPa (270 ksi). The yield strength for this type of strand is taken as $f_{py} = 0.9 f_{pu}$. Mild steel reinforcement used for slab beams and deck is specified to be ASTM A615 Grade 60 steel with yield strength, $f_{y} = 414$ MPa (60 ksi).

9.4 PRECAST PRESTRESSED CONCRETE PANEL DESIGN

Figure 9.2(a) presents the PCP cross section used in the preliminary design. The width and depth of the PCP is 1626 mm (5 ft-4 in.) and 165 mm (6.5 in.) Compared with traditional 102 mm (4 in.) thick panels, the new section has a greater depth which permits two rows of 12.7 mm (0.5 in.) diameter low relaxation strands, resulting in larger prestressing forces. The mild steel used for transverse reinforcement is the same as the TxDOT standard PCP design (#4(US)@152), which is designed to extend the rebar 914 mm (3 ft) out of the panel section for the purpose of making the transverse reinforcement continuous by overlapping and saving the CIP construction time. In the fabrication process, it is also

recommended to tie the necessary longitudinal rebars to the extended hooks so that the extra field reinforcing steel placement activities can be negated in the CIP construction.

Figure 9.2 shows (a) the applied construction load and (b) the corresponding bending moment diagram for the PCP design. The panel segments are pre-tensioned to resist 1.2 times dead load to provide a safety factor of 20 percent for the additional flexural stresses due to transportation, erection and construction. The two lifting points during the transportation and erection process are considered to be 0.21 times the span length from both ends, resulting in in the same maximum positive and negative moment values as shown in Figure 9.2(b). By conducting allowable stress analysis, it is found that the maximum span length of the PCP may span up to 22.7 m with a top and bottom pair of prestressing strands concentrically arranged at an even spacing of 152 mm (6 in.) on center. When the PCPs with thicker depth and longer span come into use, the PCPs and slab beams may be erected using cranes on the same day. The CIP deck concrete could be poured immediately after side forms are placed. Finally, it should be noted that no field placement of steel is needed.

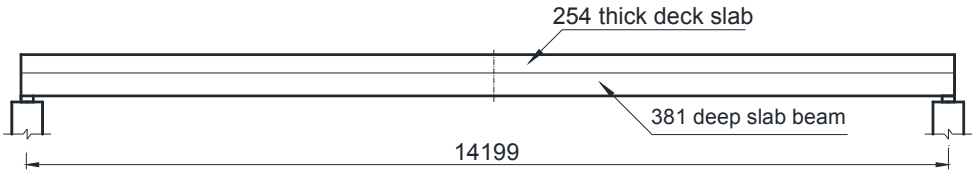

(a) Simple Span Bridge

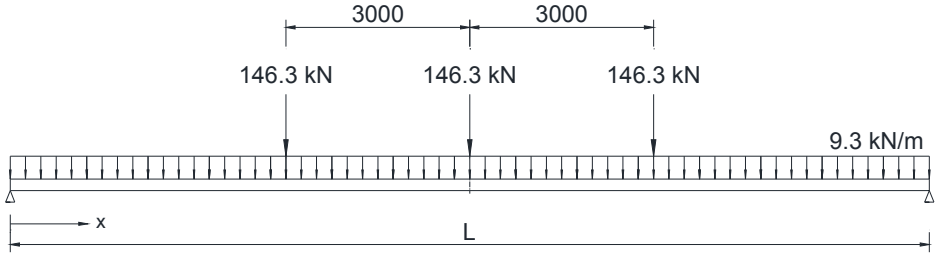

(b) Alternative Live Load Model

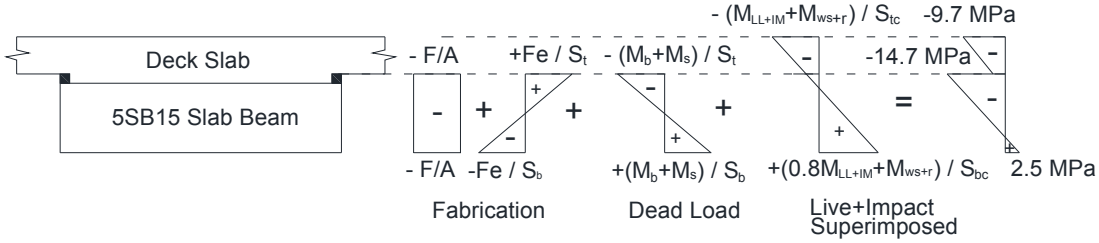

(c) Service Stress Block at Midspan

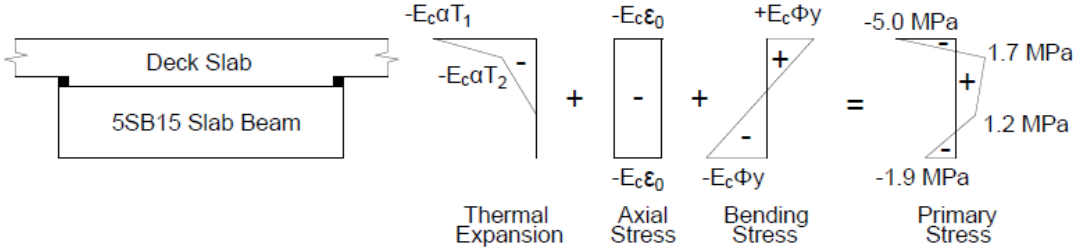

(d) Temperature Effect

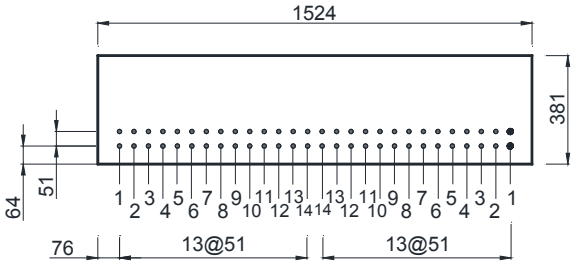

Debonding Data		
Measurement from End	**Strand No. (Bottom Row)**	**Debonded Numbers**
0 - 1823 mm	No. 5, 9, 13	6

(e) Pre-tensioned Strand Design

Figure 9.3. Preliminary Design for Simple Span Design.

9.5 DESIGN OF THE SIMPLY SUPPORTED SPANS

Figure 9.3(a) shows the elevation view of the simple span bridge. The span length, bridge width, cross section geometry are the same with the design case performed by Hueste et al. (2015), but the 165 mm (6.5 in.) thick PCPs are adopted herein. The prestressed concrete slab beams are designed to satisfy allowable stresses during fabrication, construction and at service; this prevents cracking during various stages of construction and service. Service stress analysis is carried out under the effects of pre-tensioned prestress forces, dead loads, live plus impact load and temperature gradients.

In the design, 12.7 mm (0.5 in.) diameter pretensioning prestressed strands are adopted and the initial stress at transfer f_{pi} is taken as 0.75 f_{pu}. Prestress losses are assumed to be 20 percent for pre-tensioning. The dead loads of the slab beam, PCPs and deck slab are considered to act on the non-composite beam section while the self-weight of the wearing surface and barriers were assumed to be in place after the composite action between the slab beams and deck slab becomes effective.

Figure 9.3(b) shows the alternative symmetric live load model developed in a previous section to provide bridge engineers a more direct and simpler option for rapid design. For a simple span bridge with span length longer than 12.3 m, it is recommended to use live plus impact load pattern as the following combination to determine the moment and shear forces per traffic lane: three-axle design truck load ($P_1 = P_2 = P_3 = 146.3$ kN) with equal axle spacing of 3 m and uniform design lane load ($w = 9.3$ kN/m). Because all loads are longitudinally symmetric, the maximum lane moment value would be achieved at midspan location.

The girder moment and shear force demands are determined using the following two proposed equations:

$$M_g = k_M \frac{S}{D_M} M_l \tag{9.1}$$

$$V_g = k_V \frac{S}{D_V} V_l \tag{9.2}$$

where M_g and V_g are the respective girder moment and shear demands; M_l and V_l are the lane moments and shears over the prescribed lane width; S = girder spacing in feet; $D_M = 3.66$ m (12 ft) and $D_V = 3$ m (10 ft); k_M and k_V are the respective correction factors. For a simply supported configuration, $k_M = 0.95$ and $k_V = 1.05$; for a continuous configuration, $k_M = 0.95$ and $k_V = 0.95$.

Figure 9.3(c) shows the service stress analysis under effects of prestress, dead load, live plus impact load and superimposed dead load. The stress block induced by bilinear thermal gradients is shown in Figure 9.3(d). The minimum required number of pre-tensioning strands were determined based on the allowable stress limits. Note that to mitigate the top tensile stress exceedance immediately after transfer at end regions, some debonding of strands is necessary. The final number and location of the pre-tensioned strands and debonding location information is presented in Figure 9.3(e), which conforms to the design solutions of Hueste et al. (2015) based on the AASHTO LRFD Bridge Design Specifications (2012).

Figure 9.4 presents the on-site activities needed to construct the entire deck slab system. The headed U-bars are designed as shear studs to enhance the interface shear between beam and slab. After the slab beams are erected on the pier supports, the PCPs are lifted and placed between the slab beams using the same crane on the same day as the slab beam erection is carried out. Because all necessary steel reinforcement for the deck slab is embedded in the PCPs, no extra reinforcement placement work is needed at the construction site – completely eliminating this costly field operation. The topping concrete is designed to be cast in two phases: 1) the concrete with specified strength of 45 to 55 MPa is first poured to the same level with the top surface of PCPs, as represented with green hatches; 2) the wearing surface is then placed to the required finished deck elevation, as shown with orange hatches. From the construction process, it is seen that fewer CIP construction activities are need to complete the entire deck system by using the new PCPs, thus much proposed long occupation time is saved and overall construction cost decreases.

9.6 CONTINUOUS BRIDGE DESIGN

9.6.1 Load Balance Design Philosophy and Construction Sequence

Load balancing with pretensioning and post-tensioning (PT) is adopted for the design of the three-span continuous spread slab beam bridge. Figure 9.5(a) presents the pretensioning strands applied inside the slab beam segments. Table 9.1 lists the number, the eccentricity and design force for the prestress strands in different precast slab beam segments. The pretensioning is designed to balance the dead load of slab beam and portion of PCPs. The harped tendon technique is adopted in the fabrication process so that are no end moments developed due to end eccentricity.

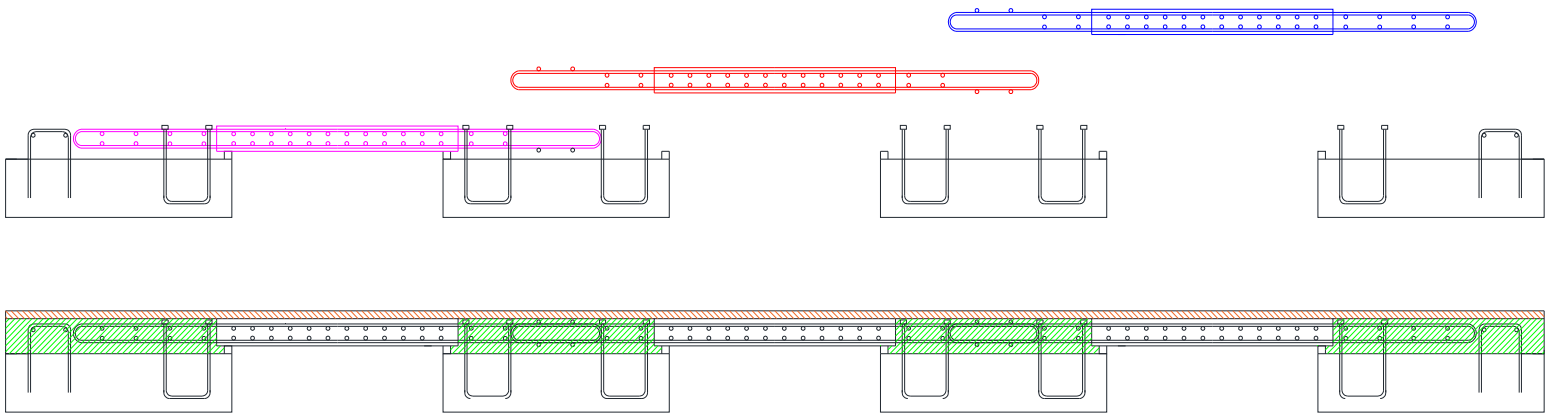

Figure 9.4. On-site Construction Activities for Spread Slab Beam Bridge with New PCPs. Note precast deck slab panels must be placed rom left to right.

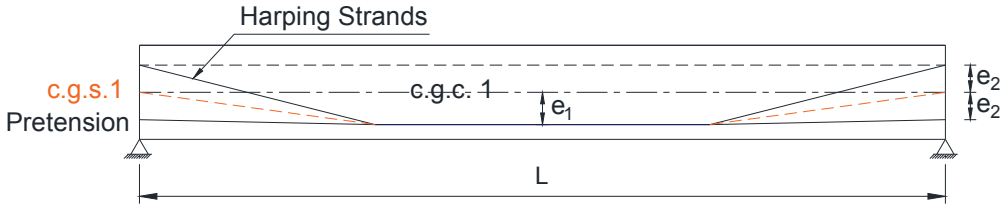

(a) Pre-tensioning Strands for the Slab Beam Fabrication Elevation View

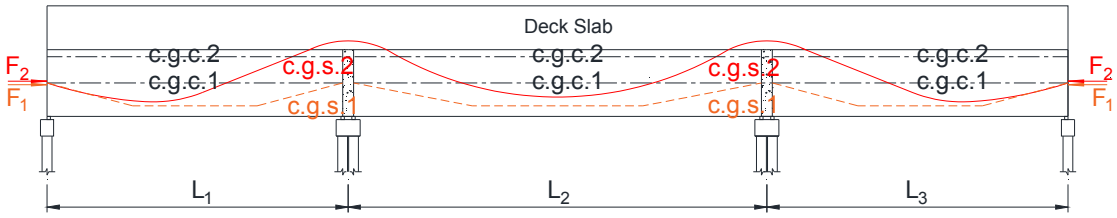

(b) Post-tensioning Tendon Profiles for the Continuous Bridge

Figure 9.5. Prestress Strand Design for the Continuous Bridge Configuration.

Table 9.1. Pretensioning Strands Design for the Precast Slab Beam Segments.

	Item	Non-harped	Harped	Prestress (Total)
21.3 m (70 ft) Slab Beam	Strands (15.2 mm diameter)	26	26	52
	Force at Transfer, F_{1i} (kN)	5075	5075	10150
	Force at Service, F_1 (kN)	4065	4065	8130
	Eccentricity at end (mm)	102	-102	0
	Eccentricity at midspan (mm)	127	127	127
16.8 m (55 ft) Slab Beam	Strands (15.2 mm diameter)	18	18	36
	Force at Transfer, F_{1i} (kN)	3514	3514	7028
	Force at Service, F_1 (kN)	3705	3705	7410
	Eccentricity at end (mm)	102	-102	0
	Eccentricity at midspan (mm)	127	127	127

Figure 9.5(b) shows the PT design for the continuous bridge configuration. Table 9.2 summarizes the numbers and design forces for the PT tendons. The PT tendons are jacked to essentially balance the self-weight of the extra deck slab. The overall system is designed to resist live plus impact load and superimposed dead load without cracking. The tendon profile considered for the preliminary design is smooth and parabolic without any sharp curvature to facilitate the tendon placement, thus the practical tendon profile over the interior support is draped with a reverse curve that results in a downward load in the neighborhood of the two interior supports.

Table 9.2. Post-tensioning Tendons Design for Continuous Bridge Configuration.

Item	Exterior Span	Interior Span
Strands (15.2 mm diameter)	19 (1 duct)	19 (1 duct)
Force at Transfer, F_{1i} (kN)	3020	3020
Force at Service after Losses, F_1 (kN)	2513	2513
Drape (mm)	178	330

Figure 9.6 shows the conceptual construction procedure based on the design philosophy. The construction process of the superstructure consists of the following eight main phases:

1. Precast the slab beams at the fabrication yard;
2. Erect the precast slab beams on the bridge supports;
3. Place PCPs between slab beams to act as stay-in-place (SIP) forms;
4. Pour cast-in-place (CIP) concrete joints and concrete between deck panels;
5. Place PT tendon in the duct;
6. Place wearing surface;
7. Jack PT tendon at construction site;
8. Install the traffic barrier.

9.6.2 Allowable Stress Analysis and Temperature Check

Structural analysis is undertaken to enable stress checks under the effects of prestress, dead load, live plus impact load and temperature gradient. The dead load includes self-weight of slab beams, PCPs, CIP deck slab, traffic barrier and wearing surface. The alternative live load model and proposed design models described in previous section were also adopted in the preliminary design of the continuous bridge configuration.

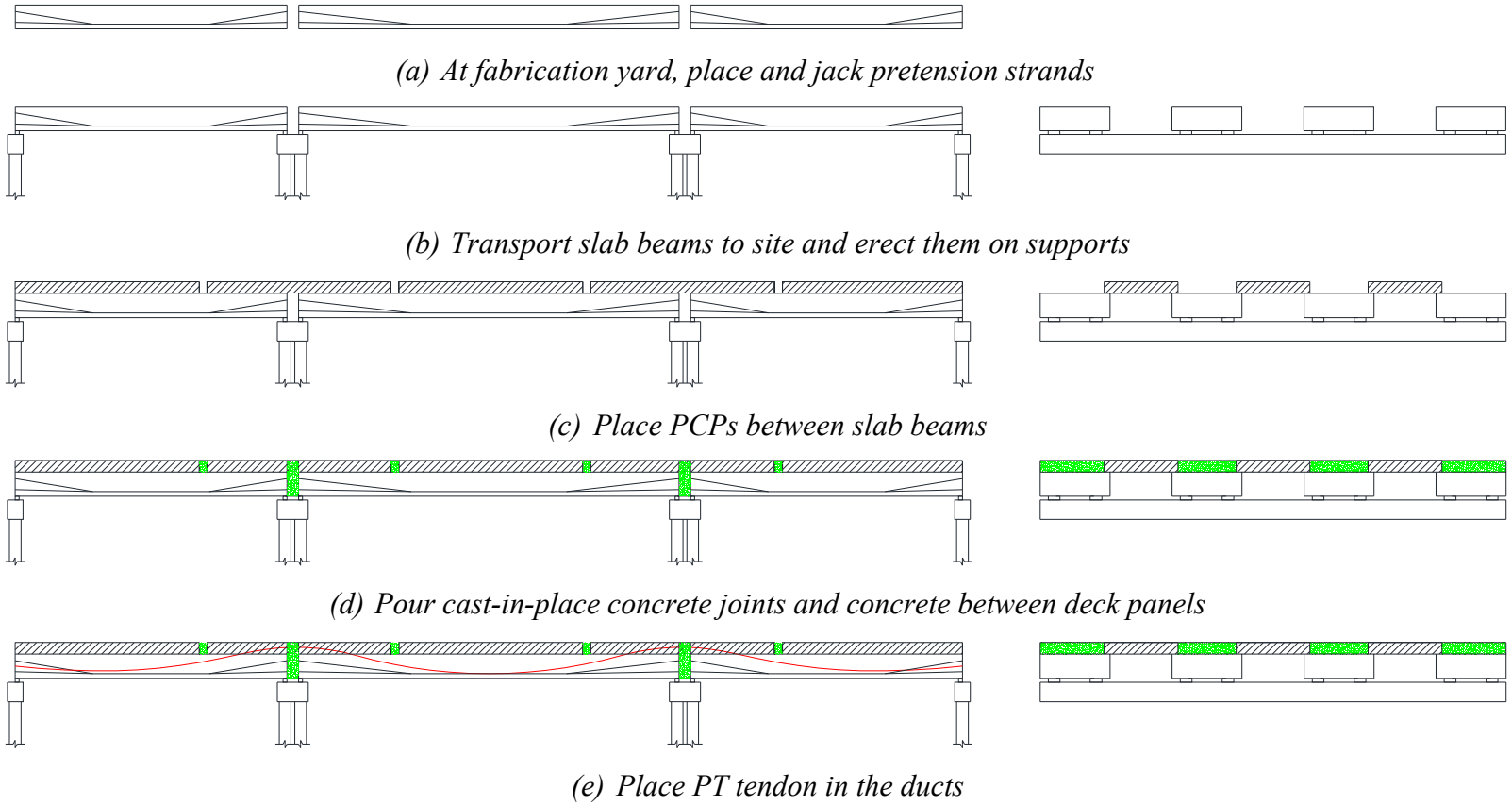

(a) At fabrication yard, place and jack pretension strands

(b) Transport slab beams to site and erect them on supports

(c) Place PCPs between slab beams

(d) Pour cast-in-place concrete joints and concrete between deck panels

(e) Place PT tendon in the ducts

Figure 9.6. Conceptual Construction Procedure.

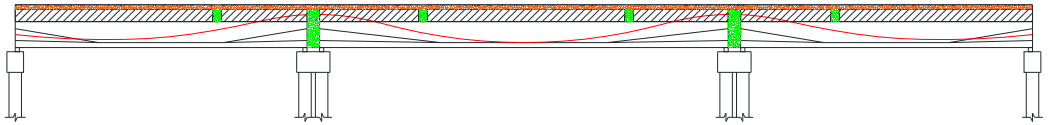

(f) Place wearing surface

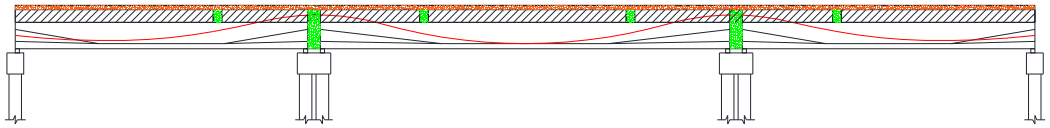

(g) Post-tension tendons

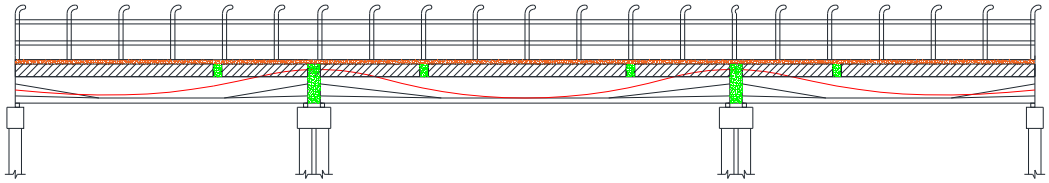

(h) Install guardrail

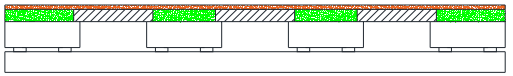

Figure 9.6. Continued.

Figure 9.7(a, b and c) shows three critical live load placement schemes to produce maximum moments and shear forces per traffic lane. In particular, two design trucks require placement in adjacent spans with minimum spacing of 15.2 m (50 ft) to generate maximum force effects at the interior supports (AASHTO 2012). The girder moment and shear demands were then determined according to the proposed design models shown in Equations (9.1) and (9.2). The stress check was carried out at the interior supports and midspan locations under the combination of service loads, as shown in Figure 9.7(d) to ensure the allowable stress limits are satisfied.

Secondary thermal stresses are critical in the design of continuous bridges (Priestley 1978). Figure 9.7(e) illustrates the procedure for calculating the secondary moments developed in the three-span continuous bridge as a result of restraint to the bending caused by primary thermal stresses. Figure 9.7(f) shows the total thermal stress, obtained by the summation of the primary thermal stresses and the secondary thermal stresses, at the interior span of the continuous spread slab beam bridge.

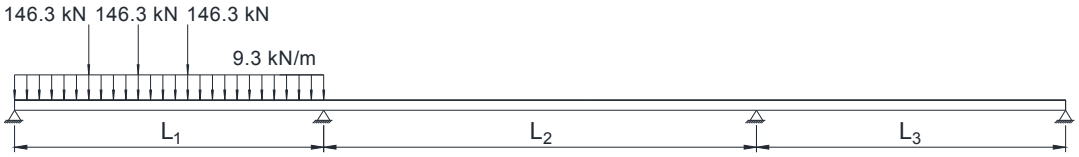

(a) Maximum Positive Moment at Exterior Span

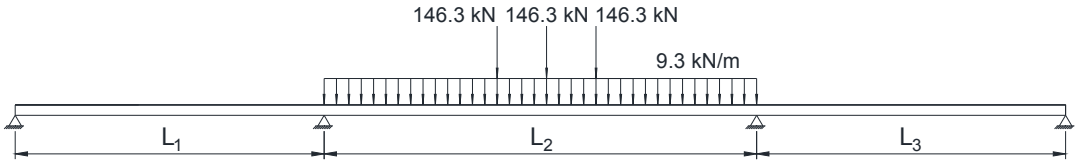

(b) Maximum Positive Moment at Interior Span

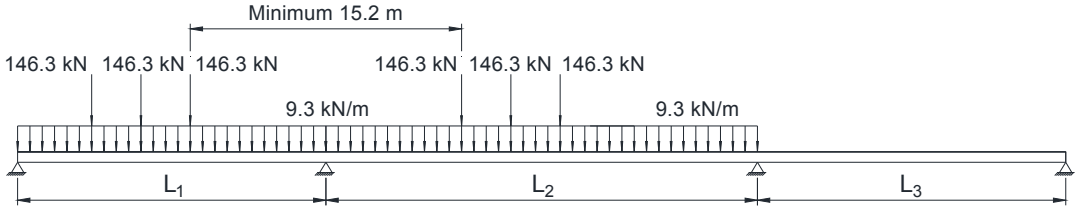

(c) Maximum Negative Moment and Shear Force at Interior Span

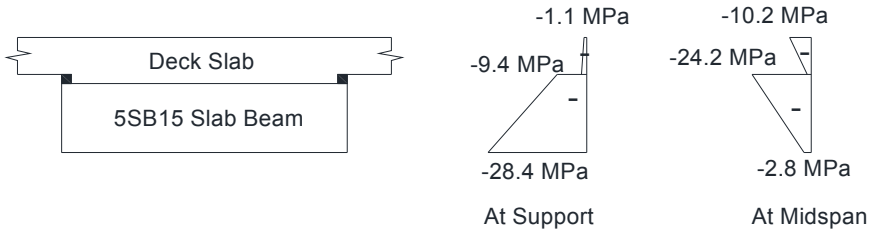

(d) Stress Blocks at Service (Interior Span)

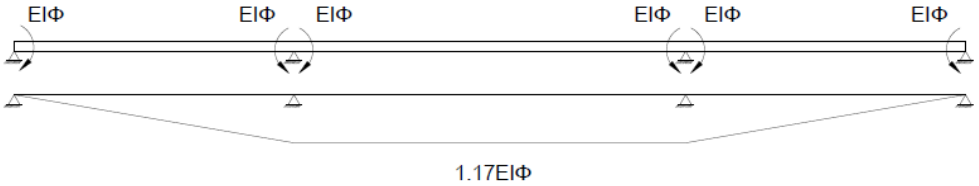

(e) Continuity moments that induce secondary thermal stresses

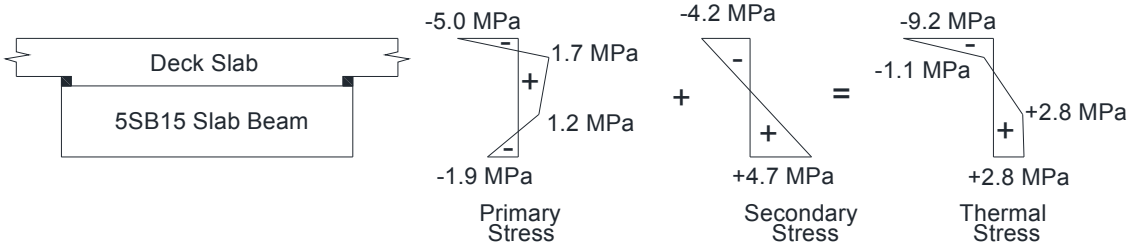

(f) Total Thermal Stress (Interior Span)

Figure 9.7. Preliminary Design for Three-span Continuous Bridge.

Figure 9.8 shows the final prestress strands arrangement at critical locations based on the load-balancing design. Both new and conventional PCPs were considered in the design process and they were shown as blue line in Figure 9.8. Since applied loads are identical for two designs, the number of prestress strands and their arrangement are the same. However, the transverse reinforcement in the new long PCPs is effectively fully anchored to the slab beams with the extended rebar, resulting in a more reliable deck slab connection system. Note that the number and location of prestressing strands follow the standard strand configuration that is set for TxDOT slab beam types. Based on geometric constraints and cover requirements, only 56 positions in two rows with 51 mm (2 in.) center-to-center spacing are available to arrange the prestress strands.

9.7 PLASTIC OVERSTRENGTH ANALYSIS

To ensure the bridge safety under the ultimate load conditions the strength limit state needs to be checked. Plastic analysis methods described in Section 8 are utilized herein to investigate the reserve strength capacity of the spread slab beam bridge system. To investigate the sufficiency of a design the plastic overstrength factor defined in Equation (8.1) is used.

Figure 9.9 depicts three potential failure modes considered in the analysis of bridge superstructures: beam-only mechanism, slab-only mechanism and mixed beam-slab mechanism. As compared to the simple span bridge configuration, negative moment capacities need to be taken into account at interior support to determine the plastic overstrength factor of the continuous bridge case.

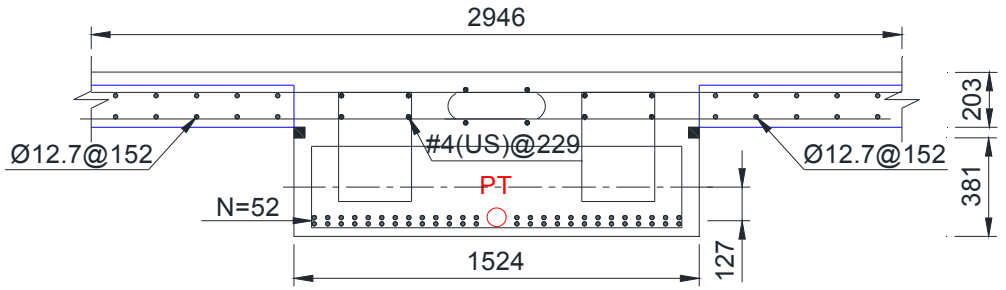

(a) Cross Section with Proposed PCP Solution at Midspan

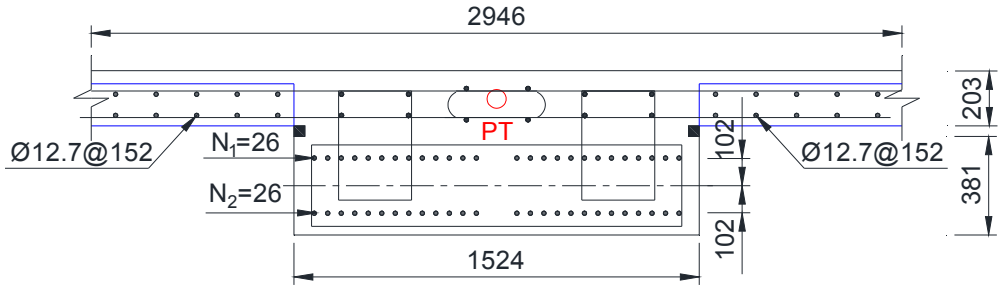

(b) Cross Section with Proposed PCP Solution at Interior Support

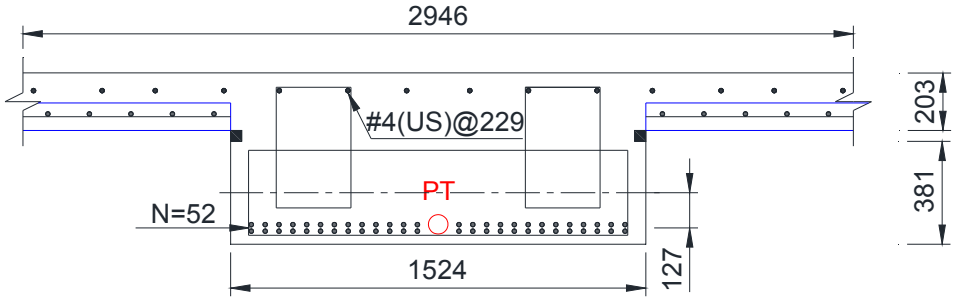

(c) Cross Section with Conventional PCPs at Midspan

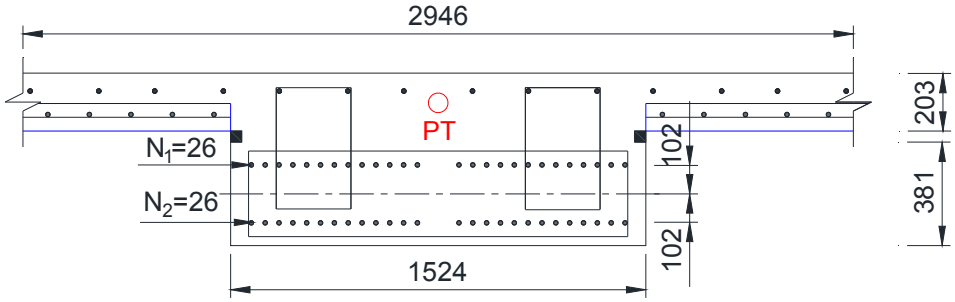

(d) Design Cross Section for Three-span Continuous Bridge

Figure 9.8. Design Cross Section for the Three-span Continuous Bridge.

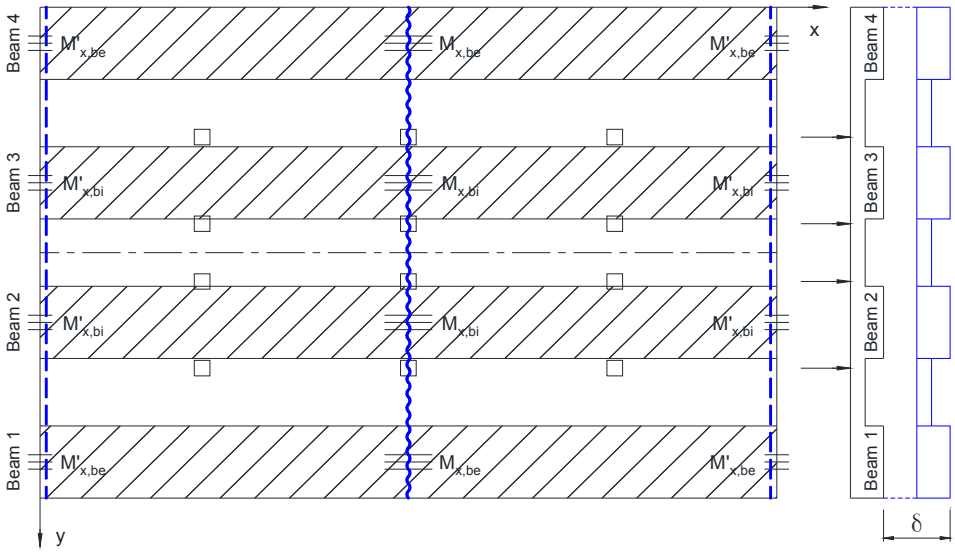

(a) Beam-only Mechanism

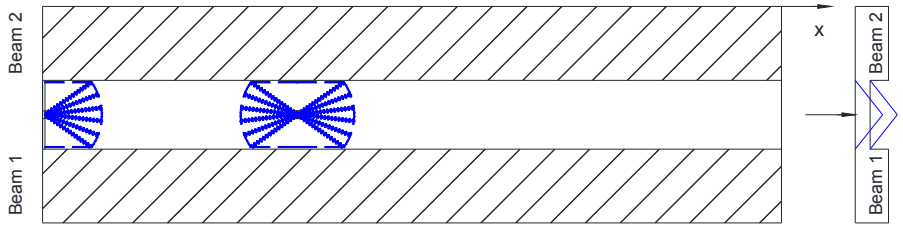

(b) Slab-only Mechanisms

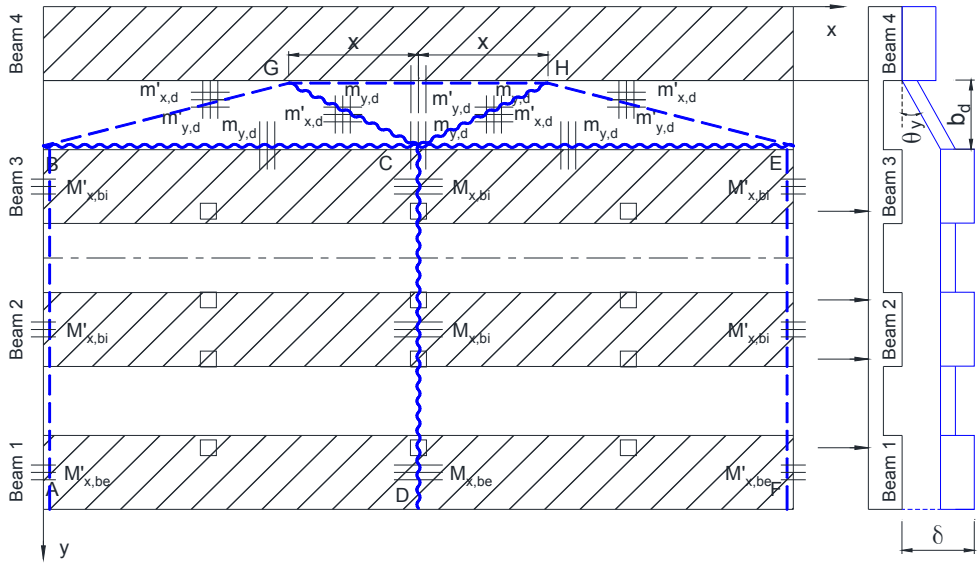

(c) Mixed Beam-slab Mechanism

Figure 9.9. Plastic Overstrength Analysis of the Spread Slab Beam Bridge.

Table 9.3 lists the computed overstrength factors for the multi-span spread slab beam bridges. For the design with conventional PCPs, the slab-only failure is the most critical mechanism that generates the lowest overstrength factor. This is because the bottom SIP presressing strands in the conventional SIP PCPs are not capable of providing the full positive flexural resistance at the slab-to-beam connection. Besides, a seam exists between conventional PCPs in the longitudinal direction, resulting in a more vulnerable connecting deck slab. When the new PCPs come into use, the transverse steels in the SIP PCPs are effectively anchored to the beam with the extended rebar and the longitudinal prestressing strands are continuous due to a longer span length of the PCP. All these advantages could effectively improve the moment capacity of the deck slab and further improve the reserve strength capacity.

For the three-span continuous spread slab beam bridge, it is found from Table 9.3 that the critical failure always occurs in the interior span (70') for both mixed beam-slab and beam-only mechanisms. It is also evident that the overstrength factors for various failure mechanisms increase when new PCPs come into use. Moreover, the desirable global beam failure mechanism becomes the most critical failure mode for both simply supported and continuous bridge configurations because the design of slab component is improved with utilizing new PCPs.

Table 9.3. Summary of Overstrength Factors

Failure Mechanisms		Conventional PCPs	Long PCPs
Slab - only Flexure Failure	One Wheel at end	**1.04***	2.68
	One Wheel inside	2.09	5.35
	Two Wheels at end	3.87	5.58
	Two Wheels inside	4.48	6.92
	Three Wheels at end	6.34	8.74
	Three Wheels inside	6.88	9.93
Mixed Beam - Slab Failure	Simple span (14.2 m)	**2.03**	2.13
	Continuous span (16.8 m)	2.46	2.64
	Continuous span (21.3 m)	**2.13**	2.34
Beam – only Failure	Simple span (14.2 m)	2.04	**2.04**
	Continuous span (16.8 m)	2.56	2.64
	Continuous span (21.3 m)	2.13	**2.23**

* Lower bound solution, all bottom steel neglected in mechanism.

9.8 CLOSURE AND KEY FINDINGS

The design of a multi-span prestressed concrete spread slab beam bridge was undertaken, and the results of that process are presented in this section. The design used the alternative live load model and proposed design models. Service stress analysis and plastic overstrength analysis at the ultimate limit state were carried out as an integral part of the design process. A key feature the results presented herein is where an alternative design based on the principles of accelerated construction was explored. This resulted in using a

thicker and longer PCP that is longitudinally prestressed in panel lengths up to 23 m. thereby providing an alternative accelerated construction option for the general contractor. The following findings are made based on the comparative designs and analysis results:

1. For this class of low profile spread slab beam bridge, span lengths up to 21.3 m are viable with only four spread slab beams. To achieve this span it is necessary to make at least three spans continuous and use load balancing principles along with some supplementary post-tensioning.
2. A longitudinally pretensioned 165 mm (6.5 in.) thick PCP may span up to 22.7 m. The design proposed herein uses all the required deck reinforcement cast into the panel; no field placement of deck reinforcement is necessary thereby accelerating construction with significant savings in site occupation time. Moreover, due to improved steel anchorage the more reliable deck slab system results, which tends to avoid a mixed beam-slab failure mechanism.
3. The use of the proposed LDF design models and plastic analysis methods for checking are quite direct and easy to apply. They lead to rapid and reliable solutions which conform to the basic tenants of solutions based on the AASHTO LRFD Bridge Design Specifications. Moreover, the plastic overstrength analysis offers the opportunity for the designer to check the hierarchy of failure mechanisms and then “rebalance” the design, if necessary.

10 SUMMARY, CONCLUSIONS AND RECOMMENDATIONS

10.1 SUMMARY

A new class of spread slab beam bridge superstructure has recently been developed and implemented in Texas. In order to investigate its structural performance in general, and load distribution behavior in particular, comprehensive static and dynamic tests were performed on an in-service spread slab beam bridge, the US 69 Bridge located in Denison, Texas. Different computational techniques including the historic grillage analysis and the more rigorous finite element method (FEM) were utilized to model the moment and shear actions for this new bridge system. Satisfactory agreement was obtained with comparisons between experimental and computational results.

Current service load design practice reveals that the asymmetric AASHTO HS20 truck load and complicated LRFD LDF formulas bring inconvenience to the design process. Alternative symmetric live load models and new design models with a familiar "*S/D*" format are developed in this dissertation for the purpose of providing bridge engineers a more straight-forward option to determine the moment and shear demands at the service load design or for the rapid checking of computer output. The applicability of the proposed design models for the prestressed concrete girder bridges commonly used in Texas and elsewhere is evaluated by comparing accuracy with more exacting FEM analysis results. Comparative results show that the proposed design formulas are mostly conservative for these bridge types.

Following service load design, the adequacy under factored ultimate strength conditions requires checking. Due to their expediency and ease of use, plastic limit analysis methods were used to evaluate the reserve strength capacity of slab-on-beam bridge systems. It was shown that by taking a holistic view of several different potential failure modes the "balance" of the design could be judged in terms of a hierarchy of failure mechanisms – flexural mechanism being preferable to shear mechanisms, for example. Therefore, it is possible to make minor adjustments to the design to obtain a preferred outcome.

The proposed design methods were adopted in the service load design of a multi-span spread slab beam bridge to explore the potential for extending the span length of this low profile bridge system. The design results indicated that span lengths up to 21.3 m are viable with only four spread slab beams. To achieve this span it is necessary to make at least three spans continuous and use load balancing principles along with some supplementary post-tensioning.

10.2 KEY CONCLUSIONS

The key conclusions that can be drawn from this research follows:

10.2.1 Field Testing

Comprehensive static and dynamic tests were conducted on the US 69 northbound bridge over Day Street in Denison, Texas, to investigate the in-service performance and load distribution behavior of the spread slab beam bridge system. Several types of instruments (strain gages, LVDTs, string potentiometers, and accelerometers) were installed on the

bridge to measure the structural responses under static and dynamic vehicular loading. By analyzing the data collected from all tests and coupled with companion FEM analyses, the following observations are drawn for this specific spread slab beam bridge geometry.

1. From the experimental tests conducted, it was shown that the presently used design methods are conservative for moment LDFs and unconservative for shear LDFs for the edge beams in particular.
2. The existence of integrally cast sidewalk and guardrail elements not only stiffens the edge beam, but markedly increases the moment demand for such beams. This is not effectively accounted for in the AASHTO bridge design process. In terms of shear action, the secondary elements relieve the shear demand. With the presence of a thicker slab (sidewalk) or an edge stiffening element (either median or guardrails) the normal design process should be handled with caution.
3. As the vehicle speed increases, so do the dynamic moment and shear demands while the LDFs do not markedly change with the vehicle speed. It is shown that the code-based uniform impact factor of 1.33 was unconservative for the tested bridge at speeds above 50 km/h. Until this aspect of vehicle-structure interaction is better understood, a more conservative approach to the service load design is recommended for this class of short span bridges. For example, it is suggested that the allowable tensile stress for a no-crack design criteria be restricted to $f_t = 0.5\sqrt{f_c'}$ (MPa).

10.2.2 Computational Analysis

Computational models were developed for a spread box beam bridge (Drehersville Bridge) and the tested spread slab beam bridge (US 69 Bridge) applying different analysis methods (grillage and FEM) and utilizing different commercial software. By comparing computational results with experimental values, the following conclusions were drawn:

1. For the spread box beam bridge, the grillage model more accurately captured the girder moments and LDFs than the FEM solutions. It is reasonable to simplify this type of bridge as several major longitudinal grillage members due to the comparatively greater box beam depth.
2. For the spread slab beam bridge tested as part of the present research, the FEM solutions provide moderately accurate deflections but given the small magnitude of deflection, it is difficult to discriminate where the errors arise; whether they are predominantly from measurement error or modeling simplifications.
3. The grillage and FEM LDFs for the tested spread slab beam bridge are similar to the observed test values with some small differences. For the exterior beam with sidewalk and guardrail in the US 69 Bridge, grillage analysis provides unconservative (-10%) moment LDFs compared with the experimental values.
4. By developing the models carefully, the historic grillage method could be utilized for the analysis and design of the spread slab beam bridge. It is recommended that the spacing of transverse grillage member is less than 10 percent of the overall span length. Also, an additional transverse beam member at the loading position could help to improve the analysis accuracy.

5. The general conclusion from this dual experimental and computational study is: given the ease of developing and applying advanced computational FEM solutions, one should use the best available analysis tools. Regardless of the claimed accuracy, it remains prudent to validate results against realistic experimental evidence, if available.

10.2.3 Live Load Models

A symmetric live load model was developed in an attempt to provide bridge engineers a more direct and simpler approach to design. The moment and shear effects of simple spans under the proposed live load model were evaluated and compared with those produced by the AASHTO LRFD HL-93 live model. The following observations were made based on the comparative results:

1. When the span length is over 12.3 m, more critical moment values are produced by the HS20 truck load rather that the tandem load. Similarly, the HS20 truck load generates more critical shear forces as the span length is larger than 7.6 m.
2. The proposed alternative truck load produces similar but slightly conservative moment and shear envelope curves as the AASHTO HS20 truck load does. Due to the symmetric property, the maximum moment generated by the alternative truck load always occurs at the midspan location.
3. It is recommended to use live load pattern as one of the following combinations for rapid design, whichever produce maximum force effects. The impact factor (33%) is only applied to the design truck or tandem load when the dynamic allowance is considered in the design.

- Alternative design truck plus lane load. $P = P_1 = P_2 = P_3 = 25 \text{ kips} = 110 \text{ kN}$, $b = c = 10 \text{ ft} = 3 \text{ m}$, $w = 0.64 \text{ kips/ft} = 9.3 \text{ kN/m}$.
- Design tandem load plus lane load. $P_1 = P_2 = 25 \text{ kips} = 110 \text{ kN}$, $b = c = 4 \text{ ft} = 1.2 \text{ m}$, $w = 0.64 \text{ kips/ft} = 9.3 \text{ kN/m}$.

10.2.4 LDF Models

New LDF models were proposed for prestressed concrete girder bridges to determine the moment and shear demands at the service load stage of design or for the rapid checking of computer output. The FEM technique was utilized to develop and analyze 61 simply supported and 38 continuous bridge models, each having a different superstructure geometry. The "exact" moment and shear force values were determined and further utilized to evaluate the applicability of the proposed design models. Based on the comparative study conducted amongst design values, FEM solutions and code-specified results, the following observations for simply supported and continuous bridge configurations were made:

10.2.4.1 Simply Supported Bridges

1. For simply supported prestressed concrete I-girder bridges, the design models provide 10 percent conservative moment and 6 percent conservative shear force values as compared to computational results. A similar degree of conservatism was obtained from the values specified by the AASHTO LRFD formulas.

2. For simply supported prestressed concrete slab beam bridge decks, the proposed design models provide about 5 percent conservative moment and shear values when compared to computational solutions.
3. For simply supported prestressed concrete spread slab beam bridges, the AASHTO LRFD spread box beam formulas provide unconservative shear design values as compared to exact FEM solutions, which indicates that AASHTO shear equations are not applicable for this new class of bridge.
4. For simply supported prestressed concrete spread slab beam bridge, the proposed design models provide about 16 percent conservative moments and 2 percent shear forces when compared to computational results. For this specific bridge type, it is suggested to adjust the correction factors in the proposed models with 0.95 and 1.05 for moment and shear actions respectively.

10.2.4.2 Continuous Bridges

1. For continuous prestressed concrete I-girder bridge decks, the design models with adjusted correction factors provide over 9 percent conservative moment and 8 percent conservative shear force values when compared to the "exact" computational results. It was also observed that AASHTO LRFD LDF formulas provide slightly unconservative design values for negative moment at continuous interior supports and positive moment at midspan when compared with the "exact" FEM solutions.
2. For continuous prestressed concrete slab beam bridge cases, the final design formulas generate conservative moment and shear design values at critical locations and are suitably reliable for the service load phase of a design.

3. For continuous prestressed concrete spread slab beam bridge, the design models with adjusted correction factors provide over 15 percent conservative positive moment values at both side and mid spans and 8 percent higher negative moment values at interior support as compared to computational results. In terms of shear forces, the proposed design values are 4 percent higher at end support and over 10 percent higher at interior pier than FEM solutions. Moreover, the AASHTO LRFD formulas generate unconservative design values for negative moments over continuous supports and shear forces at the simple end supports.
4. Generally, the proposed LDF models provide conservative design values for moment and shear actions, which could be used for service load design of prestressed concrete girder bridges. The two recommended equations for moment and shear force demands are:

   For moments: $M_g = k_M \frac{S}{D_M} M_l$

   For shears: $V_g = k_V \frac{S}{D_V} V_l$

where $D_M = 12$ ft $= 3.66$ m; $D_V = 10$ ft $= 3$ m; The correction factors, k_M and k_V, for simply supported and continuous bridge configurations are tabulated in Table 7.5.

10.2.5 Plastic Overstrength Analysis

Plastic limit methods of analysis were used to define the overstrength capacity of slab-on-beam bridge systems at the ultimate limit state collapse load. Three different limiting behavior modes were considered: slab-only mechanisms, a beam-only mechanism and

mixed beam-slab mechanisms. Then, the upper bound yield line method and lower bound strip methods were applied to the investigated new class of spread slab beam bridges. It was demonstrated that the different analysis methods, when accurately applied, are in agreement even though results are slightly different due to underlying assumptions. Based on the analysis results, the following bridge-type specific conclusions are drawn:

1. Although all methods show that the plastic overstrength is adequate whereby $\Omega > 1$, the designs may not be "balanced" in the most appropriate way. More specifically, a deck-slab failure from a single wheel load at a slab-end region was indicated ($\Omega = 1.04$). This may be simply ameliorated by placing a strong band of reinforcing slab steel parallel to the end-of-slab free edge.
2. A mixed beam-slab flexure failure was found to be critical for the Riverside Bridge ($\Omega = 2.03$) which is close to a global beam failure ($\Omega = 2.04$). This is attributed to the CIP half-slab on the half-depth SIP panels where the bottom SIP prestressing strands cannot be depended on to provide full positive moment flexural resistance at the slab-to-beam connection. To increase the positive moment slab capacity, the SIP strand or rebar should be adequately anchored into the beam, in this way the design may be "rebalanced" such that the global beam failure remains the preferred failure mechanism.
3. In terms of beam-slab failure mechanism in the spread slab beam bridge system, wider clear spacing decreases the transverse flexure capacity of the connecting deck slab and the transverse flexure failure is more likely to occur in this situation. Conversely, shear failure tends to occur when the beams are closely spaced. Such performance potential

is neither desirable nor recommended; beams should, ideally, be placed at a sufficiently wide spacing to lead to a secondary flexural failure in the deck slab, with the primary failure being beam flexure of the main spread slab beams.

10.2.6 Preliminary Design Study

A preliminary design of multi-span prestressed concrete spread slab beam bridge was performed using the proposed design methods. Service stress analysis and plastic overstrength analysis at ultimate limit state were carried out as an integral part of the design process. In addition, a thicker and longer PCP that is longitudinally prestressed was developed to provide an alternative construction option for the general contractor. The following conclusions are made based on the design and analysis results:

1. The use of the proposed LDF design models and plastic analysis methods checking are quite direct and easy to apply. They lead to rapid and reliable solutions which conform to the solutions based on the AASHTO LRFD Bridge Design Specifications (2012). Moreover, the plastic overstrength analysis offers the opportunity for the designer to check the hierarchy of failure mechanisms and then "rebalance" the design, if necessary.
2. The post-tensioning technique may make permit a solution for longer span spread slab beam bridge spans; spans of 21.3 m (70 ft) may be achieved in a continuous configuration.
3. A longitudinally pretensioned 165 mm (6.5 in.) thick PCP may span up to 22.7 m. The design proposed herein uses all the required deck reinforcement cast into the panel; no field placement of deck reinforcement is necessary thereby accelerating construction

with significant savings in site occupation time. Moreover, due to improved steel anchorage a more reliable deck slab system results, which also avoids a mixed beam-slab failure mechanism.

10.3 RECOMMENDATIONS FOR IMPLEMENTATION INTO PRESENT PRACTICE

The key recommendations for present practice follow:

1. The normal bridge design process should be handled with caution with the presence of a thicker slab (sidewalk) or an edge stiffening element (either median or guardrails) because these secondary elements not only stiffen the edge beam, but markedly alter the load distribution and increase the moment demand for the edge beam.
2. The proposed alternative live load model and LDF formulas produce similar but slightly conservative moment and shear envelope curves as compared to existing AASHTO LRFD provisions, thus they may be utilized for rapid design of bridge structures that consists of several competing alternatives.
3. Plastic limit analysis methods, including the upper bound yield line theory and lower bound strip methods, should be considered in the capacity and failure mode evaluation for the reserve strength capacity of slab-on-beam bridges at ultimate limit state. As the analysis methods take a holistic collapse mechanism approach they provide an opportunity for the designer to check the "balance" of a given design and thereby modify it, if necessary.
4. Post-tensioning of spread slab beam bridges permit the construction of more efficient longer spans; in a continuous configuration span length up to 21.3 m may be achieved.

5. The usage of the 165 mm (6.5 in.) thick PCP could save much site occupation time involving CIP construction activities, thus reduce the overall construction cost. In addition, the new PCPs could help to provide a more reliable deck slab system with continuous steel placement.

10.4 RECOMMENDATIONS FOR FUTURE RESEARCH

Following the research conducted and presented herein, certain research questions remain and new questions have arisen. Therefore the following questions pertain to future work.

What is the effect of vehicle-structure interaction on the bridge dynamic responses? And under what circumstances the uniform impact factor specified by current code is sufficient?

From the experimental observations it is evident that the code-based uniform impact factor of 1.33 is unconservative for the spread slab beam class of bridge when speeds exceed 50 km/h. Vehicle-structure interaction effects should therefore be investigated to evaluate under what circumstances the dynamic amplification factor sufficient. Hence derive modifications for bridge-specific cases.

Are the proposed design models applicable for prestressed concrete girder bridges with skew or curvature? If not, what kind of correction factors should be included for curvature and skew effects?

The applicability of proposed design models to the design of slab on prestressed concrete girder bridges with no skew or curvature has been validated. However, it is unknown whether the curvature and skew significantly affects the girder moment and shear demands. Additional parametric studies need to be undertaken to evaluate the effects of

these parameters, and further correction factors should be included in the proposed design models for curvature and skew effects.

Are the proposed design models applicable to determine the moment and shear demands of slab-on-steel girder bridges?

The proposed design models generally produce conservative design values for moment and shear actions of prestressed concrete girder bridges. However, their applicability to the slab-on-steel girder bridges remains in question. In order to broaden the applicable ranges of the proposed design models, it is suggested that parametric FEM analyses be conducted on representative slab-on-steel girder bridge configurations to determine the "exact" moment and shear demands and further evaluate the applicability of the proposed design models.

What is the constructability and structural performance of the continuous spread slab beam bridges with using new PCPs?

A three-span spread slab beam bridge has been successfully designed using the post-tensioning technique, but its constructability and performance are unknown at this stage. If sufficient research funding is available, it is suggested to build a full-scale continuous spread slab beam bridge and further investigate the static and dynamic performance of the bridge under vehicle loads. In the construction process, it is recommended to utilize new PCPS for the purpose of evaluating their effectiveness and in-service performance. The entire research procedure would be a companion to the Riverside Bridge tests as given in TxDOT Project 0-6722.

REFERENCES

AASHO (1931). AASHO Standard Specifications for Highway Bridges and Incidental Structures, American Association of State Highway Officials, Washington, D.C.

AASHTO (1941). AASHTO Standard Specifications for Highway Bridges, American Association of State Highway and Transportation Officials, Washington, D.C.

AASHTO (1965). AASHTO Standard Specifications for Highway Bridges, American Association of State Highway and Transportation Officials, Washington, D.C.

AASHTO (1977). AASHTO Standard Specifications for Highway Bridges, American Association of State Highway and Transportation Officials, Washington, D.C.

AASHTO (1994). "AASHTO LRFD Bridge Design Specifications, 1st Edition." American Association of State Highway and Transportation Officials (AASHTO), Customary US Units, Washington, DC.

AASHTO (2002). AASHTO Standard Specifications for Highway Bridges, American Association of State Highway and Transportation Officials, Washington, D.C.

AASHTO (2012). "AASHTO LRFD Bridge Design Specifications, 6th Edition." American Association of State Highway and Transportation Officials, Washington, DC.

Al-Mahaidi, R., Taplin, G., and Giufre, A. (2000). "Load distribution and shear strength evaluation of an old concrete T-beam bridge." Transportation Research Record: Journal of the Transportation Research Board, 1696(1), 52-62.

Albert, G., and David, V. (1967). "Lateral Distribution of Dynamic Loads in a Prestressed Concrete Box-beam Bridge." Fritz Engineering Laboratory Department of Civil Engineering Lehigh University, Bethlehem, Pennsylvania.

Amer, A., Arockiasamy, M., and Shahawy, M. (1999). "Load distribution of existing solid slab bridges based on field tests." Journal of Bridge Engineering, 4(3), 189-193.

CSA. (2006). Canadian highway bridge design code, Canadian Standards Association, Rexdale, Ont.

Bakht, B., Cheung, M., and Aziz, T. (1979). "Application of a simplified method of calculating longitudinal moments to the Ontario highway bridge design code." Canadian Journal of Civil Engineering, 6(1), 36-50.

Bakht, B., and Moses, F. (1988). "Lateral distribution factors for highway bridges." Journal of Structural Engineering, 114(8), 1785-1803.

Barker, R. M., and Puckett, J. A. (2007). Design of highway bridges: An LRFD approach, John Wiley & Sons, Inc., Hoboken, NJ.

Barker, R. M., and Puckett, J. A. (2013). Design of Highway Bridges: An LRFD Approach, John Wiley & Sons, Inc., Hoboken, NJ.

Barr, P., and Amin, M. N. (2006). "Shear live-load distribution factors for I-girder bridges." Journal of Bridge Engineering, 11(2), 197-204.

Barr, P. J., Eberhard, M. O., and Stanton, J. F. (2001). "Live-load distribution factors in prestressed concrete girder bridges." Journal of Bridge Engineering, 6(5), 298-306.

Barr, P. J., Woodward, C. B., Najera, B., and Amin, M. N. (2006). "Long-Term Structural Health Monitoring of the San Ysidro Bridge." Journal of performance of constructed facilities, 20(1), 14-20.

Brockenbrough, R. L. (1986). "Distribution factors for curved I-girder bridges." Journal of Structural Engineering, 112(10), 2200-2215.

BSI (1972). Code of Practice for the Structural Use of Concrete, British Standards Institution, London.

Cai, C. S., Shahawy, M., and Peterman, R. J. (2002). "Effect of diaphragms on load distribution of prestressed concrete bridges." Transportation Research Record: Journal of the Transportation Research Board, 1814(1), 47-54.

CALTRANS (2014). "Bridge Design Practice." California Department of Transportation. <http://www.dot.ca.gov/hq/esc/techpubs/manual/bridgemanuals/bridge-design-practice/pdf/bdp_3.pdf>. (January 15, 2015).

Chen, C.-H., and VanHorn, D. (1971). "Static and Dynamic Flexural Behavior of a Prestressed Concrete I-beam Bridge, Bartonsville Bridge." Fritz Engineering Laboratory· Report(349.2).

Chen, Y., and Aswad, A. (1996). "Stretching Span Capability of Prestressed Concrete Bridges under AASHTO LRFD." ASCE Journal of Bridge Engineering, 1(3), 112–120.

Chen, Y., and VanHorn, D. (1970). "Structural behavior of a prestressed concrete box-beam bridge--hazleton bridge, December 1970."Bethlehem, Pennsylvania.

Cheung, M., Gardner, N., and Ng, S. (1987). "Ultimate load distribution characteristics of a model slab-on-girder bridge." Canadian Journal of Civil Engineering, 14(6), 739-752.

Chung, W., Phuvoravan, K., Liu, J., and Sotelino, E. (2005). "Applicabiliy of the Simplified Load Distribution Factor Equation to PSC Girder Bridges." KSCE J Civ Eng, 9(4), 313-319.

Clough, R. "The Finite Element Method in Plane Stress Analysis. Pro. 2nd." Proc., ASME Conference on Electronic Computation, Pittsburgh, PA.

OHBDC (1991). Ontario Highway Bridge Design Code, Ministry of Transportation, Downsview, Ontario, Canada.

Cohen (1990). Truck Weight Limits: Issues and Options, Transportation Research Board.

Computers and Structures (2013). "CSI Knowledge Base." Computers and Structures, Inc., Berkeley, CA.

Courant, R. (1943). "Variational methods for the solution of problems of equilibrium and vibrations." Bulletin of the American Mathematical Society, 49(1), 1-23.

Dassault Systemes (2013). Abaqus, version 6. Abaqus, Inc., Velizy-Villacoublay, France.

Deng, L., Ghosn, M., Znidaric, A., and Casas, J. R. (2001). "Nonlinear flexural behavior of prestressed concrete girder bridges." Journal of Bridge Engineering, 6(4), 276-284.

Douglas, W. J., and Vanhorn, D. A. (1966). "Lateral Distribution of Static Loads In A Prestressed Concrete Box-Beam Bridge. Drehersville Bridge." Fritz Engineering Laboratory Report No. 350.1, Bethlehem, Pennsylvania.

Douglas, W. J., and VanHorn, D. A. (1966). "Static Loads in a Prestressed Concrete Box-beam Bridge." Fritz Engineering Laboratory Department of Civil Engineering Lehigh University, Bethlehem, Pennsylvania.

Eamon, C. D., and Nowak, A. S. (2002). "Effects of edge-stiffening elements and diaphragms on bridge resistance and load distribution." Journal of Bridge Engineering, 7(5), 258.

Elms, D. (1992). "Consistent crudeness in system construction." Optimization and Artificial Intelligence in Civil and Structural Engineering, Springer, 71-85.

Eom, J., and Nowak, A. S. (2001). "Live load distribution for steel girder bridges." Journal of Bridge Engineering, 6(6), 489-497.

Eom, J., and Nowak, A. S. (2001). "Live load distribution for steel girder bridges." Journal of Bridge Engineering, 6(6), 489.

Ghosn, M., Casas, J., and Xu, J. M. (1996). "Development of an efficient program for the nonlinear analysis of bridges." Computers & structures, 61(3), 459-470.

Ghosn, M., and Moses, F. (1998). Redundancy in highway bridge superstructures, Transportation Research Board.

Ghosn, M., Moses, F., and Gobieski, J. (1986). "Evaluation of steel bridges using in-service testing." Transportation Research Record (1072), 71-78.

Ghosn, M., Yang, J., Beal, D., and Sivakumar, B. (2014). Bridge system safety and redundancy (No. Project 12-86).

Google Maps (2014). <https://www.google.com/maps>. (July 15, 2014).

Graddy, J. C., Kim, J., Whitt, J. H., Burns, N. H., and Klingner, R. E. (2002). "Punching-shear behavior of bridge decks under fatigue loading." ACI Structural Journal, 99(3).

Grubb, M. A., and Schmidt, R. E. (2012). "Steel Bridge Design Handbook Design Example 1: Three-Span Continuous Straight Composite Steel I-Girder Bridge."

Guilford, A. A. (1967). "Lateral Distribution of Dynamic Loads in a Prestressed Concrete Box-beam Bridge, Drehersville Bridge." Fritz Engineering Laboratory Department of Civil Engineering Lehigh University, Bethlehem, Pennsylvania.

Guilford, A. A., and VanHorn, D. A. (1967). "Lateral Distribution of Vehicular Loads in a Prestressed Concrete Box-beam Bridge, Berwick Bridge." Fritz Engineering Laboratory Department of Civil Engineering Lehigh University, Bethlehem, Pennsylvania.

Guilford, A. A., and VanHorn, D. A. (1968). "Lateral Distribution of Vehicular Loads in a Prestressed Concrete Box-beam Bridge, White Haven Bridge." Fritz Engineering Laboratory Department of Civil Engineering Lehigh University, Bethlehem, Pennsylvania.

Hambly, E. C. (1976). Bridge Deck Behaviour, Halsted Press, New York, NY.

Hambly, E. C. (1991). Bridge Deck Behaviour, Taylor & Francis, New York, NY.

Harris, D. K., Cousins, T., Sotelino, E. D., and Murray, T. M. (2010). "Flexural Lateral Load Distribution Characteristics of Sandwich Plate System Bridges: Parametric Investigation." ASCE Journal of Bridge Engineering, 15(6), 684-694.

Hays Jr, C., Sessions, L., and Berry, A. (1986). Further studies on lateral load distribution using a finite element method.

Hazell (1999). "Strength Assessment of Concrete Beam-and-Slab Bridges." MEng Report, University of Cambridge.

Hillerborg, A. (1956). "Equilibrium theory for reinforced concrete slabs." Betong, 41(4), 171-182.

Hindman, W. S., and Vandegrift, L. E. (1945). Load distribution over continuous deck type bridge floor systems, College of Engineering, the Ohio State University.

Holcomb, R. M. (1956). "Distribution of loads in beam-and-slab bridges."

Holt, J. (2011). "Spread Box and Slab Beams." <http://ftp.dot.state.tx.us/pub/txdot-info/brg/0611_webinar/holt.pdf>. (November 11, 2014).

Hueste, M. B., Mander, J., Terzioglu, T., Jiang, D., and Petersen-Gauthier, J. (2015). "Spread Prestressed Concrete Slab Beam Bridges." Research Report No. 0-6722-1, Texas A&M Transportation Institute, College Station, TX, 406.

Hueste, M. B. D., Adil, M. S., Adnan, M., and Keating, P. B. (2006). "Impact of LRFD Specifications on Design of Texas Bridges Volume 1: Parametric Study." Texas Transportation Institute and Texas Department of Transportation, College Station, TX, 285-306.

Hueste, M. B. D., Adil, M. S., Adnan, M., and Keating, P. B. (2006). "Impact of LRFD Specifications on Design of Texas Bridges Volume 2: Prestressed Concrete Bridge Girder Design Examples." Texas Transportation Institute and Texas Department of Transportation, College Station, TX, A.1-1-B.2-67.

Hughs, E., and Idriss, R. (2006). "Live-Load Distribution Factors for Prestressed Concrete, Spread Box-Girder Bridge." ASCE Journal of Bridge Engineering, 11(5), 573-581.

Huo, X. S., Wasserman, E. P., and Zhu, P. S. (2004). "Simplified Method of Lateral Distribution of Live Load Moment." Journal of Bridge Engineering, 9(4), 382-390.

Jackson, A., and Middleton, C. (2013). "Closely correlating lower and upper bound plastic analysis of real slabs." Structural Engineer, 91, 34-40.

Jensen, V. P. (1938). "Solutions for certain rectangular slabs continuous over flexible supports; a report of an investigation conducted by the Engineering experiment station, University of Illinois in cooperation with the United States Bureau of public roads and the Illinois Division of highways."

Jensen, V. P., Kluge, R. W., and Williams, C. B. (1943). Highway slab-bridges with curbs: laboratory tests and proposed design method; a report of an investigation conducted by the Engineering experiment station, University of Illinois in cooperation with the Public roads administration, Federal works agency and the Division of highways, state of Illinois, University of Illinois.

Johansen, K. W. (1962). Yield-line theory, Cement and Concrete Association.

JRA (1996). Japanese Specifications for Highway Bridges, Japan Road Association, Maruzen, Tokyo.

Kianoush, H. M. (2015). "Experimental Study on the Ultimate Capacity of Deck Joints in Prefabricated Concrete Bulb-Tee Bridge Girders." Bridge Structures Assessment Design and Construction, 55(71).

Kim, S., and Nowak, A. S. (1997). "Load distribution and impact factors for I-girder bridges." Journal of Bridge Engineering, 2(3), 97-104.

Kocsis, P. (2004). "Evaluation of AASHTO live load and line load distribution factors for I-girder bridge decks." Practice Periodical on Structural Design and Construction, 9(4), 211.

Laman, J. A., Pechar, J. S., and Boothby, T. E. (1999). "Dynamic Load Allowance for Through-Truss Bridges." Journal of bridge engineering, 4(4), 231-241.

Lightfoot, E., and Sawko, F. (1959). "Structural Frame Analysis by Electronic Computer: Grid Frameworks Resolved by Generalised Slope-Deflection." Engineering, 187, 18-20.

Lin, C.-S., and VanHorn, D. A. (1968). "The Effect of Midpan Diaphragms on Load Distribution in a Prestressed Concrete Box-beam Bridge, Philadelphia Bridge." Fritz Engineering Laboratory, Department of Civil Engineering, Lehigh University, Bethlehem, Pennsylvania.

Lowe, S. (1999). "Collapse behavoir of reinforced concrete beam and slab bridges." MPhil. Thesis, University of Cambridge.

Mabsout, M. E., Tarhini, K. M., Frederick, G. R., and Kesserwan, A. (1998). "Effect of continuity on wheel load distribution in steel girder bridges." Journal of Bridge Engineering, 3(3), 103-110.

Mabsout, M. E., Tarhini, K. M., Frederick, G. R., and Tayar, C. (1997). "Finite-element analysis of steel girder highway bridges." Journal of Bridge Engineering, 2(3), 83.

Mander, T. J., Henley, M. D., Scott, R. M., Head, M. H., Mander, J. B., and Trejo, D. (2010a). "Experimental Performance of Full-Depth Precast, Prestressed Concrete Overhang, Bridge Deck Panels." Journal of Bridge Engineering, 15(5), 503-510.

Mander, T. J., Mander, J. B., and Head, M. H. (2010b). "Compound Shear-Flexural Capacity of Reinforced Concrete–Topped Precast Prestressed Bridge Decks." Journal of Bridge Engineering, 16(1), 4-11.

Mander, T. J., Mander, J. B., and Hite Head, M. (2010c). "Modified yield line theory for full-depth precast concrete bridge deck overhang panels." Journal of Bridge Engineering, 16(1), 12-20.

Marx, H. J., Khachaturnian, N., and Gamble, W. L. (1986). "Development of design criteria for simply supported skew slab-and-girder bridges." University of Illinois Engineering Experiment Station. College of Engineering. University of Illinois at Urbana-Champaign.

Middleton, C. (1997). "Concrete bridge assessment: an alternative approach." Structural engineer, 75(23/24).

Middleton, C. (2008). "Generalised collapse analysis of concrete bridges." Magazine of Concrete Research, 60(8), 575-585.

Motarjemi, D., and VanHorn, D. A. (1969). "Theoretical analysis of load distribution in prestressed concrete box-beam bridges." Fritz Engineering Laboratory, Department of Civil Engineering, Lehigh University, Bethlehem, Pennsylvania.

Newmark, N. M. (1938). "A distribution procedure for the analysis of slabs continuous over flexible beams."

Newmark, N. M. (1943). "Design of Slab and Stringer Highway Bridges." Public Roads, 23(7), 157-166.

Newmark, N. M. (1946). Studies of Slab and Beam Highway Bridges: Tests of simple-span right I-beam bridges, by NM Newmark, CP Siess, and RR Penman, University of Illinois.

Newmark, N. M. (1949). "Highway Bridge Floors: A Symposium: Design of I-Beam Bridges." Transactions of the American Society of Civil Engineers, 114(1), 997-1022.

Newmark, N. M., and Siess, C. P. (1942). "Moments in I-beam Bridges", University of Illinois.

Newmark, N. M., Siess, C. P., and Peckham, W. M. (1948). "Studies of slab and beam highway bridges: part II, tests of simple-span skew I-beam bridges."

Nowak, A. S. (1993). "Live Load Model for Highway Bridges." Journal of Structural Safety, 13(1-2), 53-66.

Nowak, A. S., and Hong, Y.-K. (1991). "Bridge live-load models." Journal of Structural Engineering, 117(9), 2757-2767.

Nutt, R. V., Schamber, R. A. , and Zokaie, T. (1988). "Distribution of wheel loads on highway bridges." Imbsen and Associates, Sacramento, California.

O'Connor, C., and pritchard, R. (1985). "Impact Studies on Small Composite Girder Bridge." Journal of structural engineering, 111(3), 641-653.

Park, R., and Gamble, W. L. (2000). Reinforced concrete slabs, John Wiley & Sons.

Parke, G., and Hewson, N. (2008). ICE Manual of Bridge Engineering, Thomas Telford, London.

Paultre, P., Proulx, J., and Talbot, M. (1995). "Dynamic Testing Procedures for Highway Bridges Using Traffic Loads." Journal of structural engineering, 121(2), 362-376.

Phuvoravan, K., Chung, W. S., Liu, J., and Sotelino, E. D. (2004). "Simplified live load distribution factor equation for steel girder bridges." Design of Structures 2004, 1892(1892), 88-97.

Pirayeh Gar, S., Mander, J. B., Head, M., and Hurlebaus, S. (2014). "FRP Slab Capacity Using Yield Line Theory." Journal of Composites for Construction, 18(6).

Priestley, M. N. "Design of concrete bridges for temperature gradients." Proc., ACI Journal Proceedings, ACI.

Puckett, J. A., Mertz, D., Huo, X. S., C., J. M., Peavy, M. D., and Patrick, M. D. (2005). "Simplified Live Load Distribution Factor Equations for Bridge Design." Journal of the Transportation Research Board, 11(S), 67-78.

Razaqpur, A. G., and Nofal, M. (1990). "Analytical modeling of nonlinear behavior of composite bridges." Journal of Structural Engineering, 116(6), 1715-1733.

Reddy, J. N. (1993). An introduction to the finite element method, McGraw-Hill New York.

Ryall, M. J., Parke, G. A. R., and Harding, J. E. (2000). "ICE Manual of Bridge Engineering." E. Institution of Civil, ed., Thomas Telford, London.

Samaan, M. S. K. S. J. (2002). "Distribution of Wheel Loads on Continuous Steel Spread-Box Girder Bridges." Journal of Bridge Engineering, 7(3), 175.

Sanders, W. W., and Elleby, H. A. (1970). "Distribution of wheel loads on highway bridges." NCHRP Report(83).

Sawko, F., and Saha, G. (1967). "Ultimate load analysis of bridge decks." Building Science, 2(3), 223-237.

Schaffer, T., and VanHorn, D. A. (1967). Structural Response of a 45°degree Skew Prestressed Concrete Box-girder Highway Bridge Subjected to Vehicular Loading: Brookville Bridge, Fritz Engineering Laboratory, Department of Civil Engineering, Lehigh University.

Schwarz, M., and Laman, J. A. (2001). "Response of prestressed concrete I-girder bridges to live load." Journal of Bridge Engineering, 6(1), 1-8.

Shahawy, M., and Huang, D. (2001). "Analytical and field investigation of lateral load distribution in concrete slab-on-girder bridges." ACI Structural Journal, 98(4).

Siess, C., and Viest, I. (1953). "Studies of slab and beam highway bridges: part V. tests of continuous right I-beam bridges." Bulletin(416).

Sotelino, E., Liu, J., Chung, W., and Phuvoravan, K. (2004). "Simplified Load Distribution Factor for Use in LRFD Design." Joint Transportation Research Program, Indiana Department of Transportation and Purdue University, West Lafayette, IN, 1-148.

Sotelino, E., Liu, J., Chung, W., and Phuvoravan, K. (2004). "Simplified Load Distribution Factor for Use in LRFD Design." Joint Transportation Research Program, 191.

Suksawang, N., Nassif, H., and Su, D. (2013). "Verification of shear live-load distribution factor equations for I-girder bridges." KSCE J Civ Eng, 17(3), 550-555.

Surana, C. S., and Agrawal, R. (1998). Grillage Analogy in Bridge Deck Analysis, Narosa Publishing House, London, UK.

Tanbsh, S., and Tabatabai, M. (2001). "Live Load Distribution in Girder Bridges Subject to Oversize Trucks." ASCE Journal of Bridge Engineering, 6((1)), 9-16.

Tarhini, K. M., and Frederick, G. R. (1992). "Wheel load distribution in I-girder highway bridges." Journal of Structural Engineering, 118(5), 1285-1294.

TxDOT (2012). "Bridge Division Standards." Texas Department of Transportation. <http://www.txdot.gov/insdtdot/orgchart/cmd/cserve/standard/bridge-e.htm>. (September 10, 2012).

VanHorn, D., and Chen, C. (1971). "Structural Behvior of a Prestressed Concrete I-beam Bridge, Lehighton Bridge." Fritz Engineering Laboratory Report.

VanHorn, D. A. (1969). "Structural behavior characteristics of prestressed concrete box-beam bridges." Lehigh University, Office of Research, Bethlehem, Pennsylvania, 92 Pages.

Wegmuller, A. W., and Kostem, C. N. (1973). "Finite element analysis of plates and eccentrically stiffened plates."

Westergaard, H. (1930). "Computation of stresses in bridge slabs due to wheel loads." Public Roads, 11(1), 1-23.

White, A., and Purnell, W. B. (1957). "Lateral Load Distribution on I-beam Bridge." Journal of the Structural Division, 83.

Zokaie, T. (2000). "AASHTO-LRFD Live Load Distribution Specifications." ASCE Journal of Bridge Engineering, 5(2), 131-138.

Zokaie, T., Imbsen, R. A., and Osterkamp, T. A. (1991). "Distribution of Wheel Loads on Highway Bridges." NHCRP Project Report 12-26, Transportation Research Board, Washington, D.C.

APPENDIX A1

MOMENTS AND SHEAR FORCES TABLES FOR THE CONSIDERED SIMPLY SUPPORTED BRIDGE GEOMETRIES

This appendix presents the moment and shear force values determined by proposed design models, available AASHTO LRFD empirical formulas and FEM analysis for simply supported bridge configurations. This appendix supports material in Section 6.

A1.1 INTRODUCTION

New design models are proposed in Section 6 to determine the moment and shear demands in the preliminary design stage for slab on prestressed concrete girder bridges. A total of 61 simply supported bridge configurations were selected and analyzed using the finite element method (FEM) approach to provide "exact" moment and shear force solutions. For each bridge configuration, the design moment and shear demands were also calculated based on the proposed design models plus the available AASHTO LRFD empirical formulas. The comparison between the design values and computational solutions are made to verify the applicability of the proposed design models. The moment and shear force values for different types of bridge superstructures determined by proposed design models, AASHTO LRFD empirical formulas and FEM analysis are listed in this Appendix: prestressed concrete I-girder bridge (Table A1.1-Table A1.3), prestressed concrete slab beam bridge (Table A1.4-Table A1.5) and prestressed concrete spread slab beam bridge (Table A1.6-Table A1.8).

Table A1.1. Critical Moment and Shear Values for Simply Supported I-girder Bridge Cases.

No.	One Lane Loaded				Multiple Lanes Loaded			
	Exterior Beam		Interior Beam		Exterior Beam		Interior Beam	
	M (kN-m)	*V* (kN)	*M* (kN-m)	*V* (kN)	*M* (kN-m)	*V* (kN)	*M* (kN-m)	*V* (kN)
1	1349	294	1006	300	1249	246	1291	309
2	2011	328	1502	302	2064	283	2045	329
3	2474	354	1891	320	2652	306	2618	354
4	1464	315	1142	336	1405	268	1542	374
5	2218	361	1624	338	2325	315	2366	406
6	2727	388	2004	357	2972	342	2969	431
7	1577	341	1277	371	1550	293	1763	432
8	2398	379	1768	372	2576	343	2618	452
9	2469	381	1837	383	2592	339	2683	462
10	2518	383	1898	393	2599	337	2740	470
11	3003	407	2182	394	3315	375	3281	480
12	3078	409	2247	404	3337	371	3346	489
13	3467	433	2534	388	4004	404	3899	486
14	1476	326	1186	349	1463	278	1611	392
15	2312	365	1715	361	2449	322	2464	420
16	2884	392	2103	381	3148	351	3076	446
17	1411	315	1129	335	1399	268	1521	373
18	2077	359	1532	326	2289	318	2241	395
19	2146	362	1589	336	2314	316	2301	403
20	2194	363	1638	344	2329	314	2350	410
21	2572	387	1897	346	2915	347	2797	420
22	2642	388	1943	355	2946	343	2857	427
23	3102	405	2316	354	3586	371	3394	434

Table A1.2. Comparison of FEM and Design Values for Simply Supported I-girder Bridges.

No.	FEM Analysis		Design Values (Proposed Model)		Model/FEM	
	M (kN-m)	V (kN)	M (kN-m)	V (kN)	M	V
1	1349	309	1277	313	0.95	1.01
2	2064	329	2126	352	1.03	1.07
3	2652	354	2751	376	1.04	1.06
4	1542	374	1532	375	0.99	1.00
5	2366	406	2550	423	1.08	1.04
6	2972	431	3301	451	1.11	1.05
7	1763	432	1788	438	1.01	1.01
8	2618	452	2976	493	1.14	1.09
9	2683	462	2976	493	1.11	1.07
10	2740	470	2976	493	1.09	1.05
11	3315	480	3852	526	1.16	1.10
12	3346	489	3852	526	1.15	1.08
13	4004	486	4796	557	1.20	1.15
14	1611	392	1628	399	1.01	1.02
15	2464	420	2710	449	1.10	1.07
16	3148	446	3508	479	1.11	1.07
17	1521	373	1532	375	1.01	1.01
18	2289	395	2550	423	1.11	1.07
19	2314	403	2550	423	1.10	1.05
20	2350	410	2550	423	1.09	1.03
21	2915	420	3301	451	1.13	1.07
22	2946	427	3301	451	1.12	1.05
23	3586	434	4111	477	1.15	1.10
Median (50^{th} Percentile)					1.10	1.06
Lognormal Standard Deviation, β_D					0.061	0.034

Table A1.3. Comparison of FEM and AASHTO Design Values for Simply Supported I-girder Bridges.

No.	FEM Analysis		Design Values (AASHTO)		AASHTO/FEM	
	M (kN-m)	*V* (kN)	*M* (kN-m)	*V* (kN)	*M*	*V*
1	1349	309	1472	337	1.09	1.09
2	2064	329	2291	380	1.11	1.16
3	2652	354	2896	405	1.09	1.14
4	1542	374	1676	382	1.09	1.02
5	2366	406	2606	430	1.10	1.06
6	2972	431	3292	459	1.11	1.06
7	1763	432	1875	425	1.06	0.98
8	2618	452	2824	479	1.08	1.06
9	2683	462	2910	479	1.08	1.04
10	2740	470	2986	479	1.09	1.02
11	3315	480	3585	511	1.08	1.06
12	3346	489	3674	511	1.10	1.05
13	4004	486	4387	541	1.10	1.11
14	1611	392	1753	398	1.09	1.01
15	2464	420	2721	449	1.10	1.07
16	3148	446	3436	479	1.09	1.07
17	1521	373	1676	382	1.10	1.02
18	2289	395	2530	430	1.11	1.09
19	2314	403	2606	430	1.13	1.07
20	2350	410	2671	430	1.14	1.05
21	2915	420	3208	459	1.10	1.09
22	2946	427	3292	459	1.12	1.07
23	3586	434	3931	486	1.10	1.12
Median (50th Percentile)					1.10	1.06
Lognormal Standard Deviation, β_D					0.016	0.041

Table A1.4. Critical Moment and Shears for Simply Supported Slab Beam Bridges.

No.	One Lane Loaded				Two Lanes Loaded			
	Exterior Beam		Interior Beam		Exterior Beam		Interior Beam	
	M (kN-m)	*V* (kN)	*M* (kN-m)	*V* (kN)	*M* (kN-m)	*V* (kN)	*M* (kN-m)	*V* (kN)
1	210	141	186	145	229	129	241	161
2	248	152	222	149	287	141	298	173
3	285	165	259	151	348	155	357	185
4	323	176	296	154	416	168	418	194
5	363	185	340	157	492	178	495	202
6	415	193	392	160	578	188	580	210
7	165	115	149	95	175	107	172	120
8	193	124	175	100	214	116	209	125
9	218	133	199	105	256	126	245	133
10	244	140	222	109	300	135	290	138
11	271	146	247	113	348	143	336	144
12	304	151	275	116	404	150	386	148

Table A1.5. Comparison of FEM and Design Values (Slab Beam Bridges).

No.	FEM Analysis		Design Model		Model/FEM	
	M (kN-m)	V (kN)	M (kN-m)	V (kN)	M	V
1	580	210	609	219	1.05	1.05
2	495	202	515	211	1.04	1.04
3	418	194	433	201	1.04	1.04
4	357	185	365	190	1.02	1.03
5	298	173	301	177	1.01	1.02
6	241	161	239	159	0.99	0.99
7	404	151	465	168	1.15	1.11
8	348	146	393	161	1.13	1.11
9	300	140	331	154	1.1	1.1
10	256	133	279	145	1.09	1.1
11	214	125	230	135	1.07	1.08
12	175	120	183	121	1.04	1.02
Median (50^{th} Percentile)					1.06	1.05
Lognormal Standard Deviation, β_D					0.051	0.040

Table A1.6. Critical Moment and Shear Values for Simply Supported Spread Slab Beam Bridges.

No.	One Lane Loaded				Multiple Lanes Loaded			
	Exterior Beam		Interior Beam		Exterior Beam		Interior Beam	
	M (kN-m)	*V* (kN)	*M* (kN-m)	*V* (kN)	*M* (kN-m)	*V* (kN)	*M* (kN-m)	*V* (kN)
1	308	180	279	243	344	157	377	243
2	353	197	324	254	420	173	453	254
3	397	211	371	261	502	185	531	261
4	446	223	430	267	592	197	632	267
5	508	234	496	271	696	208	743	278
6	353	196	327	280	378	167	435	280
7	400	214	370	292	456	184	510	294
8	446	230	416	301	538	198	588	307
9	494	242	472	307	629	212	682	318
10	555	254	538	312	731	224	793	327
11	396	209	374	296	416	179	508	331
12	450	228	416	309	500	197	583	350
13	500	244	460	318	588	213	660	364
14	552	258	511	326	683	227	752	375
15	439	222	409	296	453	193	575	366
16	503	242	453	308	548	213	652	385
17	560	259	498	317	645	230	755	400
18	617	273	548	323	747	246	879	412
19	381	205	359	294	403	174	481	319
20	433	224	397	306	481	192	549	338
21	479	239	438	315	563	208	622	351
22	525	253	483	322	645	222	721	362
23	415	215	385	289	431	185	536	348
24	473	234	426	301	519	204	607	367
25	525	251	468	309	609	220	686	382
26	576	265	512	316	700	235	788	393

Table A1.7. Comparison of FEM and Design Values for Simply Supported Spread Slab Beam Bridges.

No.	FEM Analysis		Design Values (Proposed Model)		Model/FEM	
	M (kN-m)	*V* (kN)	*M* (kN-m)	*V* (kN)	*M*	*V*
1	377	243	400	235	1.06	0.97
2	453	254	487	254	1.08	1.00
3	531	261	576	269	1.08	1.03
4	632	267	694	281	1.10	1.05
5	743	278	819	292	1.10	1.05
6	435	280	477	280	1.09	1.00
7	510	294	579	302	1.14	1.03
8	588	307	686	319	1.16	1.04
9	682	318	827	334	1.21	1.05
10	793	327	975	348	1.23	1.07
11	508	331	553	325	1.09	0.98
12	583	350	672	350	1.15	1.00
13	660	364	796	371	1.20	1.02
14	752	375	960	388	1.28	1.03
15	575	366	629	370	1.09	1.01
16	652	385	765	399	1.17	1.03
17	755	400	904	422	1.20	1.05
18	879	412	1091	442	1.24	1.07
19	481	319	529	311	1.10	0.97
20	549	338	643	335	1.17	0.99
21	622	351	761	355	1.22	1.01
22	721	362	918	371	1.27	1.03
23	536	348	587	345	1.10	0.99
24	607	367	713	371	1.17	1.01
25	686	382	843	393	1.23	1.03
26	788	393	1017	412	1.29	1.05
Median (50th Percentile)					1.16	1.02
Lognormal Standard Deviation, β_D					0.068	0.028

Table A1.8. Comparison of FEM and AASHTO Design Values for Simply Supported Spread Slab Beam Bridges.

No.	FEM Analysis		Design Values (AASHTO)		AASHTO/FEM	
	M (kN-m)	V (kN)	M (kN-m)	V (kN)	M	V
1	377	243	409	234	1.09	0.96
2	453	254	479	248	1.06	0.98
3	531	261	549	259	1.03	0.99
4	632	267	643	269	1.02	1.01
5	743	278	738	276	0.99	1.00
6	435	280	465	269	1.07	0.96
7	510	294	544	286	1.07	0.97
8	588	307	622	298	1.06	0.97
9	682	318	729	309	1.07	0.97
10	793	327	837	318	1.06	0.97
11	508	331	518	303	1.02	0.91
12	583	350	606	322	1.04	0.92
13	660	364	693	336	1.05	0.92
14	752	375	812	347	1.08	0.93
15	575	366	569	336	0.99	0.92
16	652	385	664	356	1.02	0.93
17	755	400	761	372	1.01	0.93
18	879	412	892	386	1.01	0.94
19	481	319	502	292	1.04	0.92
20	549	338	587	310	1.07	0.92
21	622	351	671	324	1.08	0.92
22	721	362	786	335	1.09	0.93
23	536	348	541	318	1.01	0.91
24	607	367	632	337	1.04	0.92
25	686	382	723	352	1.06	0.92
26	788	393	847	364	1.07	0.93
Median (50th Percentile)					1.05	0.94
Lognormal Standard Deviation, β_D					0.029	0.029

APPENDIX A2

MOMENTS AND SHEAR FORCES TABLES FOR THE CONSIDERED CONTINUOUS BRIDGES

This appendix presents the moment and shear force values determined by proposed design models, available AASHTO LRFD empirical formulas and FEM analysis for continuous bridge configurations. This appendix supports material in Section 7.

A2.1 INTRODUCTION

New design models are proposed in Section 6 to determine the moment and shear demands in the preliminary design stage for slab on prestressed concrete girder bridges. A total of 38 continuous bridge FEM models were developed and analyzed, with each bridge model having a different superstructure geometry, to determine the "exact" moment and shear force values which would be further utilized to evaluate the applicability of the proposed design models for continuous bridges. The moment and shear force values for different types of bridge superstructures determined by proposed design models, available AASHTO LRFD empirical formulas and FEM analysis are listed in this Appendix: prestressed concrete I-girder bridge (Table A2.1-Table A2.6), prestressed concrete slab beam bridge (Table A2.7-Table A2.10) and prestressed concrete spread slab beam bridge (Table A2.11-Table A2.16).

Table A2.1. Critical Moment and Shear Values for Continuous I-girder Bridge Cases (One Lane Loaded).

No.	Exterior Beam					Interior Beam				
	Moment (kN-m)			Shear (kN)		Moment (kN-m)			Shear (kN)	
	$+M$ (Side Span)	$-M$ (Support)	$+M$ (Mid Span)	End Support	Interior Pier	$+M$ (Side Span)	$-M$ (Support)	$+M$ (Mid Span)	End Support	Interior Pier
1	3054	-4002	3246	422	526	2296	-2838	2466	388	464
2	3172	-4083	3371	426	528	2375	-2937	2541	400	473
3	3858	-5087	3941	464	572	2970	-3560	3074	407	488
4	4015	-5208	4097	468	576	3056	-3642	3156	420	497
5	2865	-3758	3047	407	500	2134	-2654	2290	367	439
6	2976	-3836	3168	410	503	2215	-2752	2362	380	447
7	3600	-4761	3675	447	543	2775	-3311	2871	383	460
8	3754	-4882	3831	451	547	2846	-3403	2944	396	469
9	2742	-3596	2921	396	482	2054	-2553	2227	355	423
10	2846	-3670	3036	399	485	2130	-2648	2286	367	432
11	3442	-4549	3515	436	523	2680	-3199	2766	369	444
12	3591	-4667	3667	440	527	2759	-3273	2847	382	453
13	3798	-5374	4055	455	556	3013	-3833	3275	375	460
14	3969	-5475	4239	459	560	3105	-3885	3375	389	470

Table A2.2. Critical Moment and Shear Values for Continuous I-girder Bridge Cases (Multiple Lanes Loaded).

No.	Exterior Beam					Interior Beam				
	Moment (kN-m)			Shear (kN)		Moment (kN-m)			Shear (kN)	
	$+M$ (Side Span)	$-M$ (Support)	$+M$ (Mid Span)	End Support	Interior Pier	$+M$ (Side Span)	$-M$ (Support)	$+M$ (Mid Span)	End Support	Interior Pier
1	3533	-4363	3878	389	512	3509	-4233	3816	483	576
2	3594	-4370	3951	386	510	3595	-4322	3901	493	582
3	4747	-5811	4937	443	572	4652	-5430	4838	513	614
4	4841	-5831	5041	439	570	4752	-5533	4937	525	622
5	3305	-4094	3620	370	481	3215	-3896	3551	448	536
6	3370	-4121	3699	367	478	3292	-3984	3597	458	543
7	4394	-5438	4563	423	537	4380	-5028	4591	474	571
8	4498	-5468	4676	418	535	4434	-5075	4649	486	578
9	3162	-3917	3466	358	459	3046	-3707	3322	431	519
10	3226	-3948	3544	354	457	3136	-3795	3384	441	526
11	4187	-5189	4347	410	513	4066	-4725	4247	455	552
12	4294	-5222	4463	405	510	4133	-4823	4319	467	559
13	4731	-6291	5175	436	559	4657	-5785	5157	465	579
14	4861	-6307	5326	431	556	4735	-5816	5243	478	586

Table A2.3. Comparison of FEM and Proposed Design Moment Values for Continuous Prestressed Concrete I-girder Bridge Cases.

No.	FEM Analysis (kN-m)			Design Model (kN-m)			Model/FEM		
	$+M$ (Side Span)	$-M$ (Support)	$+M$ (Mid Span)	$+M$ (Side Span)	$-M$ (Support)	$+M$ (Mid Span)	$+M$ (Side Span)	$-M$ (Support)	$+M$ (Mid Span)
1	3533	-4363	3878	4235	-5028	4714	1.20	1.15	1.22
2	3595	-4370	3951	4235	-5028	4714	1.18	1.15	1.19
3	4747	-5811	4937	5905	-6800	6188	1.24	1.17	1.25
4	4841	-5831	5041	5905	-6800	6188	1.22	1.17	1.23
5	3305	-4094	3620	3857	-4579	4293	1.17	1.12	1.19
6	3370	-4121	3699	3857	-4579	4293	1.14	1.11	1.16
7	4394	-5438	4591	5378	-6193	5636	1.22	1.14	1.23
8	4498	-5468	4676	5378	-6193	5636	1.20	1.13	1.21
9	3162	-3917	3466	3630	-4310	4040	1.15	1.10	1.17
10	3226	-3948	3544	3630	-4310	4040	1.13	1.09	1.14
11	4187	-5189	4347	5062	-5829	5305	1.21	1.12	1.22
12	4294	-5222	4463	5062	-5829	5305	1.18	1.12	1.19
13	4731	-6291	5175	5887	-7395	6579	1.24	1.18	1.27
14	4861	-6307	5326	5887	-7395	6579	1.21	1.17	1.24
	Median (50^{th} Percentile)						1.19	1.14	1.21
	Lognormal Standard Deviation, β_D						0.0355	0.0269	0.0353

Table A2.4. Comparison of FEM and Proposed Design Shear Values for Continuous Prestressed Concrete I-girder Bridge Cases.

No.	FEM Analysis (kN)		Design Model (kN)		Model/FEM	
	V End Support	V Interior Pier	V End Support	V Interior Pier	V End Support	V Interior Pier
1	483	576	524	660	1.08	1.15
2	493	582	524	660	1.06	1.13
3	513	614	579	725	1.13	1.18
4	525	622	579	725	1.10	1.17
5	448	536	477	600	1.06	1.12
6	458	543	477	600	1.04	1.11
7	474	571	528	660	1.11	1.16
8	486	578	528	660	1.09	1.14
9	431	519	449	565	1.04	1.09
10	441	526	449	565	1.02	1.08
11	455	552	496	621	1.09	1.13
12	467	559	496	621	1.06	1.11
13	465	579	520	670	1.12	1.16
14	478	586	520	670	1.09	1.14
	Median (50^{th} Percentile)				1.08	1.13
	Lognormal Standard Deviation, β_D				0.0312	0.0284

Table A2.5. Comparison of FEM and AASHTO Design Moment Values for Continuous Prestressed Concrete I-girder Bridge Cases.

No.	FEM Analysis (kN-m)			Design Model (kN-m)			Model/FEM		
	$+M$ (Side Span)	$-M$ (Support)	$+M$ (Mid Span)	$+M$ (Side Span)	$-M$ (Support)	$+M$ (Mid Span)	$+M$ (Side Span)	$-M$ (Support)	$+M$ (Mid Span)
1	3533	-4363	3878	3800	4331	3921	1.08	0.99	1.01
2	3595	-4370	3951	3746	4267	3861	1.04	0.98	0.98
3	4747	-5811	4937	4981	5543	4901	1.05	0.95	0.99
4	4841	-5831	5041	4905	5456	4822	1.01	0.94	0.96
5	3305	-4094	3620	3555	4053	3667	1.08	0.99	1.01
6	3370	-4121	3699	3501	3989	3606	1.04	0.97	0.97
7	4394	-5438	4591	4662	5193	4591	1.06	0.96	1.00
8	4498	-5468	4676	4586	5106	4511	1.02	0.93	0.96
9	3162	-3917	3466	3408	3885	3515	1.08	0.99	1.01
10	3226	-3948	3544	3354	3821	3455	1.04	0.97	0.97
11	4187	-5189	4347	4464	4984	4400	1.07	0.96	1.01
12	4294	-5222	4463	4389	4896	4321	1.02	0.94	0.97
13	4731	-6291	5175	5060	6134	5457	1.07	0.97	1.05
14	4861	-6307	5326	4971	6023	5358	1.02	0.95	1.01
	Median (50^{th} Percentile)						1.05	0.96	0.99
	Lognormal Standard Deviation, β_D						0.0222	0.0194	0.0256

Table A2.6. Comparison of FEM and AASHTO Design Shear Values for Continuous Prestressed Concrete I-girder Bridge Cases.

No.	FEM Analysis (kN)		Design Model (kN)		Model/FEM	
	V End Support	V Interior Pier	V End Support	V Interior Pier	V End Support	V Interior Pier
1	483	576	508	641	1.05	1.11
2	493	582	508	641	1.03	1.10
3	513	614	563	704	1.10	1.15
4	525	622	563	704	1.07	1.13
5	448	536	476	600	1.06	1.12
6	458	543	476	600	1.04	1.11
7	474	571	527	659	1.11	1.15
8	486	578	527	659	1.08	1.14
9	431	519	456	575	1.06	1.11
10	441	526	456	575	1.03	1.09
11	455	552	505	632	1.11	1.14
12	467	559	505	632	1.08	1.13
13	465	579	529	681	1.14	1.18
14	478	586	529	681	1.11	1.16
	Median (50^{th} Percentile)				1.08	1.13
	Lognormal Standard Deviation, β_D				0.0316	0.0242

Table A2.7. Critical Moment and Shear Values for Continuous Slab Beam Bridge Cases (One Lane Loaded).

No.	Exterior Beam					Interior Beam				
	Moment (kN-m)			Shear (kN)		Moment (kN-m)			Shear (kN)	
	$+M$ (Side Span)	$-M$ (Support)	$+M$ (Mid Span)	End Support	Interior Pier	$+M$ (Side Span)	$-M$ (Support)	$+M$ (Mid Span)	End Support	Interior Pier
1	304	-423	336	144	197	265	-327	298	124	165
2	343	-460	371	149	202	312	-381	340	129	173
3	385	-499	407	155	208	346	-393	369	131	174
4	228	-328	248	110	155	209	-283	228	92	133
5	253	-355	271	114	160	233	-307	251	94	136
6	281	-382	295	118	164	260	-331	274	97	139

Table A2.8. Critical Moment and Shear Values for Continuous Slab Beam Bridge Cases (Two Lanes Loaded).

No.	Exterior Beam					Interior Beam				
	Moment (kN-m)			Shear (kN)		Moment (kN-m)			Shear (kN)	
	$+M$ (Side Span)	$-M$ (Support)	$+M$ (Mid Span)	End Support	Interior Pier	$+M$ (Side Span)	$-M$ (Support)	$+M$ (Mid Span)	End Support	Interior Pier
1	398	-473	452	156	200	400	-475	455	158	216
2	463	-524	510	165	207	467	-529	513	166	222
3	531	-585	569	173	214	536	-583	573	173	228
4	285	-356	320	117	150	268	-332	305	115	155
5	327	-393	358	123	155	311	-366	342	119	160
6	372	-434	397	129	160	355	-401	381	123	163

Table A2.9. Comparison of FEM and Design Moment Values for Continuous Slab Beam Bridge Cases.

No.	FEM Analysis (kN-m.)			Design Model (kN-m.)			Model/FEM		
	$+M$ (Side Span)	$-M$ (Support)	$+M$ (Mid Span)	$+M$ (Side Span)	$-M$ (Support)	$+M$ (Mid Span)	$+M$ (Side Span)	$-M$ (Support)	$+M$ (Mid Span)
1	400	-475	455	414	-488	474	1.04	1.03	1.04
2	467	-529	513	487	-547	537	1.04	1.03	1.05
3	536	-585	573	562	-605	601	1.05	1.04	1.05
4	285	-356	320	316	-373	362	1.11	1.05	1.13
5	327	-393	358	372	-418	410	1.14	1.07	1.14
6	372	-434	397	430	-463	460	1.16	1.07	1.16
	Median (50th Percentile)						1.08	1.04	1.09
	Lognormal Standard Deviation, β_D						0.0480	0.0152	0.0495

Table A2.10. Comparison of FEM and Design Shear Values for Continuous Slab Beam Bridge Cases.

No.	FEM Analysis (kN)		Design Model (kN)		Model/FEM	
	V End Support	V Interior Pier	V End Support	V Interior Pier	V End Support	V Interior Pier
1	158	216	183	232	1.16	1.07
2	166	222	193	239	1.16	1.08
3	173	228	201	247	1.16	1.08
4	117	155	140	177	1.20	1.14
5	123	160	147	183	1.20	1.15
6	129	164	154	189	1.20	1.15
	Median (50th Percentile)				1.18	1.11
	Lognormal Standard Deviation, β_D				0.0184	0.0347

Table A2.11. Critical Moment and Shear Values for Continuous Spread Slab Beam Bridge Cases (One Lane Loaded).

No.	Exterior Beam					Interior Beam				
	Moment (kN-m)			Shear (kN)		Moment (kN-m)			Shear (kN)	
	$+M$ (Side Span)	$-M$ (Support)	$+M$ (Mid Span)	End Support	Interior Pier	$+M$ (Side Span)	$-M$ (Support)	$+M$ (Mid Span)	End Support	Interior Pier
1	373	-519	410	190	234	356	-444	399	215	242
2	419	-566	452	200	242	408	-485	444	221	250
3	470	-613	496	209	248	461	-527	490	225	256
4	411	-579	444	207	252	389	-491	432	247	279
5	457	-629	487	218	260	441	-530	478	254	286
6	507	-680	531	227	267	495	-572	525	260	293
7	455	-635	487	225	275	424	-540	461	268	305
8	503	-691	532	236	283	473	-579	507	276	313
9	555	-746	576	246	291	527	-620	555	282	319
10	505	-694	535	243	301	471	-604	499	289	338
11	558	-755	582	255	310	515	-643	546	298	346
12	613	-815	629	266	318	569	-683	594	305	352
13	433	-611	460	216	260	399	-519	430	262	297
14	475	-664	499	227	268	441	-554	469	269	304
15	521	-716	538	237	275	487	-590	509	275	310
16	472	-656	499	231	279	439	-571	464	281	327
17	519	-713	540	242	288	479	-606	504	289	334
18	568	-769	581	253	295	525	-643	545	296	340

Table A2.12. Critical Moment and Shear Values for Continuous Spread Slab Beam Bridge Cases (Multiple Lanes Loaded).

No.	Exterior Beam					Interior Beam				
	Moment (kN-m)			Shear (kN)		Moment (kN-m)			Shear (kN)	
	$+M$ (Side Span)	$-M$ (Support)	$+M$ (Mid Span)	End Support	Interior Pier	$+M$ (Side Span)	$-M$ (Support)	$+M$ (Mid Span)	End Support	Interior Pier
1	478	-569	542	179	235	507	-627	579	222	271
2	556	-631	613	189	244	593	-696	654	233	281
3	639	-707	685	199	252	682	-765	732	242	290
4	509	-625	571	189	252	555	-707	627	268	313
5	586	-691	641	201	262	642	-779	703	279	322
6	669	-770	713	212	271	733	-851	781	288	330
7	551	-687	614	206	276	613	-789	683	319	364
8	631	-760	686	219	286	701	-862	760	331	374
9	716	-841	759	230	297	792	-938	840	341	383
10	600	-750	664	224	299	675	-874	737	354	404
11	685	-830	739	237	310	762	-950	816	367	414
12	773	-917	814	250	322	854	-1027	897	379	423
13	519	-658	573	198	259	583	-748	656	303	346
14	589	-726	638	210	268	672	-814	735	314	355
15	666	-799	712	221	278	766	-891	816	323	363
16	561	-705	616	210	276	640	-822	710	336	384
17	636	-779	681	223	286	731	-891	792	348	394
18	714	-859	752	235	296	827	-976	876	359	403

Table A2.13. Comparison of FEM and Design Moment Values for Continuous Spread Slab Beam Bridge Cases.

No.	FEM Analysis (kN-m)			Design Model (kN-m)			Model/FEM		
	$+M$ (Side Span)	$-M$ (Support)	$+M$ (Mid Span)	$+M$ (Side Span)	$-M$ (Support)	$+M$ (Mid Span)	$+M$ (Side Span)	$-M$ (Support)	$+M$ (Mid Span)
1	507	-627	579	551	-650	631	1.09	1.04	1.09
2	593	-696	654	648	-729	715	1.09	1.05	1.09
3	682	-765	732	748	-806	800	1.10	1.05	1.09
4	555	-707	627	656	-773	751	1.18	1.09	1.20
5	642	-779	703	772	-867	851	1.20	1.11	1.21
6	733	-851	781	891	-959	953	1.22	1.13	1.22
7	613	-789	683	761	-897	871	1.24	1.14	1.28
8	701	-862	760	895	-1006	987	1.28	1.17	1.30
9	792	-938	840	1033	-1113	1105	1.31	1.19	1.32
10	675	-874	737	866	-1021	991	1.28	1.17	1.34
11	762	-950	816	1019	-1145	1123	1.34	1.21	1.38
12	854	-1027	897	1176	-1266	1258	1.38	1.23	1.40
13	583	-748	656	728	-858	834	1.25	1.15	1.27
14	672	-814	735	857	-963	944	1.27	1.18	1.28
15	766	-891	816	989	-1065	1058	1.29	1.19	1.30
16	640	-822	710	807	-951	924	1.26	1.16	1.30
17	731	-891	792	949	-1067	1046	1.30	1.20	1.32
18	827	-976	876	1096	-1180	1172	1.32	1.21	1.34
	Median (50th Percentile)						1.24	1.15	1.26
	Lognormal Standard Deviation, β_D						0.0820	0.0572	0.0917

Table A2.14. Comparison of FEM and Design Shear Values for Continuous Spread Slab Spread Beam Bridge Cases.

No.	FEM Analysis (kN)		Design Model (kN)		Model/FEM	
	V End Support	V Interior Pier	V End Support	V Interior Pier	V End Support	V Interior Pier
1	222	271	244	308	1.10	1.14
2	233	281	257	318	1.10	1.13
3	242	290	268	328	1.11	1.13
4	268	313	290	367	1.08	1.17
5	279	322	306	379	1.10	1.18
6	288	330	319	391	1.11	1.18
7	319	364	337	426	1.05	1.17
8	331	374	355	440	1.07	1.18
9	341	383	370	454	1.08	1.18
10	354	404	383	484	1.08	1.20
11	367	414	403	501	1.10	1.21
12	379	423	421	516	1.11	1.22
13	303	346	322	407	1.06	1.18
14	314	355	339	421	1.08	1.19
15	323	363	354	434	1.10	1.20
16	336	384	357	451	1.06	1.17
17	348	394	376	467	1.08	1.18
18	359	403	392	481	1.09	1.19
	Median (50th Percentile)				1.09	1.18
	Lognormal Standard Deviation, β_D				0.0165	0.0235

Table A2.15. Comparison of FEM and AASHTO Moment Values for Continuous Spread Slab Beam Bridge Cases.

No.	FEM Analysis (kN-m.)			Design Model (kN-m.)			AASHTO/FEM		
	$+M$ (Side Span)	$-M$ (Support)	$+M$ (Mid Span)	$+M$ (Side Span)	$-M$ (Support)	$+M$ (Mid Span)	$+M$ (Side Span)	$-M$ (Support)	$+M$ (Mid Span)
1	507	-627	579	510	-578	543	1.01	0.92	0.94
2	593	-696	654	584	-634	603	0.98	0.91	0.92
3	682	-765	732	658	-686	663	0.96	0.90	0.91
4	555	-707	627	578	-656	616	1.04	0.93	0.98
5	642	-779	703	663	-719	684	1.03	0.92	0.97
6	733	-851	781	747	-779	752	1.02	0.91	0.96
7	613	-789	683	644	-730	686	1.05	0.93	1.01
8	701	-862	760	738	-801	762	1.05	0.93	1.00
9	792	-938	840	832	-867	837	1.05	0.92	1.00
10	675	-874	737	707	-802	753	1.05	0.92	1.02
11	762	-950	816	810	-879	836	1.06	0.93	1.02
12	854	-1027	897	913	-952	920	1.07	0.93	1.02
13	583	-748	656	624	-707	664	1.07	0.95	1.01
14	672	-814	735	715	-776	738	1.06	0.95	1.00
15	766	-891	816	805	-840	811	1.05	0.94	0.99
16	640	-822	710	672	-762	716	1.05	0.93	1.01
17	731	-891	792	770	-836	795	1.05	0.94	1.00
18	827	-976	876	868	-905	874	1.05	0.93	1.00
	Median (50th Percentile)						1.04	0.93	0.99
	Lognormal Standard Deviation, β_D						0.0280	0.0127	0.0339

Table A2.16. Comparison of FEM and AASHTO Shear Values for Continuous Spread Slab Spread Beam Bridge Cases.

No.	FEM Analysis (kN)		Design Model (kN)		AASHTO/FEM	
	V End Support	V Interior Pier	V End Support	V Interior Pier	V End Support	V Interior Pier
1	222	271	233	286	1.05	1.05
2	233	281	242	293	1.04	1.04
3	242	290	251	300	1.03	1.03
4	268	313	268	329	1.00	1.05
5	279	322	279	337	1.00	1.05
6	288	330	288	345	1.00	1.04
7	319	364	301	370	0.94	1.02
8	331	374	314	380	0.95	1.02
9	341	383	325	388	0.95	1.01
10	354	404	334	411	0.94	1.02
11	367	414	348	421	0.95	1.02
12	379	423	360	431	0.95	1.02
13	303	346	291	357	0.96	1.03
14	314	355	303	367	0.96	1.03
15	323	363	314	375	0.97	1.03
16	336	384	316	388	0.94	1.01
17	348	394	329	398	0.94	1.01
18	359	403	340	407	0.95	1.01
	Median (50th Percentile)				0.97	1.03
	Lognormal Standard Deviation, β_D				0.0359	0.0149

APPENDIX A3

YIELD LINE THEORY ANALYSIS FOR SLAB TO BEAM FOLDED PLATE MECHANISM

This appendix presents the derivation of ultimate load capacity corresponding to slab to beam folded plate mechanism and its application in the plastic overstrength analysis of the Riverside Bridge. This appendix supports material in Section 8.

A3.1 SLAB TO BEAM FOLDED PLATE MECHANISM

In Section 8, yield line theory method was utilized to predict the overstrength capacity of slab-on-beam bridge decks at the ultimate collapse load. When the beams are relatively widely spaced and the deck slab is relatively weak and not capable of transferring the applied load from one beam to the neighboring beam, a yield line mechanism may occur within the connecting deck slab as the beams also reach their plastic capacity. This is referred to herein as slab to beam folded plate mechanism and its yield line pattern is shown in Figure 8.3(a). The lowest collapse load, P_u, for the beam-slab system is determined based on the principle of the virtual work as follows.

External Virtual Work: $$EWD = P_u \delta \tag{A3.1}$$

The internal work done in different segments shown in Figure 8.3 (a) is tabulated as below:

Segment	**Rotation Angles**		**Internal Work Done**	
	θ_x	θ_y	$(m_x)(\theta_x)(y)$	$(m_y)(\theta_y)(x)$
ABCD	$\frac{\delta}{L/2}$	-	$M_{x,b}\left(\frac{\delta}{L/2}\right)$	-
CDEF	$\frac{\delta}{L/2}$	-	$M_{x,b}\left(\frac{\delta}{L/2}\right)$	-
BCG	$\frac{\delta}{L/2}$	$\frac{\delta}{b_d}\left(1-\frac{2x}{L}\right)$	$\left(m_{x,d}+m'_{x,d}\right)\left(\frac{\delta}{L/2}\right)(b_d)$	$\left(m_{y,d}+m'_{y,d}\right)\frac{\delta}{b_d}\left(1-\frac{2x}{L}\right)\left(\frac{L}{2}-x\right)$
ECF	$\frac{\delta}{L/2}$	$\frac{\delta}{b_d}\left(1-\frac{2x}{L}\right)$	$\left(m_{x,d}+m'_{x,d}\right)\left(\frac{\delta}{L/2}\right)(b_d)$	$\left(m_{y,d}+m'_{y,d}\right)\frac{\delta}{b_d}\left(1-\frac{2x}{L}\right)\left(\frac{L}{2}-x\right)$
GCH	-	$\frac{\delta}{b_d}$	-	$\left(m_{y,d}+m'_{y,d}\right)\left(\frac{\delta}{b_d}\right)(2x)$

$$IWD = M_{x,b}\left(\frac{4\delta}{L}\right) + 4\left(m_{x,d} + m'_{x,d}\right)\left(\frac{b_d\delta}{L}\right) + \left(m_{y,d} + m'_{y,d}\right)\left(\frac{\delta}{b_d}\right)\left(L - 2x + \frac{4x^2}{L}\right) \quad \text{(A3.2)}$$

Equating external and internal work and solving for the collapse load gives:

$$P_u = 4\frac{M_{x,b}}{L} + 4\frac{\left(m_{x,d} + m'_{x,d}\right)}{L}b_d + \left(\frac{m_{y,d} + m'_{y,d}}{b_d}\right)\left(1 - 2\frac{x}{L} + \frac{4x^2}{L^2}\right)L \quad \text{(A3.3)}$$

where θ_x and θ_y = the plastic rotation angles in x and y directions, b_d = width of deck slab between two neighboring slab beams; δ = the plastic deflection value; $M_{x,b}$ = the positive moment capacity of the composite slab beam section in the longitudinal direction; $m_{x,d}$, $m'_{x,d}$, $m_{y,d}$ and $m'_{y,d}$ = the positive and negative moment capacities of unit deck slab in the longitudinal and transverse direction.

A3.2 APPLICATION OF SLAB TO BEAM FOLDED PLATE MECHANISM ON RIVERSIDE BRIDGE

An example of applying slab to beam folded plate mechanism to calculate the plastic overstrength factor of a realistic spread slab beam bridge, Riverside Bridge, is presented herein.

The external virtual work done by self weight, truck wheel load, lane load and impact load could be expressed as follows.

$$EWD = \Omega\left[w_{du}A_{du}\delta_d + w_{lu}A_{lu}\delta_l + P_{1u}\left(1 - \frac{b}{\alpha L}\right)\delta + P_{2u}\delta + P_{3u}\left(1 - \frac{b}{(1-\alpha)L}\right)\delta\right] \quad \text{(A3.4)}$$

The total failure surface is divided into several segments as shown in Figure 8.7(b). The internal virtual work done in different segments is tabulated in the

table below.

Segment	Rotation Angles		Internal Work Done	
	θ_x	θ_y	$(m_x)(\theta_x)(y)$	$(m_y)(\theta_y)(x)$
ABCD	$\frac{\delta}{\alpha L}$	-	$\left(M_{x,be}+2M_{x,bi}\right)\left(\frac{\delta}{\alpha L}\right)$	-
CDEF	$\frac{\delta}{(1-\alpha)L}$	-	$\left(M_{x,be}+2M_{x,bi}\right)\frac{\delta}{(1-\alpha)L}$	-
BCG	$\frac{\delta}{\alpha L}$	$\frac{\delta}{b_d}\left(1-\frac{x}{\alpha L}\right)$	$\left(m_{x,d}+m'_{x,d}\right)\left(\frac{\delta}{\alpha L}\right)(b_d)$	$\left(m_{y,d}+m'_{y,d}\right)\frac{\delta}{b_d}\left(1-\frac{x}{\alpha L}\right)(\alpha L-x)$
ECF	$\frac{\delta}{(1-\alpha)L}$		$\left(m_{x,d}+m'_{x,d}\right)\frac{\delta}{(1-\alpha)L}(b_d)$	$\left(m_{y,d}+m'_{y,d}\right)\frac{\delta}{b_d}\left(1-\frac{x}{(1-\alpha)L}\right)((1-\alpha)L-x)$
GCH	-	$\frac{\delta}{b_d}$		$\left(m_{y,d}+m'_{y,d}\right)\left(\frac{\delta}{b_d}\right)(2x)$

$$IWD=\left(M_{x,be}+2M_{x,bi}+m_{x,d}b_d+m'_{x,d}b_d\right)\left(\frac{\delta}{(1-\alpha)\alpha L}\right)+\left(m_{y,d}+m'_{y,d}\right)\left(\frac{\delta}{b_d}\right)\left[\frac{x^2}{(1-\alpha)\alpha L}-2x+L\right] \tag{A3.5}$$

$$\Omega=\phi\frac{\frac{M_{x,be}+2M_{x,bi}+m_{x,d}b_d+m'_{x,d}b_d}{(1-\alpha)\alpha L}+\left(\frac{m_{y,d}+m'_{y,d}}{b_d}\right)\left[\frac{x^2}{(1-\alpha)\alpha L}-2x+L\right]}{\frac{w_{du1}A_{du1}}{2}+\frac{w_{du2}A_{du2}}{3}+\frac{w_{lu}A_{lu}}{2}+P_{1u}\left(1-\frac{b}{\alpha L}\right)+P_{2u}+P_{3u}\left(1-\frac{b}{(1-\alpha)L}\right)} \tag{A3.6}$$

where w_{du1} and w_{du2} respectively represent the dead load applied on rectangular and triangular segments. There are two unknown parameters in the expression for plastic overstrength factor: one is the length of negative yield line, x, and the other is the position of vehicle wheel loads, α, as shown in Figure 8.7(b). By substituting the known parameters into the above equation and trying different values of x and α, with numerical methods, it is determined that the lowest overstrength factor for Riverside Bridge is 2.26 when $\alpha = 0.532$ and $x = 0.249\,L$.

APPENDIX A4

PRELIMINARY DESIGN FOR SPREAD SLAB BEAM BRIDGES

This appendix presents calculation details for the preliminary design of a new precast prestressed concrete panel, simply supported spread slab beam bridge and three-span continuous spread slab beam bridge. This appendix supports material in Section 8.

Note: All computations in this appendix are presented in US customary units. The following conversion factors may be used to convert to SI units.
1 in. = 25.4 mm *1 kip-ft = 1.3558 kN-m*
1 kip = 4.4482 kN *1 ksi = 6.895 MPa*

	DESIGN FOR PRECAST PRESTRESSED CONCRETE PANEL	1 / 1

Design Section

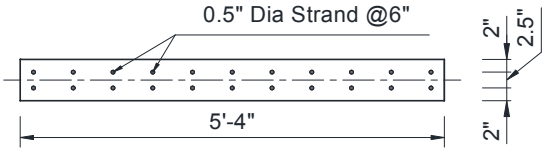

General Parameters Used

$f_c' = 6.0$ ksi $\quad f_{pu} = 270$ ksi $\quad A_{ps} = 0.153$ in^2

$A = 416$ in^2 $\quad S_x = 451$ in^3 $\quad w = 0.43$ kips/ft

Moment Demand

The panel segments are pre-tensioned to resist 1.2 times dead load to provide a safety factor of 20 percent for the additional flexural stresses due to transportation, erection and construction. The two lifting points during the transportation and erection process are considered to be 0.21 times of span length from both ends, which results in the same maximum positive and negative moment values.

$w_D = 1.2w = 0.52$ kips/ft

$M = 0.025 w_D L^2 = 0.025 \times 0.52 L^2 = 0.013 L^2$ kip-ft

Allowable Stress Analysis

The 0.5 in. diameter prestress strands are placed in a top and bottom pair with an even spacing of 6 in.

For a pair of strands: $T = 0.75 f_{pu} A_{ps} (1 - 20\%) \times 2 = 49.6$ kips/pair

Panel width is 5 ft-4 in., thus it allows 10 pairs of prestress strands.

Total force: $F = 10T = 10 \times 49.6 = 496$ kips

Stress Block:

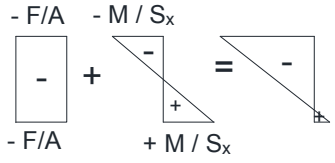

$$-\frac{F}{A} + \frac{M}{S_x} = -\frac{496}{416} + \frac{0.13L^2}{451} < 0.19\sqrt{f_c'} = 0.465$$

$L_{max} = 74.7$ ft

Bridge Layout and Cross Section

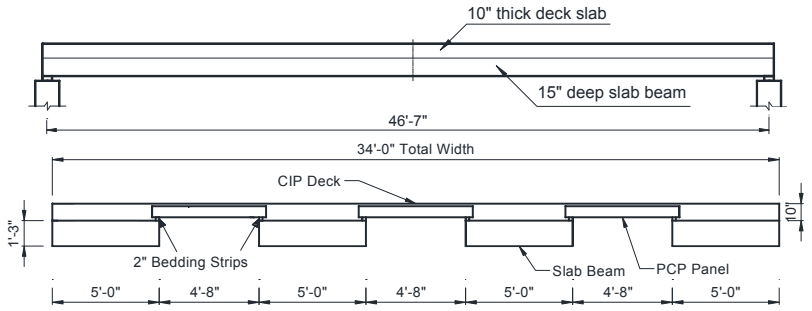

General Parameters Used

$f'_c = 8.5$ ksi $\quad f'_{ci} = 6$ ksi $\quad f_{pu} = 270$ ksi $\quad A_{ps} = 0.153\ in^2$

$A = 900\ in^2$ $\quad S_x = 2250\ in^3$ $\quad S_{x,b} = 6717\ in^3$ $\quad S_{x,t} = 7550\ in^3$

$w_b = 0.94$ kips/ft $\quad w_d = 0.98$ kips/ft $\quad w_D = 1.92$ kips/ft $\quad w_s = 0.415$ kips/ft

Load Balancing Design for Pretensioning Strands

Prestress forces for each strand:

At transfer: $T_i = 0.75 f_{pu} A_{ps} = 30.9$ kips

At service: . $T = T_i \cdot (1 - 20\%) = 24.7$. kips

Approximate load balancing for pretensioning strands to minimize the beam deflection:

$$n \cdot T \cdot e = \frac{w_D L^2}{10} \qquad n \times 24.7 \times 4 = \frac{1.92 \times 46.58^2}{10}$$

$n = 50.6$ Select even number $n = 52$ for stress check

$F_i = nT_i = 52 \times 30.9 = 1606.8$ kips

$F = nT = 52 \times 24.7 = 1284.4$ kips

Note: In the design performed by Hueste et al. (2015), T value is taken as 22.9 kips. If the designer use the same prestress force value, n value equals 54.6 and further selected 56, which is the same with Hueste et al.'s design solutions.

Allowable Stress Analysis

The stress check Is undertaken in different construction stages to satisfy the allowable stress limitation.

a. 5SB15 Slab Beam Fabrication

Due to the high pretensioning forces at transfer, it is found that the stress limits cannot be satisfied at end regions. Therefore, it is decided to use the debonding technique to mitigate the stress exceedance, which was also adopted in Hueste et al.'s design (2015). Based on trial calculation, it is decided to debond 6 strands at bottom row.

At transfer (30 in. away from the end)

$$\frac{F_i}{A}=\frac{1421.4}{900}=1.579\ \text{ksi} \qquad \frac{F_i e}{S_x}=\frac{1421.4\times 3.87}{2250}=2.445\ \text{ksi}$$

$$M_b=\left(\frac{1}{2}w_b L x-\frac{1}{2}w_b x^2\right)_{x=30\ in.}=53.5\ \text{kip-ft} \qquad \frac{M_b}{S_x}=\frac{53.5\times 12}{2250}=0.285\ \text{ksi}$$

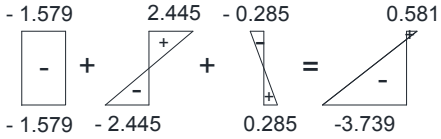

$$-\frac{F_i}{A}+\frac{F_i e}{S_x}-\frac{M_b}{S_x}=0.581<0.24\sqrt{f_{ci}'}=0.588\ \text{ksi}$$

$$-\frac{F_i}{A}-\frac{F_i e}{S_x}+\frac{M_b}{S_x}=-3.739>-0.65f_{ci}'=-3.9\ \text{ksi}$$

At Service (Midspan)

$$\frac{F}{A}=\frac{1284.4}{900}=1.427\ \text{ksi} \qquad \frac{Fe}{S_x}=\frac{1284.4\times 4}{2250}=2.283\ \text{ksi}$$

$$M_b=\frac{1}{8}w_b L^2=254.9\ \text{kip-ft} \qquad \frac{M_b}{S_x}=\frac{254.9\times 12}{2250}=1.360\ \text{ksi}$$

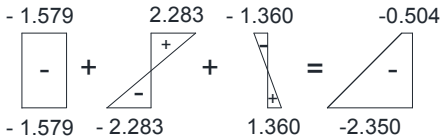

$$-\frac{F}{A}+\frac{Fe}{S_x}-\frac{M_b}{S_x}=-0.504>-0.45f_c'=-3.825\ \text{ksi}$$

$$-\frac{F}{A}-\frac{Fe}{S_x}+\frac{M_b}{S_x}=-2.35>-0.45f_c'=-3.825\ \text{ksi}$$

b. Apply PCPs and CIP Deck at the Construction Site

$$M_d=\frac{1}{8}w_d L^2=264.5\ \text{kip-ft} \qquad \frac{M_d}{S_x}=\frac{254.9\times 12}{2250}=1.410\ \text{ksi}$$

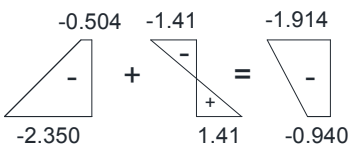

$$-0.504-\frac{M_d}{S_x}=-1.914>-0.45f_c'=-3.825\ \text{ksi}$$

$$-2.350+\frac{M_d}{S_x}=-0.94>-0.45f_c'=-3.825\ \text{ksi}$$

c. Apply Superimposed Dead Load and Live plus Impact Load

Alternative symmetric live load model and proposed design models developed in Sections 5 and 6 are used herein to determine the moment and shear demands under live plus impact load.

Alternative live load model: $P_1 = P_2 = P_3 = 25$ kips, $b = c = 10$ ft, $w = 0.64$ kips/ft

Proposed design model: $M_g = k_M \frac{S}{12} M_L$, $k_M = 0.95$ for spread slab beam bridge

$$M_L = 3P(1+IM)\left(\frac{L}{4} - \frac{b}{3}\right) + \frac{1}{8}wL^2 = 1002.8 \text{ kip-ft}$$

$$M_g = 0.95 \times \frac{9.67}{12} \times 1002.8 = 767.7 \text{ kip-ft}$$

M_g acts on the composite beam section, $S_{x,b} = 6717$ in.^{3}, $S_{x,t} = 7550$ in.^{3}.

$$\frac{M_g}{S_{x,b}} = \frac{767.7 \times 12}{6717} = 1.370 \text{ ksi} \qquad \frac{M_g}{S_{x,t}} = \frac{767.7 \times 12}{7550} = 1.220 \text{ ksi}$$

Superimposed dead load includes self-weight of barrier and wearing surface:

$$w_s = 0.217 + 0.198 = 0.415 \text{ kips/ft} \qquad M_s = \frac{1}{8}w_s L^2 = 112.6 \text{ kip-ft}$$

$$\frac{M_s}{S_{x,b}} = \frac{112.6 \times 12}{6717} = 0.201 \text{ ksi} \qquad \frac{M_g}{S_{x,t}} = \frac{112.6 \times 12}{7550} = 0.179 \text{ ksi}$$

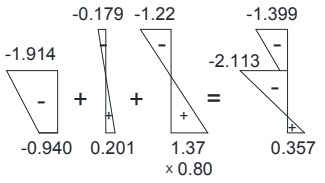

$$-1.914 - \frac{M_s}{S_{x,t}} - \frac{M_{L+I}}{S_{x,t}} = -1.399 > -0.60f_c' = -5.1 \text{ ksi}$$

$$-0.940 + \frac{M_{L+I}}{S_{x,b}} + 0.8\frac{M_s}{S_{x,b}} = 0.356 < 0.19\sqrt{f_c'} = 0.554 \text{ ksi}$$

Thus, stress limitations are satisfied during the construction procedure.

Temperature Effects Check

Based on AASHTO LRFD Article 3.12.3, the temperature gradient is specified as follows:

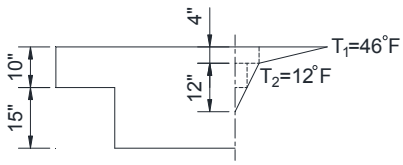

$\alpha = 6 \times 10^{-6}$ /° F, $E_c = 5590$ ksi

Transformed Composite Section: $A = 1613$ in.^{2},

$I = 88900$ in.^{4}, $y_t = 11.8$ in., $y_b = 13.2$ in.

Using segmental superposition method instead of integration:

The strain at the centroid of the composite section: $\varepsilon_o = \frac{\alpha}{A}\int bTdy = 54.2\times10^{-6}$

The curvature in the composite section: $\phi = \frac{\alpha}{I}\int bTydy = 7.82\times10^{-6}$ /in.

The strain due to thermal expansion: $\varepsilon_t = \alpha T = \begin{matrix} 276\times10^{-6}(0'-4") \\ 72\times10^{-6}(4"-16") \end{matrix}$

Primary thermal stress: $\varepsilon_t = E_c\left(\varepsilon_o + \phi y - \alpha T\right)$, the thermal stress block follows:

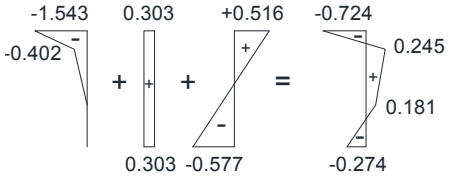

For simply supported bridge configuration, there is no secondary thermal stress due to determinate structure. The final stresses due to service loads and 0.5 times thermal effects still satisfy the allowable stress limitations. The stress block is shown as follows:

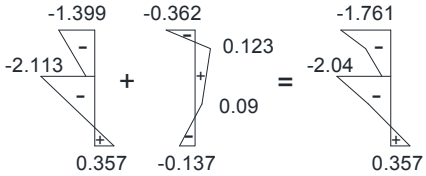

Deflection Check

According to AASHTO LRFD Article 2.5.2.6.2, the composite bending stiffness of the girders is considered and all supporting components are assumed to deflect equally. Deflection is calculated under the larger of (1) design truck load alone, or (2) 25 percent of design truck load and full Design Lane Load according to Article 3.6.1.3.2. For the preliminary designs, case (1) $\delta_1 = 0.462$ in.; case (2) $\delta_2 = 0.252$ in. Both values are smaller than the deflection limit $L/800 = 0.699$ in.

Shear Design

The shear resistance of the slab beam girder is checked based on the requirements of the AASHTO LRFD Bridge Design Specifications. Due to the high cross-sectional area of the slab beams, the shear resistance of the concrete itself satisfies the required shear strength most of time. Both transverse shear and interface shear resistances are checked herein.

a. Transverse Shear Design

Based on AASHTO LRFD: $\phi V_n \geq V_u$, where ϕ = strength reduction factor for shear, 0.9.

V_n is the nominal shear resistance at a given section, which is the sum of contributions provided by the concrete, transverse reinforcement and prestressing force. Note that the TxDOT Bridge Division Standard Drawings provide transverse steel arrangement and it will be adopted in current design process, as shown in following:

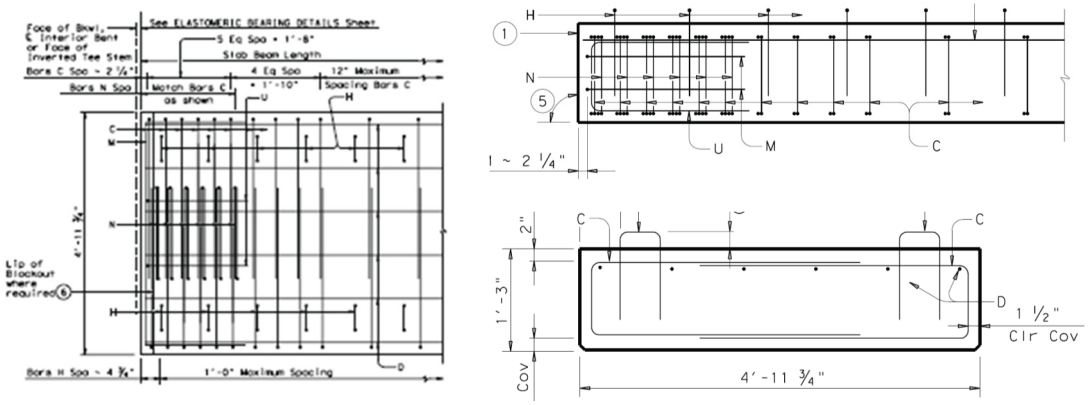

Elevation and Section View of Transverse Reinforcement (TXDOT 2013)

$$V_n = V_c + V_s + V_p \leq 0.25 f_c' b_v d_v + V_p$$

$$V_c = 0.0316 \beta \sqrt{f_c'} b_v d_v = 0.0316 \times 3.88 \times \sqrt{8.5} \times 60 \times 17.55 = 376.4 \text{ kips}$$

Transverse steel currently provided in the TxDOT drawings is 0.4 in²/ft Thus,

$$V_s = A_v f_v \frac{d_v}{s} \cot\theta = 0.4 \times 60 \times \frac{17.55}{12} \times \cot(29) = 63.3 \text{ kips}$$

$$V_n = V_c + V_s + V_p = 376.4 + 63.3 = 439.7 \text{ kips} \leq 0.25 f_c' b_v d_v + V_p = 2237.6 \text{ kips}$$

The pretensioning strand is parallel with the longitudinal axis of the slab beam. Thus, there are no shear resistance contributions provided by the prestressing force.

V_u is the factored shear force at the ultimate limit state: $V_u = 1.25 V_{DC} + 1.5 V_{DW} + 1.75 V_{L+I}$

$V_{DC} = 0.5 w_{DC} L = 44.7$ kips, $V_{DW} = 0.5 w_{DW} L = 9.67$ kips

$$V_{L+I} = 0.32 L - \frac{997.5}{L} + 99.8 = 93.3 \text{ kips}$$

$$V_u = 1.25 V_{DC} + 1.5 V_{DW} + 1.75 V_{L+I} = 1.25 \times 44.7 + 1.5 \times 9.67 + 1.75 \times 93.3 = 234 \text{ kips}$$

$\phi V_n = 0.9 \times 439.7 = 395.7$ kips $\geq V_u = 234$ kips

Therefore, the transverse steel currently provided in the TxDOT standard drawings for 5SB15 slab beam is adequate for the transverse shear design.

b. Interface Shear Design

The interface shear design should satisfy: $\phi V_{ni} \geq V_{ui}$

$$V_{ui} = \frac{12V_u}{d_v} = \frac{12 \times 234}{15.5} = 181.2 \text{ kips/ft.}$$

$V_{ni} = cA_{cv} + \mu(A_{vf} f_y + P_c) = 0.075 \times 56 \times 12 + 0.6 \times 0.8 \times 60 = 79.2$ kips/ft.

$\phi V_{ni} = 0.9 \times 79.2 = 71.6$ kips $< V_{ui} = 181.2$ kips

Based on the simple calculation, it is shown that increased amount of interface shear reinforcement is needed to achieve required interface shear strength. This issue was investigated by Hueste (2015) using global force equilibrium method and it will not further described herein. It is suggested by Hueste (2015) that the standard interface shear reinforcement between the support and quarter span length must be doubled, while the minimum interface shear reinforcement may be used for the region between the quarter span and midpsan for standard beam types.

Plastic Overstrength Analysis

The plastic analysis methods are utilized to evaluate the reserve strength capacity of the simply supported spread slab beam bridge. Different limiting behavior modes are considered herein: slab-only mechanisms, a beam-only mechanism and mixed beam-slab mechanisms.

a. Flexural Capacities of Slab and Beam Components

The flexure capacities of the connecting slab and composite beams are determined with section analysis and their values are listed as follows.

$M_{x,bi} = 3478$ kip-ft $\quad M_{x,be} = 3246$ kip-ft

$m_x = 29.7$ kip-in./in. $\quad m_y = 18.1$ kip-in./in. $\quad m_d = 23.3$ kip-in./in.

$m_x' = 16.6$ kip-in./in. $\quad m_y' = 11.2$ kip-in./in. $\quad m_d' = 13.6$ kip-in./in.

b. Deck slab Local failure Mechanisms

The deck slab local flexure failure mechanisms are shown in Figure 8.2.

The collapse loads due to single or multiple axle loads are determined with the following expressions

Single axle inside: $$P_1 = 2\varphi\left(m_d + m_d^{'}\right) + 4\left(m_y + m_y^{'}\right)\cot\frac{\varphi}{2}$$

Single axle at free end: $$P_1 = \varphi\left(m_d + m_d^{'}\right) + 2\left(m_y + m_y^{'}\right)\cot\frac{\varphi}{2}$$

Multiple axles inside: $$\sum P_i = 2\varphi\left(m_d + m_d^{'}\right) + 4\left(m_y + m_y^{'}\right)\cot\frac{\varphi}{2} + 4\left(m_y + m_y^{'}\right)\frac{b}{b_d}$$

Multiple axles at free end: $$\sum P_i = \varphi\left(m_d + m_d^{'}\right) + 2\left(m_y + m_y^{'}\right)\cot\frac{\varphi}{2} + 4\left(m_y + m_y^{'}\right)\frac{b}{b_d}$$

the lowest collapse loads for all the yield line patterns listed above are obtained when

$$\varphi = 2\sin^{-1}\sqrt{\frac{m_y + m_y^{'}}{m_d + m_d^{'}}} = 2\sin^{-1}\sqrt{\frac{18.1 + 11.2}{23.2 + 13.6}} = 0.702\pi$$

Therefore, The corresponding overstrength factors (Ω) are calculated as follows:

	Inside the deck slab	At free end
Single axle inside:	5.35	**2.68**
Two axles inside:	6.92	5.58
Three axles inside:	9.93	8.74

c. Beam-only Failure Mechanism

The plastic overstrength factors for beam-only and mixed beam-slab failure mechanisms are determined with virtual work equations.

$$IWD = N_b M_{x,b}\left(\frac{1}{\alpha L} + \frac{1}{(1-\alpha)L}\right)\delta$$

$$EWD = \Omega\left[w_{du}A_{du}\delta_d + w_{lu}A_{lu}\delta_l + P_{1u}\left(1 - \frac{b}{\alpha L}\right)\delta + P_{2u}\delta + P_{3u}\left(1 - \frac{b}{(1-\alpha)L}\right)\delta\right]$$

$$\Omega = \phi \frac{N_b M_{x,b}\left(\frac{1}{\alpha L}+\frac{1}{(1-\alpha)L}\right)}{\frac{w_{du}A_{du}}{2}+\frac{w_{lu}A_{lu}}{2}+P_{1u}\left(1-\frac{b}{\alpha L}\right)+P_{2u}+P_{3u}\left(1-\frac{b}{(1-\alpha)L}\right)}$$

By substituting the known parameters into the above equation, it is determined that the lowest overstrength factor is $\Omega = 2.04$ when $\alpha = 0.527$.

d. Mixed Beam-slab Failure Mechanism

The expressions for the internal and external virtual work are shown as follows:

$$IWD = \frac{N_b M_{x,b} + m_x b_d + m'_x b_d}{(1-\alpha)\alpha L}\delta + \left(\frac{m_y + m'_y}{b_d}\right)\left[\frac{x^2}{(1-\alpha)\alpha L} - 2x + L\right]\delta$$

$$EWD = \Omega\left[w_{du}A_{du}\delta_d + w_{lu}A_{lu}\delta_l + P_{1u}\left(1-\frac{b}{\alpha L}\right)\delta + P_{2u}\delta + P_{3u}\left(1-\frac{b}{(1-\alpha)L}\right)\delta\right]$$

$$\Omega = \phi \frac{\frac{N_b M_{x,b} + m_x b_d + m'_x b_d}{(1-\alpha)\alpha L} + \left(\frac{m_y + m'_y}{b_d}\right)\left[\frac{x^2}{(1-\alpha)\alpha L} - 2x + L\right]}{\frac{w_{du1}A_{du1}}{2}+\frac{w_{du2}A_{du2}}{3}+\frac{w_{lu}A_{lu}}{2}+P_{1u}\left(1-\frac{b}{\alpha L}\right)+P_{2u}+P_{3u}\left(1-\frac{b}{(1-\alpha)L}\right)}$$

By substituting the known parameters into the above equation, it is determined that the lowest overstrength factor is $\Omega = 2.13$ when $\alpha = 0.532$.

It is seen that the desirable global beam-only mechanism is the most critical failure mode for simply supported spread slab beam bridge.

Bridge Layout and Cross Section

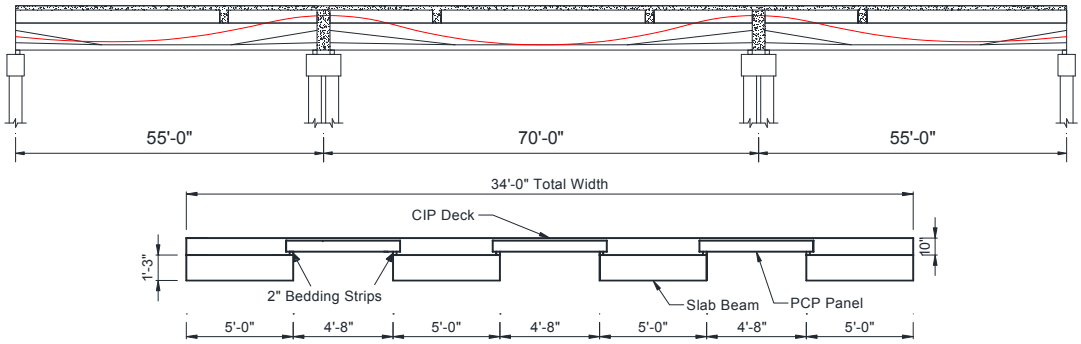

General Parameters Used

$f_c' = 8.5$ ksi	$f_{ci}' = 6$ ksi	$f_{pu} = 270$ ksi	$A_{ps} = 0.217$ in^2
$A = 900$ in^2	$S_x = 2250$ in^3	$S_{x,b} = 6717$ in^3	$S_{x,t} = 7550$ in^3
$w_b = 0.94$ kips/ft	$w_d = 0.98$ kips/ft	$w_D = 1.92$ kips/ft	$w_D = 0.415$ kips/ft

Load Balancing Design Philosophy

Load balancing with pretensioning and post-tensioning (P.T.) was used in the design of the three-span continuous spread slab beam bridge to determine the viable prestress strands arrangement. The pretensioning strands are designed to balance the dead load of slab beam and portion of PCPs. The P.T. tendons are jacked to resist the self-weight of the extra deck slab, live plus impact load and superimposed dead load. Based on geometric constraints and cover requirements, only 56 spots in two rows with 2 in. center-to-center spacing.are available to arrange the prestress strands.

Allowable Stress Analysis

The stress check Is undertaken in different construction stages to satisfy the allowable stress limitation. Herein, the analysis and design for interior span (70 ft) are described in detail as an example. The design for the exterior span slab beam (55 ft) is similar.

a. 5SB15 Slab Beam Fabrication

Based on trial calculation result, it is decided to use all as many available spots as possible for pretension strands, with exception of locations for P.T. tendons. Harping technique is adopted in the fabrication process so that is no end moments are developed due to eccentricity. Therefore, the tensile stress limitation at the end region could easily be satisfied. The elevation view and cross section of the precast slab beam for interior span (70 ft) are shown as follows.

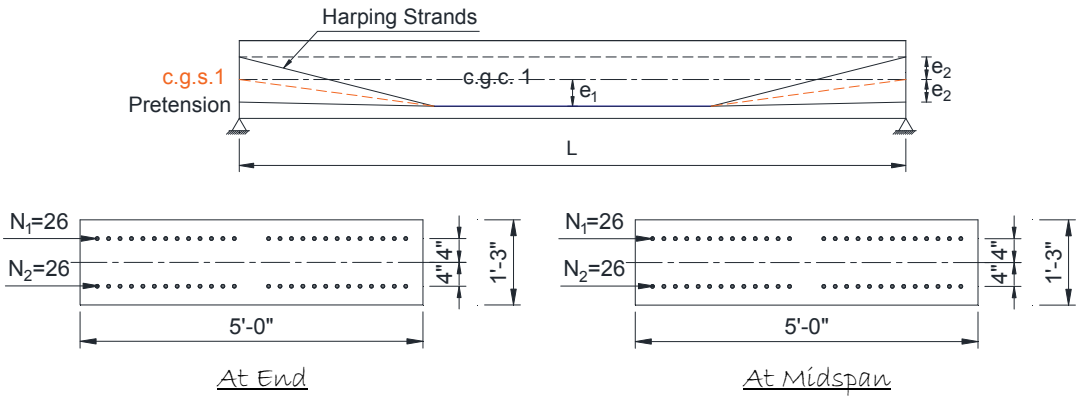

At End At Midspan

Strand numbers available for pretensioning: $N_1 = N_2 = 26$, $N = N_1 + N_2 = 52$

Prestress force: $F_i = NT_i = 52 \times 43.9 = 2283$ kips, $F = NT = 52 \times 35.2 = 1828$ kips

At transfer (at end)

$$-\frac{F_i}{A} = -2.536 > -0.65 f_{ci}' = -3.9 \text{ ksi}$$

At Service (Midspan)

$$\frac{F}{A} = \frac{1828}{900} = 2.031 \text{ ksi} \qquad \frac{Fe_1}{S_x} = \frac{1828 \times 5}{2250} = 4.062 \text{ ksi}$$

$$M_b = \frac{1}{8} w_b L^2 = 575.8 \text{ kip-ft} \qquad \frac{M_b}{S_x} = \frac{575.8 \times 12}{2250} = 4.062 \text{ ksi}$$

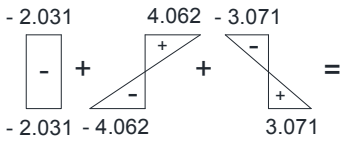

$$-\frac{F}{A} + \frac{Fe_1}{S_x} - \frac{M_b}{S_x} = -1.04 > -0.45 f_c' = -3.825 \text{ ksi}$$

$$-\frac{F}{A} - \frac{Fe}{S_x} + \frac{M_b}{S_x} = -3.02 > -0.45 f_c' = -3.825 \text{ ksi}$$

b. Place PCPs between Slab Beams

5 ft-4 in. wide, 6.5 in. thick PCP: $w_{pcp} = 0.43$ kips/ft

$$M_{PCP} = \frac{1}{8} w_{pcp} L^2 = \frac{1}{8} \times 0.43 \times 70^2 = 263.4 \text{ kip-ft} \qquad \frac{M_{PCP}}{S_x} = \frac{263.4 \times 12}{2250} = 1.405 \text{ ksi}$$

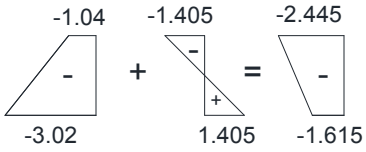

$$-1.04-\frac{M_d}{S_x}=-2.445>-0.45f_c'=-3.825 \text{ ksi}$$

$$-3.02+\frac{M_d}{S_x}=-1.615>-0.45f_c'=-3.825 \text{ ksi}$$

c. Cast Concrete Joints to Achieve Continuity and Pour the CIP deck

The continuity is achieved after casting the concrete joints and the CIP deck slab is considered to apply on the three-span continuous beam: $w_{CIP}=0.55$ kips/ft

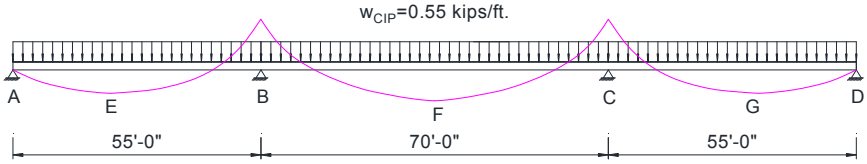

By using moment distribution method, the moment values at critical locations due to the self-weight of the PCP could be determined and listed as follows

Exterior: $M_E=112$ kip-ft Support: $M_B=-218$ kip-ft Interior: $M_F=118$ kip-ft

The allowable stress check is undertaken at midspan point F and interior support B:

At Interior Support B: $\frac{M_B}{S_x}=\frac{218\times12}{2250}=1.163$ ksi

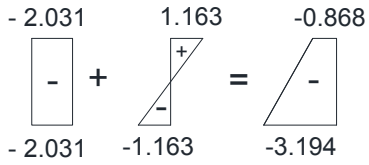

$$-2.031+\frac{M_B}{S_x}=-0.868>-0.45f_c'=-3.825 \text{ ksi}$$

$$-2.031-\frac{M_B}{S_x}=-3.194>-0.45f_c'=-3.825 \text{ ksi}$$

At Midspan Location F: $\frac{M_F}{S_x}=\frac{118\times12}{2250}=0.629$ ksi

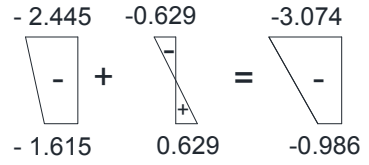

$$-2.445+\frac{M_F}{S_x}=-3.074>-0.45f_c'=-3.825 \text{ ksi}$$

$$-1.615+\frac{M_F}{S_x}=-0.986>-0.45f_c'=-3.825 \text{ ksi}$$

d. Jack Post-tensioning Tendons

19 strands are allowed inside one duct. With considering the frictional losses, the prestress forces are determined as follows:

$T = 0.67 f_{pu} A_{ps} \cdot (1 - 20\%) = 31.4$ kips, $\quad F = 19T = 19 \times 31.4 = 596.7$ kips

The post-tensioning tendon profile and equivalent upward load is presented as follows:

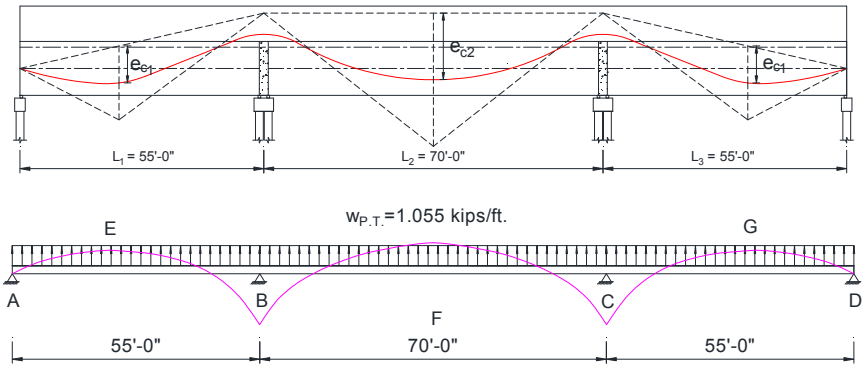

$e_{c1} = 7$ in. $\quad e_{c2} = 13$ in. $\quad w_{P.T.} = \dfrac{8 \times 596.7 \times 13}{70^2 \times 12} = 1.055$ kips/ft

Exterior: $M_E = -215$ kip-ft $\quad$ Support: $M_B = 418$ kip-ft $\quad$ Interior: $M_F = -226$ kip-ft

At Interior Support B: $\dfrac{M_B}{S_{x,b}} = \dfrac{418 \times 12}{6717} = 0.747$ ksi $\quad \dfrac{M_B}{S_{x,t}} = \dfrac{418 \times 12}{7550} = 0.665$ ksi

Compressive stress due to post-tensioning prstress forces: $\dfrac{F_{P.T.}}{A} = \dfrac{596.7}{1613.4} = 0.37$ ksi

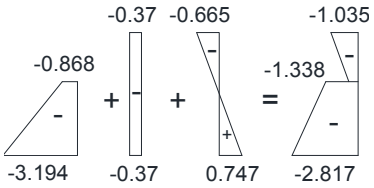

$-\dfrac{F_{P.T.}}{A} - \dfrac{M_B}{S_{x,t}} = -1.035 > -0.45 f_c' = -3.825$ ksi

$-3.194 - \dfrac{F_{P.T.}}{A} + \dfrac{M_B}{S_{x,t}} = -2.817 > -0.45 f_c' = -3.825$ ksi

The stress at the top surface of slab beam is also checked to satisfy allowable stress limits.

At Midspan Location F: $\dfrac{M_F}{S_{x,b}} = \dfrac{226 \times 12}{6717} = 0.404$ ksi $\quad \dfrac{M_F}{S_{x,t}} = \dfrac{226 \times 12}{7550} = 0.360$ ksi

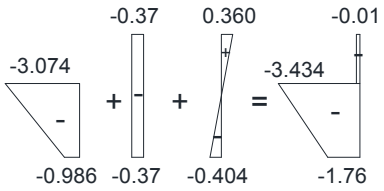

$-\dfrac{F_{P.T.}}{A} + \dfrac{M_F}{S_{x,t}} = -0.01 > -0.45 f_c' = -3.825$ ksi

$-0.986 - \dfrac{F_{P.T.}}{A} - \dfrac{M_F}{S_{x,b}} = -1.76 > -0.45 f_c' = -3.825$ ksi

The stress at the top surface of slab beam is also checked to satisfy allowable stress limits.

e. Apply the superimposed Dead load

$w_s = 0.415$ kips/ft, applied on the three-span continuous beam similar as CIP deck.

Exterior: $M_E = 84.5$ kip-ft Support: $M_B = -164.5$ kip-ft Interior: $M_F = 89$ kip-ft

At Interior Support B: $\frac{M_B}{S_{x,b}} = \frac{164.5 \times 12}{6717} = 0.294$ ksi $\frac{M_B}{S_{x,t}} = \frac{164.5 \times 12}{7550} = 0.261$ ksi

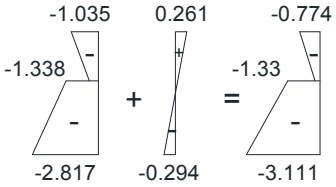

$$-1.035 + \frac{M_B}{S_{x,t}} = -0.774 > -0.45 f_c' = -3.825 \text{ ksi}$$

$$-2.817 - \frac{M_B}{S_{x,b}} = -3.111 > -0.45 f_c' = -3.825 \text{ ksi}$$

The stress at the top surface of slab beam is also checked to satisfy allowable stress limits.

At Midspan Location F: $\frac{M_F}{S_{x,b}} = \frac{89 \times 12}{6717} = 0.159$ ksi $\frac{M_F}{S_{x,t}} = \frac{89 \times 12}{7550} = 0.141$ ksi

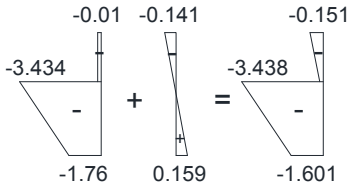

$$-0.01 - \frac{M_F}{S_{x,t}} = -0.151 > -0.45 f_c' = -3.825$$

$$-1.76 + \frac{M_F}{S_{x,b}} = -1.601 > -0.45 f_c' = -3.825$$

The stress at the top surface of slab beam is also checked to satisfy allowable stress limits.

f. Apply Live plus Impact Load

Alternative symmetric live load model and proposed design models developed in Sections 5 and 6 are used herein to determine the moment and shear demands under live plus impact load.

Alternative live load model: $P_1 = P_2 = P_3 = 25$ kips, $b = c = 10$ ft, $w = 0.64$ kips/ft; Impact factor = 33 %. The maximum positive and negative moment values at critical locations are determined based on the following load placement schemes. Note that for negative moment at interior support, a second truck is allowed to add into the live load model, but the magnitude is multiplied by 0.9 in accordance with AASHTO code.

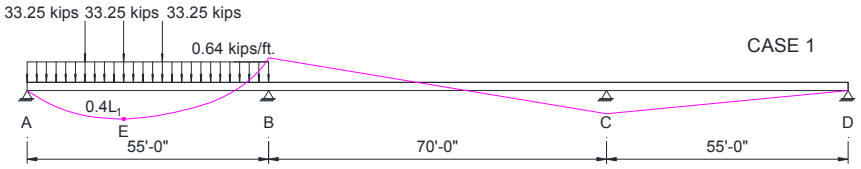

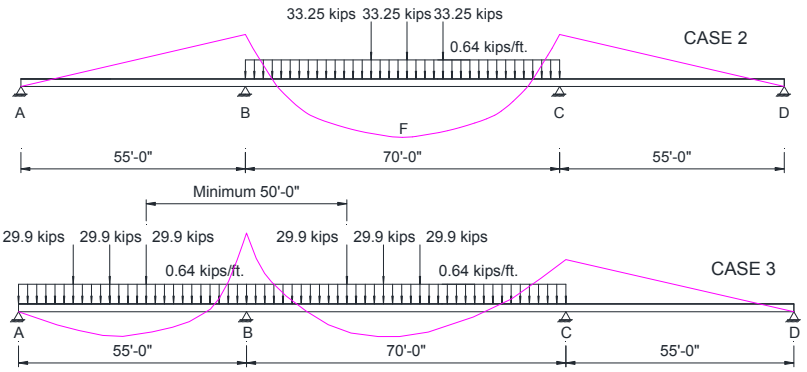

The maximum moments at critical locations due to different load placement schemes could be determined with moment distribution method. The values are listed as follows:

Exterior: $M_E = 1008$ kip-ft Support:. $M_B = -1172$ .kip-ft Interior: $M_F = 1092$ kip-ft

Proposed design model: $M_g = k_M \frac{S}{12} M_L$, $k_M = 0.95$ for spread slab beam bridge

The moment demands for 70 ft long composite beam section are:

$$M_{g,B} = 0.95 \times \frac{9.67}{12} \times 1172 = 897 \text{ kip-ft} \qquad M_{g,F} = 0.95 \times \frac{9.67}{12} \times 1092 = 836 \text{ kip-ft}$$

At Interior Support B: $\frac{M_B}{S_{x,b}} = \frac{897 \times 12}{6717} = 1.602$ ksi $\frac{M_B}{S_{x,t}} = \frac{897 \times 12}{7550} = 1.425$ ksi

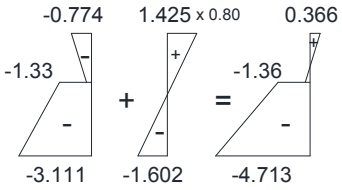

$$-0.774 + 0.8 \times \frac{M_B}{S_{x,t}} = 0.366 < 0.19\sqrt{f_c'} = 0.554 \text{ ksi}$$

$$-3.111 - \frac{M_B}{S_{x,b}} = -4.713 > -0.6 f_c' = -5.1 \text{ ksi}$$

At Midspan Location F: $\frac{M_F}{S_{x,b}} = \frac{836 \times 12}{6717} = 1.494$ ksi $\frac{M_F}{S_{x,t}} = \frac{836 \times 12}{7550} = 1.329$ ksi

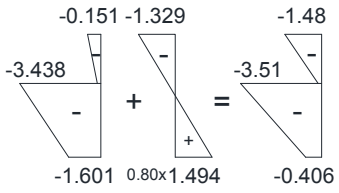

$$-0.151 - \frac{M_F}{S_{x,t}} = -1.48 > -0.45 f_c' = -3.825 \text{ ksi}$$

$$-1.601 + 0.8 \times \frac{M_F}{S_{x,b}} = -0.406 > -0.6 f_c' = -5.1 \text{ ksi}$$

Thus, stress limitations are satisfied during the construction procedure.

Temperature Effects Check

The primary thermal stress due to temperature gradients has been calculated for the simply supported spread slab beam bridge. For continuous bridge configuration, secondary thermal stress exists due to the indeterminacy. The secondary moment could be determined with moment distribution method.

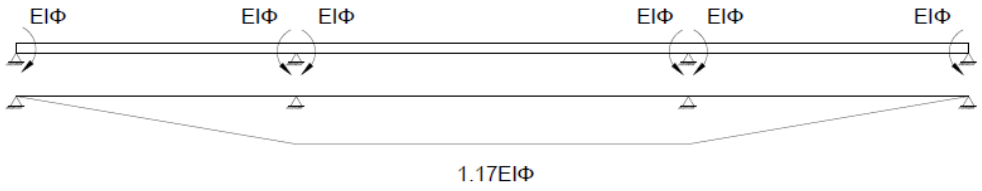

$M_{t,sec} = 1.17EI\phi$

$\sigma_{t,sec} = \frac{M_{t,sec}y}{I} = 1.17EI\phi$

Thermal Stress:

$\sigma_t = \sigma_{t,pri} + \sigma_{t,sec}$

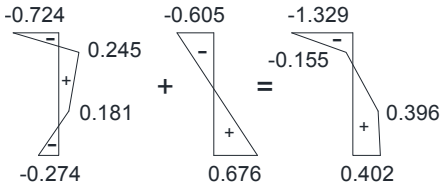

The final stresses due to service loads and 0.5 times thermal effects still satisfy the allowable stress limitations. The stress block is shown as follows:

At Interior Support B

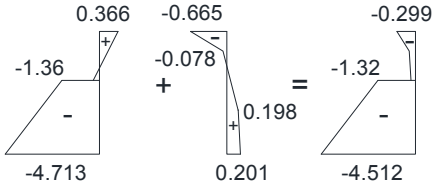

At Midspan Location F

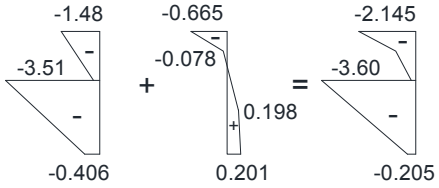

Deflection Check

According to AASHTO LRFD Article 2.5.2.6.2, the composite bending stiffness of the girders is considered and all supporting components are assumed to deflect equally. Deflection is calculated under the larger of (1) design truck load alone, or (2) 25 percent of design truck load and full Design Lane Load according to Article 3.6.1.3.2. For exterior span, the deflection values for case (1) $\delta_1 = 0.564$ in. and case (2) $\delta_2 = 0.331$ in. are smaller than the deflection limit $L_1/800 = 0.825$ in. Similarly, For interior span, the deflection values for case (1) $\delta_1 = 0.859$ in. and case (2) $\delta_2 = 0.545$ in. are smaller than the deflection limit $L_2/800 = 1.05$ in.

Shear Design

The transverse and interface shear resistance of the slab beam girder is checked based on the requirements of the AASHTO LRFD Bridge Design Specifications. The methodology for the calculation of shear resistance and demand has been described in the design for simple spans. The transverse shear steel arrangement, capacity and demand in different regions of the interior span (70 ft) are listed as follows:

Distance from the Support	Shear Reinforcement	Shear Capacity (kips)	Shear Demand (kips)
0 – 1 ft-8in.	#4@4"	509.7	264.7
1 ft-8in – 3 ft 6 in.	#4@6"	452.7	255.1
3 ft- 6 in. - midspan	#4@12"	395.7	245.6

Similar with simple span design, the amount of interface shear reinforcement is not adequate to achieve required interface shear strength for not intentionally roughed surface. Current TxDOT standard slab beam details (#4@12" H bar) provide a 0.8 in.^{2}/ft reinforcing bar area crossing the interface plane. It is suggested to increase the rebar amount to #4@4" in the end region close to the support.

Plastic Analysis

The plastic analysis methods are utilized to evaluate the reserve strength capacity of the Continuous spread slab beam bridge. The calculation for slab-only failure mechanism is the same with the simply supported case and will not described herein. The flexure capacities of the composite slab beam at different locations are listed as follows.

	Exterior span	Interior support	Interior span
M_x	4649 kip-ft	2370 kip-ft	5122 kip-ft

As compared with simply supported configurations, the negative flexure capacity at interior support needs to be considered in the calculation of plastic overstrength factors for mixed beam-slab and beam-only failure mechanisms.

a. Interior Span

When the beam-only failure mechanism occurs, the plastic overstrength factor, Ω, is determined based on virtual work equations as follows:

$$\Omega = \phi \frac{N_b\left(M_{x,b} + M'_{x,b}\right)\left(\frac{1}{\alpha L} + \frac{1}{(1-\alpha)L}\right)}{\frac{w_{du}A_{du}}{2} + \frac{w_{lu}A_{lu}}{2} + P_{1u}\left(1 - \frac{b}{\alpha L}\right) + P_{2u} + P_{3u}\left(1 - \frac{b}{(1-\alpha)L}\right)}$$

By substituting the known parameters into the above equation, it is determined that the lowest overstrength factor is . $\Omega = 2.23$. when $\alpha = 0.515$

When the mixed beam-slab failure mechanism occurs, the expression for the plastic overstrength factor is shown as follows:

$$\Omega = \phi \frac{\frac{N_b\left(M_{x,b} + M'_{x,b}\right) + m_x b_d + m'_x b_d}{(1-\alpha)\alpha L} + \left(\frac{m_y + m'_y}{b_d}\right)\left[\frac{x^2}{(1-\alpha)\alpha L} - 2x + L\right]}{\frac{w_{du1}A_{du1}}{2} + \frac{w_{du2}A_{du2}}{3} + \frac{w_{lu}A_{lu}}{2} + P_{1u}\left(1 - \frac{b}{\alpha L}\right) + P_{2u} + P_{3u}\left(1 - \frac{b}{(1-\alpha)L}\right)}$$

By substituting the known parameters into the above equation, it is determined that the lowest overstrength factor is $\Omega = 2.34$ when $\alpha = 0.518$.

b. Exterior Span

When the beam-only failure mechanism occurs, the plastic overstrength factor, Ω , is determined based on virtual work equations as follows:

$$\Omega = \phi \frac{N_b M_{x,b}\left(\frac{1}{\alpha L} + \frac{1}{(1-\alpha)L}\right) + N_b M'_{x,b}\frac{1}{(1-\alpha)L}}{\frac{w_{du}A_{du}}{2} + \frac{w_{lu}A_{lu}}{2} + P_{1u}\left(1 - \frac{b}{\alpha L}\right) + P_{2u} + P_{3u}\left(1 - \frac{b}{(1-\alpha)L}\right)}$$

By substituting the known parameters into the above equation, it is determined that the lowest overstrength factor is $\Omega = 2.64$ when $\alpha = 0.478$

When the mixed beam-slab failure mechanism occurs, the expression for the plastic overstrength factor is shown as follows:

$$\Omega = \phi \frac{\frac{N_b M_{x,b} + m_x b_d + m'_x b_d}{(1-\alpha)\alpha L} + \frac{N_b M'_{x,b}}{(1-\alpha)L} + \left(\frac{m_y + m'_y}{b_d}\right)\left[\frac{x^2}{(1-\alpha)\alpha L} - 2x + L\right]}{\frac{w_{du1}A_{du1}}{2} + \frac{w_{du2}A_{du2}}{3} + \frac{w_{lu}A_{lu}}{2} + P_{1u}\left(1 - \frac{b}{\alpha L}\right) + P_{2u} + P_{3u}\left(1 - \frac{b}{(1-\alpha)L}\right)}$$

By substituting the known parameters into the above equation, it is determined that the lowest overstrength factor is $\Omega = 2.64$ when $\alpha = 0.486$

From the analysis results above, it is seen that the most critical collapse load is generated by the beam-only mechanism at interior span.

APPENDIX A5

EVALUATION OF LIVE LOAD MODELS FOR PIN-FIXED AND FIXED-FIXED SPANS

This appendix presents the evaluation of the proposed live load model described in Section 5 for pin-fixed and fix-fixed spans which are the basic span units for the multiple span continuous bridge. This appendix supports material in Section 5.

Note: All computations in this appendix are presented in US customary units. The following conversion factors may be used to convert to SI units.
1 in. = 25.4 mm *1 kip-ft = 1.3558 kN-m*
1 kip = 4.4482 kN *1 ksi = 6.895 MPa*

A5.1 APPLICATION OF SLAB TO BEAM FOLDED PLATE MECHANISM ON RIVERSIDE BRIDGE

An alternative symmetric live load model is developed in Section 5 to provide bridge engineers a more direct and simpler option for rapid design. The load effects of the proposed live load model for a wide range of simple spans has been validated by comparing with the "exact" actions generated by the HL-93 live load model that is designated in the AASHTO LRFD Bridge Design Specifications (AASHTO 2012). However, it remains in question whether the proposed live load model is applicable to the preliminary design of the multi-span continuous bridge.

Figure A5.1(a) presents an example of three-span continuous bridge design. By utilizing the moment distribution method, it is possible to determine the moment demands per traffic lane by hand calculations. As a starting point, the exterior and interior spans of the continuous bridge were be treated as two basic span units, pin-fixed and fixed-fixed spans as shown in Figure A5.1(b), respectively. Then, the fixed end moment values would be balanced through several rounds of iterations with using distribution factors and carryover factors which are irrelevant to the live load models. Therefore, it is reasonable to evaluate the load effects of live load models for these two basic span units as representatives of the multi-span continuous bridge. In this appendix, the moment and shear force envelopes generated by the proposed live load model were calculated for a wide range of pin-fixed and fixed-fixed spans; and they are compared with the load effects caused by the HL-93 live load model for the purpose of evaluating the applicability of the proposed live load model to the continuous bridge configuration.

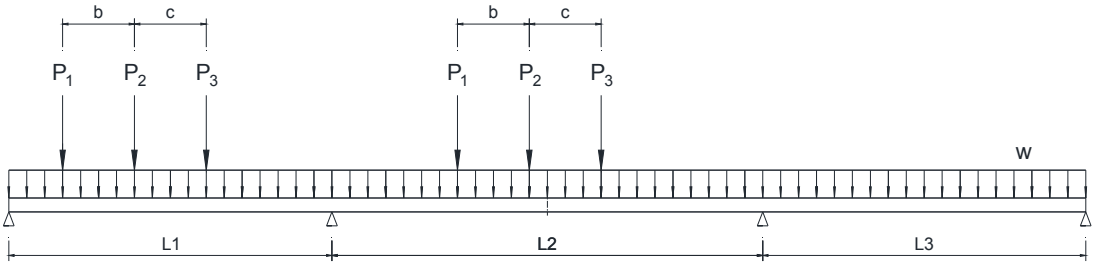

(a) An Example of Continuous Bridge Design

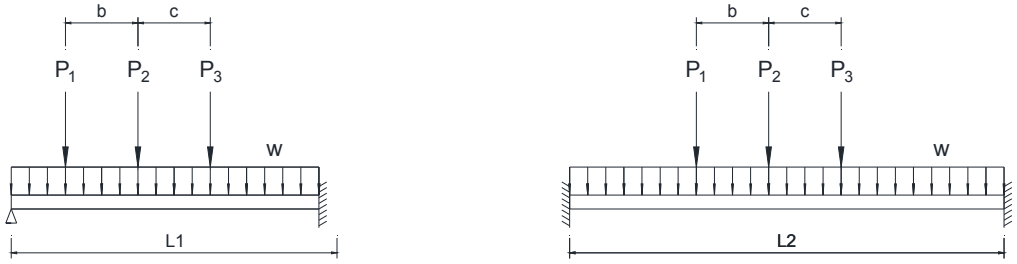

(b) Two Basic Span Units

Figure A5.1. Design of Continuous Bridge Configurations under Live Load.

A5.2 COMPARISONS AMONG DIFFERENT LIVE LOAD MODELS

A5.2.1 Results for Pin-Fixed Spans

Figure A5.2 shows the comparison amongst maximum positive and negative moment and shear values of pin-fixed spans under different live load models. When L > 49 ft, more critical positive moment values are produced by the design truck load rather than the tandem axles. The critical span length for maximum negative moment is 31 ft It is evident that the proposed alternative live load produces slightly more conservative maximum moment values than the HL-93 live load does in the region where the truck load governs the design, which demonstrates that the alternative truck load may be utilized to determine moment effects of pin-fixed spans in the design process. As for the shear action, it is shown from Figure A5.2(c) that the design truck load generates more critical design shear force values than the tandem load when L > 22 ft. In this span range, the maximum shear design values provided by the proposed live load are slightly conservative when compared to the values generated by HS20 truck along with lane load.

Figure A5.3 shows the top and bottom moment envelope curves of pin-fixed beams with different span lengths when various moveable truck or tandem loads plus impact and lane loads are applied. The blue dash and orange solid lines represent the respective maximum moment envelopes produced by the HS20 truck load and tandem axle load along with lane load. The moment envelope generated by the proposed live load model is represented with red solid line, from which it can be found that the

maximum positive moment generally occurs at 0.4 times from the pin end while the maximum negative moment always occurs at the fixed end. By comparing the moment envelopes from different live load models, it is evident that the moment envelopes generated by the alternative live load model are close to, but slightly higher than those produced by HL-93 live load, thus it is conservative to adopt the alternative design model for design usage.

Figure A5.4 represents the top and bottom lines of the shear force envelopes for pin-fixed span beams under various live load models. It is shown that for short spans the tandem load produces a more critical shear envelope due to the closer axle spacing ($b = 4$ ft). When compared to the shear effects caused by the HS20 truck along with lane load, the proposed live load generates slightly conservative shear force values, which may be utilized for rapid analysis or design of bridge spans.

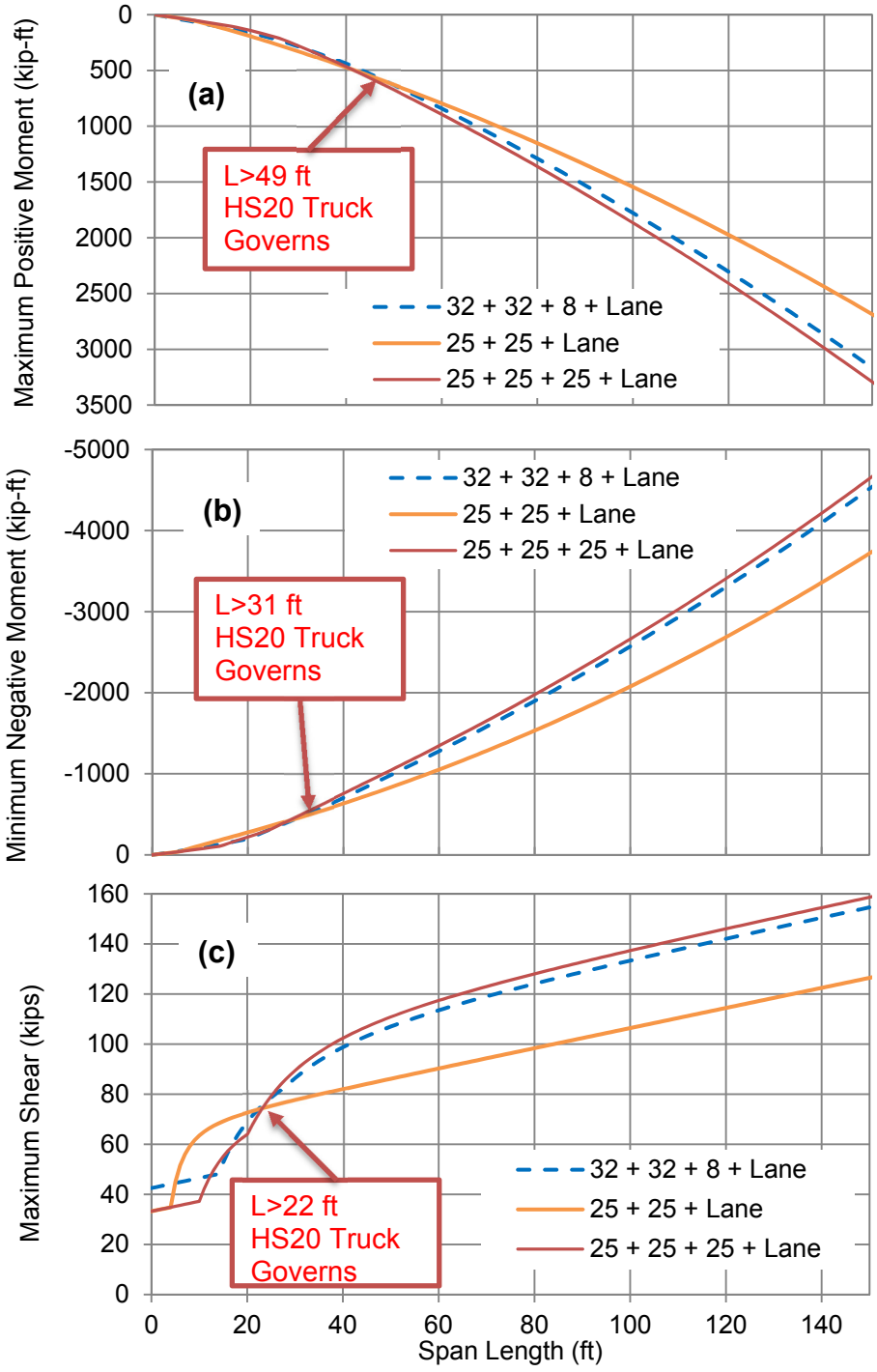

Figure A5.2. Design Actions for (a) Positive Moment, (b) Negative Moment and (c) Shear Values of Pin-fixed Spans under Various Live Load Models.

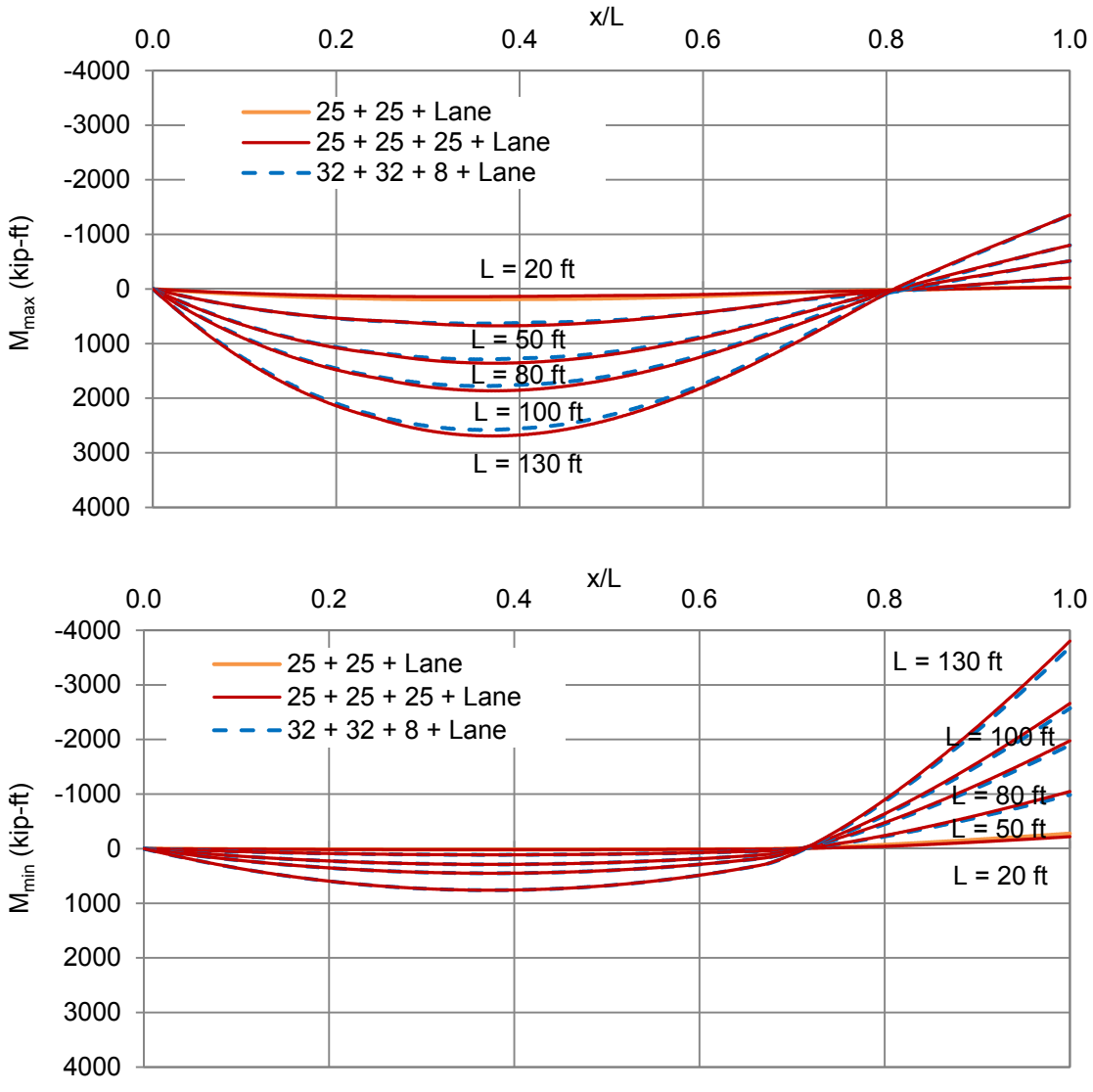

Figure A5.3. Maximum and Minimum Moment Envelopes of Pin-fixed Span Beams under Various Types of Live Loads plus Lane Load.

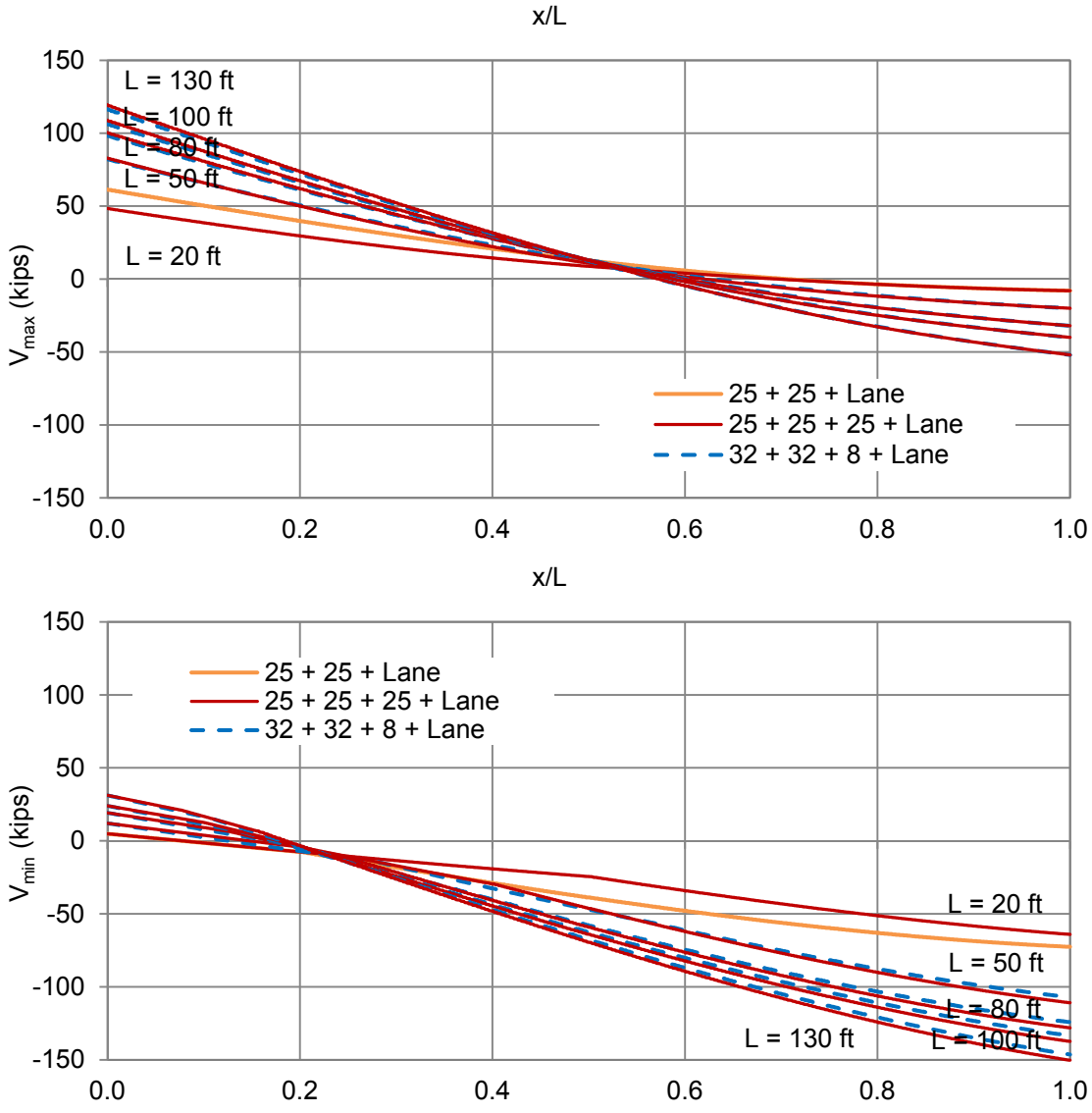

Figure A5.4. Maximum and Minimum Shear Envelopes of Pin-fixed Span Beams under Various Types of Live Loads plus Lane Load.

A5.2.2 Results for Fixed-fixed Spans

Figure A5.5 shows the comparison amongst maximum positive and negative moment and shear values of fixed-fixed spans under different live load models. Similar with the results for pin-fixed spans, the proposed alternative live load produces slightly more conservative maximum moment and shear force values than the HL-93 live load does in the region where the truck load governs the design, which demonstrates that the alternative truck load may be utilized to determine moment effects of fixed-fixed spans in the design process.

Figure A5.6 shows the top and bottom lines of moment envelope curves of fixed-fixed beams with different span lengths when various moveable truck or tandem loads plus impact and lane loads are applied. It is found that the maximum positive and negative moments always occur at mid-span and fixed-end locations, respectively, which conforms to the symmetric property of fixed-fixed beam. By comparing the moment envelopes from different live load models, it is evident that the moment envelopes generated by the alternative live load model are close to, but slightly higher than those produced by HL-93 live load, thus it is conservative to adopt the alternative design model for design usage. Figure A5.7 represents the top and bottom lines of shear force envelopes for pin-fixed span beams under various live load models. When compared to the shear effects caused by HS20 truck along with lane load, the proposed live load generates slightly conservative shear force values.

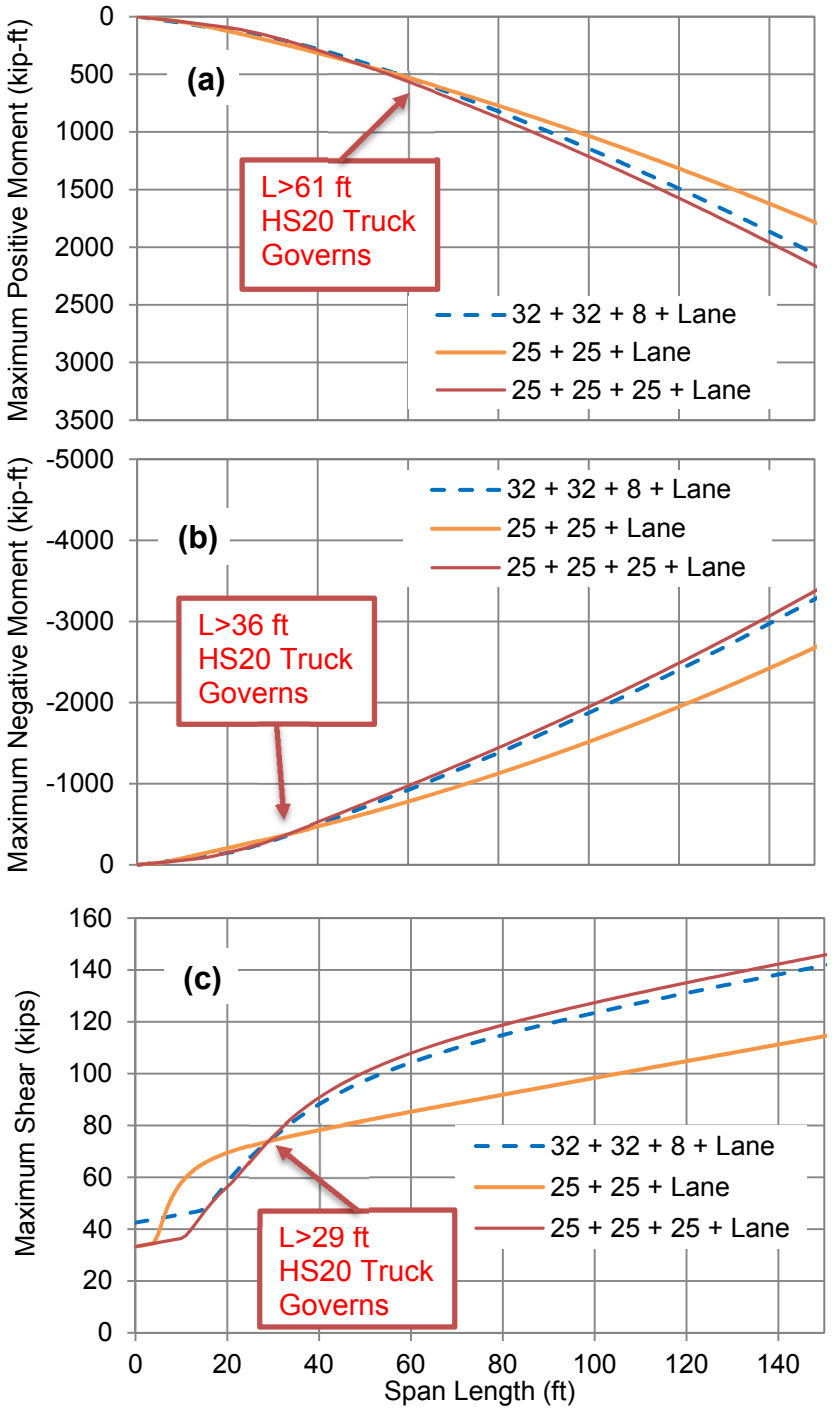

Figure A5.5. Design Actions for (a) Positive Moment, (b) Negative Moment and (c) Shear Values of Fixed-fixed Spans under Various Live Load Models.

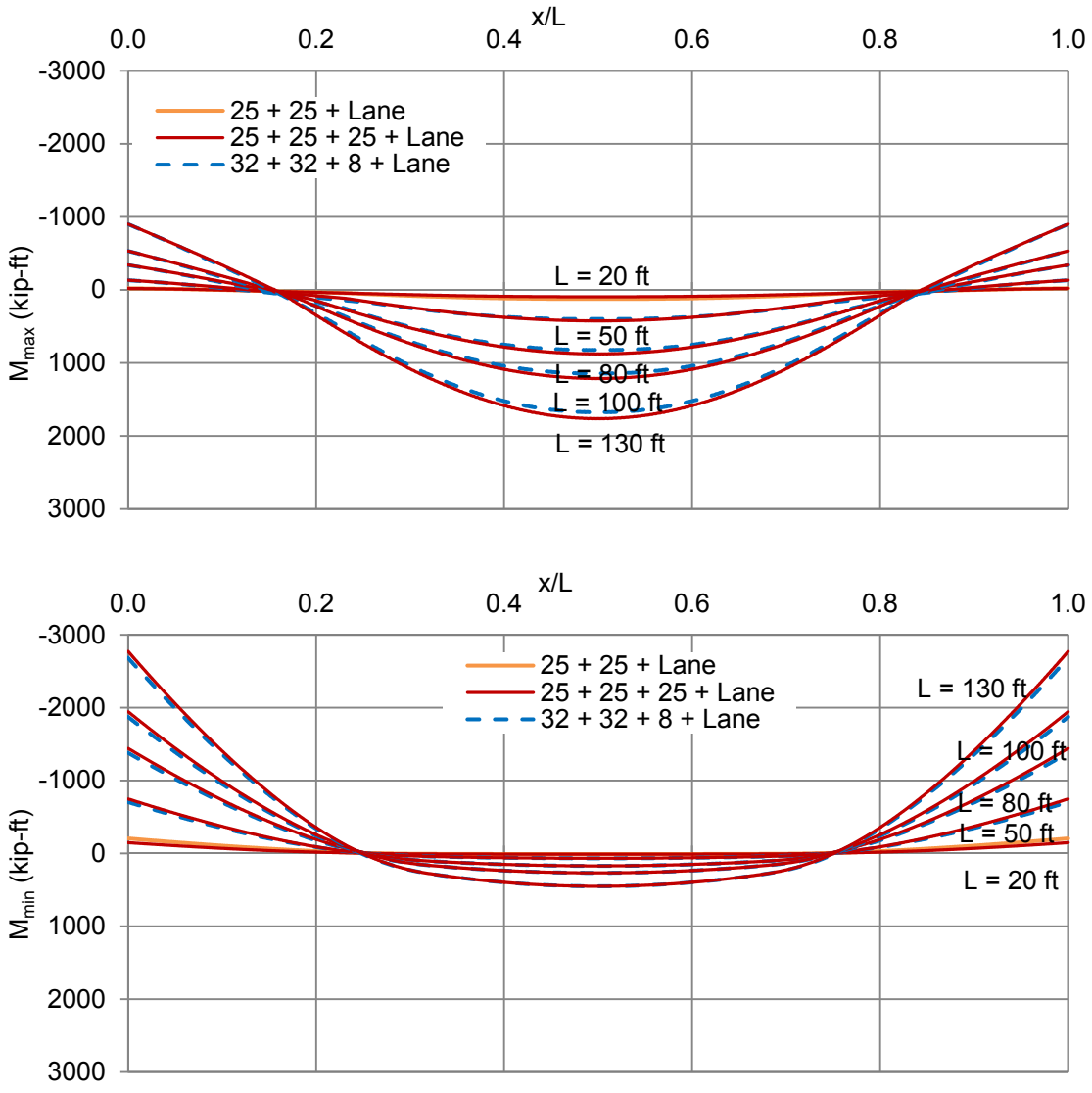

Figure A5.6. Maximum and Minimum Moment Envelopes of Fixed-fixed Span Beams under Various Types of Live Loads plus Lane Load.

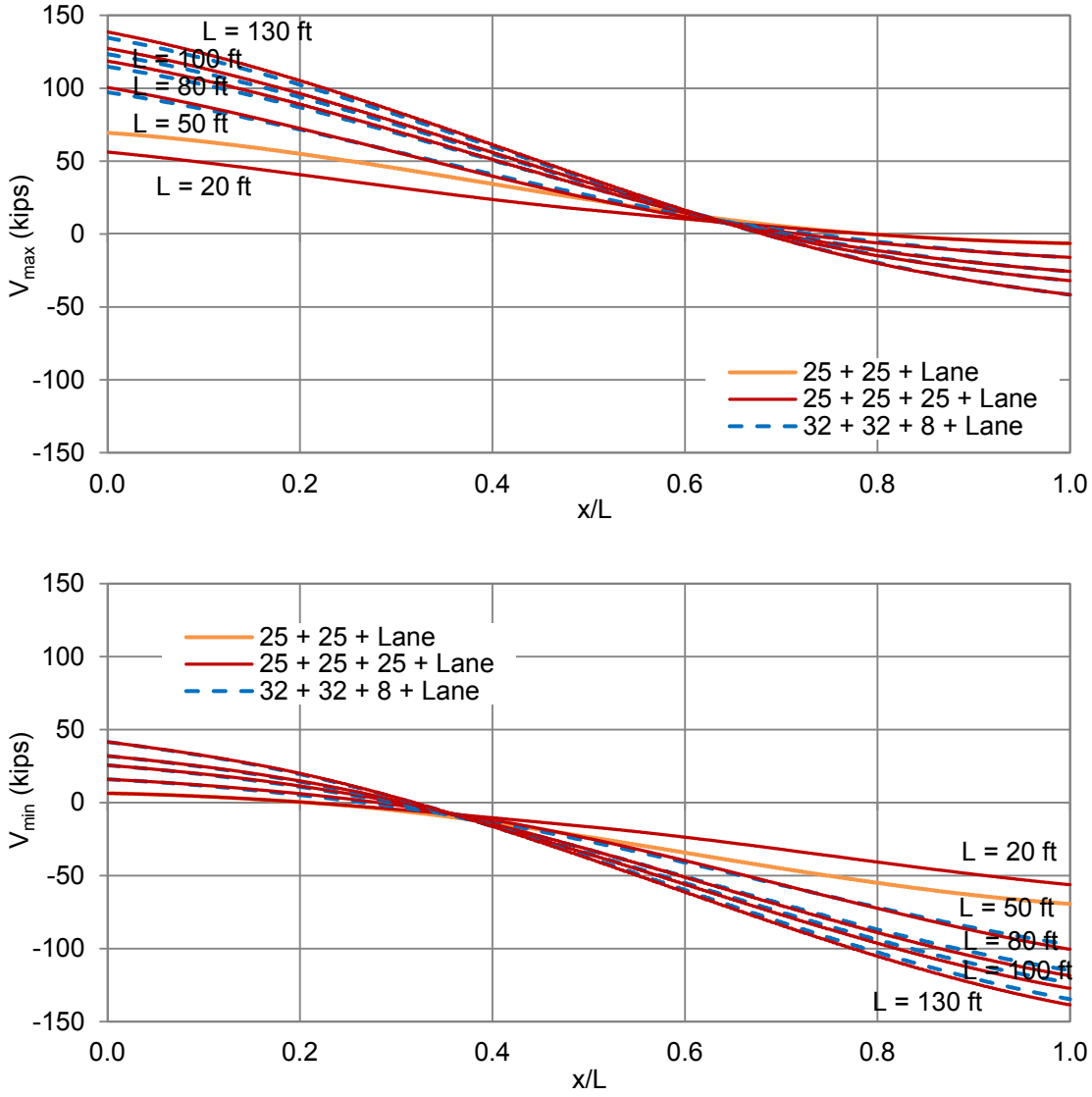

Figure A5.7. Maximum and Minimum Shear Envelopes of Fixed-fixed Span Beams under Various Types of Live Loads plus Lane Load.

A5.3 CLOSURE AND KEY FINDINGS

The moment and shear effects of pin-fixed and fixed-fixed spans under the proposed live load model were evaluated and compared with those produced by AASHTO LRFD HL-93 live model. The following conclusions may be drawn:

1. For pin-fixed spans, the maximum positive moment generally occurs at 0.4 times from the pinned end while the maximum negative moment always occurs at the fixed end. For fixed-fixed spans, the maximum positive and negative moments always occur at mid-span and fixed-end locations, respectively, which conforms to the symmetric property.

2. The proposed alternative truck load produces similar but slightly conservative moment and shear envelope curves for both pin-fixed and fixed-fixed spans as the AASHTO HS20 truck load does, which demonstrates that the alternative truck load may be utilized to determine load effects of continuous bridge configurations in the design process.